Structural Control Optimisation and Health Monitoring using Newly Developed Techniques

A thesis submitted in fulfilment
of the requirements for the degree of
Doctor of Philosophy

By

Mohsen Askari

Faculty of Engineering and Information Technology
University of Technology, Sydney

March, 2014

To My Beautiful Sister:

Raheleh

CERTIFICATE OF ORIGINAL AUTHORSHIP

I certify that the work in this thesis has not previously been submitted for a degree nor has it been submitted as part of requirements for a degree except as fully acknowledged within the text.

I also certify that the thesis has been written by me. Any help that I have received in my research work and the preparation of the 0thesis itself has been acknowledged. In addition, I certify that all information sources and literature used are indicated in the thesis.

Signature of Candidate

Production Note:
Signature removed prior to publication.

Date

22 March 2014

ACKNOWLEDGMENTS

I am truly fortunate to have spent four years at the Centre for Built Infrastructure Research (CBIR) at University of Technology, Sydney (UTS) that provided me the great opportunity to accomplish my graduate studies in a friendly but highly competitive environment. I would first like to thank my PhD supervisors, Associate Prof. Jianchun Li and Prof. Bijan Samali who guided, mentored and encouraged me throughout my thesis with their knowledge, jovial disposition and patience.

I would like to acknowledge the members of CBIR Dynamics and Control Group, in particular Dr. Yancheng Li for his generous help during my experimental tests and Dr. Amir Ali Zad for his valuable guidelines about student life in UTS and Australia.

I am also indebted to my true friends who gave me so many helps in different ways during my study at UTS. My special thanks go to Dr. Saad Mahbub Subhani, Dr. Yukari Aoki, Dr. Ikram Mohammad Kabir, Dr. Vahid Behbood, Dr. Ali Parsa Pajouh, Alireza Radman, Kianoosh Keynejad, Amir Reza Bahrami, Rowshanak Rahrooh, Mona Parvaresh, Leila & Peyman, Zubin Kalchuri, Tina Nyhammer…

Last, but not the least, I thank my family for their support through my entire life. My special appreciation goes out to my brother Meisam without whose motivation and encouragement, completion of this degree would be impossible.

LIST OF PUBLICATIONS RELATED TO THIS THESIS

Journal Articles

1. Semi-Active LQG Control of Seismically Excited Nonlinear Buildings using Optimal Takagi-Sugeno Inverse Model of MR Dampers, M Askari, J Li, B Samali, Procedia Engineering 14, 2765-2772

2. Cost effective Multi Objective Placement of Actuators and MR Dampers in High-Rise Structures using a Modified Integer Coded NSGAII, M. Askari, B. Samali, J. Li, Engineering Applications of Artificial Intelligence (Under Review)

3. Intelligent Semi-Active Control of Building-MR Damper Systems using Novel TSK-Inv and Max-Min Algorithms, M.Askari, J. Li, B. Samali, Journal of intelligent material systems and structures, (Revised sent).

4. Application of extended, unscented, iterated extended and iterated unscented Kalman filter for real-time structural identification; an experimental comparison study, M.Askari, J. Li, B. Samali, International Journal of Structural Stability and Dynamics, (Under Review)

5. Experimental forward and inverse modelling of MR dampers using an optimal TSK fuzzy scheme M.Askari, J. Li, B. Samali, Journal of intelligent material systems and structures, (Revised sent).

6. Adaptive Multiple Forgetting Factor Recursive Least Square (AMFF-RLS) for Real-Time Structural Identification with Unknown Input, Advances in Structural Engineering, (Under Review)

.

Book Chapter

7. A Multi-objective Subtractive FCM Based TSK Fuzzy System with Input Selection, and Its Application to Dynamic Inverse Modelling of MR Dampers, M. Askari, J Li, B Samali, Artificial Intelligence and Soft Computing, 215-226

Conference Papers

8. Adaptive Multiple Forgetting Factor Recursive Least square (AMFF-RLS) for real-time structural identification, M Askari, J Li, B Samali, 22nd ACMSM: "Materials to Structures: Advancement through Innovation", Sydney, Australia December 2012.

9. Application of extended, unscented, iterated extended and iterated unscented Kalman filter for real-time structural identification, M Askari, J Li, B Samali, 7th Australasian Congress on Applied Mechanics (ACAM 7), Adelaide, December 2012.

10. Adaptive multiple forgetting factor recursive least square (AMFF-RLS) for Real-Time Structural Identification with Unknown Input, M Askari, J Li, B Samali, 7th Australasian Congress on Applied Mechanics (ACAM 7), Adelaide, December 2012.

11. Multi Objective Optimal Placement of Structural Control Actuators, M Askari, 6th Australasian Congress on Applied Mechanics (ACAM 6), Perth, December 2010.

12. Future Intelligent Civil Structures: Challenges and Opportunities, J. Li, Y. Li, M. Askari, QP. Ha, The International Symposium on Automation and Robotics in Construction and Mining (ISARC 2014), Sydney, July 2014

TABLE OF CONTENTS

LIST OF FIGURES

LIST OF TABLES

ABSTRACT

Vibration is usually undesirable and yet it occurs in most machines, vehicles, structures, buildings and dynamic systems. The resulting unpleasant motions and the dynamic stresses may lead to fatigue and failure of the structure or machines. In the field of civil engineering, control and identification of the state of health of the structure during the dynamic loads, such as earthquakes and attempt to suppress the vibrations and detect any damage or potential hazard are of vital importance and have posed a great challenge to the research community.

This thesis presents new techniques for optimisation, real-time health monitoring and semi-active vibration control of structures subjected to seismic loads.

First, a new encoding scheme is presented for a fuzzy-based nonlinear system identification methodology, using subtractive Fuzzy C-Mean clustering and non-dominated sorting genetic algorithm. The method is able to automatically select the best inputs as well as the structure of the fuzzy model in such a way that both accuracy and compactness of model are guaranteed. The proposed method is then employed to identify the forward and inverse models of a MR damper. Numerical and Experimental results show that the developed evolving TSK fuzzy model can identify and grasp the nonlinear dynamics of both forward and inverse systems very well, while a small number of inputs and fuzzy rules are required for this purpose.

The optimal design and placement of control devices, is an important problem that affects the control of civil engineering structures. This study also presents a multi-objective optimisationmethod for simultaneous finding of optimal number and location of actuators and MR dampers, in active and semi-active controlled structures. The method is applied to a nonlinear 20-storey benchmark building. The obtained optimal layout of active actuators is compared to the original benchmark problem definition in which 25 actuators are located in non-optimal places. Results show the effect of proposed strategy where similar level of structural performance, in terms of proposed objective indices, is achieved by use of only 7 actuators in optimal locations. Also, the

optimal configuration of different number of MR dampers in the same nonlinear benchmark building is also studied. Results are then compared with optimal locations of actuators in the equivalent active system and the differences are shown.

Two new semi-active control algorithms named TSKInv and MaxMin, are also introduced in this research study to convert the force generated by nominal controller to the required voltage of MR dampers. TSKInv algorithm is developed by modelling the inverse dynamics of MR damper using TSK fuzzy inference systems and MaxMin controller is designed based on the maximum ($maximum\ voltage$) and minimum ($minimum\ voltage$) load of MR damper at each time-step. Applications of these two newly developed methods are compared to some other semi-active control strategies through the 20-storey nonlinear benchmark building. Results show the superiority of these two models over the other algorithms in tracking the desired force using less amount of control force and power.

Also, an investigation on different Kalman Filtering algorithms used in system identification is carried out in this dissertation work, on which EKF, IEKF, UKF and IUKF have been applied to some numerical examples to estimate the parameters of targeted structures in real-time using acceleration responses only. Results demonstrate that IUKF and UKF are the most reliable and robust estimators even if the structure is highly nonlinear and measured data are contaminated with noise. Then, a novel recursive least square based method with adaptive multiple forgetting factor is proposed and applied to different structural identification problems with unknown excitations. It is found from the results that, the proposed algorithm can effectively identify the time-varying parameters as well as the unknown inputs to the structure with high computational efficiency.

Using the developed techniques, this project aims to prepare a platform for real-time structural integrity assessment of civil infrastructures, during or after earthquakes.

CHAPTER 1

INTRODUCTION

Structural safety, both for the structure itself, its occupants, and contents is of great importance because of the devastating consequence of severe dynamic loadings including winds, waves, earthquakes and traffic. Such loads can cause large amplitude and/or sustained vibratory motions, which can be detrimental to the structure and human occupants. For example, the earthquake of magnitude 6.7 that happened in Northridge, U.S.A. on January17 1994 was responsible for the death of 57 people, injury to 9,000 people, displacement of more than 20,000 people from their homes and causing about $20 billion in losses. Another earthquake of magnitude 6.9 happened on the first anniversary of the Northridge Earthquake (January 17 1995) in the city of Kobe, Japan. In that event 5,500 lives were lost, 35,000 people were injured and the estimated loss was over $147 billion. On the 26th of December 2003 the city of Bam in Iran was struck by an earthquake with a magnitude of 6.6. More than 37,000 people died and another 20,000 were injured by the quake. In the India-Pakistan border on October 8, 2005 an earthquake of magnitude 7.6 struck. More than 75,000 people were killed, 80,000 injured and 2.5 million people became homeless. Peru's earthquake of magnitude 8.0 on August 15, 2007 killed at least 500 people and over 34,000 houses were destroyed.

Earthquakes often cause huge casualties, which is due to the failure of constructed facilities such as collapse of buildings, bridges, and dams. Therefore, it is a great challenge for structural engineers to develop technologies to protect civil structures

including their contents and occupants from hazard of strong earthquakes. Safe and performance-based designs of structures are keys to mitigate the effects of such events. To achieve this goal, it is very important to understand the behaviour of structures subjected to vibratory motion of the ground surface during an earthquake.

Figure 1.1. Kobe earthquake, 1995, Japan

To face the environmental forces like earthquake, traditionally structures have been designed through a combination of strength, deformability and energy absorption capacity. This can be achieved through a combination of structural components such as shear walls, braced frames and moment resisting frames to form lateral load resisting systems. The shape of the building is also an important consideration in this approach, since square or rectangular buildings (symmetrical in plan) perform better than other shapes such as L, U or T type buildings (asymmetrical in plan). Materials selection is another important factor, since ductile materials, such as steel and timber are found to perform better than brittle ones, such as brick, concrete and masonry. Seismic design relies on the ability of structural elements to dissipate the seismic energy input to the structure during an earthquake. Therefore, a certain level of deformation and damage is accepted. During minor and moderate earthquakes, structures resist the seismic forces mainly by elastic deformation and hence there is no significant damage. But during strong ground motions caused by a severe earthquake, ductile structures are allowed to deform well beyond the elastic limit. In such a case, there is significant damage to the structure.

It is very difficult, and sometimes impossible and expensive, to repair such damage and excessive deformation of the structure may lead to collapse. Therefore, integrating a supplemental energy dissipation system (supplemental damping system) into the structural system appears to be an elegant solution to reduce the demand on energy dissipation through inelastic deformation, and accordingly to control the response of a structure and minimise its vibration during earthquake events. Integration of such systems into the structure is an essential part of structural control or protective systems. As it is a great challenge for engineers to protect structures as well as human lives and economy, a significant amount of effort has been made to employ various control strategies in the design of engineering structures to increase their safety and reliability against strong earthquakes. As a result, different control technologies have been advanced and are at various stages of development. Such control algorithms offer the advantage of being able to modify dynamically the response of a structure in a desirable manner. Moreover, such control systems can be used in existing structures to be retrofitted or strengthened to withstand future seismic activities.

There are three primary classes of supplemental damping devices, categorised into three corresponding control strategies; namely, passive, active and semi-active control devices. Passive damping treatments have been used extensively in many structural systems to reduce vibration response. Once the passive dampers are incorporated into a structure, the damping cannot be adjusted. Full-scale implementation of active control systems have also been accomplished in several structures such as the 298 meter tall Yokohama Landmark Tower in Japan. However, cost effectiveness and reliability considerations have limited their wide spread acceptance. Semi-active systems, on the other hand, due to their mechanical simplicity, low power requirements, and large, controllable force capacity, provide an attractive alternative to active and hybrid control systems for structural vibration reduction. Therefore, because of advantages inherent in these devices, they are often employed as smart structural members. Some of the semi-active devices available for civil engineering applications are: (a) Variable orifice fluid dampers, (b) Controllable friction dampers, (c) Adjustable tuned liquid dampers, (d) Controllable fluid dampers.

Even though, structural control strategies, reduce the structural vibration, it is still important to develop efficient techniques that can accurately detect damage severity

and location in civil structures, if occurs, in order to determine the remaining life of structure, repair the damaged parts, avoid extra cost as well as updating the mathematical model of the structure. To this end visual inspection, which is labour-intensive and expensive, is still the most widely used method, to date, to check structural safety. However, it is a very subjective process as the accuracy of the damage detection depends highly on the expertise and the experience of the inspecting staff. Moreover, many instances of structural damage, like the corrosion of steel bars in reinforce concrete structure, are hidden inside the structure and cannot be observed from the outside; under such circumstances, visual inspection cannot accomplish its intended purpose.

Hence, in research communities there is an intensive and growing interest in developing efficient structural health monitoring (SHM) techniques, which provide an objective and reliable way to assess the structural health condition and detect the existence of any damage. Generally, SHM techniques are classified into two large categories. The first kind, is known as non-destructive evaluation (NDE), including acoustic emission monitoring, ultrasonic wave, radiography imagining, eddy current detection, and many other methods (Chang & Liu 2003). These techniques require some experimental tests to be carried out in the immediate vicinity of the damage locations to detect the damage. In order to perform NDE testing, the approximate locations of the damage must be known a priori and be accessible for testing, making these methods unsuitable to detect structural damage in the entirety of a complex structure. The second kinds of techniques are known as vibration-based structural health monitoring methods and make use of structural vibration responses to detect and locate structural damage on global structure basis. The basic premise of these SHM methods is that structural damage will alter the structural stiffness, mass and/or energy dissipation, which in turn change the dynamic behaviours of structures. Thus, by tracking these changes SHM systems can, theoretically, detect the occurrence of structural damage, and even locate and quantify them.

1.1 MOTIVATION FOR THIS RESEARCH

As discussed earlier, semi-active control uses the measured structural response to determine the required control force. Therefore, they have the ability to deal with the

changes in external loading conditions. Furthermore, they cannot input any energy into the system and have properties that can be adjusted in real time and can only absorb or dissipate energy. Because of these properties, there is no stability problem associated with this system (Yang 2001). Another advantage of this system is that, they have an extremely low power requirement which is particularly critical during seismic events when the main power source to the structure may fail. These systems also offer the reliability of a passive system, yet maintain the versatility and adaptability of fully active systems. Moreover, they are fail-safe systems as can act as passive control system in the case of power failure.

A magneto-rheological (MR) damper is a type of controllable fluid damper which uses magneto-rheological (MR) fluid. MR fluid consists of micron-sized, magnetically polarisable particles suspended in a liquid such as water, glycol, mineral or synthetic oil (Dyke et al. 1996b). MR fluid has the properties to change reversibly from a free flowing, linear viscous fluid to a semi-solid with controllable yield strength. Because of this property, MR dampers are quite promising for civil engineering applications. However, the semi active control of MR damper-systems is still a challenging issue in the research community. A vibration control system using an MR damper requires two main controllers: (i) a primary system controller, and (ii) an MR damper voltage regulator. The former controller computes the desired damping force required for given system conditions. This is typically done through a sliding mode control, linear quadratic Gaussian (LQG) algorithm or any other optimal control theory which makes the real system to emulate an idealised reference system. The function of the voltage regulator is to command the damper to produce the desired force. The effectiveness of this controller depends on its ability to deal with the nonlinear nature of the device (i.e. the nonlinear relationship between damper force and relative velocity across it) and its semi-active nature.

Optimisation of structure is another issue which has an important effect on structural control performance. In structural control, the type, location and number of active/semi-active control devices should first be optimally determined for the building. The sensory system, data acquisition and signal transmission system should then be designed properly to provide essential feedback information to the control system in which the feedback information is processed according to the control algorithm to

determine control signals. Finally, the beneficial control signals are sent to the control devices to change their parameters to achieve beneficial control forces by which the maximum building response reduction can be achieved. This way of designing, helps to decrease the amount of load on the members and prevent them from damage.

As mentioned in the previous section, an important objective of health monitoring systems for civil infrastructures is to identify the state of the structure and to evaluate its possible damage. If such identification is carried out after the entire data sets are collected, the identification method is called off-line method which can be used when the final state of the structural parameters at the end of loading is of interest. However, in some cases, real-time system identification is absolutely necessary. For example, in structural control, during severe loadings such as earthquakes, access to the updated structural model, to produce optimal control actions, requires real-time structural identification.

Advances in the aforementioned areas can provide a platform for the next generation of smart structures where structural control is integrated with structural damage detection.

1.2 OBJECTIVES OF THE PRESENT RESEARCH

The civil engineering profession and construction industry in many countries are conservative and generally reluctant to apply new technologies. To increase the confidence of adopting new technologies in the field of structural control and health monitoring, more research and implementation is needed. The objectives of the present research are then as follows:

- To study and develop a new optimal concise and precise system identification method.
- To obtain new forward and inverse models of MR dampers.
- To evaluate the effect of control device locations in the structure and introduce new algorithms for optimal number and placement of the actuators and MR dampers in multi-storey structures.
- To design new semi-active control frameworks for the smart devices to be incorporated into the structure.

- To apply some recently developed online system identification methods to civil engineering structures.

- To present a new online real-time structural identification method to track any abrupt changes of structural parameters.

1.3 ORGANISATION OF THE THESIS

This thesis has been organised into six chapters. The introduction, motivation and innovation of this research are presented in the current chapter. It should be mentioned that, since the current dissertation is a multi-disciplinary study, the literature review relevant to each discipline area is conducted and provided in the corresponding chapter for better understanding and discussing the challenges. Hence, no specific chapter is dedicated to Literature Review. The overviews of the other chapters are as follows:

- **Chapter 2**: In this chapter, a new encoding scheme is presented for a fuzzy-based nonlinear system identification methodology, using the subtractive fuzzy C-Mean clustering and a modified version of non-dominated sorting genetic algorithm. Due to the simplicity of the procedure, the most suitable minimal inputs and rules are searched simultaneously, such that the resulting fuzzy model is of compact size and acceptable accuracy. The proposed method is then employed to identify the inverse model of an MR damper. From numerical and experimental modelling point of view, it is shown that the developed Takagi–Sugeno-Kang (TSK) fuzzy model can represent the dynamic behaviour of the MR damper accurately using a concise model.

- **Chapter 3**: This chapter presents a multi-objective optimisation method for simultaneous finding of optimal number and placement of actuators and MR dampers, in active and semi-active vibration control of seismically excited nonlinear structures. First, a modified integer coded version of non-dominated sorting genetic algorithm II (MI-NSGAII) is introduced. This method can increase the accuracy as well as the convergence speed of the original NSGAII, particularly when the adjustable parameters are integers. Using this method, a hybrid algorithm is then designed to find the optimum number and location of structural control devices. As a case study, the proposed strategy is then used to

find the optimal number and location of actuators and MR dampers in a 20-storey nonlinear benchmark structure in which the objective functions, i.e. reduction of peak inter-storey drift ratio, peak floor acceleration and peak base shear, are simultaneously achieved.

- **Chapter 4:** New technologies for improving structural resistance to earthquake loading are investigated in this chapter. Two new semi-active control algorithms named TSKInv and MaxMin, are designed to convert the force generated by the primary controller to the required voltage of MR dampers. The first technique uses an optimal compact TSK fuzzy inverse model of MR damper to predict the required voltage to actuate the MR dampers (TSKFInv). To find the inverse model of MR damper, the method introduced in Chapter 2, is used here. Another semi-active voltage controller is also presented which works based on the maximum and minimum capacities of MR damper at each time-step. Using the response of the structure, the maximum and minimum loads that can be generated by an MR damper at each time-step are obtained by a simple forward model of MR damper. Considering a linear relation between these two operating points, the required voltage to produce a desired force is then estimated. The method is designated as MaxMin Optimal Controller. For both algorithms, the acceleration response of building is only used as the input. However, in case the acceleration measurement is not available at some storeys, a Kalman filter is designed to estimate the required unknown response. For the case study, the proposed control strategies are applied to a 20-storey nonlinear benchmark building subjected to 10 different earthquake signals. The numerical results are compared to clipped optimal control (COC) and modified COC and the results discussed.

- **Chapter 5:** In this chapter, a comparative study on different Kalman filtering algorithms was carried out, where EKF, IEKF, UKF and IUKF have been applied to estimate the parameters of linear and nonlinear structures in real-time using acceleration responses only. Such comparison has not been conducted before in civil engineering applications. Also, a recursive least square (RLS) based method with adaptive multiple forgetting factors is proposed and applied to different structural identification problems with unknown excitations. The

covariance matrix in this method has the same size as the unknown parameters, which makes the proposed algorithm compact and capable of real-time tracking of the unknown system's parameters. The efficiency of this method is validated using various numerical examples. It is found from the results that, the proposed algorithm can effectively identify and track the time-varying structural parameters with high computational efficiency, as well as the unknown inputs to the structure.

- **Chapter 6**: A summary of all chapters together with concluding remarks are presented in this chapter. Some future works are also suggested in this chapter.

CHAPTER 2

MR DAMPER MODELLING

2.1 CHAPTER OUTLINE

In this chapter, a new encoding scheme is presented for a fuzzy-based nonlinear system identification methodology, using the subtractive Fuzzy C-Mean clustering and a modified version of non-dominated sorting genetic algorithm. This method is able to automatically select the best inputs as well as the structure of the fuzzy model such as rules and membership functions. Moreover, three objective functions are considered to satisfy both accuracy and compactness of the model. The proposed method is then employed to identify the inverse model of a highly nonlinear structural control device, i.e. Magnetorheological (MR) damper. It is shown that the developed evolving Takagi–Sugeno-Kang (TSK) fuzzy model can identify and grasp the nonlinear dynamics of both forward and inverse systems very well, while a small number of inputs and fuzzy rules are required for this purpose.

2.2 INTRODUCTION AND BACKGROUND

2.2.1 Magnetorheological Dampers

In recent years, smart structures have been adopted in many engineering fields because the performance of structural systems can be improved without either significantly

increasing the structure mass or requiring high cost of control power. They may be called intelligent structures, adaptive structures, active structures, smart structures, etc. These terminologies refer to a structure which is an integration of actuators, sensors, control units, and signal processing units within a structural system. The materials that are usually used to make a smart structure are: piezoelectrics, shape memory alloys (SMA), electrostrictive/magnetostrictive materials, polymer gels, and magnetorheological/electrorheological fluids (Hurlebaus & Gaul 2006).

In particular, one of the controllable-fluid dampers, magnetorheological (MR) damper developed by Lord Corporation, has attracted attention in recent years because it has many attractive characteristics. A MR damper consists of a hydraulic cylinder, magnetic coils, and MR fluids that consist of micron-sized magnetically polarisable particles floating within oil-type fluids as shown in Figure 2.1. The MR damper is operated as a passive damper; however, when a magnetic field is applied to the MR fluids, the MR fluids are changed into a semi-active device in a few milliseconds. Its characteristics are summarised as: 1) a MR damper is operated by low power sources, e.g., SD-1000 MR damper can generate force of up to 3000 N using a small battery with capacity less than 10 W; 2) it has high yield strength level, e.g., its maximum yield strength is beyond 80 kPa; 3) the performance is stable in a broad temperature range, e.g., MR fluids can operate at temperatures between $-40^{\circ}C$ and $15^{\circ}C$; 4) the response time is a few milliseconds; 5) the performance is not sensitive to contamination during manufacturing the MR damper. Moreover, the operating point of the MR damper, which is a current-controlled device, can be changed by a permanent magnet.

To fully use the best features of the MR damper, a mathematical model that portrays nonlinear behaviour of the MR damper has to be developed first. However, this is challenging because the MR damper is a highly nonlinear hysteretic device. Therefore, research related to response control of building structures using MR dampers first started from development of a model that can describe the behaviour of MR damper. In this section, several models for the MR damper are introduced.

In this chapter, literatures on different types of forward and inverse models of MR dampers are discussed. Some concluding remarks are made and a new approach to

capture the behaviour of inverse model of MR damper, to be used later in this thesis, is introduced and validated through numerical and experimental case studies.

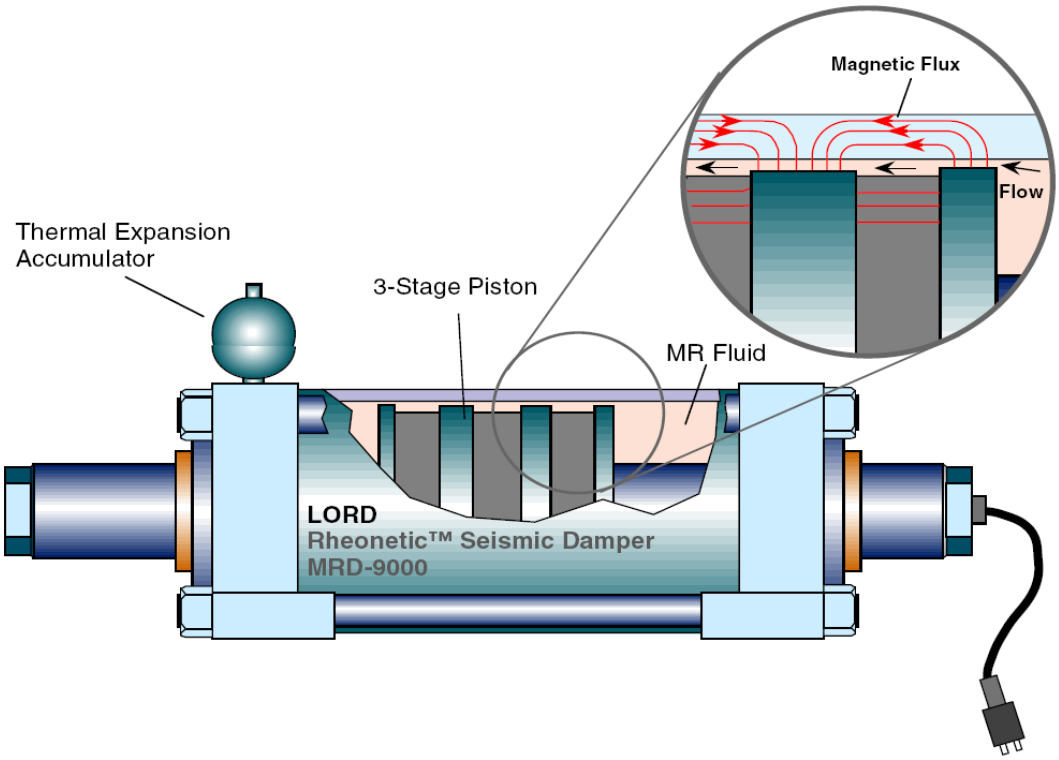

Figure 2.1. A schematic of the prototype 20-ton large-scale MR damper (Yang et al. 2002)

2.2.2 Forward Models of a MR Damper

A model that can predict the hysteresis force of the MR damper is called forward model and will take advantage of the exceptional characteristics of MR dampers. There have been many efforts devoted to model the non-linear behaviour of the MR damper. These models are classified as the quasi-static and dynamic models. Although the quasi-static models are capable of describing force–displacement behaviour of MR dampers reasonably well, they are not sufficient to describe the nonlinear force–velocity behaviour of these dampers. Many dynamic models have been developed to overcome this shortcoming. These models include parametric and non-parametric models. Parametric models have been proposed for describing the dynamic behaviour of MR dampers. The parametric modelling technique characterises the device as a collection of linear and/or nonlinear springs, dampers and other physical elements.

In general, the simplest model for a damper would be a viscous dashpot model:

$$f = c\dot{x}, \tag{2-1}$$

where the damper force f is linearly related to the applied velocity $\dot{x}$. However, this can not be used for the MR damper modelling because the relationship between MR damper forces and piston velocities is highly nonlinear. Furthermore, a MR damper has two more design parameters: the piston displacement and the applied voltage. Stanway suggested a viscoplastic model, called Bingham model, by adding a Coulomb friction element into the viscous damper model for the highly nonlinear hysteretic behaviour of an electrorheological damper as shown in Figure 2.2 (Stanway, Sproston & Stevens 1985).

Such a Bingham model can also be applied to a MR damper (Spencer et al. 1997):

$$f_{MR} \triangleq F = f_C sgn(\dot{x})v + c\dot{x} + f_0, \tag{2-2}$$

where f_C is Coulomb friction coefficient, $\dot{x}$ is the piston velocity, v is the applied voltage, c is the damping coefficient, and f_0 is an offset value to adjust a non-zero force value due to accumulator. When a MR damper is designed, an accumulator can be incorporated into the MR damper in order to adjust expansion or contraction of MR fluids due to changing temperature.

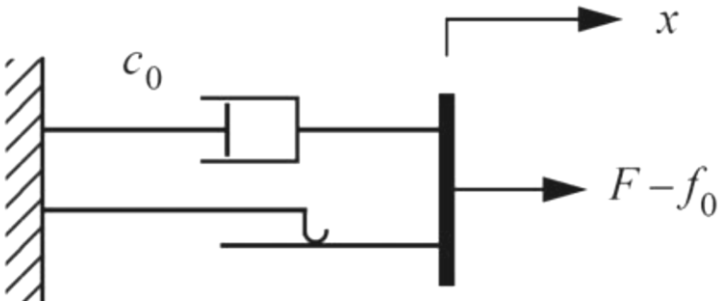

Figure 2.2. Bingham model of an ER/MR damper (Stanway, Sproston & Stevens 1985)

The reason that the Bingham model can be used to describe the behaviour of a MR damper is that a MR damper has approximately two operating stages, i.e., pre-yielding and post-yielding stages. Note that it is simple and easy for this Bingham model to be incorporated with a control system for analysis and design purposes; however, the piston displacement is not considered in this model, i.e., the effects of stiffness of the MR damper is ignored. In addition, the performance is degraded when the magnitude of the piston velocity is small. The problem of performance of the Bingham model being degraded at low velocity range can be solved by a polynomial model.

One of the most popular mathematical models for modelling a MR damper is the Bouc-Wen model (Spencer et al. 1997) depicted in Figure 2.3.

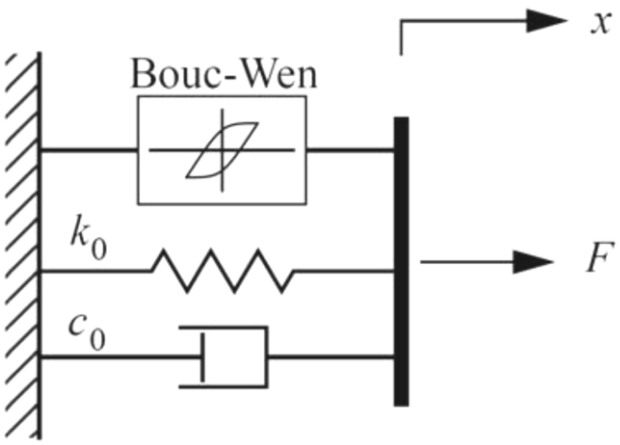

Figure 2.3.Bouc-Wen model of the MR Damper (Spencer et al. 1997)

The hysteretic behaviour of the Bouc-Wen model for a MR damper is governed by the following equations (Spencer et al. 1997; Tse & Chang 2004):

$$f_{MR} \triangleq F = c_0\dot{x} + k_0(x - x_0) + \alpha z_{BW},$$

$$\dot{z}_{BW} = -\gamma|\dot{x}|z_{BW}|z_{BW}|^{n-1} - \beta\dot{x}|z_{BW}|^n + A\dot{x},$$

$$\alpha = \alpha_a + \alpha_b u + \alpha_c u^2, \tag{2-3}$$

$$c_0 = c_{0a} + c_{0b}u,$$

$$\dot{u} = -\eta(u - v),$$

where z_{BW} and α, called evolutionary variables, describe the hysteretic behaviour of the MR damper; c_0 is the viscous damping; k_0 is the stiffness; x_0 is the initial displacement, which is caused by an accumulator, of the spring that corresponds to the stiffness$k0$; γ, β and A are adjustable shape parameters of the hysteresis loops; and v and u are input and output voltages of a first-order filter, respectively.

Although this model describes the hysteretic behaviour of the MR damper, it is still difficult for the Bouc-Wen model to capture the response behaviour at the small piston velocities (Spencer et al. 1997).

Such a drawback of the Bouc-Wen model can be solved by modifying the Bouc-Wen model, i.e., the modified Bouc-Wen model which has good performance at both high velocity as well as low velocity ranges (Spencer et al. 1997) as shown in Figure 2.4. The MR damper force predicted by the modified Bouc-Wen model is governed by the following differential equations according to (Spencer et al. 1997):

$$
\begin{aligned}
F &= c_1\dot{y} + k_1(x - x_0) \\
\dot{y} &= \frac{1}{c_0 + c_1}[\alpha z + c_0\dot{x} + k_0(x - y)] \\
\dot{z} &= -\gamma|\dot{x} - \dot{y}|z|z|^{n-1} - \beta(\dot{x} - \dot{y})|z|^n + A(\dot{x} - \dot{y}) \\
\alpha &= \alpha_a + \alpha_b u \\
c_1 &= c_{1_a} + c_{1_b} u \\
c_0 &= c_{1_a} + c_{1_b} u \\
\dot{u} &= -\eta(u - v)
\end{aligned}
\tag{2-4}
$$

where z and α , called evolutionary variables, describe the hysteretic behaviour of the MR damper; c_0 and c_1 are viscous damping at high and low velocities, respectively; k_0 and k_1 are the stiffness at large velocities and the accumulator stiffness, respectively; the x_0 is the initial displacement of spring with stiffness k_1; γ, β and A are adjustable shape parameters of the hysteresis loops; and v and u are input and output voltages of a first-order filter, respectively. Note that the modified Bouc-Wen model is one of the most effective models to describe the behaviour of a MR damper; however, it is not easy to derive the inverse model for control system design purpose. In the following sections, the corresponding inverse models are introduced. Other kinds of parametric dynamic models for MR dampers based on mechanical idealisations, including Bingham-model-based dynamic models, bi-viscous models, viscoelastic–plastic models, stiffness–viscosity-elasto-slide models, Bouc–Wen hysteresis operator-based models, Dahl hysteresis operator-based models, LuGre hysteresis operator-based models, hyperbolic tangent function-based models, sigmoid function-based models, equivalent models and phase transition models have been also explored and validated. More literature on different types of forward models can be found in (Wang & Liao 2011).

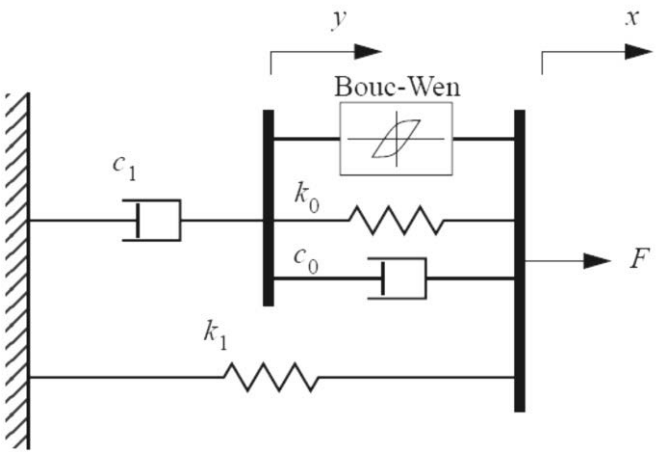

Figure 2.4. Modified Bouc-Wen model of the MR Damper (Spencer et al. 1997)

These parametric models can model the dynamics of MR dampers within a limited range by identifying the parameters for the parametric dynamic models. However, parametric identification methods require assumptions with regards to the structure of the mechanical model that simulates the behaviour. Once a model is selected, the values of system parameters are determined in such a way that the error between the experimental data and the simulated responses is minimised. The approach could be divergent if the starting assumptions for the structure of the model are flawed, or if proper constraints are not applied to the parameters and thus unrealistic parameters such as negative mass or stiffness may be obtained.

2.2.3 Non-parametric models

Another class of dynamic models mentioned above are non-parametric models. The non-parametric modelling methods employ analytical expressions to describe the characteristics of the modelled devices based on both testing data analysis and device working principles. Non-parametric methods could avoid some pitfalls of the parametric approaches for modelling, and they are robust and applicable to linear, nonlinear and hysteretic systems. For modelling MR dampers, non-parametric models, including the polynomial model, the multi-function model, the black-box model, the query-based model, the neural network model, the fuzzy model, the wavelet model and the Ridgenet model, have been proposed in the literature (Wang & Liao 2011).

2.2.4 Inverse Models of a MR Damper

A MR damper force cannot be directly controlled, but only applied voltage can be directly controlled, i.e., control force signals that are provided by a control algorithm should be converted into voltage or current signals to operate the MR damper. For the signal transformation, two ways might exist: 1) use of an algorithm to be able to convert control forces into voltage or current signals, 2) use of an inverse model of the MR damper. The inverse dynamic models for MR dampers represent the relationships between the applied voltage/current and the displacement to the MR dampers and damper force.

Recently, several types of inverse models of a MR damper are introduced. They include a Bingham, a polynomial, a Bouc-Wen, and a modified Bouc-Wen model. These models however are difficult to solve numerically and also can not fully capture the behaviour of inverse model of MR dampers and thus can not be used in real-time applications. Therefore, non-parametric models, such as Neural Network based models and Fuzzy Inference based models have been proposed by some researchers (Askari, Li & Samali ; Askari & Markazi). In this chapter, a novel non-parametric approach based on Takagi-Sugeno-Kang (TSK) fuzzy inference systems will be presented which is able to track the inverse behaviour of MR dampers.

2.3 A NEW NON-PARAMETRIC APPROACH FOR MR DAMPER MODELLING

One of the common algorithms in identification of nonlinear systems is Fuzzy modelling where TSK approach is the most popular one and is recently used in mechanical and civil engineering application.

The TSK fuzzy model uses IF–THEN rules to approximate a wide class of nonlinear systems by fuzzy blending of local linear approximations. This method employs linear models in the consequent part of the Fuzzy System (FS). The schematic structure of a TSK fuzzy model is shown in Figure 2.5.

Various methods, such as clustering algorithms, linear least squares and nonlinear optimisation methods are used for tuning of antecedent and consequent parameters of

the FS (Jang, Sun & Mizutani 2010; Yager & Filev 1994). To accommodate new input data, adaptive online learning of TSK fuzzy models has been developed (Kasabov & Song 2002). From another point of view, the design of a fuzzy model can be formulated as a search problem in an appropriate multidimensional space, where every point represents a possible fuzzy model with specific rule structure, membership functions (MFs), and their associated parameters. Due to the capability of search within irregular and multidimensional spaces, evolutionary algorithms (EAs), such as the GA and evolutionary strategies have extensively been used.

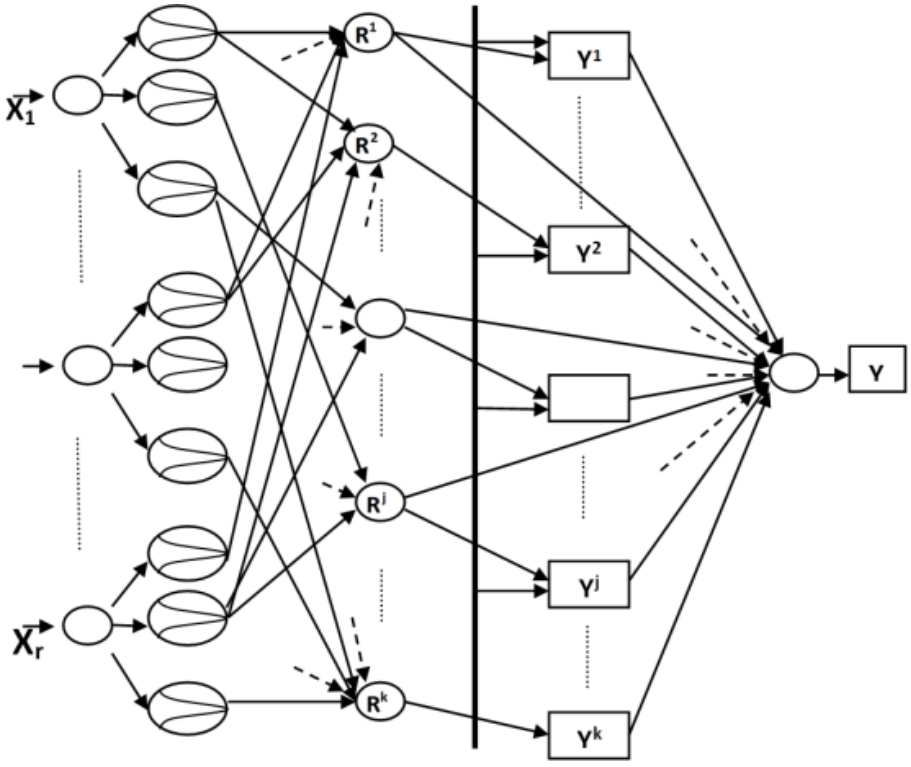

Figure 2.5. Structure of a TSK Fuzzy Model (r: number of inputs; k: number of rules)

In conventional EA-based fuzzy modelling methods, the structure of the FS, e.g., the suitable inputs, are prescribed and parameters of the rules and MFs are optimised. Some methodologies have been developed to modify the rules structure of the FS, using a single objective GA and by encoding the required information into a chromosome (Chiu 1994). However, selection of the most relevant inputs, among numerous possible options, is an important and challenging problem for construction of an FS. Therefore, some studies on finding the best possible combination of relevant inputs are reported (Yager & Filev 1994). Due to the fact that, the process for selection of inputs and the rule bases for nonlinear systems are co-dependent, a new GA based

methodology is then introduced (Du & Zhang 2008), where an encoding scheme for simultaneous selection of the most appropriate inputs, numbers of rules and parameters of the MFs, using a single-objective GA algorithm, is studied. Such encoding scheme, however, deals with a large number of to-be-tuned parameters, causing a huge computational burden and hence making the optimisation process very time consuming. Furthermore, application of such method requires a good knowledge of the expected bounds of every parameter at the outset of the design, which may not be available. On the other hand, the excessive number of inputs and rules, not only affect the compactness and transparency of the underlying model, but also increases the complexity of the computations necessary for real-time implementation of the resulting model.

In order to develop an accurate, yet compact FS, in this chapter, an evolving TSK fuzzy model is introduced. The proposed method is based on subtractive clustering technique combined with fuzzy c-mean clustering method (FCM) and a new modified version of non-dominated sorting genetic algorithm (MNSGAII). For this purpose, an encoding scheme, using a bi-section chromosome is introduced. The first section of the chromosome encodes the selected inputs and the second one encodes the rules and the MFs parameters. The best chromosome is searched and evolved through a suitably defined multi-objective MNSGAII with three objective functions, i.e., the number of inputs, the number of rules and the RMS error between the target and predicted outputs.

2.3.1 Preliminaries

2.3.1.1 TSK Fuzzy Structure

Most neural fuzzy systems employ the inference method proposed by Mamdani (Mamdani, Assilian 1975) in which the consequent parts are defined by fuzzy sets. A Mamdani-type fuzzy rule has the form:

$$If\, x_1 \; is \; A_{1j}(m_{1j}, \sigma_{1j}) \; and \; x_2 \; is \; A_{2j}(m_{2j}, \sigma_{2j}) \ldots and \; x_n \; is \; A_{nj}(m_{nj}, \sigma_{nj})$$

$$THEN \; y \; is \; B_j(m_j, \sigma_j) \, .$$

where m_{ij} and σ_{ij}represent a Gaussian membership function with mean and standard deviation respectively, of the ith dimension and the jth rule node. The consequent B_j of the jth rule is aggregated into one fuzzy set for the output variable y. The crisp output is obtained through defuzzification, which calculates the centroid of the output fuzzy set. In addition, Takagi, Sugeno and Kang introduced a modified inference scheme which in the first two parts of the fuzzy inference process, fuzzifying the inputs and applying the fuzzy operator, are exactly the same as Mamdani model (Takagi & Sugeno 1985). However, a TSK fuzzy inference model employs different implication and aggregation methods than the standard Mamdani model. Instead of fuzzy sets being used, the conclusion part of a rule in TSK fuzzy model, is a linear combination of the crisp inputs, as follows:

$$If\, x_1\ is\ A_{1j}(m_{1j}, \sigma_{1j})\ and\ x_2\ is\ A_{2j}(m_{2j}, \sigma_{2j})\ \dots and\ x_n\ is\ A_{nj}(m_{nj}, \sigma_{nj})$$

$$THEN\ y = w_{0j} + w_{1j}x_1 + \cdots + w_{nj}x_n$$

where m_{ij} and σ_{ij} represent a Gaussian membership function with mean and standard deviation, respectively, of the ith dimension and the jth rule node. Since the consequent of a rule is crisp, the defuzzification step becomes obsolete in the TSK inference scheme. Instead, the model output is computed as the weighted average of the crisp rule outputs. This computation is less expensive than calculating the centre of gravity.

2.3.1.2 Scatter Partitioning

Scatter partitioning, or clustering, aims at partitioning data into quasi-homogenous groups with intra-group data similarity greater than inter-group similarity. This approach attempts to obtain an approximation of the fuzzy model without making assumptions about the structure of the data (Jang, Sun & Mizutani 1997). Clustering is used in fuzzy modelling for data compression and model construction. In order to divide data into groups, similarity metrics are used to evaluate the homogeneity of normalised input vectors. Comparable input-output data pairs in the training set are assembled into groups or clusters. After data partitioning, one rule is associated with each data cluster, usually leading to rules scattered in the input space at locations with sufficient concentration of data. This results in a greatly reduced number of rules, in contrast to grid-partitioned models. Also, as opposed to models using grid partitioning,

fuzzy sets are not shared by all the rules. Off-line clustering algorithms used for fuzzy modelling include the fuzzy C-means (FCM) clustering (Bezdek, Ehrlich & Full 1984), the mountain clustering method (Yager & Filev 1994) and the subtractive clustering technique (Chiu 1994).

2.3.1.3 Subtractive Clustering

The subtractive clustering algorithm considers each of the available data points as a possible candidate for the centres of data clusters. To do so, a matrix consisting of n sets of m-dimensional input–output data, $\{x_1, .., x_n\}$, normalized within the hypercube of dimension *M* is considered.

The density measure for every data point, x_i, is defined as

$$D_i = \sum_{j=1}^{n} \exp\left(-\frac{\|x_i - x_j\|^2}{(r_a/2)^2}\right), \tag{2-5}$$

where, $\|\ \|$ denotes the Euclidean distance and r_a is the prescribed radius of the hyperspheres, within which the neighbouring points are considered to be more important than the others. Hence, a data point will have a high density value if it has many neighbouring data points. The data point, x_{C_1}, with the highest density, D_{C_1}, is then selected as the first cluster centre.

In order to select the next cluster centre, the data points near the first cluster centre, x_{C_1}, should be forced to be less important. For this purpose, the modified densities are defined as:

$$D_{mi} = D_i - D_{C_1} \exp\left(-\frac{\|x_i - x_{C_1}\|^2}{(r_b/2)^2}\right), \tag{2-6}$$

The constant r_b specifies a neighbourhood of x_{C_1} where the modified density must become smaller. Generally, r_b should be selected larger than r_a, e.g. $1.5r_a$ (Chiu 1994). Now, the next data point, x_{C_2}, with the largest modified density is selected as the next cluster centre, and so on.

2.3.1.4 FCM based TSK model identification

Regarding TSK models, both the clusters (fuzzy regions) and the linear sub-models' parameters are requested. By premise structure identification, we mean to determine the specific input variables and partition the input space properly. Fuzzy C-Mean is one of the strongest clustering algorithms that can be used to identify the clusters.

The objective function of the FCM is defined by:

$$J_b(U,Z) = \sum_{i=1}^{c}\sum_{k=1}^{N}(\mu_{ik})^m \|x_k - z_i\|^2, \tag{2-7}$$

where x_k signifies the point in data space, k =1, 2,..., N ; N signifies the number of data points; Z_i stands for the final cluster centre, i =1,2,..., c ; c corresponds to the number of fuzzy rules; $\mu_{ik} \in [0,1]$ is the fuzzy membership degree of the kth data pair pertaining to the ith fuzzy subset.

It is assumed that μ_{ik} is constrained by the following equation:

$$\sum_{i=1}^{c}\mu_{ik} = 1,\ k = 1,2,\dots,N. \tag{2-8}$$

The C-means algorithm for clustering in n dimensions produces C-means vectors that present c classes of data. The problem of finding the fuzzy clusters in the data set is now solved as a constrained optimisation problem using FCM algorithm, considering the minimisation of the function in Eq.2-7 over the domain data set and taking into account the constraints in Eq.2-8. The results of FCM imply the clustering centres together with the corresponding membership degrees. The main steps for identifying the TSK fuzzy model based on FCM are given as follows:

Step 1: Given c, m, and the initial clustering centres for all k =1, 2,..., N and i =1, 2,..., c . set an initial fuzzy c-partition matrix $U = [\mu_{ik}]$ to indicate the membership value for the ith cluster representatives.

Step 2: Calculate the following equation:

$$z_i = \frac{\sum_{k=1}^{N} z_k(\mu_{ik})^m}{\sum_{k=1}^{N}(\mu_{ik})^m}, \qquad i = 1,2,\dots,c \tag{2-9}$$

Step 3 Update U to adjust

$$\mu_{ik} = \left[\sum_{j=1}^{c}\left(\frac{x_k - Z_i}{x_k - Z_j}\right)^{\frac{2}{m-1}}\right]^{-1} \tag{2-10}$$

Step 4 Check for termination. If

$$\|U_k - U_{k-1}\| < \varepsilon \tag{2-11}$$

stop; otherwise, let k = k +1 and return to step 2.

Step 5: Identify the consequent parameters using orthogonal least squares (OLS) method. We have:

$$y = \emptyset\theta, \tag{2-12}$$

where $\emptyset = [\beta_1, \dots, \beta_n, \beta_1 x_1, \dots, \beta_n x_1, \dots, \beta_1 x_m, \dots, \beta_n x_m]$, and $\theta = [p_0^1, \dots, p_m^1, p_0^2, \dots, p_m^2, p_0^n, \dots, p_m^n]^T$ signify the consequent parameters.

In regard to the least squares solutions,

$$\theta = (\emptyset^T\emptyset)^{-1}\emptyset^T y. \tag{2-13}$$

Here we convert $[\emptyset^T\emptyset]$ into an orthogonal matrix [W^T W]. By implementing iteration and conversion algorithms, the $(m+1) \times n$ coupled equations become mutually independent, thereby calculating the consequent parameters θ.

2.3.1.5 Non-Dominated Sorting Genetic Algorithm II (NSGA II)

In solving multi-objective optimisation problems, one may be interested in a set of Pareto optimal solutions that provide some sort of flexibility and freedom to the final decision. The NSGA-II algorithm has been demonstrated to be one of the efficient algorithms for solving multi-objective optimisation on a number of benchmark problems (Deb 2001; Deb et al. 2002). In addition, it has been shown that NSGA-II outperforms two other contemporary multi-objective evolutionary algorithms: Pareto-archived evolution strategy (PAES) (Knowles & Corne 1999) and Strength-Pareto Evolutionary Algorithm (SPEA) (Zhihuan, Yinhong & Xianzhong 2010) in terms of finding a diverse set of solutions and in converging near the true Pareto-optimal set. It also provides an efficient procedure for introducing elitism into a multi-objective

optimisation algorithm while guarantees a diversity-preserving mechanism, assuring a good convergence towards the Pareto optimal front without losing solution diversity.

In this algorithm, the population size, N, and number of generations are initialised first. The population is then sorted based on non-domination into each front (Figure 2.6). The first front is a completely non-dominant set in the current population, and the second one is dominated by the individuals in the first front only, and so on. Based on the relevant front, each individual is assigned a fitness value. Individuals in the first front are given a fitness value of 1 and individuals in the second one are associated with a fitness value of 2 and so on. In addition to the fitness value, a crowding distance (CD) parameter is also introduced in this algorithm for a uniform distribution of the individuals in each front. CD is a measure of how close an individual is to its neighbours. A better diversity in the solution will be achieved with the individuals with larger CD. Parents are then selected from the population using binary tournament selection based on the rank. However, if one individual is supposed to be chosen between two from the same front, the priority is with the one with larger CD. The off-springs will be generated after and combined with the parents to make a new population of size 2N. The new population will be sorted again, based on non-domination, and only the best N individuals are selected. These steps are repeated for a number of generations to get the final Pareto front.

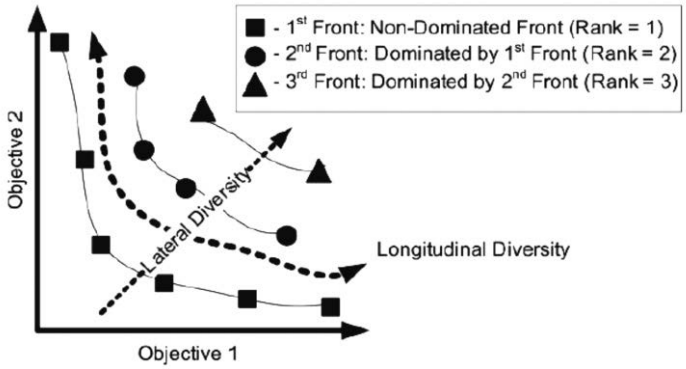

Figure 2.6. Non-Dominated Sorting Concept

The original form of Real-Coded NSGAII, uses simulated binary crossover (SBX) operator and polynomial mutation and is designed for optimisation of continues adjustable parameters. Here, Laplace Crossover and Power Mutation are going to be

used which make the optimisation faster and able to work with discrete adjustable parameters.

2.3.2 Proposed Hybrid Learning Algorithm

As outlined before, subtractive clustering can be used for initial estimation of the number of clusters as well as the centres. In order to find the efficient clusters for each dimension, m, in the input space, the only variable parameter that must be chosen appropriately is the neighbourhood radius r_a. Furthermore, to design an accurate yet compact model, a minimal number of inputs which are the most relevant ones to the model should be selected carefully. To this end, the aforementioned genetic algorithm is hired to intelligently select the required inputs as well as the initial clusters to be modified by FCM to obtain an accurate and concise TSK fuzzy model.

2.3.2.1 Genetic Encoding Scheme

All the inputs in m dimensions are considered to be involved into the fuzzy model for which the corresponding r_as are incorporated into a single chromosome, as shown in Figure.2.7. The length of the chromosome, representing the fuzzy model, would then be equal to 2m+1, where m is the number of candidate inputs.

The first part of chromosome indicates the selected inputs, where the value 1 in each gene shows that the corresponding input is used in the fuzzy model and then the corresponding r_a in the second part of chromosome is searched for. If the value of 0 is assigned to the gene m in the first part, it means that the proposed input would not be selected and hence the gene n + m in the next part is irrelevant.

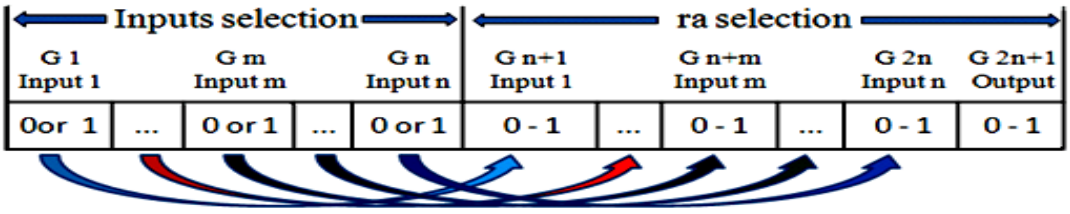

Figure.2.7. Encoding scheme for individual chromosomes

As the evolutionary operation of NSGA-II with objective functions for the number of inputs, number of rules and the modelling error proceeds, the values of genes in the chromosome are modified, and the complete structure of the FS is optimised simultaneously. The final result provides an accurate and compact fuzzy model, with a minimum number of inputs and fuzzy rules.

Based on the encoding scheme proposed above, the proposed TSK fuzzy learning algorithm is developed as follows:

Step 1: Encode all the parameters into one chromosome using the proposed encoding scheme.

Step 2: Generate the initial population of the chromosomes.

Step 3: Find the initial clusters from the collected data using subtractive clustering method and based on the selected inputs and their corresponding neighbourhood radius values of each chromosome.

Step 4: Update the clusters using FCM using the number and centre of clusters achieved in step 3 for each chromosome.

Step 5: Derive a TSK fuzzy model out of each chromosome, using the proposed obtained clusters and least squares estimator.

Step 6: Based on the resulting rules, fuzzy input structure and the MF parameters, for every chromosome, evaluate three objective functions, namely, *the number of inputs*, *the number of rules* and *the modelling RMSE*. In fact, considering the first two factors as objective functions leads us to have a concise model while the last objective function is the representative of accuracy and can be measured from the following equation, where L is the length of data points, $\hat{Y}$ is the predicted output and Y is the target output:

$$J_{RMSE} = \sqrt{\frac{1}{L}\sum_{i=1}^{n}\left(Y_i - \hat{Y}_i\right)^2} \tag{2-13}$$

Step 7: Rank all the chromosomes based on the objective function values.

Step 8: Choose parents using tournament selection method, to be used in the next step for crossover and mutation.

Step 9: Perform crossover and mutation operators to the parents to generate new set of individuals called off-springs.

Step 10: Evaluate the objective function of the new individuals and rank them. Steps 3-8 will be repeated for a fixed number of generations. The final answer is the chromosome whose objective function is smaller in the last generation.

2.4 INVERSE MODEL OF MR DAMPER (NUMERICAL STUDY)

In this section, the proposed evolving TSK fuzzy modelling approach is applied to develop an inverse model of MR damper. As mentioned earlier, this is a challenging problem due to the inherent hysteretic and highly nonlinear dynamics of the MR damper.

2.4.1 Data Collection

In order to obtain a high quality trained fuzzy model, high quality training and testing data must be collected first. To make the identified model fully represent the underlying system, the training samples should cover all possible combinations and ranges of input variation in which the MR damper will operate. This is to ensure that the TSK model trained by these samples can accurately represent the behaviour of the MR damper.

As mentioned before, the phenomenological model for a prototype MR damper developed by Spencer et al. (Spencer et al. 1997) can well capture the behaviour of the MR damper. Therefore, and in order to collect an accurate set of data, the phenomenological model is considered here in this study to collect training data.

According to the model shown in Figure 2.4, force, f, of the damper is obtained if the patterns of displacement x and voltage v are prescribed. Therefore to derive an applicable model of the MR damper, the acceleration data as well as displacement and

the voltage data will be collected from the aforementioned mathematical model, in this study.

A set of typical parameters of the 1000kN MR damper is presented in Table 2-1. Note that the maximum operational voltage of this MR damper is 10 V, which is defined as the saturation voltage of the damper and is obtained experimentally. Moreover, the situation of 0 V will also be common during operation of the MR damper. Therefore, range of the voltage signal is set as 0–10 V, in this study. Likewise, the displacement range of the MR damper is ± 20 cm while its frequency ranges from approximately 0–5 Hz.

Generated signals for training the fuzzy model are shown in Figure 2.8. A time step of 0.005 second is used to produce a total of 10,000 data sets through a 50s simulation.

2.4.2 Numerical Results

In this section, a TSK inverse model of MR damper has been obtained using the described method.

For the current study, it is assumed that the input vector for the TSK fuzzy model consists of 11 input variables. The candidates to the model include the past and current displacement $x(T-2)$, $x(T-1)$, $x(T)$, velocities, $v(T-2)$, $v(T-1)$, $v(T)$, accelerations $a(T-2)$, $a(T-1)$, $a(T)$, as well as forces $F(T-1)$, and $F(T)$ where T denotes the time step. The output is the predicted voltage v(t). The GA parameters used in the optimisation are given in Table 2-2.

Table 2-1. Typical Parameters of a 1000kN MR Damper

Parameter	Values	Parameter	Values
$\mathbf{c_{0_a}(kNs/m)}$	110.0	$\boldsymbol{\alpha_a}\mathbf{(kN/m)}$	46.2
$\mathbf{c_{0_b}(kNs/mV)}$	114.3	$\boldsymbol{\alpha_b}\mathbf{(kN/mV)}$	41.2
$\mathbf{k_0\ (kN/m)}$	0.002	$\boldsymbol{\gamma}\mathbf{(m^{-2})}$	164.0
$\mathbf{c_{1_a}(kNs/m)}$	8359.2	$\boldsymbol{\beta}\mathbf{(m^{-2})}$	164.0
$\mathbf{c_{1_b}(kNs/m)}$	7481.9	$\mathbf{A}$	1107.2
$\mathbf{k_1\ (kN/m)}$	0.0097	$\mathbf{n}$	2
$\mathbf{x_0\ (m)}$	0.18	$\boldsymbol{\eta}\mathbf{(s^{-1})}$	100

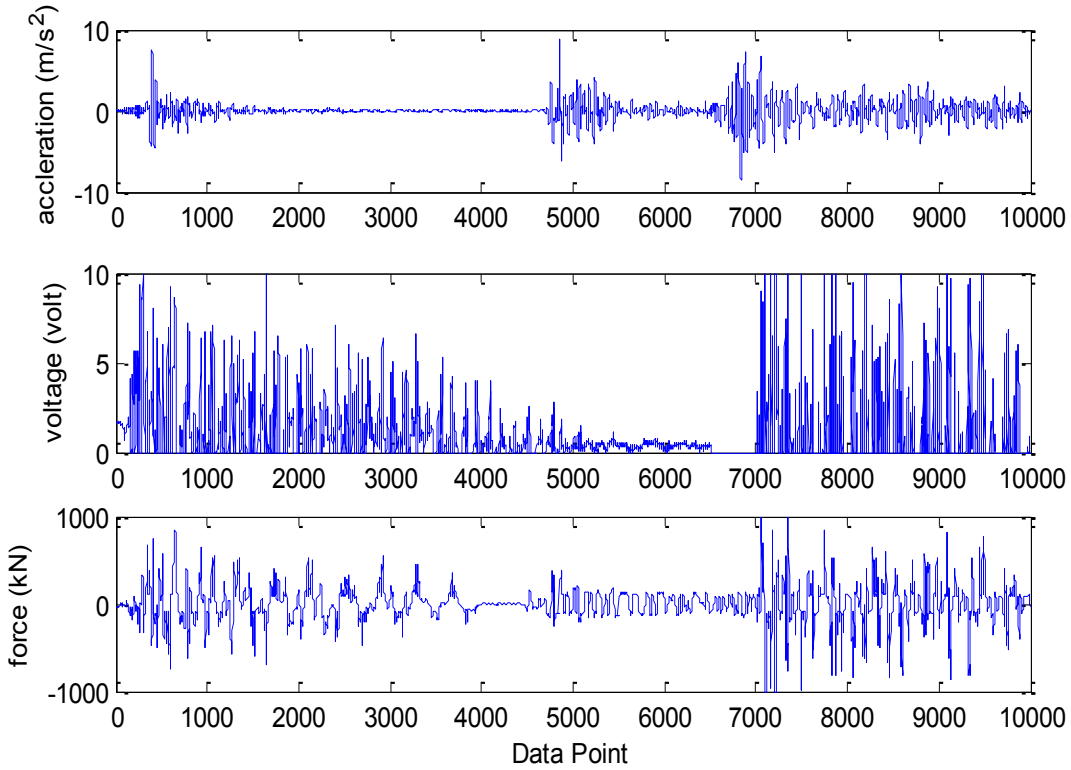

Figure 2.8. Collected Data (Inverse model, Numerical study)

Table 2-2. GA parameters used in inverse MR damper Modelling optimisation (Numerical)

Population NO	40	Crossover probability	0.8
Generation NO	60	mutation probability	0.1

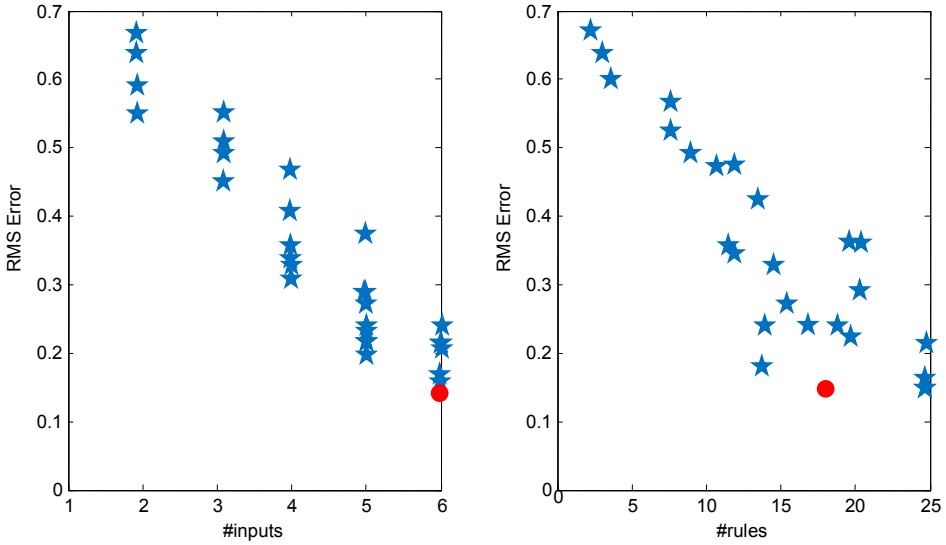

Figure 2.9. Pareto Front for Inverse Model of MR Damper (numerical study)

Figure ***2.9*** shows the final obtained Pareto front. As can be seen, there is a trade-off between model complexity and accuracy. It must be mentioned that, if the complexity is not very important for the designer, the point with the minimum RMS error can be selected as the final solution or the optimisation can be run with the only objective bring error minimisation. Here however, the red point is chosen as the compromised solution to consider both accuracy and compactness of the model. This solution results in a simple fuzzy model with only six inputs, eighteen rules and an acceptable RMS error of 0.154. The selected inputs are $x(T-1)$, $x(T)$, $v(T)$, $a(T-2)$, $a(T)$ and $F(T)$. The predicted voltage of the designed model, shown in Figure 2.11, should be sent to the forward model to generate the applied force (Figure 2.10). Figure 2.12, is the comparison between the target force and the generated one where the excellent tracking of the original signal using the new approach is depicted. The RMS error between the target and the predicted force is about 37.87 kN which compared to the maximum capacity of the proposed MR damper (1,000 kN) is acceptable (less than 4%).

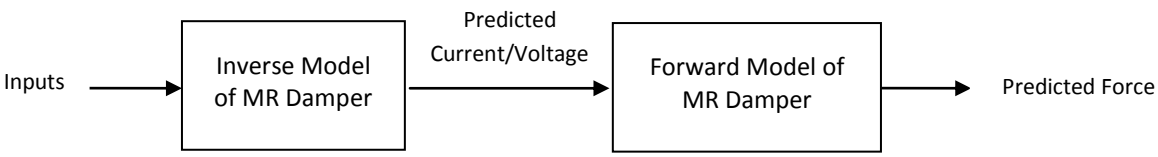

Figure 2.10. Block diagram for the inverse model validation strategy of MR damper

2.4.3 Model validation

To validate the effectiveness, ability and accuracy of the developed TSK fuzzy model in identifying the inverse dynamic behaviour of an MR damper, a set of validation data is generated from the Phenomenological model of a 1000kN MR damper. The time duration for the collected validation data is 10s and the time increment is 0.001 which amounts to a total of 10000 data points. Figure 2.13 shows the histories of validation data for acceleration, voltage and force.

Using the proper validation data set, including acceleration and voltage, the predicted forces are as shown in Figure 2.14, which almost follow the target force generated by

the phenomenological model. The maximum error is 75N which is 4% of the maximum target force.

It should be mentioned that the dynamics of MR damper is such that when the velocity is close to zero, the generated force will be near zero regardless of the voltage. In other words, when the generated force is close to zero, the voltage can be assigned any values and that is why the predicted voltage at some points are very different to the target, although the generated force derived from the predicted voltage, is very close to the target one.

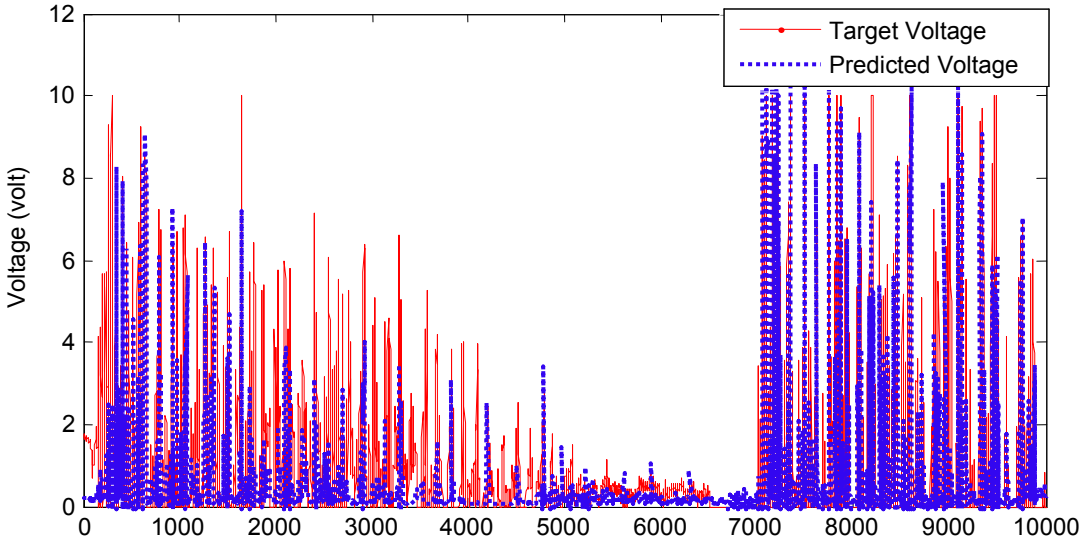

Figure 2.11. The comparison between the target and generated voltage (Numerical training data)

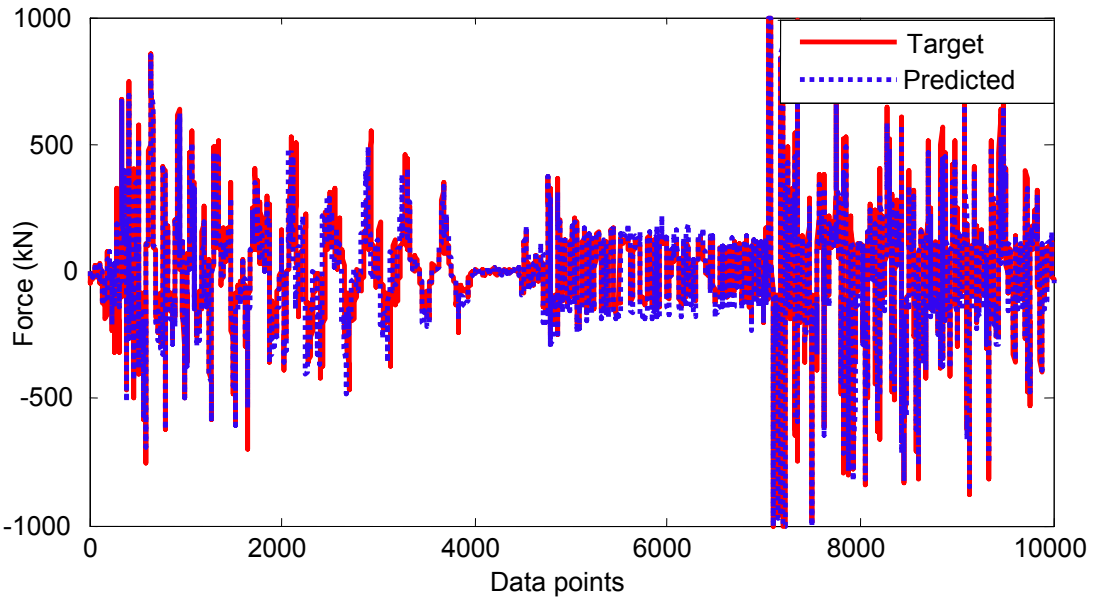

Figure 2.12. The comparison between the target and generated force (Numerical training data)

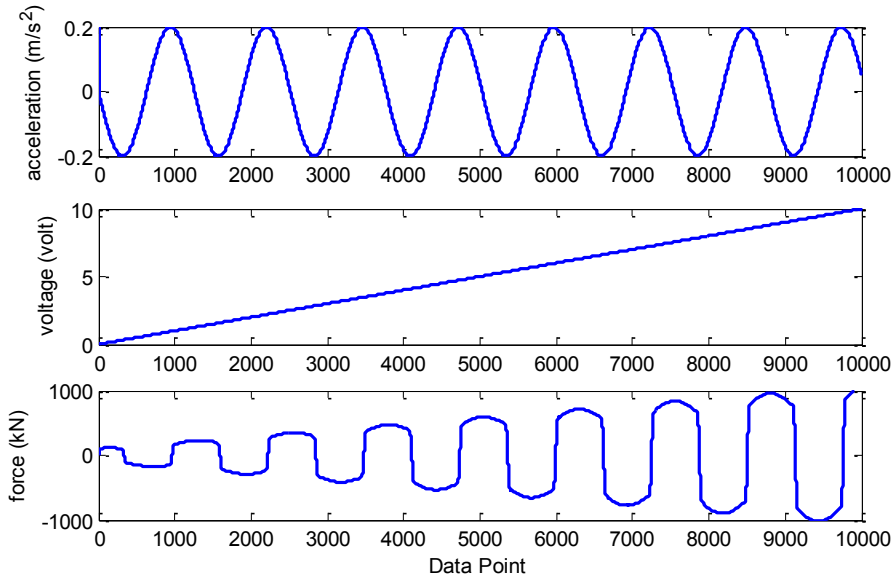

Figure 2.13. Numerical Validation data

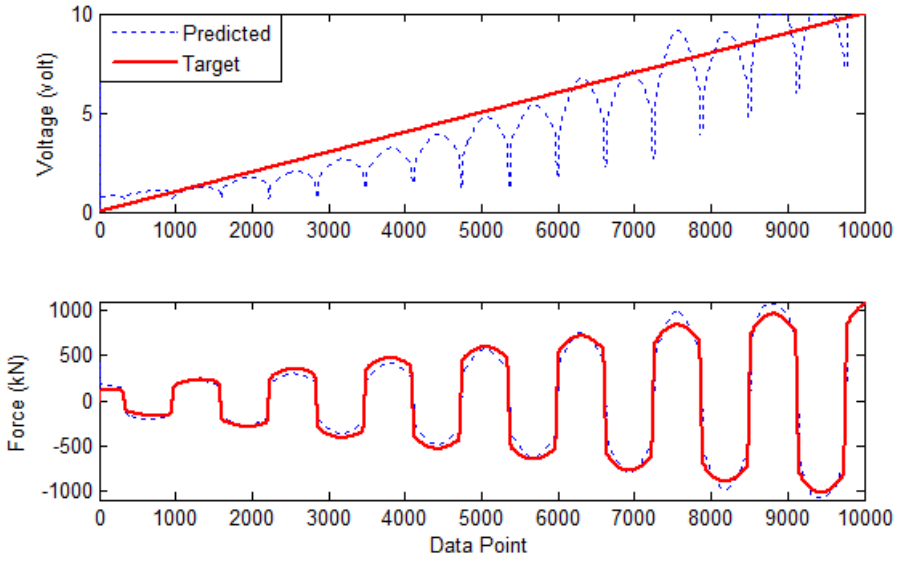

Figure 2.14. Comparison between the predicted and target voltages and forces (Numerical validation data)

2.5 MR Damper Modelling (Experimental Study)

An experimental test program has been conducted to obtain the data necessary for modelling the MR damper through parametric identification. These data have been used to model both forward and inverse behaviour of the MR damper using the proposed method explained here.

The experimental test was set up on a Schenck material testing machine, as shown in Figure 2.15. Connecting plates were designed and fabricated to install the MR damper between the actuator and load cell, as shown in Figure 2.16. The actuator of the Schenck material testing machine was employed to drive the damper. The machine also measured the displacement of damper rod. A ±5kN load cell was inserted between the damper and the machine to measure the reaction force of the damper.

Figure 2.15. MR damper test on Schenck material testing machine

The type of MR damper used in this experimental test was RD-1005-3 damper, manufactured by the Lord Corporation, as shown in Figure 2.16. The main cylinder of the damper is 112.3 mm in length and 41.4 mm in diameter. The damper has an

extended length of 208 mm and a compressed length of 155 mm, so it has a ±25 mm stroke. The main cylinder houses the piston, where the magnetic circuit is located, accumulator and MR fluid. The MR fluid can be activated by a current applied to the magnetic circuit. The current for the electromagnet is supplied by a constant current power supply which generates a 0-2 A current. For more details, please refer to (Djajakesukma 2003).

Figure 2.16. MR damper installation

By using this experimental set up, the responses of MR damper were measured under sinusoidal and quasi-static excitations, as shown in Figure 2.17. The magnetic field

strength was varied as measured by current which was applied in the range of 0-2 A. The sinusoidal input disturbances have frequencies of 1 and 2 Hz and varying displacement amplitudes. While the quasi static has a frequency of 0.25 Hz and displacement amplitude of ±25 mm. Table 2-3 shows the number of operating conditions for discrete values of applied current and excitation.

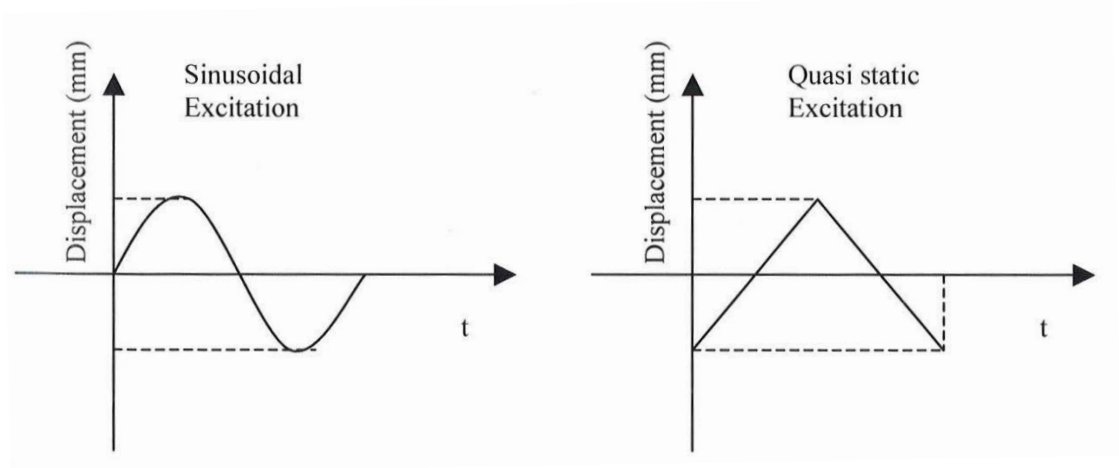

Figure 2.17. Input excitation for MR damper testing: sinusoidal and quasi static excitations

Table 2-3.MR damper testing conducted for 42 operating conditions

Applied Current (A)	Sinusoidal Excitation						Quasi Static
	Frequency : 1 Hz			2 Hz			0.25Hz
	Displacement (mm)						
	8	12	15	4	6	8	25
0.00	Case 1	Case 2	Case 3	Case 4	Case 5	Case 6	Case 7
0.25	Case 8	Case 9	Case 10	Case 11	Case 12	Case 13	Case 14
0.50	Case 15	Case 16	Case 17	Case 18	Case 19	Case 20	Case 21
0.75	Case 22	Case 23	Case 24	Case 25	Case 26	Case 27	Case 28
1.00	Case 29	Case 30	Case 31	Case 32	Case 33	Case 34	Case 35
2.00	Case 36	Case 37	Case 38	Case 39	Case 40	Case 41	Case 42

MR damper testing was conducted for the 42 experiments. Piston rod was always located at zero position at the beginning of the test. During each test, 20 cycles of force vs displacement were generally measured, while velocity was calculated from the measured displacement. It is observed that the measured force is not centered at zero, due to presence of accumulator in the damper. The accumulator helps to avoid cavitation in the fluid during normal operations and accounts for the volume of fluid

displaced by the piston rod as well as thermal expansion of the fluid. From the graphs of force vs. time, it is seen that the increase of applied current will increase the damper force.

2.5.1 Experimental Data collection for Training and Validation

In order to collect the most comprehensive data sets for the purpose of modelling, 400-500 data points from each case (except quasi static cases) have been put together to form a total set of 17,000 data points. These data points from each set have been picked carefully in a way their corresponding starting and ending velocity are close to zero. After each set, 10 zero data points have been added to avoid the effect of previous data sets on output prediction of next set as the model may use the data in the previous time steps. Figure 2.18 shows the training data collected and selected from experimental tests. The data of quasi static tests are left for verification of designed models.

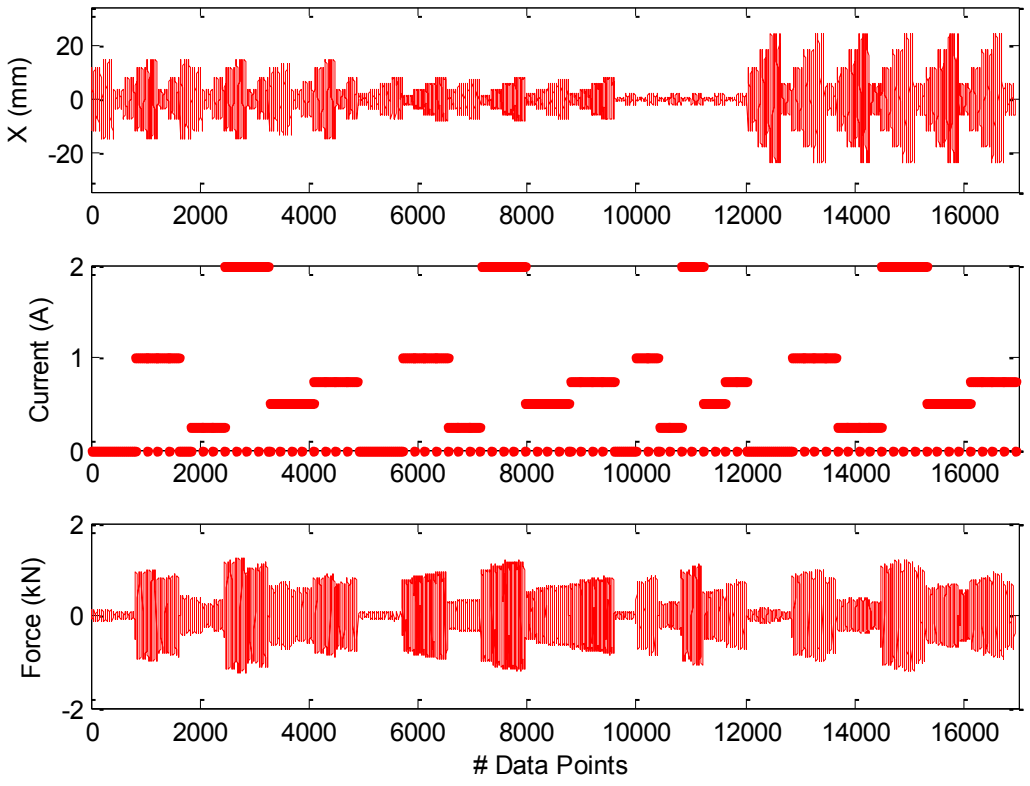

Figure 2.18. Training data (Inverse model, experimental study)

Like the numerical study, an accurate forward model is needed to evaluate the performance of the developed inverse model of MR damper. The forward model uses the output of inverse model, i.e. predicted current, to generate and estimate the force (Figure 2.10). By comparing this force with the target force, the accuracy and performance of developed inverse model can be checked. Therefore, in the next section a forward model of MR damper will be built using the training data.

2.5.2 Forward model of MR damper (experimental study)

To find the best inputs to be considered for the purpose of MR damper forward modelling, 11 candidates have been chosen for the mapping which are $F(T-1)$, $x(T-2)$, $x(T-1)$, $x(T)$, $v(T-2)$, $v(T-1)$, $v(T)$, $a(T-2)$, $a(T-1)$, $a(T)$, $I(T)$ where F, x, v, a and I, represent force, displacement, velocity, acceleration and current, respectively. T is also showing the current time step. The output of the model, which is going to be estimated, is set to be force; $F(T)$.

Using the approach explained earlier in this chapter and also the GA parameters as shown in Table 2-4, the best Pareto front have been obtained based on minimisation of three objective functions: number of inputs, number of fuzzy rules and the RMSE of the model. The best Pareto front is shown in Figure 2.19.

Table 2-4.GA parameters used in forward MR damper Modelling optimisation

Population NO	30	Crossover probability	0.8
Generation NO	50	mutation probability	0.1

To make a trade off between all three objective functions and considering the fact that minimising the error is of priority, the point which is marked by a red star in Figure 2.19 is selected to build a forward model of MR damper. This designing point makes a concise model with 5 inputs, 10 fuzzy rules and RMSE of 0.86. The inputs to the model are $F(T-1)$, $x(T)$, $v(T-2)$, $v(T)$ and $I(T)$. The comparison between the predicted and target forces are shown in Figure 2.20 where a perfect match between these two is clear.

To validate the model, the experimental data sets from case 14 (displacement: 0.25mm, current: 0.25 A, Frequency: 0.25 Hz) is chosen (Figure 2.21). Using the developed

model, a comparison between the predicted damping force of MR fluid damper and target force is shown in Figure 2.22. As can be seen, the predicted force using the designed TSK forward model track the target force quite closely and the nonlinearity behaviour of MR damper is also captured. This proves the efficiency of the proposed forward model in terms of both accuracy and compactness.

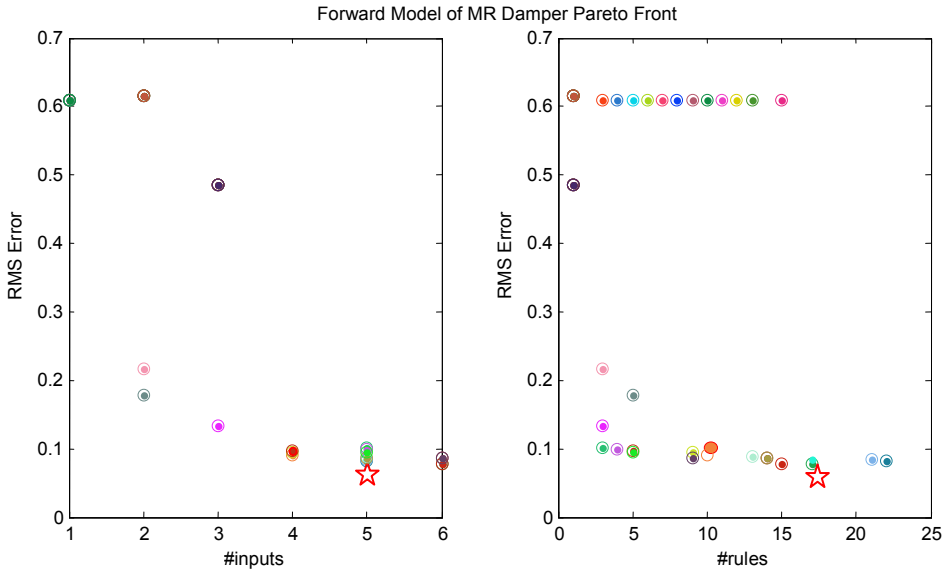

Figure 2.19. Pareto Front for Forward Model of MR damper (experimental study)

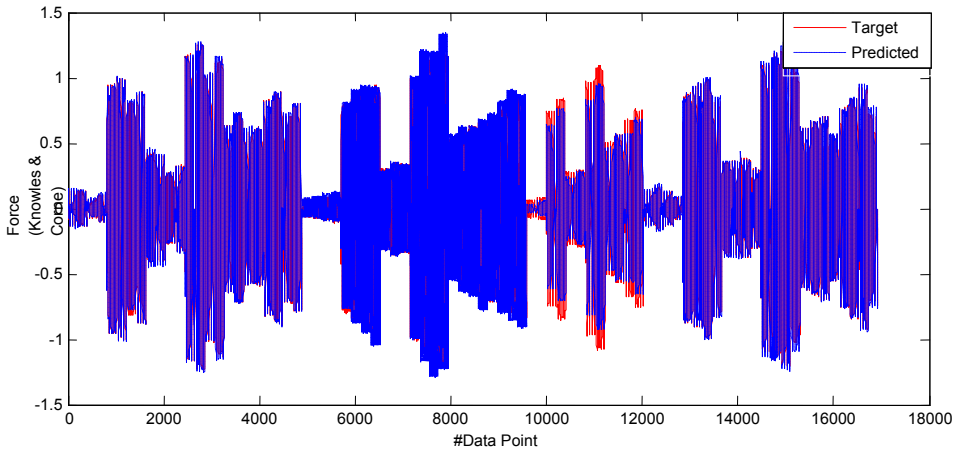

Figure 2.20. Comparison between original and predicted force of MR damper forward model (experimental study, training data)

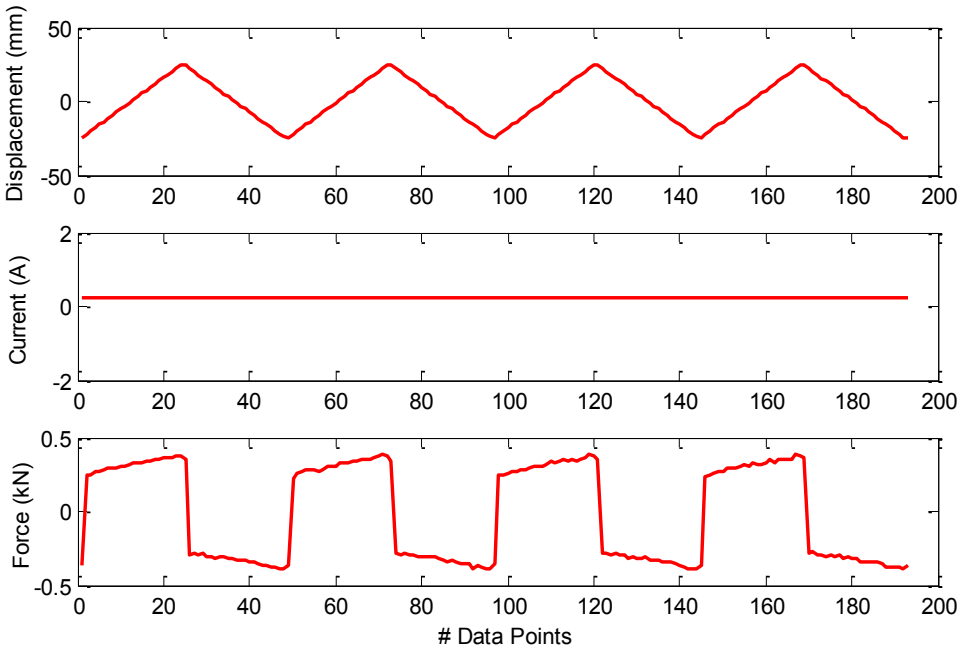

Figure 2.21. Validation data set (forward Model, experimental data)

2.5.3 Inverse model of MR damper (experimental study)

A similar identification scheme is used for the inverse dynamic model of the MR damper. Like the previous sections, the candidate inputs to be used in the proposed approach should be chosen first. As mentioned earlier, finding a model that can capture the inverse behaviour of MR damper and predict the required current of damper is mathematically hard and complicated. Therefore, more inputs, i.e. 15, have been considered in this case which are $F(T-2)$, $F(T-1)$, $F(T)$, $x(T-3)$, $x(T-2)$, $x(T-1)$, $x(T)$, $v(T-3)$, $v(T-2)$, $v(T-1)$, $v(T)$,$a(T-3)$, $a(T-2)$, $a(T-1)$, $a(T)$. The output is the applied current, $I\ (T)$, that will generate the desired force. A larger number of populations and generations are also used here due to high complexity of the optimisation problem. The GA parameters used in the proposed optimisation algorithm are shown in Table 2-5.

Table 2-5. GA parameters used in inverse MR damper modelling optimisation

Population NO	60	Crossover probability	0.8
Generation NO	50	mutation probability	0.1

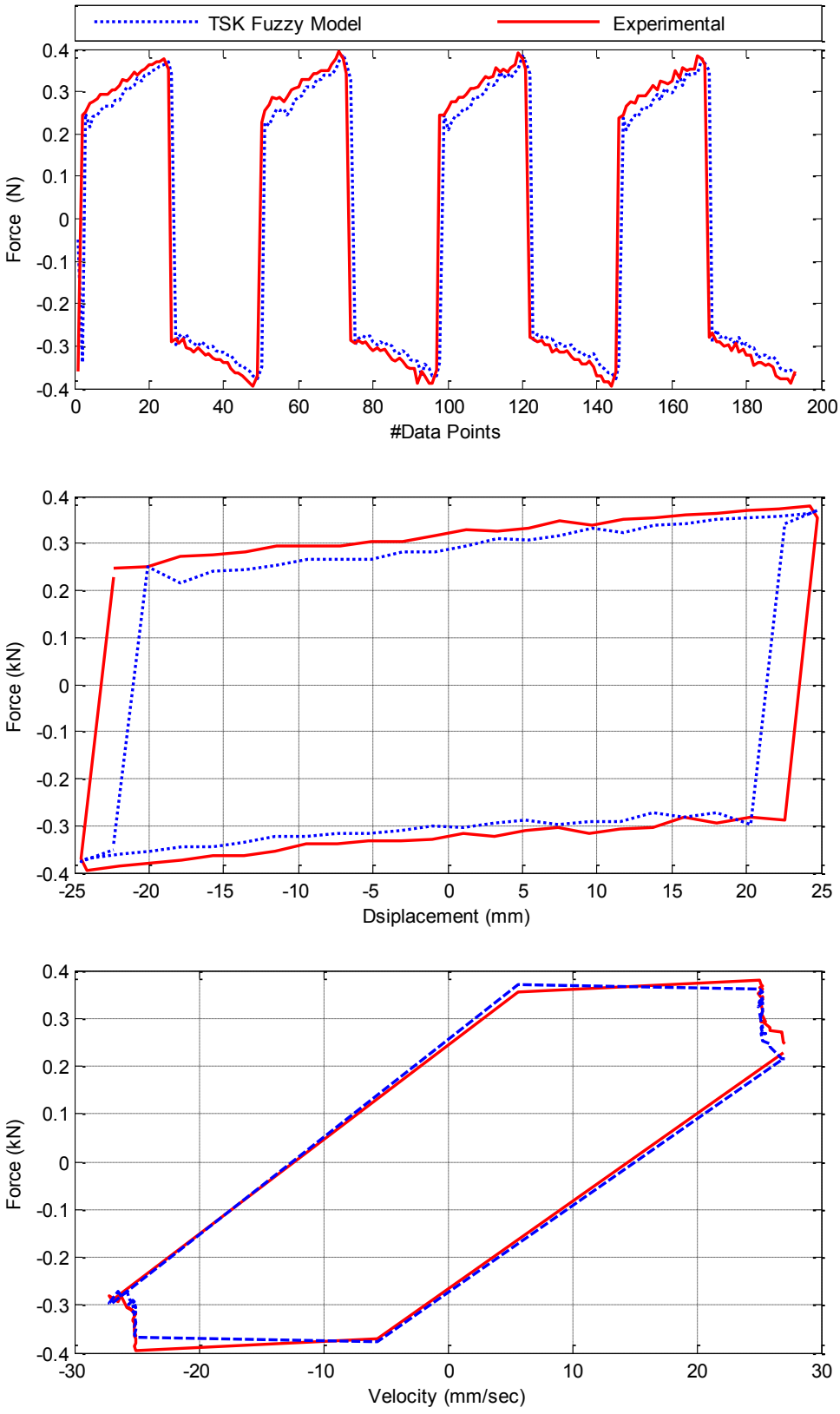

Figure 2.22. Comparison between predicted and target force (Forward model, experimental data)

Using the training data shown in Figure 2.18, the best Pareto front obtained at the end of optimisation is plotted in Figure 2.23 which helps the designer to achieve the best model based on his desire. Here the point marked by a red star is picked for building a compact and accurate inverse model.

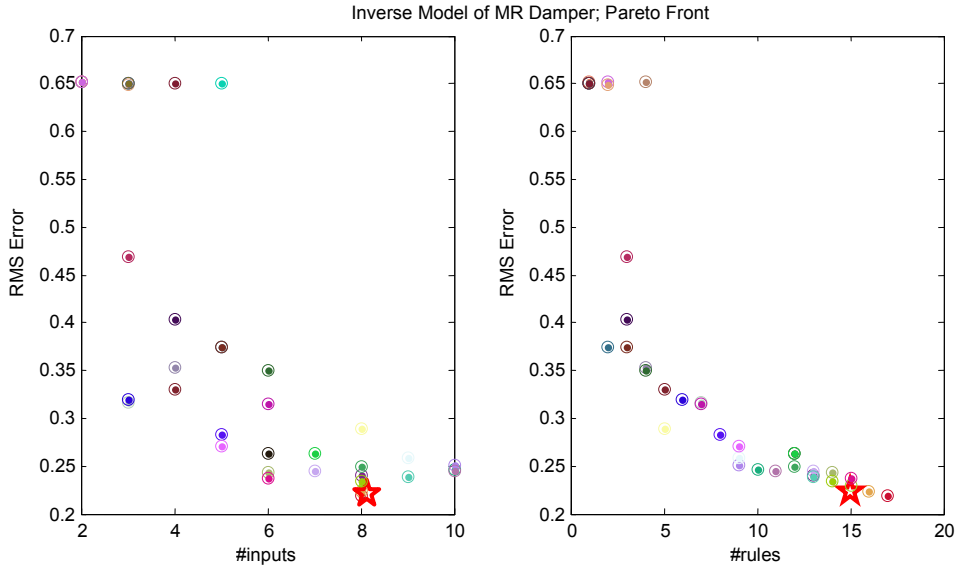

Figure 2.23. Preto Front for inverse modelling of MR damper (experimental study)

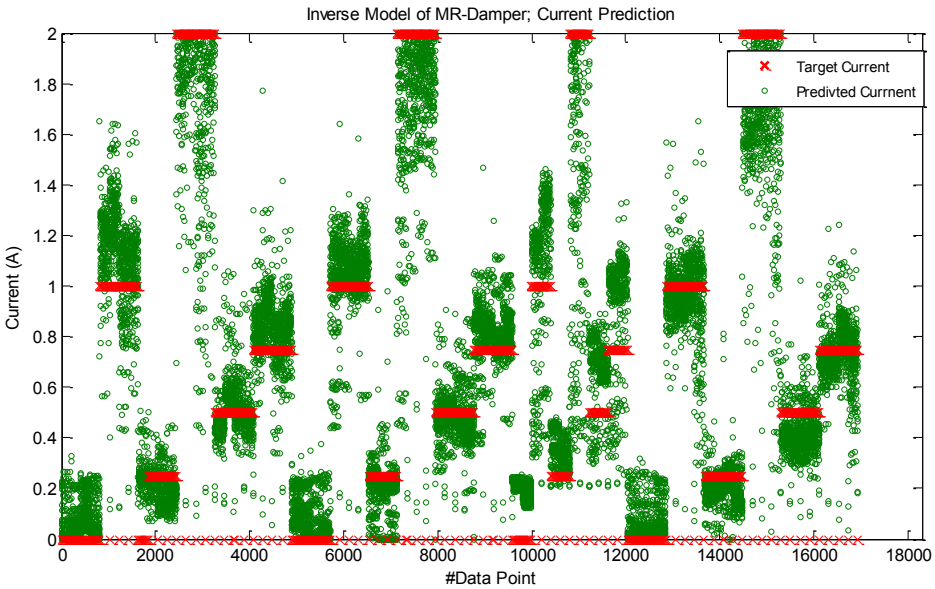

Figure 2.24. Comparison between target and predicted current of MR damper inverse model (experimental study, training data)

The obtained dynamic TSK inverse model of MR damper is using 8 inputs, 15 fuzzy rules and has the RMSE of 0.217. The selected inputs to the model are $F(T-2)$, $F(T)$, $x(T-2)$, $x(T)$, $v(T-3)$, $v(T-2)$, $v(T)$ and $a(T-1)$.

The predicted current of the inverse model is compared to the target one in Figure 2.24. As can be found from the figure, the predicted current can not fully track the target signal. However, the RMS error between these two signals is 0.217 which is acceptable with respect to the maximum range of current (2A). Moreover, if the error between these two outputs is considered separately for each step, it can be figured out that at each segment, around 80% of the predicted data points (green dots) are within ±0.25 A of the target output (red lines). This is mainly satisfactory in the high range of target force. On the other hand, when the velocity, and consequently generated force, is close to zero, the impact of current on the behaviour of MR damper is negligible. Therefore, no unique current can be estimated in these cases and thus the predicted current fluctuates a lot and gets far from the target values in high frequencies where zero-velocities occur.

To prove the above points and show the performance of the proposed inverse model, the previously designed forward model is combined with it to generate force using the predicted currents coming out of inverse model as shown in Figure 2.10. As shown in Figure 2.25, the error between target and predicted force is very small and ignorable in high range of forces. However, when the force is small and close to zero, this error is more.

The proposed model is validated using the data sets for cases 14, 28 and 42. This process has been done in two steps. In the first step, the validation test signals, x, v, a, and F were acquired directly from the test rig and fed into the trained inverse TSK fuzzy model. Secondly, the signals x, v, a, F and predicted I were fed into the designed TSK forward model and the resulting damper force was measured for comparison with the originally desired force F (T). The results of these two steps are shown in Figure 2.26 to Figure 2.28, where it is clearly seen that the trained TSK fuzzy inverse model, together with the forward model, can perfectly track the direct dynamic behaviour of the MR damper. However, the results show that when the target force is close to zero (Figure 2.28), the error between target and predicted force is more.

2.6 SUMMARY

A new TSK fuzzy modelling approach, using the evolving combination of subtractive clustering, FCM and NSGA-II is presented. Due to the simplicity of the procedure, the most suitable minimal inputs and rules are searched simultaneously, such that the resulting fuzzy model is of compact size and acceptable accuracy. The developed methodology is then applied to emulate the inverse dynamic behaviour of an MR damper. From numerical and experimental modelling, it is shown that the developed TSK fuzzy model can represent the dynamic behaviour of the MR damper accurately using a concise model. The use of proposed TSK fuzzy model to represent a MR damper will make the application of MR dampers for control engineering purposes more practical, since the linear control theory can be applied directly. This model will be used later in Chapter 4, to semi-active vibration control of a 20-storey nonlinear benchmark building.

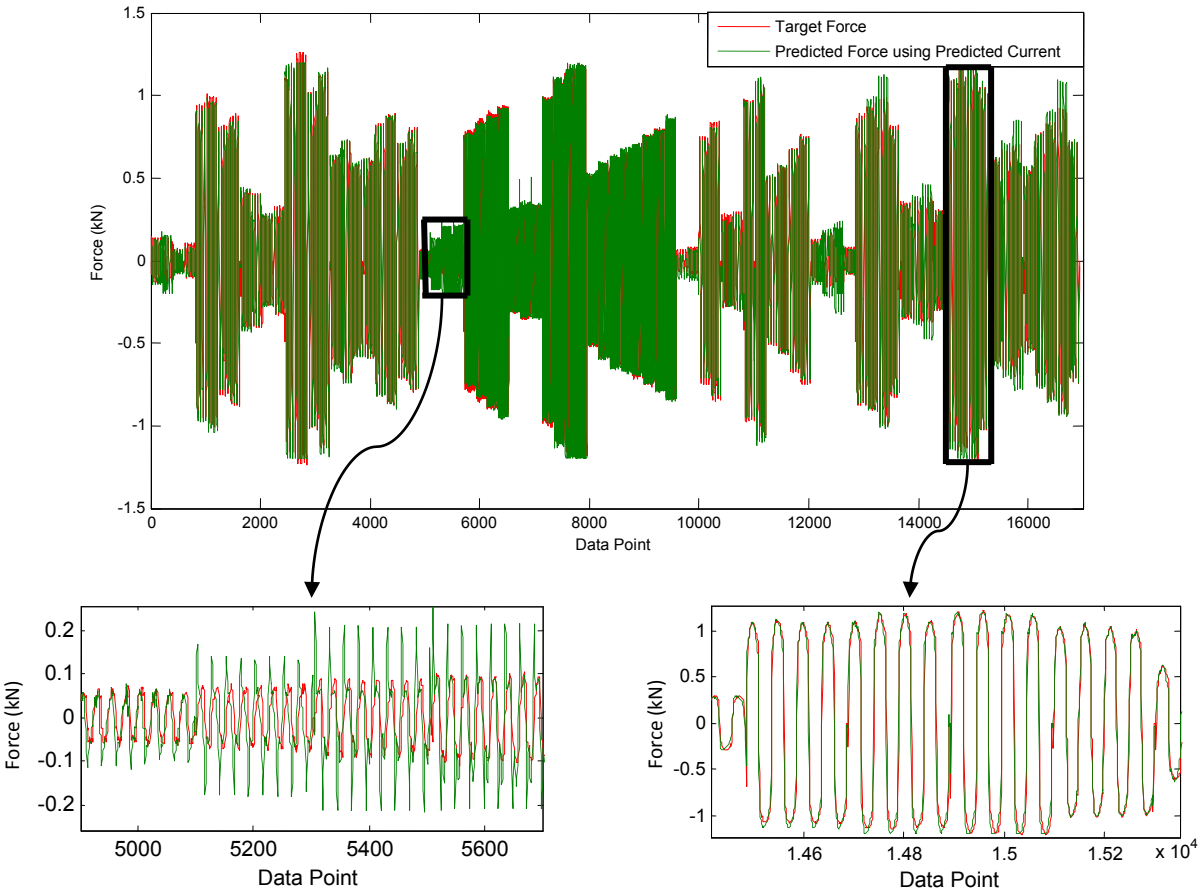

Figure 2.25. Comparison between target and generated force using MR damper inverse model (experimental study, training data)

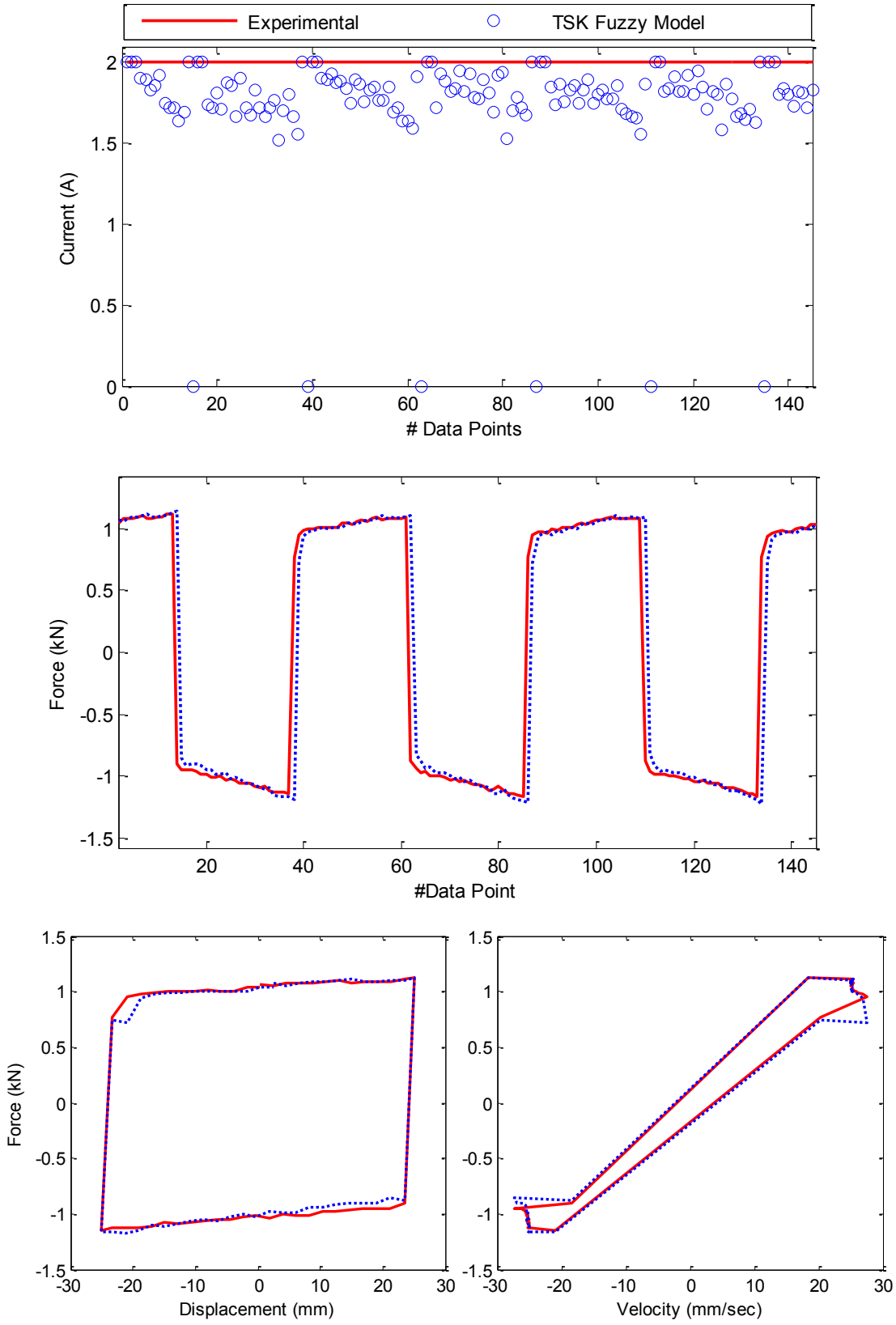

Figure 2.26. Comparison between target and generated force using inverse model of MR damper (Experimental validation data, case 42)

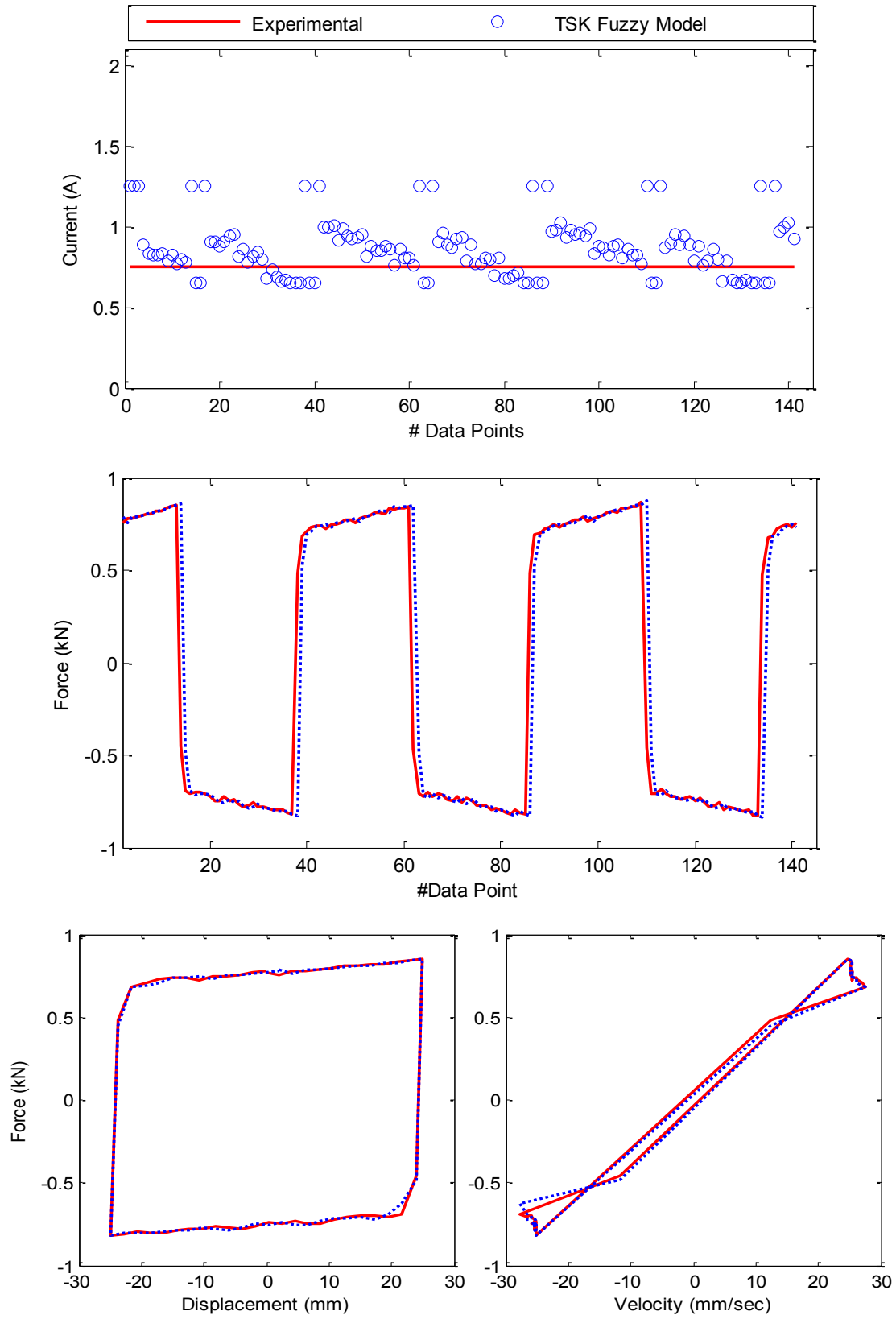

Figure 2.27. Comparison between target and generated force using inverse model of MR damper (Experimental validation data, case 28)

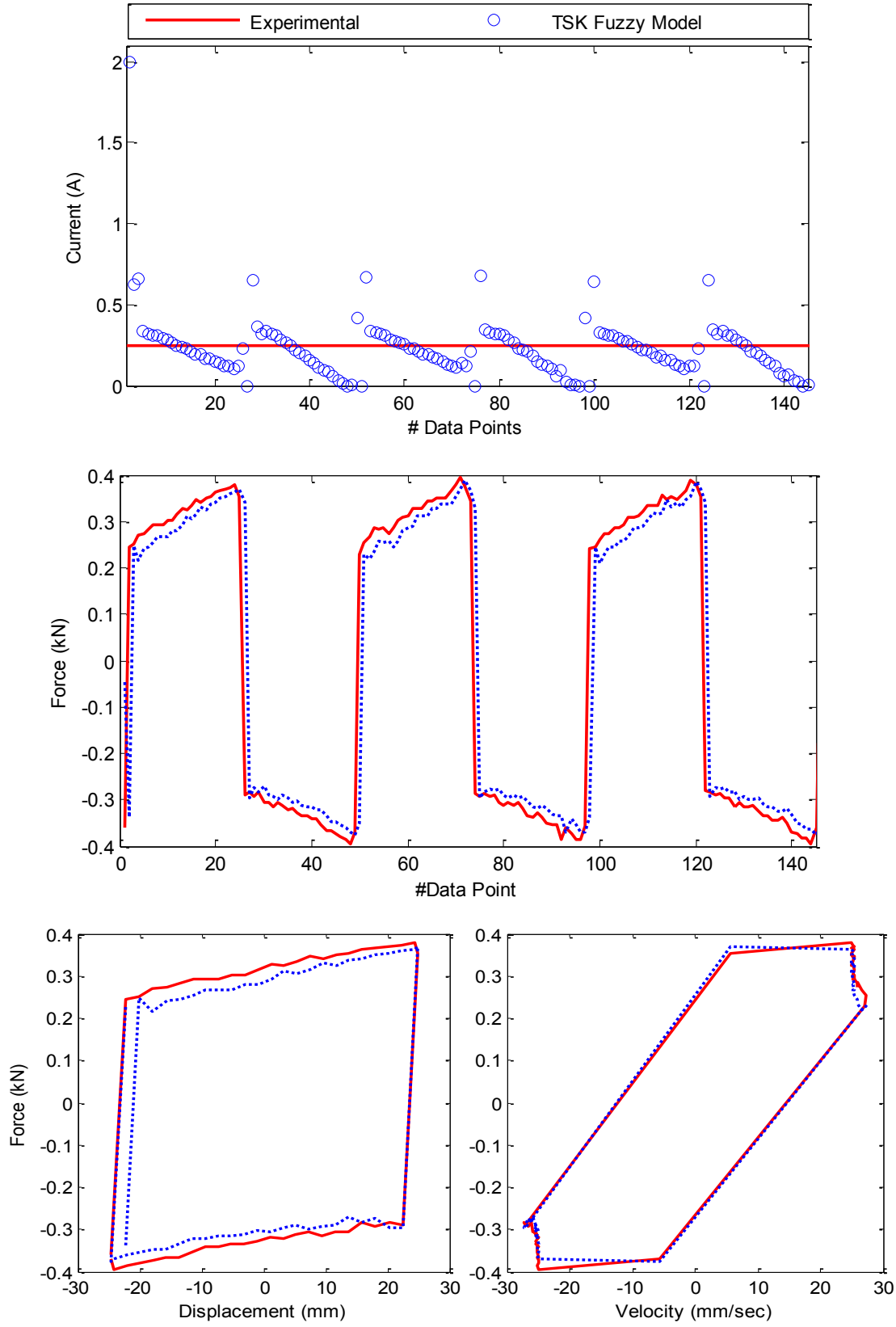

Figure 2.28. Comparison between target and generated force using inverse model of MR damper (Experimental validation data, case 14)

CHAPTER 3

MULTI-OBJECTIVE OPTIMAL PLACEMENT OF STRUCTURAL CONTROL DEVICES

3.1 CHAPTER OUTLINE

The optimal design and placement of control devices, is an important problem that affects the control of civil engineering structures. This chapter presents a multi-objective optimisation method for simultaneous finding of the optimal number and placement of actuators and MR dampers, in active and semi-active vibration control of seismically excited nonlinear structures.

This chapter is structured as follows. First a literature and background on the methods and approaches used by other researchers in order to obtain the optimum places of control devices are provided. This, specifically, includes a comprehensive study on optimal MR damper placement methods. The challenges are then discussed and the concluding remarks are made. In the next section, a modified integer coded version of non-dominated sorting genetic algorithm II (MI-NSGAII) is introduced. This method can increase the accuracy as well as the convergence speed of the original NSGAII, particularly when the adjustable parameters are integers. Then, a hybrid algorithm to find the optimum number and places of structural control devices is presented. Next, the case study, i.e. the 20-storey nonlinear benchmark structure is introduced briefly; the proposed strategy is then used to find the optimal number and places of active and

semi-active control devices in it. Results are discussed and finally conclusions are drawn in the last section.

3.2 INTRODUCTION AND BACKGROUND

Structural controls, including passive control, semi-active control, and active control, have been demonstrated effective in mitigating earthquake damage. It is well known that certain locations in a structure are better suited for placement of control devices in the sense that these locations effectively reduce structural response while using minimum control effort. It is also expected that practically the number of control devices to be used in a structure is limited. Moreover, fewer control devices, can reduce system's complexity and power consumption. It has, therefore, been of great motivation and challenge for researchers to design a strategy for optimising the number and placement of actuators and dampers in structures subjected to seismic excitation. Search algorithms have been widely used for optimal placement of control devices in the structures.

Arbel used the concepts of controllability measures for optimal placement of actuators within an oscillatory system (Arbel 1981). As an alternative, a guided random search method, the simulated annealing method, was employed to optimally place control devices in a structure (Liu, Begg & Matravers 1997). Brown et.al used LQG optimal control theory-based Pareto optimal trade-off curves for various placements of actuators and sensors within civil structures (Brown, Ankireddi & Yang 1999). Xu and Teng developed an incremental algorithm for placement of active/passive control devices within the structure (Xu & Teng 2002). Cheng et.al used a sequential iterative procedure for optimal placement of dampers and actuators in a three-storey building subjected to earthquake excitations (Cheng, Jiang & Zhang 2002). Chen and Chen proposed a step-by-step procedure for optimal placement of piezoelectric friction dampers within a 20-storey benchmark building (Chen & Chen 2004). Amini and Tavassoli developed a new method for optimising the control force and the number and location of a closed-open loop control system (Amini & Tavassoli 2005). Rao et.al proposed a novel multiple start guided neighbourhood search (MSGNS) algorithm by integrating the best features of SA and Tabu search algorithms for optimal placement of actuators within seismically excited tall buildings (Rama Mohan Rao & Sivasubramanian 2008).

Another versatile global approach used in structural control optimisation is genetic algorithm (GA). Furuya and Haftka used GA in solving optimisation problems to find locations of optimal actuators within large space structural systems (Furuya & Haftka 1995). Dhingra and Lee applied a hybrid gradient based GA to an across-four space structure for finding actuator locations and minimum weights of structures (Dhingra & Lee 1995). Li et.al, developed a multi-level GA in order to optimise the actuator locations and linear quadratic regulator (LQR) controller gains within buildings subjected to wind loads (Li et al. 2000). Abdullah et al. combined genetic algorithms and a gradient-based optimisation technique to design the optimal position of direct velocity feedback control controllers in buildings (Abdullah, Richardson & Hanif 2001). Singh and Moreschi examined optimal placement of passive energy dissipative devices in a multi-storey building for seismic protection using GA (Singh & Moreschi 2002). Liu, et.al, applied GA to a 16-storey tall building structure under different earthquake excitations for optimal actuator distribution (Liu, Yang & Li 2003). Wongprasert and Symans employed GA for identifying the optimal damper distribution to control the nonlinear seismic response of a 20-storey benchmark building (Wongprasert & Symans 2004). Li et.al, also demonstrated the effectiveness of a two-level GA by solving the optimal distribution problems of actuators within building structures subjected to an earthquake load(Li et al. 2004). Tan et.al, applied GA in order to find the optimal actuator locations and control gains for hazard mitigation of a 40-storey shear building and a nine-storey irregular structure (Tan et al. 2005). Onoda and Hanawa utilized GA to solve the actuator placement optimisation problem for statistical static distortion correction of truss structures (Onoda & Hanawa 2012).

Recently, Cha et.al, proposed a multi-objective genetic algorithm (MOGA) for optimal placements of actuators and sensors in two nonlinear benchmark building structures (Cha et al. 2012). They considered the total number of actuators and accelerometers (J_1) as well as the dynamic response of the structure (J_2) as two objective functions to be minimised. However, the use of accelerometers, in terms of cost and installation, is not an issue compared to the difficulties incorporated in both cost and installation of control devices. Therefore using as few as possible number of actuators is more desirable while using many accelerometers is not a challenging problem. Thus, considering the total number of actuators and accelerometers as an objective function may result in an irrational answer. For example, using the proposed method by Cha and

Agrawal, between two possible optimal set points whose J_1s (total number of sensors and accelerometers) are the same, i.e:

P_1: {J_1=14 (8 actuators+6 accelerometers), J_2= 0.950 and P_2: {J_1=14 (5 actuators+9 accelerometers), J_2= 0.951},

the latter will be automatically ignored as its peak drift ratio (J_2) is slightly larger than the first point. However, a designer will be more interested in the second point as it offers to use 3 fewer actuators than the first point and at the same time, the difference between the second objective functions of these two points is negligible. Therefore, it is more rational to fix the number of sensors and find the optimal number/ or location of control devices only. Moreover, in the proposed method, the only structural dynamic response which has been taken into account, as an objective function to be minimised, is the maximum drift ratio. Consequently, the final arrangement may not satisfy the other objective indices which conflict with the drift ratio such as peak level acceleration and peak base shear force.

The other aim of this chapter, besides introducing an algorithm to be used in optimal placement of control devices, is to particularly apply the proposed algorithm to building-MR damper systems and compare the optimum arrangements of MR dampers and actuators in a structure. In the majority of research presented to date, only the optimal placement of control devices in an active or passive control system is investigated and not many works have been reported to find the best location/ or number of semi-active control devices such as MR dampers, in linear and nonlinear structures. Shi et.al discussed some methods of optimal placement of MR dampers in a high-rise linear building (Shi, Xin & Ningwei 2004). Kwok et.al, presented a multi-objective binary-coded GA to optimise the location and number of MR dampers in linear structures (Kwok, Ha & Samali 2007). Li et.al, proposed a two-phase optimisation process using single objective genetic algorithm for the placement of semi-active MR dampers in a nonlinear benchmark structure (Li, Song & Ou 2010). They, in the first phase, developed a proper optimised active control using GA and then tried to distribute the MR dampers such that it mimics the optimal active control force obtained in the first phase. They considered three objective functions, i. e, peak inter-storey drift ratio (E_1), peak semi-active control force (E_2) and an evaluation index for the effect of semi-active control tracing the active control force (E_3), where the last one

should be maximised while the other two are to be minimised. The proposed multi-objective optimisation is then converted to a single objective optimisation problem by defining a new objective function as: $E = \alpha E_1 + \beta E_2 + (1 - E_3)$. However, adjusting the coefficients α and β needs some trial and error. Moreover, by using this method, only one solution can be found at the end of the optimisation. The optimisation is also done using only one type of earthquake. Amini et.al, adopted an improved ant colony algorithm to find the optimal locations of MR dampers in a small linear structure using one objective function only (Amini & Ghaderi 2012). In order to make the problem simple, they also assumed that only one MR damper can be installed between two consecutive storeys which creates some limitations for the designer although, computationally it reduces the search space.

Third generation benchmark control problems for seismically excited nonlinear buildings is an effort to systematically evaluate the performance of various control strategies, especially in the case of nonlinear building structures. This chapter particularly focuses on finding and comparing the optimum layouts for actuators and MR dampers within the 20-storey highly nonlinear benchmark structure subjected to a variety of seismic loadings. Since for a nonlinear case the analytical method of optimisation is difficult to apply, and also because of the integer constraints on the adjustable parameters, i.e. locations of control devices, a modified integer coded multi-objective GA has been developed and considered as the optimisation method in this study. This method uses the best features of a recently developed integer coded algorithm named MI-LXPM into the framework of a well-known Pareto front based GA named NSGAII and is referred to as MI-NSGAII. Using the proposed approach, a Pareto front will be generated using three considered objective indices, i.e. peak inter-storey drift ratio, peak acceleration and peak base shear force. This Pareto front gives freedom to the designer to choose the best design based on his desire. Moreover, by choosing a pre-defined level of performance on dynamic responses of a structure, the designer can decide on decreasing or increasing the number of control devices. In other words, both control cost and dynamic performance is considered in this optimisation problem to be minimised. For an active control system, an LQG algorithm is proposed and 1000 kN hydraulic actuators together with accelerometers are considered to be installed in the building. For the semi-active case on the other hand, an LQG-COC

algorithm is to be designed and 1000 kN MR dampers and accelerometers are to be placed within the structure.

3.3 MODIFIED INTEGER-CODED NSGAII

Genetic algorithms are general purpose population based stochastic search techniques which mimic the principles of natural selection and genetics laid down by Charles Darwin. This approach was first used to solve optimisation problems by De-Jong (Jong 1975). A detailed implementation of GA can be found in (Goldberg 1989).

The way the variables are coded in GA is critical for its efficiency. Real coded genetic algorithms (RCGAs), which use real numbers for encoding, have faster convergence towards optimal than binary and grey coded Gas (Deb 2001). Also, RCGAs overcome the difficulty of ‘‘Hamming Cliff” as in binary coded GAs.

In the case when the adjustable parameters are integer, many applications of GAs are available in the literature, some of them use binary coded GA (Cheung, Langevin & Delmaire 1997; Luo, Guignard & Chen 2001), while some others use real coded representation (Maiti, Bhunia & Maiti 2006; Ponsich et al. 2007; Yokota, Gen & Li 1996). Recently, a robust GA, namely, MMI-LXPM, for solving integer and mixed integer nonlinear programming problems, is introduced by Deep et.al (Deep et al. 2009). The proposed algorithm, however, uses a single objective function. In this study, the main features of MI-LXPM, including Laplace Crossover, Power Mutation together with a truncation procedure for handling the integer parameters have been adopted into one of the most common multi objective GAs, Non-Dominated Sorting Genetic Algorithm type II (NSGAII), to find a non-dominated sorting Pareto front for control device assignment.

As discussed earlier in Chapter 2, NSGAII provides an efficient procedure for introducing elitism into a multi-objective optimisation algorithm while guaranteeing a diversity-preserving mechanism, ensuring a good convergence towards the Pareto optimal front without losing solution diversity. The original form of Real-Coded NSGAII uses simulated binary crossover (SBX) operator and polynomial mutation and is designed for optimisation of continuous adjustable parameters. Here, Laplace

Crossover and Power Mutation are going to be used which make the optimisation faster and able to work with discrete adjustable parameters.

3.3.1 Laplace Crossover

Crossover has always been considered to be the fundamental search operator in genetic algorithms. Deep and Thakur introduce a new parent centric real coded crossover operator, based on Laplace Distribution, known as Laplace Crossover (LX) to improve the performances of Real Coded Genetic Algorithms for function optimisation (Deep & Thakur 2007a). A new version of Laplace crossover operator, has also been introduced by Deep et.al, to take care of integer adjustable parameters in the optimisation problems (Deep et al. 2009).

Using the proposed operator, two offsprings $y^1 = (y_1^1, y_2^1, \dots, y_n^1)$ and $y^2 = (y_1^2, y_2^2, \dots, y_n^2)$ are generated from two parents, $\bar{x}^1 = (\bar{x}_1^1, \bar{x}_2^1, \dots, \bar{x}_n^1)$ and $\bar{x}^2 = (\bar{x}_1^2, \bar{x}_2^2, \dots, \bar{x}_n^2)$ in the following way. First, uniform random numbers $u_i, r_i \in [0, 1]$ are generated. Then a random number β_i, which satisfies the Laplace distribution, is generated as:

$$\beta_i = \begin{cases} a - b\,log(u_i), & r_i \le {}^1/_2; \\ a + b\,log(u_i), & r_i > {}^1/_2 \end{cases}, \tag{3-1}$$

where a is location parameter and $b > 0$ is scaling factor. If the adjustable parameters are integer, then $b = b_{int}$, otherwise, it can take real values. With smaller values of b, offsprings are expected to be nearer to parents and for larger values of b, offsprings will be generated far from parents. After computing β_i, the two offsprings produced from parents are as follows:

$$\begin{aligned} y_i^1 &= \bar{x}_i^1 + \beta_i \left| \bar{x}_i^1 - \bar{x}_i^2 \right|, \\ y_i^2 &= \bar{x}_i^2 + \beta_i \left| \bar{x}_i^1 - \bar{x}_i^2 \right|. \end{aligned} \tag{3-2}$$

3.3.2 Power Mutation

Power mutation is based on power distribution and defined, in original form, in (Deep & Thakur 2007b). However, in order to deal with mixed integer optimisation problems, it is modified in (Deep et al. 2009). The working of the modified power mutation is as

follow: First, a random number, s, which follows the power distribution, $s = (s_1)^p$, where s_1 is a uniform random number between 0 and 1, is created. p is called the index of mutation. It governs the strength of perturbation of power mutation. $p = p_{real}$ or $p = p_{int}$ depending on integer or real restriction on the adjustable parameters. In other words, for real adjustable parameters, $p = p_{real}$ and for integer adjustable parameters, the value of p is integer. After determining s, a muted solution is created in the vicinity of a parent $\bar{x}$ as follows:

$$y = \begin{cases} \bar{x} - s\,(\bar{x} - x^l), & \mathrm{t} < r; \\ \bar{x} + s\,(x^u - \bar{x}), & \mathrm{t} \geq r\,. \end{cases} \tag{3-3}$$

where $\mathrm{t} = \frac{\bar{\mathrm{x}} - \mathrm{x}^{\mathrm{l}}}{\mathrm{x}^{\mathrm{u}} - \bar{\mathrm{x}}}$, x^{l} and x^{u} are the lower and upper bounds of adjustable parameters and r is a uniformly distributed random number between 0 and 1.

3.3.3 Truncation procedure for integer adjustable parameters

To ensure that after mutation and crossover operations the offsprings, $\mathrm{y_i}$, generated from integer parents remain integer, the following truncation procedure is used in this study:

If y_i is integer then new chromosome $\bar{x}_i = y_i$, otherwise,

$\bar{x}_i$ is equal to either $[y_i] - 1, [y_i]$ or $[y_i] + 1$ each with probability 0.33, ($[y_i]$ is the rounded value of y_i).

This provides more randomness in the solution and clearly helps not to generate the same integer values.

3.4 THE PROPOSED MI-NSGAII BASED APPROACH TO FIND THE OPTIMAL NUMBERS AND PLACES OF CONTROL DEVICES

In the proposed method, a multi-objective genetic algorithm, MI-NSGAII, is employed to find the optimum number and places of control devices. For this purpose, an initial guess of the required number of control devices is taken first. Next, the genetic algorithm is employed to find the optimal configuration of the control devices to

minimise some suitably defined objective indices. At this stage, a Pareto front will be generated by MI-NSGAII which represents a set of good non-dominated arrangement of control devices. The proposed front can help the designer to select the best point according to his desire. After choosing the proper assignment of devices based on the proposed level of performance, the minimised value of objective indices is compared to the maximum allowable limit (desirable structural performance). If the obtained values of the indices are higher (lower) than the allowable limit, the number of control devices is increased (decreased), and the optimisation procedure is repeated until the minimised level of structural performance is almost equal to the specified limit. Figure 3.1 illustrates a functional flowchart of the proposed algorithm.

The objective indices for the proposed benchmark building are divided into four categories: building responses, building damage, control devices, and control strategy requirements. In this study, three of the conflicting indices are considered as the objective functions to be minimised through the proposed genetic algorithm. These indices are, respectively, the peak inter-storey drift (J_1), maximum level acceleration of storeys (J_2) and base shear force J_3 subjected to 10 different earthquakes and defined as below:

$$J_1 = \underset{\substack{El-Centro \\ Hachinohe \\ Northridge \\ Kobe}}{\boldsymbol{Max}} \left\{ \frac{max_{i,t}(\frac{|d_i(t)|}{h_i})}{\delta^{max}} \right\}$$

$$J_2 = \underset{\substack{El-Centro \\ Hachinohe \\ Northridge \\ Kobe}}{\boldsymbol{Max}} \left\{ \frac{max_{i,t}(\ddot{x}_{ai}(t))}{\ddot{x}_{\mathrm{a}}^{\max}} \right\}$$

$$J_3 = \underset{\substack{El-Centro \\ Hachinohe \\ Northridge \\ Kobe}}{\boldsymbol{Max}} \left\{ \frac{max_t|\sum_{\mathrm{i}} m_i \ddot{x}_{ai}(t)|}{F_b^{max}} \right\}$$

where i shows the storey number; $d_i(t)$is the inter-storey drift of the above ground level over the time history of each earthquake; h_{i} is the height of corresponding stories; δ^{max} is the maximum inter-storey drift ratio of the uncontrolled structure calculated by

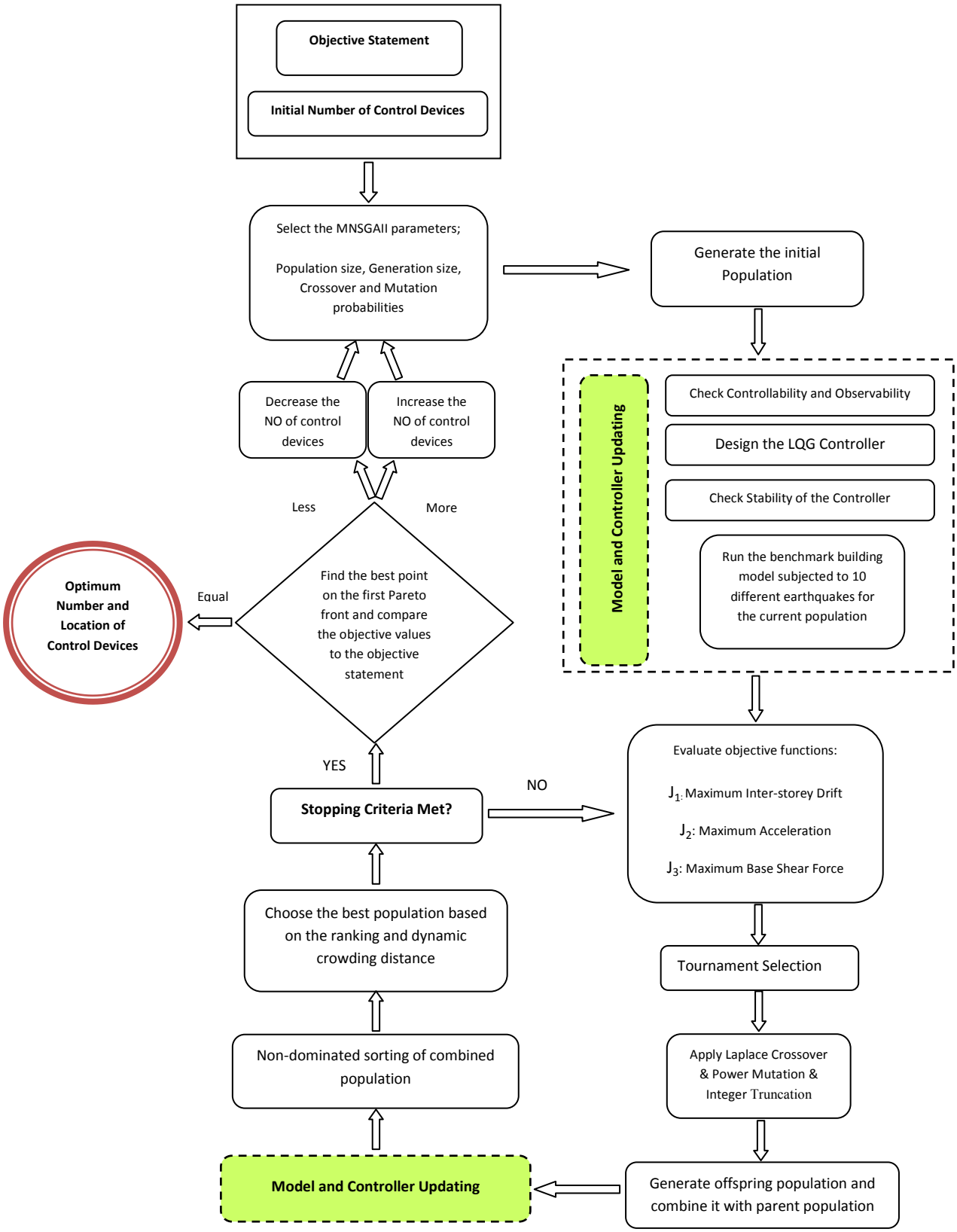

Figure 3.1. Proposed Optimisation Flowchart

the relation $\max_{i,t}(\frac{|d_i(t)|}{h_i})$, $\ddot{x}_i(t)$ and $\ddot{x}_a^{max}$ are maximum absolute acceleration of the i^{th} level with control devices and maximum absolute acceleration of uncontrolled structure, respectively. m_i is the mass of the ith storey. It is worth noting that, the structure of controller, which determines the desired control forces, will be updated by changing the control device configurations. Here in this study, the same LQG control algorithm as designed in the benchmark problem definition is considered in order to compare the final results. However, for the semi-active case, clipped optimal control (COC) is also combined with LQG to control the required voltage of MR dampers.

In order to use the aforementioned optimisation strategy, the adjustable parameters need to be defined and encoded into a chromosome to be evolved through the optimisation. Here, the length of chromosome is chosen to be equal to the number of control devices. So, the adjustable parameters are the locations of control devices and, therefore, each gene, an integer number in the [1-20] interval, represents the floor number (Figure 3.2). For example, the chromosome [1 4 5 20] is interpreted as 4 actuators (length of matrix) located on 1st, 4th, 5th, and 20th floor of the structure, respectively. Similarly, the chromosome [2 18 2 2] represents that 3 actuators are placed on floor 2 and 1 actuator is assigned to floor 18.

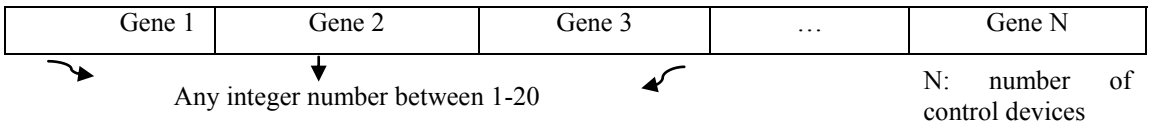

Figure 3.2 Encoding scheme for individual chromosome

3.5 CASE STUDY: 20-STOREY NONLINEAR BENCHMARK STRUCTURE

A nonlinear benchmark building of 20-storey which was designed and developed by Ohtori et al to facilitate comparison of performances of different control algorithms and control devices, has been used here as case study (Ohtori et al. 2004). The 20-storey benchmark structure is 30.48 m by 36.58 m in plane, and 80.77 m in elevation and consists of moment resisting frames: five bays in NS-direction and six bays in EW-direction (see Figure 3.3). Based on the physical description of the 20-storey structures described in (Ohtori et al. 2004), in-plane finite element models of the N-S MRFs have been developed. Structural member nonlinearities were included to capture the inelastic

behaviour of buildings during strong earthquakes. The beams and columns of the structure are modelled as plane-frame elements, and mass and stiffness matrices for the structure are determined. A bilinear hysteretic model is used to characterise the nonlinear bending stiffness of the structural members. The damping matrix is determined based on an assumption of Rayleigh damping. More information can be found in (Ohtori et al. 2004).

Two far-field and two near-field historical ground motion earthquake records with different intensities are selected as excitations to the structure. These records are the El Centro (1940) and Hachinohe (1968) earthquake records with 0.5, 1.0, and 1.5 intensity and, Northridge (1994) and Kobe (1995) earthquake records with 0.5 and 1.0 intensity. Control devices are placed throughout the stories of the building, connecting the adjacent levels. The size of both active actuators and MR dampers are limited to provide maximum control force of 1000 kN. Although there are multiple control devices acting on each floor, it is assumed that all control devices on a single floor experience the same inputs, and respond in the same way. The control strategy implemented on the building is based on acceleration feedback. For this purpose, a total of five accelerometers are used on levels 4, 8, 12, 16, and 20 as proposed in the benchmark problem. An LQG controller is also designed, based on the measurements and places of control devices. Therefore, the design of LQG controller, as mentioned earlier, should be updated with respect to number and places of control devices through the optimisation algorithm. More details on the control design can be found in the benchmark problem definition (Ohtori et al. 2004).

3.5.1 Optimal Number and Places of Active Actuators

The aforementioned methodology is applied to the proposed benchmark structure to optimise the number and position of actuators within it. The control forces are applied to the structure through a to-be-determined number of actuators, at the locations which should be obtained via the proposed optimisation procedure. As mentioned before, J_1, J_2 and J_3, are selected as the objective functions. Therefore, the following objective statements are considered:

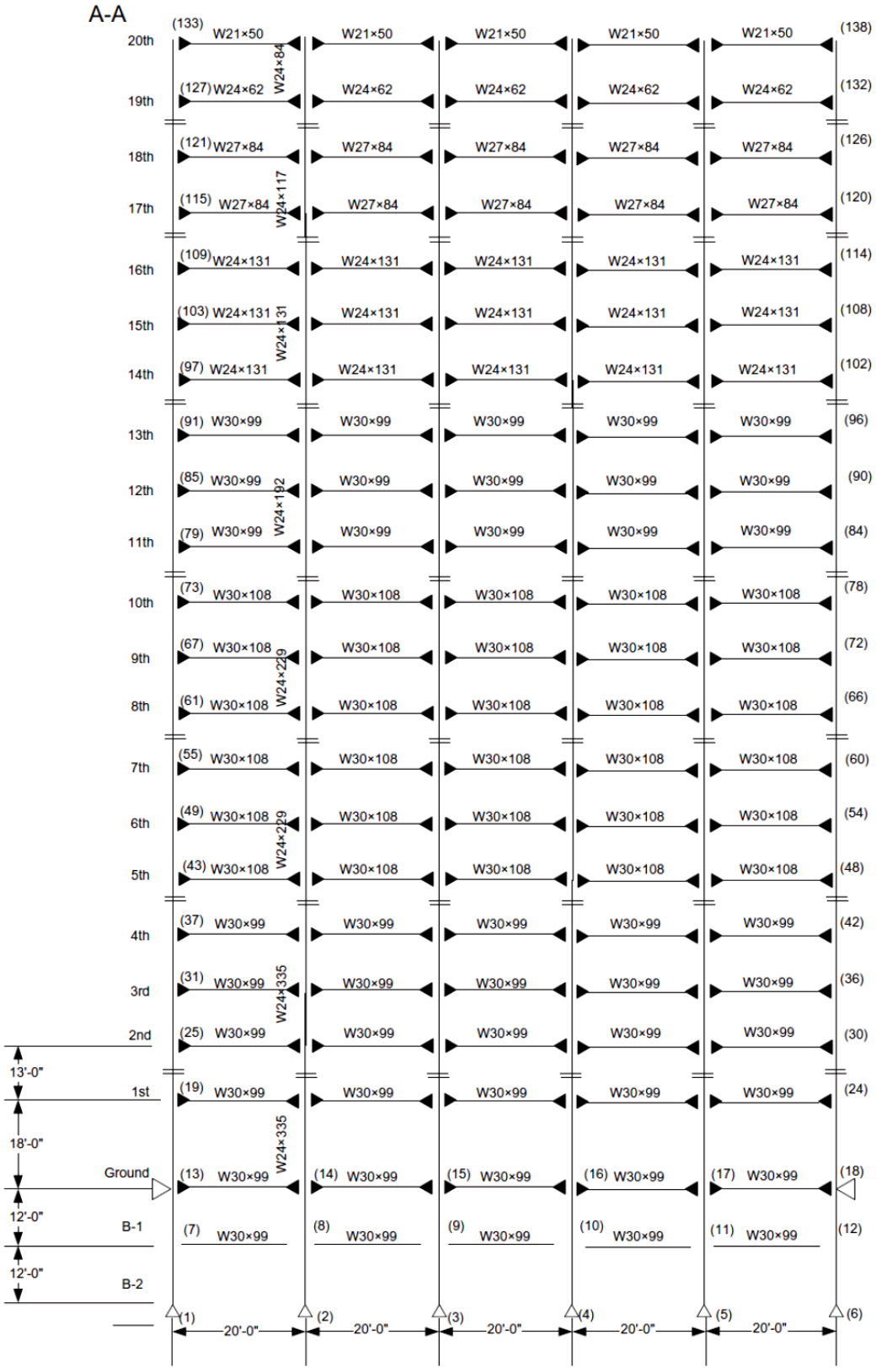

Figure 3.3. 20 -Storey benchmark building proposed in this study

$$J_1(maximum\ of\ the\ inter-storey\ drifts\ ratio) \leq J_{1,max}$$
$$J_2(maximum\ of\ the\ floor\ acceleration) \leq J_{2,max}$$
$$J_3(maximum\ of\ shear\ base) \leq J_{3,max}$$

For the sake of comparison, and as a reference, we select the value of $J_{1,max}$ =0.9421, $J_{2,max}$=0.9043, and $J_{3,max}$ = 1.0656 as the proposed level of performance as achieved by the control strategy in (Ohtori et al. 2004).

Here we started with 20 actuators which is 5 actuators fewer than what was used in the reference (Ohtori et al. 2004). After completion of optimisation, a Pareto front presenting a set of best configuration of actuators is achieved. It should be mentioned that since we are dealing with three objective functions, we need to study two different graphs at the same time, i.e J_1 vs J_3 and J_2 vs J_3, where the points with the same colour represent the same configuration. As expected and can be seen from Figure 3.4, there are many points with better level of performance, in terms of proposed objective indices, compared to the reference. Therefore, the number of actuators was decreased for the next optimisation procedure to be close to the allowable limit of performance. To do so, 10 actuators are considered to be placed in the optimum positions in the second step. The corresponding Pareto front is also sketched in Figure 3.4 where still many points have smaller values of J_1, J_2 and J_3, compared to the reference point which is marked by star. Therefore, it is assumed that the number of actuators can still be decreased. Next Pareto front in Figure 3.4, shows the best configurations of 5 actuators, where none of the points in the first front, lead to a more efficient arrangement of actuators compared to the original work. This means that, the optimum number of actuators should be between 5 and 10. However, it is worth to note that selecting the proper configuration depends on the designer's desire. If designer is more interested to keep the maximum of inter-storey drift ratio at the minimum level, then 5 actuators can still be used for this purpose since some points on the corresponding Pareto front have smaller values of J_1 compared to the reference point.

As the last run, 7 actuators were used to find their optimum layout. The generated Pareto front, plotted in Figure 3.4, shows that the point marked by a green square, can capture the reference point quite well. In other words, the same objective indices as the 25 placed actuators in the benchmark problem definition can be achieved if only 7 actuators were incorporated into the structure with the proposed optimum arrangement

shown in Figure 3.6. This clearly demonstrates that a more efficient control strategy can not be necessarily achieved by only increasing the number of control devices. Placing fewer number of devices in optimal locations, on the other hand, is more effective in terms of cost and safety.

For the sake of comparison, the optimisation is also run for 25 and 15 actuators whose Pareto fronts are depicted in Figure 3.5. The best configuration in each optimisation case that makes a trade-off between all three proposed objective indices is marked by a green square. In order to provide a more comprehensive solution and also to compare devices arrangements for different purposes, the best configuration of actuators, are also considered and shown in Figure 3.6. The GA parameter settings used here are given in Table 3-1.

Table 3-1. GA parameters used in actuators distribution optimisation

Population NO	60	Crossover probability (*pc*)	0.8	a	0	p_{int}	4
Generation NO	100	Mutation probability (*pm*)	0.1	b_{int}	0.35	-	

Each of the Pareto-optimal fronts shown in Figure 3.4 and Figure 3.5 defined almost 30 control device layout designs, and each layout design represents a different trade-off between maximum drift, maximum floor acceleration and shear force controllability and instrumentation cost. Engineers can use this information to select the appropriate design that best meets their performance criteria.

It needs to be mentioned that, although the optimisation procedure is performed using three objective indices, J_1, J_2 and J_3, the effect of designed control system on other indices should be studied as well.

Figure 3.7 displays the value of some indices for different number of optimally placed actuators (trade-off scenario) and compares the results with the original work (Ohtori et al. 2004). The point marked by solid circle in each graph, represents the original work.

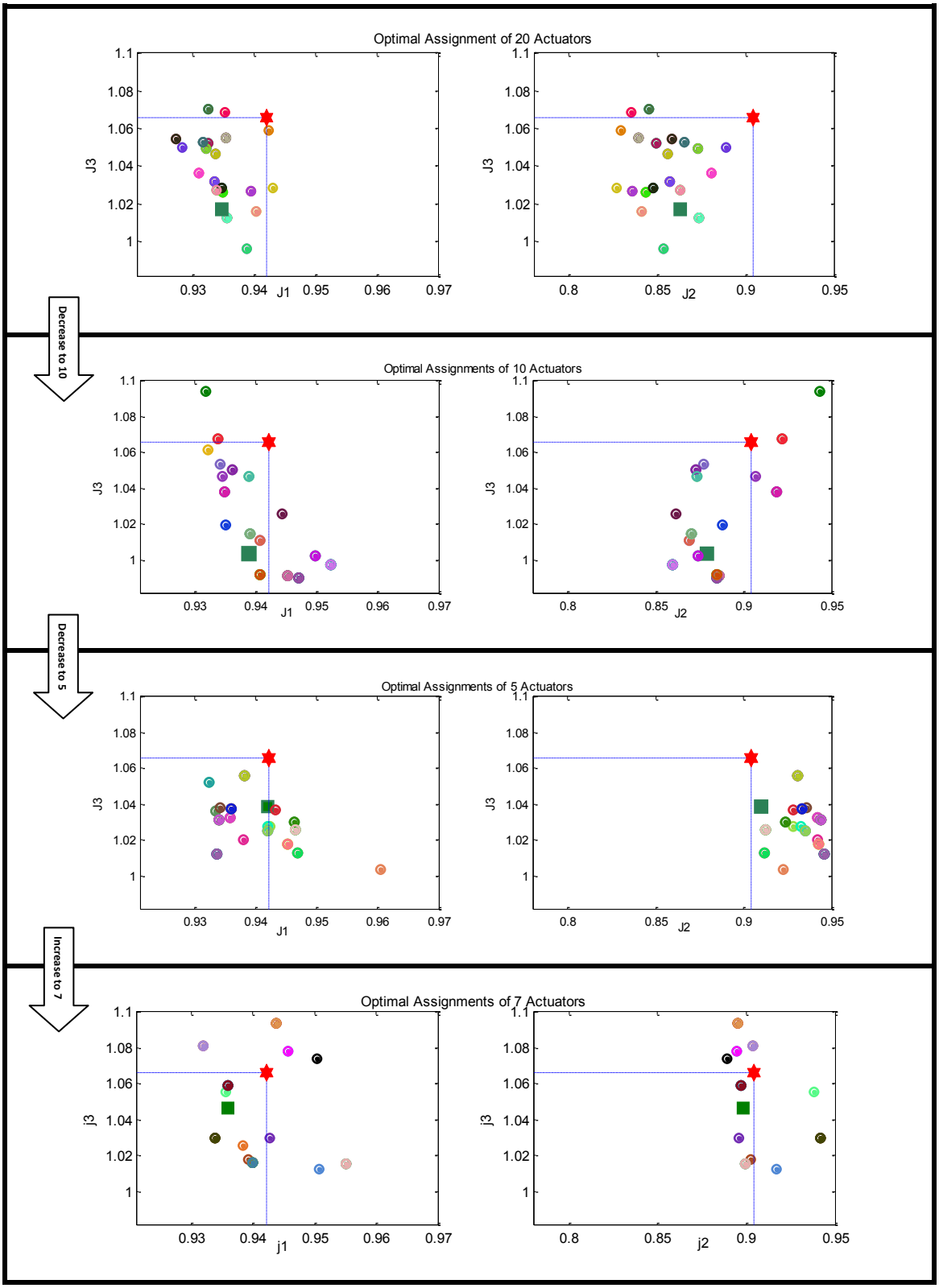

Figure 3.4 Pareto Fronts Obtained for Optimal Places of Different Number of Actuators

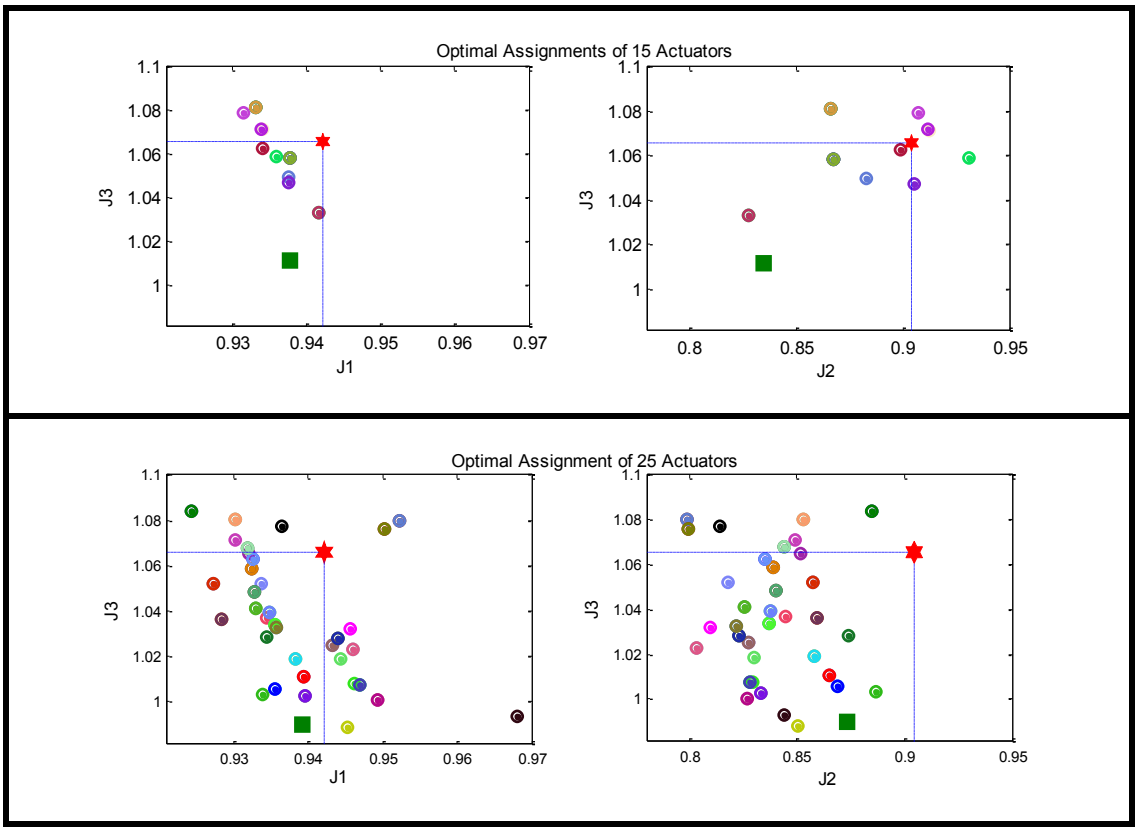

Figure 3.5 Pareto Front for optimal placement of 15 and 25 actuators

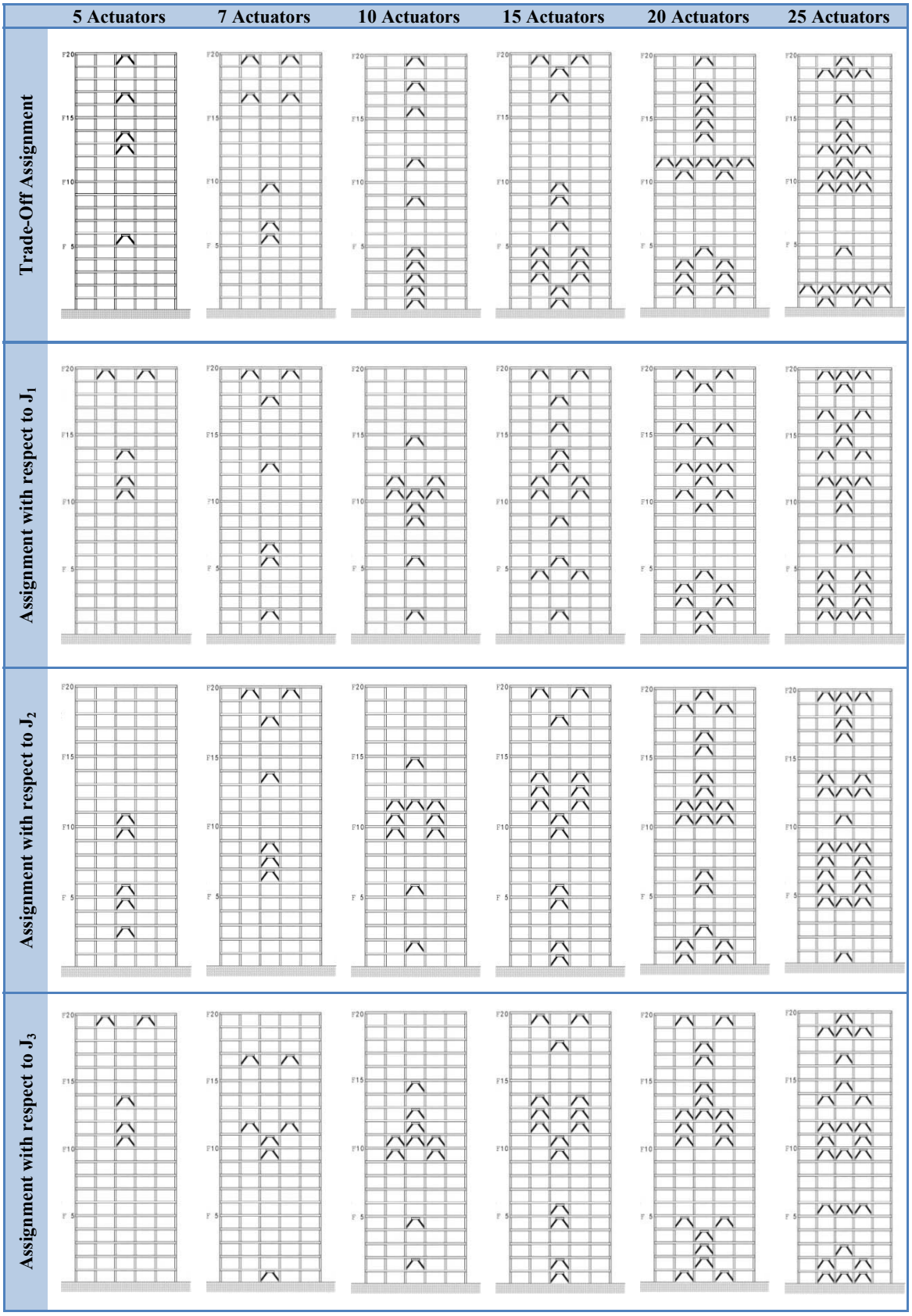

Figure 3.6 Optimal Actuator Placement in 20-storey benchmark structures for different purposes

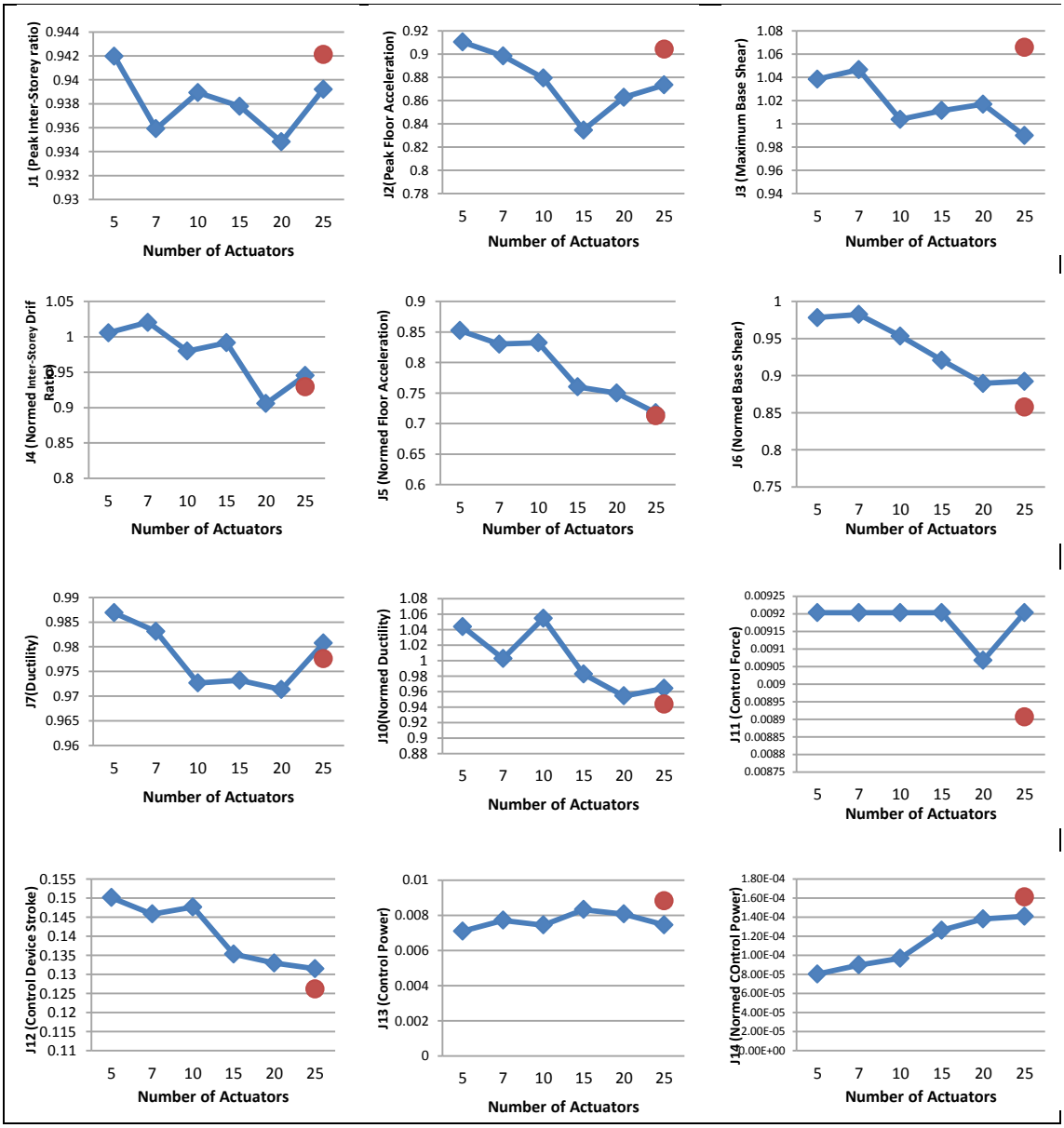

Figure 3.7 Changes of Performance Indices vs. Number of Actuators (Trade-Off Scenario)

As shown in above figures, the optimisation procedure can help to reduce the magnitude of many indices compared to the original work while it increases the performance indices in some cases. For instance, similar or smaller values of J_1, J_2, J_3, J_7, J_{13} and J_{14} can be achieved using 7 optimally placed actuators. On the other hand Normed Inter-Storey Drift (J_4), Normed Floor Acceleration (J_5), Normed Base Shear (J_6), Normed Ductility Index (J_{10}), Control Force (J_{11}), the stroke of control devices (J_{12}) will be increased by reducing the number of control devices. Furthermore, it is interesting to see that Control Power indices (J_{13} and J_{14}) are increasing by the number of actuators which is reasonable.

3.5.2 Optimal MR Damper Number and Places

Magneto-Rheological (MR) dampers are one of the most promising semiactive devices that do not inject energy into the system they are attached to. They can absorb the vibratory energy due to motion of the MR damper and input control voltage applied to them. Due to their mechanical simplicity, high dynamic range, low power requirements, low cost, large force capacity, and inherent stability, these devices have successfully been employed as shock absorbers, suspension systems in vehicle seats, brakes in aerobic exercise equipment and more recently, in prosthetics and seismic and wind mitigation (Duan, Ni & Ko 2006).

Traditionally, an optimal controller like LQR, LQG, H_∞ etc., is designed for the ideal active control devices due to their simplicity, and then the actuators are replaced by semi-active control devices. In other words, it is assumed that the critical locations of actuators and semi-active control devices such as MR dampers are the same. The main aim of this section is to numerically show the difference between the best places of actuators and MR dampers. Therefore, the optimal locations of a specific number of MR dampers will be compared to those obtained for the active actuators. To this end, MR dampers with the same capacity as the active actuators employed in the previous section, i.e. 1000 kN, need to be chosen. It is worth noting that, firstly, such a comparison can not be found in the literature and secondly, finding the multi-objective optimal number and places of MR dampers in high-rise nonlinear buildings has not been reported by the researchers, to date.

For simulation purposes, the phenomenological model proposed by Spencer et al, is used in this study (Spencer et al. 1997). A set of typical parameters of the 1000 kN MR damper used here in the simulations, is presented in Table 2-1 (Ze-bing, Jin-zhi & Hong-xia 2004). Note that the maximum operational voltage of this MR damper is 10 V, which is defined as the saturation voltage of the damper and is obtained experimentally. Moreover, the situation of 0 V will also be common during operation of the MR damper. Therefore, the range of the voltage signal is set as 0–10 V in this study. Likewise, the displacement range of the MR damper is $\pm$20 cm while its frequency ranges from approximately 0 to 5 Hz.

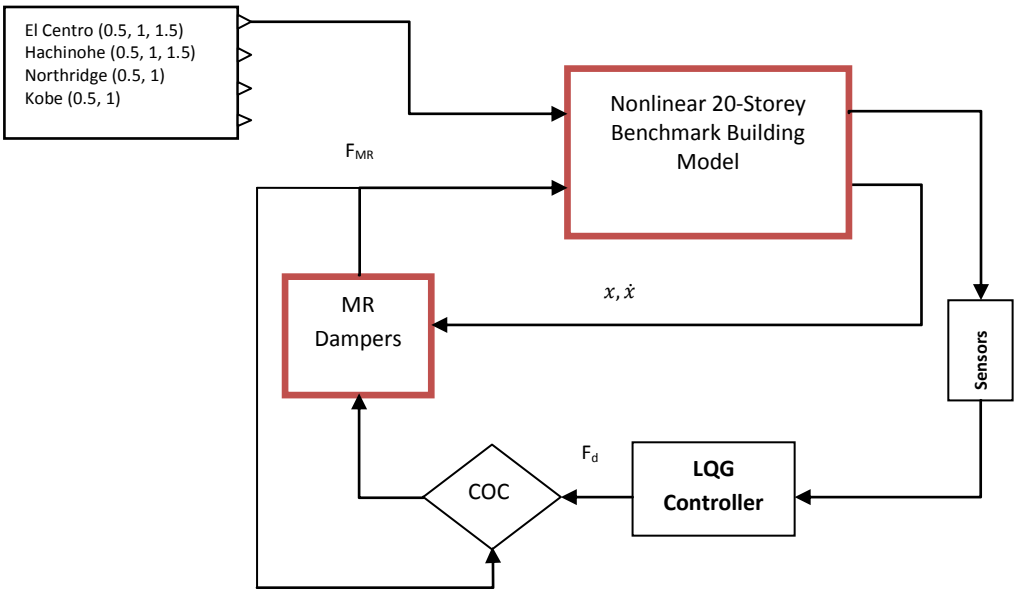

Figure 3.8 Block diagram of the proposed semi-active control algorithm

Like the previous section, an LQG controller is designed as the target optimal controller to estimate the required force that should be generated by the MR dampers. This controller, however, needs to be combined with another algorithm to provide the MR dampers with a proper voltage to produce such control force. The most commonly used semi-active strategy to be used together with the target controller is the clipped-optimal control (COC) (Dyke et al. 1996a). Therefore in this study, a COC is also considered between the main controller and MR dampers. A schematic block diagram of the proposed control loop is sketched in Figure 3.8.

Using the optimisation strategy described earlier and also the explained semi-active control algorithm, the Pareto fronts for optimal places of different number of MR dampers were obtained and shown in Figure 3.9 and Figure 3.10. Remember, the Pareto fronts advance in each generation until the last Pareto front whose points possess rank 1. However the number of points on the final front might be less than the population number as not all the points in the last population are ranked 1. Also note that, the final point can be selected based on designer's desire. Here the selected points which make a trade-off between proposed objective indices, are marked by green squares and their corresponding arrangements are shown in Figure 3.9 and Figure 3.10. Like the previous section, the optimum distribution of different number of MR dampers for various purposes, i.e. minimising J1 only, minimising J2 only, minimising J3 only and a trade-

off between all three indices, is shown in Figure 3.11. The GA parameters settings used here are given in Table 3-2.

Table 3-2. GA parameters used in MR dampers distribution optimisation

Population NO	30	Crossover probability (pc)	0.8	a	0	p_{int}	4
Generation NO	50	mutation probability (pm)	0.1	b_{int}	0.35	-	

The range of designs, provided here, allows the engineer to understand the trade-off that is occurring and also to pick the minimum number of devices required to provide the proposed control effectiveness one seeks. Moreover, the structural engineer can choose the best layout architecture that fits the constraints present in a specific structure due to installation of control devices because of architectural and mechanical system requirements or other features.

The effects of optimal arrangements of MR dampers (Trade-Off Scenario), together with the designed control system on other indices are studied and results are shown in Figure 3.12.

The value of three proposed objective indices for the under-study structure considering optimal assignments of different number of control devices, i.e. actuators and MR dampers, are depicted in Figure 3.14 for different scenarios. These scenarios include;

(a) optimal arrangement of control devices considering a trade-off between all three indices,
(b) optimal arrangement of control devices considering minimisation of J1 only,
(c) optimal arrangement of control devices considering minimisation of J2 only,
(d) optimal arrangement of control devices considering minimisation of J3 only.

Comparison between the performances of the active controlled structure using optimally placed actuators to the semi-active controlled structure using optimally placed MR dampers, shows that the MR dampers with optimal arrangements are better choices in reducing peak inter-storey drifts. However, actuators in optimal locations are more effective in reducing the maximum floor acceleration and base shear. The results also indicated that increasing the number of control devices had a beneficial effect on controlling drift and acceleration if they are installed in the optimal places for each

case. However, using more devices does not necessarily decrease the base shear force, even though the optimisation would be done for minimisation of J_3 only.

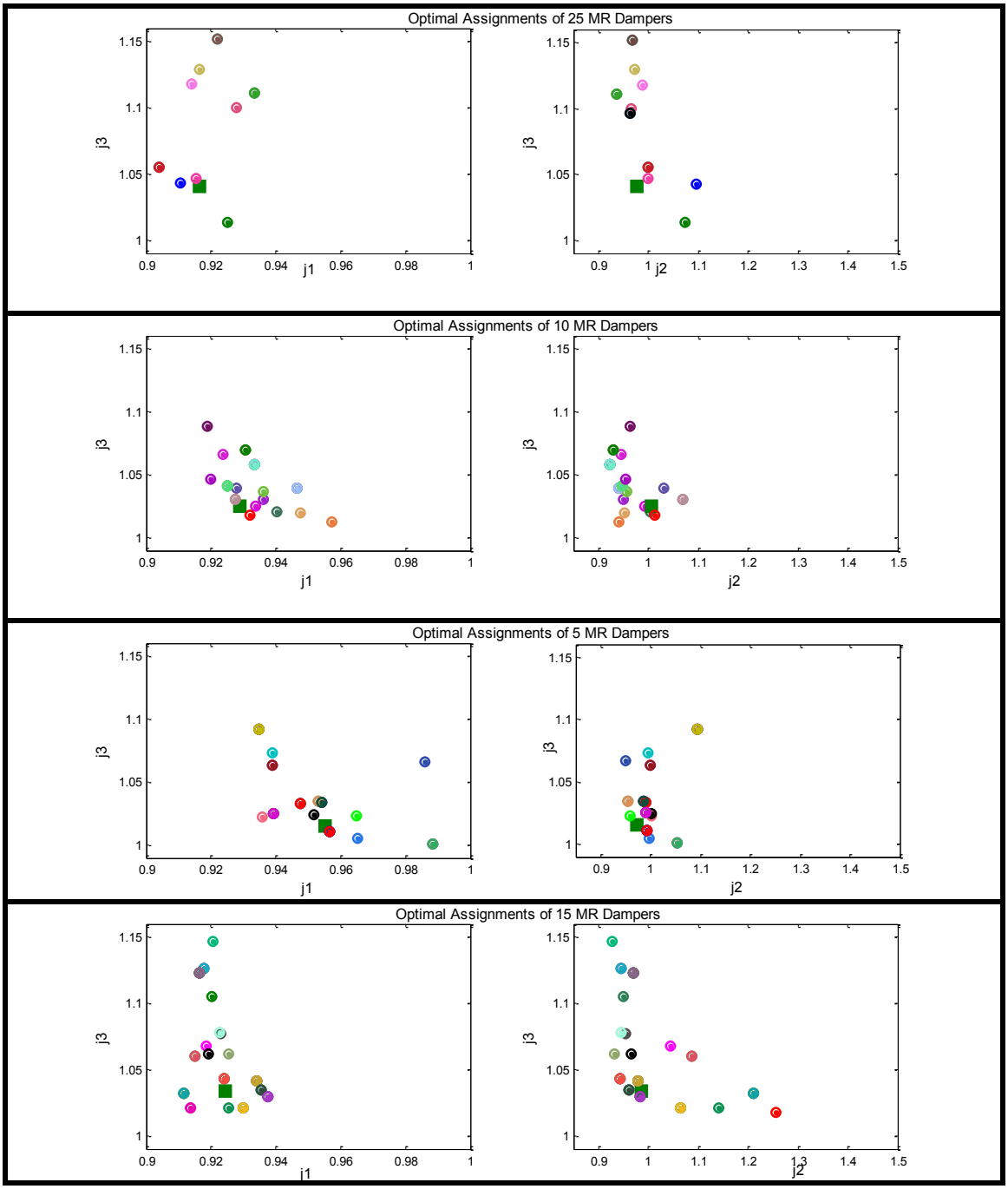

Figure 3.9. Pareto Fronts for optimal assignment of different number of MR dampers

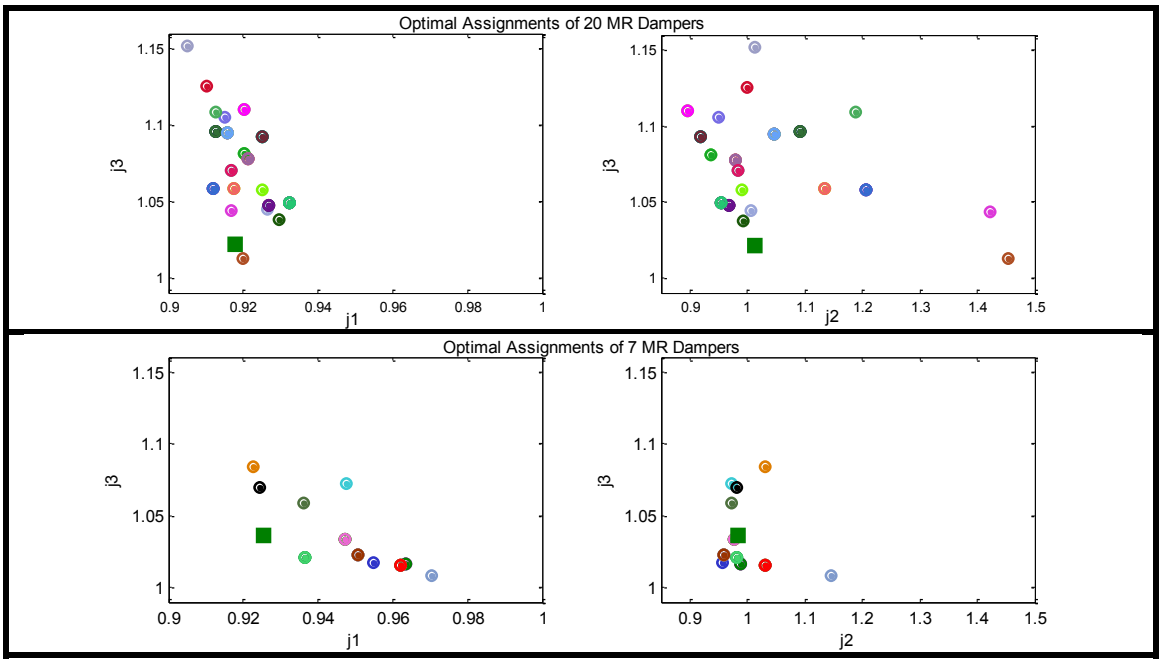

Figure 3.10. Pareto Fronts for optimal assignment of different number of MR dampers (Continue)

Figure 3.13 compares the maximum displacement and acceleration responses of the 20-storey building using optimally placed actuators, MR dampers and 25 non-optimally placed actuators (benchmark). It can be observed that, the green line (7 actuators) matches the blue line (25 actuators) which shows same levels of performance in these two systems.

As discussed earlier, one of the foci of this study is to compare the optimal places of actuators in an active controlled system, and MR dampers in a semi-active controlled structure. It is also of interest to prove the fact that, the optimal arrangement of MR dampers can be only achieved if the proposed optimisation algorithm is run through the semi-active controlled structures even though it takes a longer time compared to the active system. Therefore, the performance of active and semi-active structure, using optimum assignment of actuators and MR dampers obtained in this section, is given in the second column of Table 3-3 and Table 3-4, respectively. Moreover, the active and semi-active performance of the structure is also checked using the best configuration of MR dampers and actuators and the results are shown in the last column of Table 3-3 and Table 3-4. The comparison between these two columns for both active and semi-active structures shows that, larger values of J_1, J_2 and J_3 can be achieved when MR dampers are placed in optimal locations of actuators and also when actuators are incorporated into the structure in the optimal places of MR dampers in an active

system. In other words, optimal locations of actuators (MR dampers) are not optimal for semi-active (active) control systems.

3.6 SUMMARY

This chapter has addressed the problem of optimal number and placement of active and semi-active devices in the control of civil structures against earthquake excitations. The problem is tackled from a multi-objective optimisation perspective where a modified integer coding genetic algorithm is introduced and used to obtain near-optimum number and places of actuators and MR dampers in an active and semi-active controlled 20-storey nonlinear benchmark building subjected to 10 different earthquakes. The new optimisation algorithm (MI-NSGAII) is developed through the integration of the MI-LXPM and NSGAII. The NSGAII is adopted as a dynamic multi-objective optimisation search algorithm whereas MI-LXPM is adopted to deal with discrete to-be-optimised parameters.

The use of Pareto-based NSGAII, together with new integer-coded operators, is effective in this problem domain in which the objective functions, i.e. reduction of peak inter-storey drift ratio, peak floor acceleration and peak base shear, are simultaneously achieved. These objective functions are selected in such a way that both human comfort (J_2) and safety level (J_1, J_3) of the structure is guaranteed.

The results of optimal placement of active actuators were compared to the benchmark problem definition (Ohtori et al. 2004) in which 25 actuators are located in non-optimal locations. Results showed the effect of proposed strategy where the same level of structural performance, in terms of proposed objective functions, is obtained by use of only 7 actuators in an optimal layout. However, some indices are slightly increased compared to the original work. This problem can be solved by using more control devices or taking more performance indices into account during the optimisation. As can be found from the results, the proposed algorithm can lead to a cost effective distribution of control devices.

The optimal configuration of different number of MR dampers in the same nonlinear benchmark building is also studied in this chapter. Due to highly nonlinear behaviour of these devices, and thus complexity of the problem, few reported studies have been

conducted in this area. Results proved the fact that optimal places of actuators and MR dampers are totally different. It should be mentioned that using different Pareto fronts, design engineers can select the number and arrangement of devices based on the level of performance that is acceptable. It also demonstrated the superiority of optimally assigned MR dampers on actuators in reduction of structural peak inter-storey drift. On the other hand, optimally allocated actuators perform better than MR dampers in reducing the peak floor acceleration as well as peak base shear force. The optimal number of control devices, however, might be slightly different for different applied control strategies as various control algorithms work with different objective functions. This can be more elaborated in future studies.

Future work will be directed towards finding the optimal location of sensors and MR dampers simultaneously to address the optimality in smart structures.

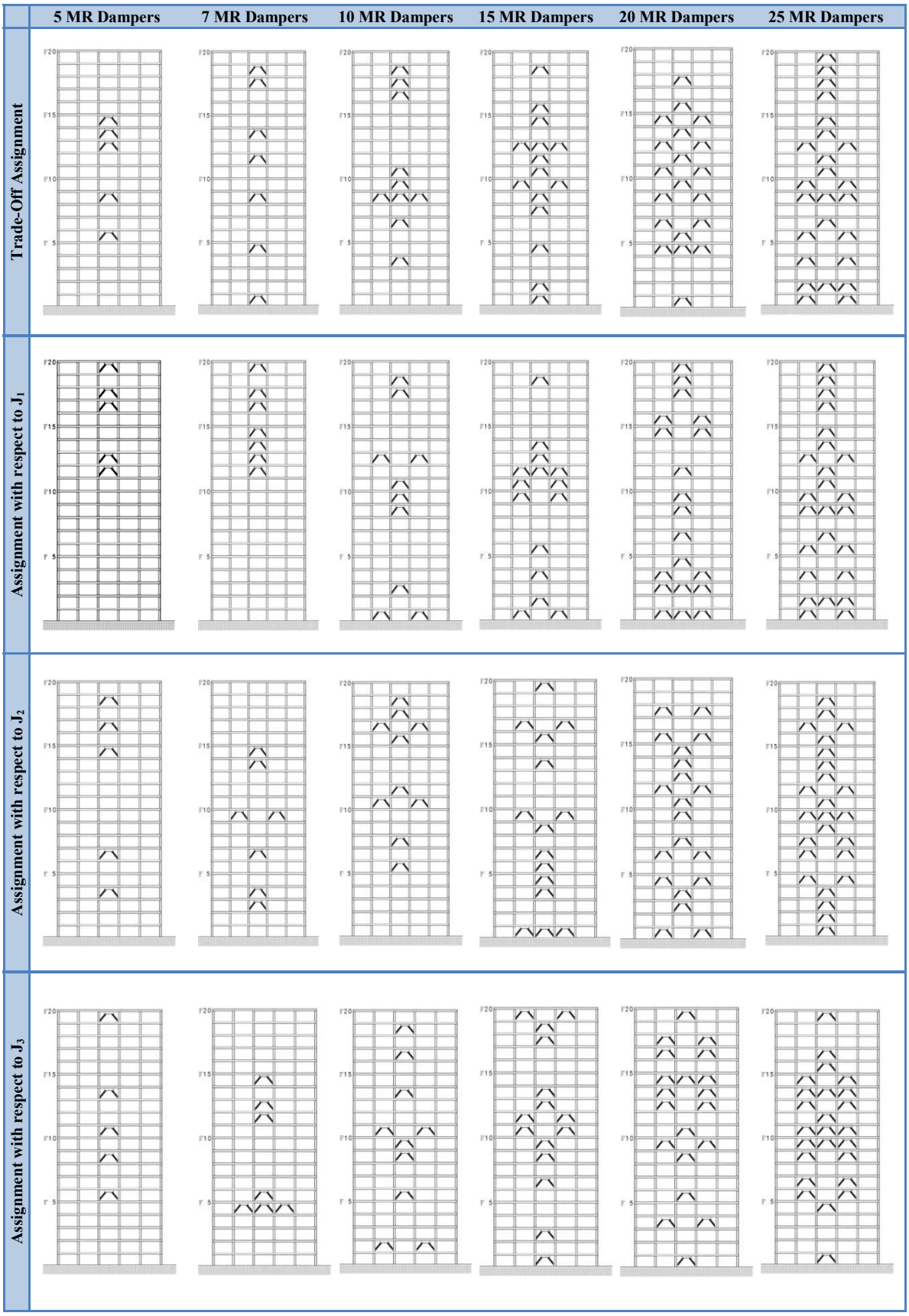

Figure 3.11. Optimal MR Dampers Placement in 20-storey benchmark structure

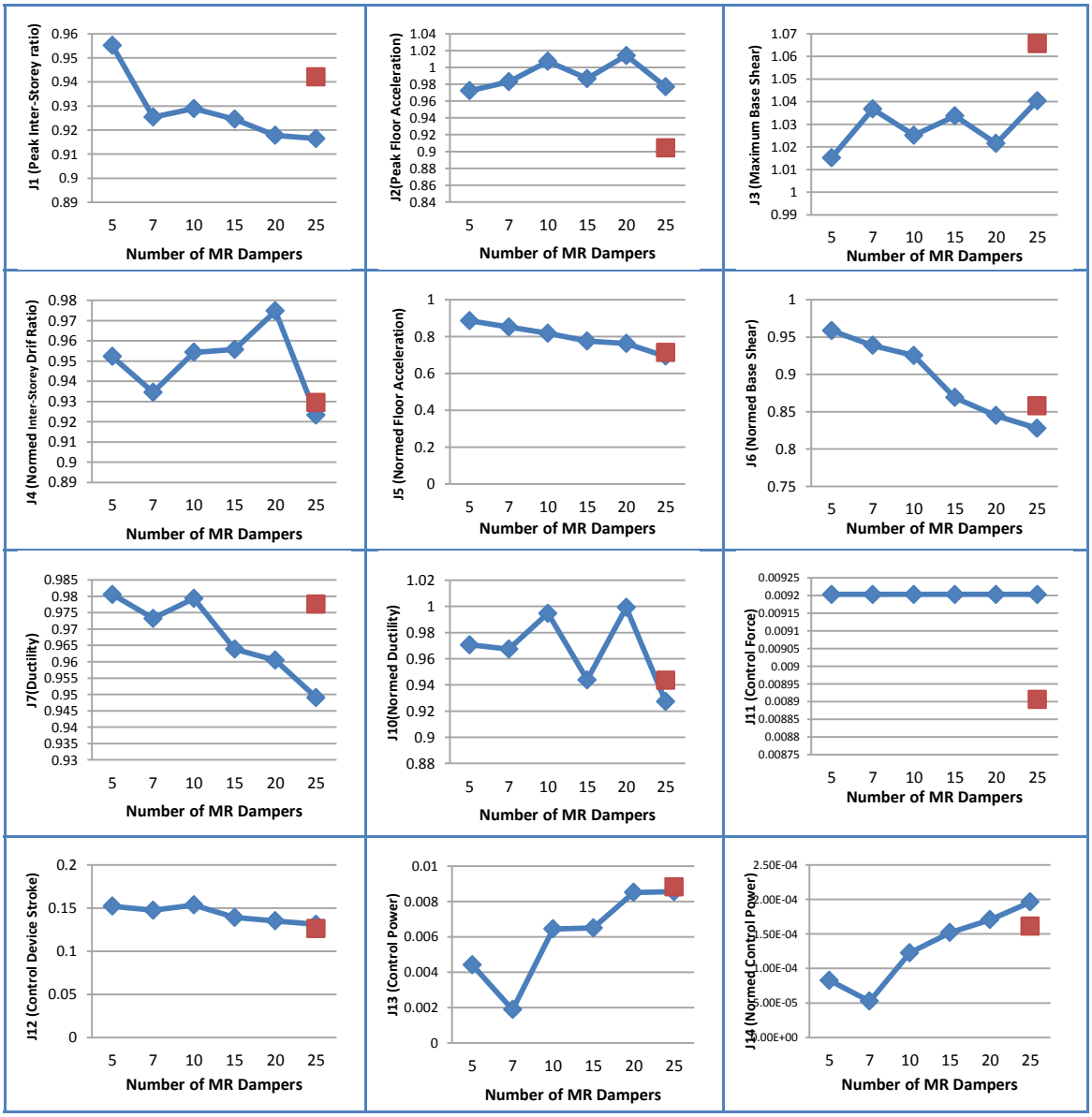

Figure 3.12. Changes of Performance Indices vs. Number of MR dampers (Trade-Off Scenario)

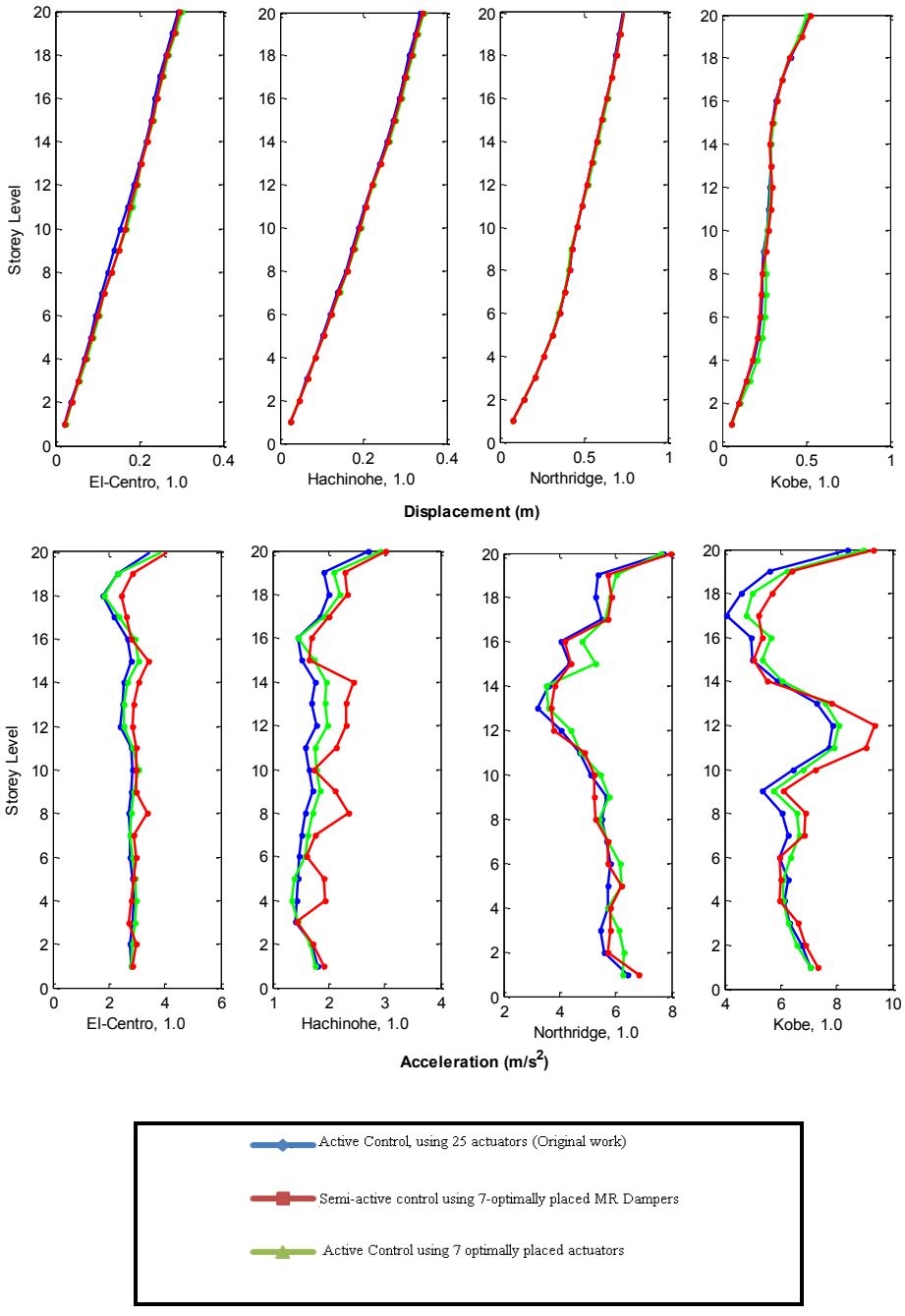

Figure 3.13. Comparison of peak floor displacement and acceleration with and without optimisation

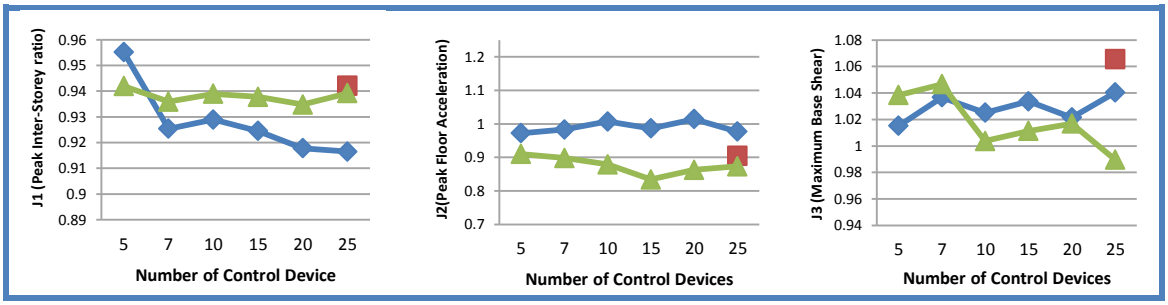

(a) Trade-Off Scenario

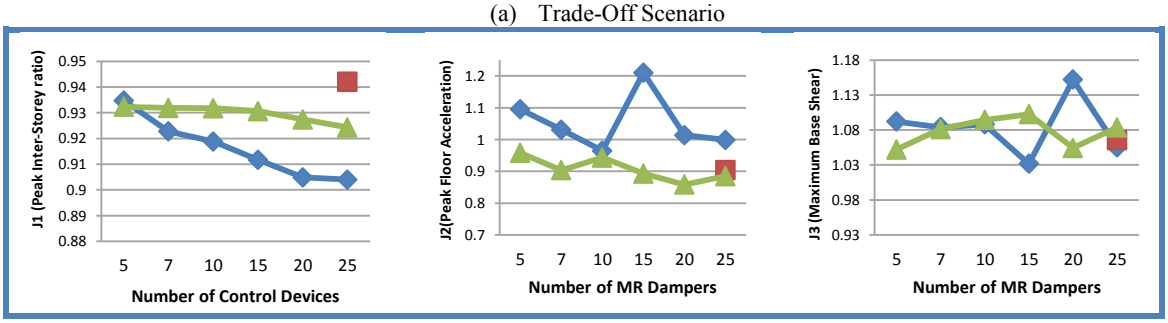

(b) J1 minimisation Scenario

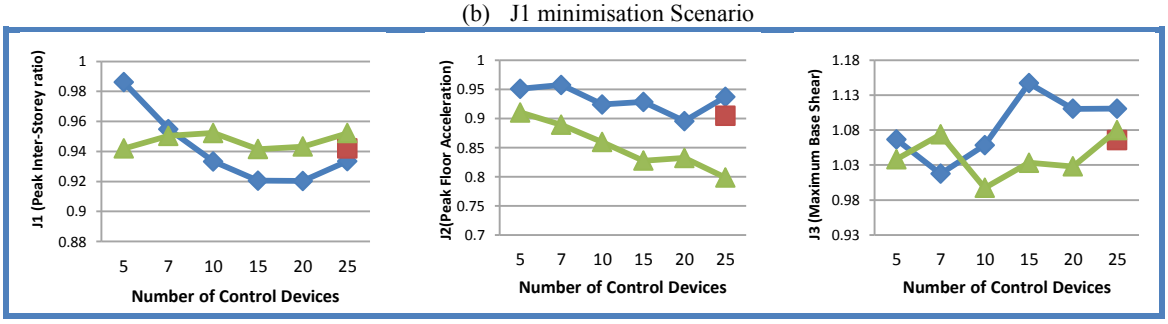

(c) J2 minimisation Scenario

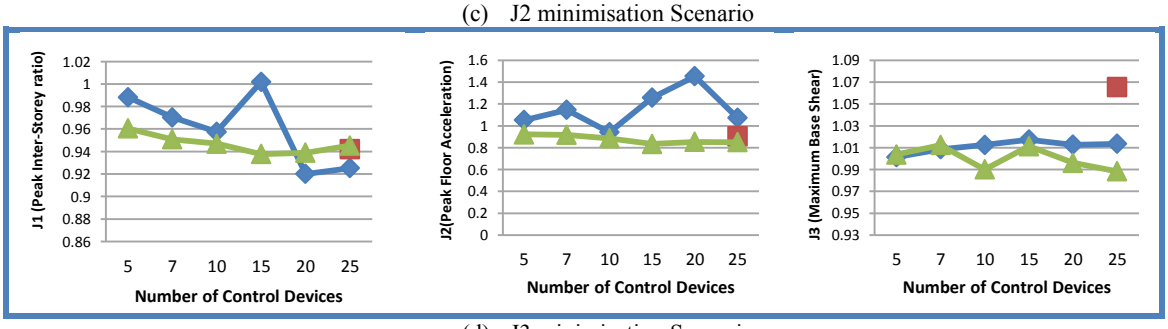

(d) J3 minimisation Scenario

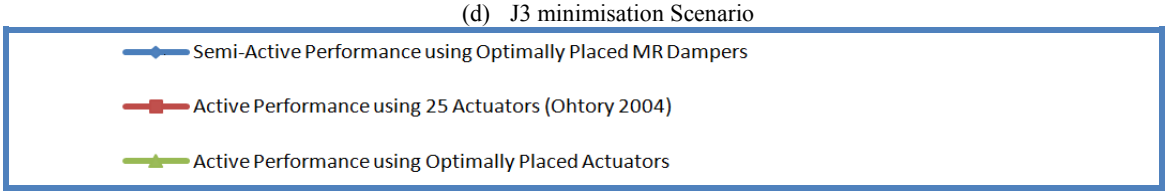

Figure 3.14. Structural Performance for Optimal Assignments of actuators and MR dampers

Table 3-3. Optimal Actuator Placements

		Optimal Assignment of Control Devices, (DESIGN 1 : Actuators)																				Active Structural Performance Using Optimal Actuator Assignments			Active Structural Performance Using Optimal MR-Damper Assignments		
		1	2	3	4	5	6	7	8	9	10	11	12	13	14	15	16	17	18	19	20	J1	J2	J3	J1	J2	J3
Trade-Off	5											1	1		1						2	0.9419	0.9103	1.0384	0.9492	0.9308	1.0472
	10		1			1					2	3	1	1		1						0.9389	0.8794	1.0038	0.9534	0.9358	1.0620
	15	1	1			1	1				1	1	2	2	2				1		2	0.9378	0.8346	1.0113	0.9422	0.8824	1.0514
	20	2	1	1	1	2						2	2	3	1	1		1	1		2	0.9348	0.8627	1.0169	0.9519	0.8639	1.0512
	25	2	5			1					3	3	1	3	1	1		1		3	1	0.9393	0.8733	0.9898	0.9473	0.8438	1.0237
	7						1	1			1							2			2	0.9355	0.8984	1.0420	0.9526	0.9825	1.0548
		1	2	3	4	5	6	7	8	9	10	11	12	13	14	15	16	17	18	19	20	J1	J2	J3	J1	J2	J3
J1 Minimisation	5						1							1	1			1			1	0.9323	0.9580	1.0521	0.9590	0.9844	1.0468
	10	1	1	1	1	1				1			1				1		1		1	0.9318	0.9433	1.0945	0.9672	0.9574	1.0492
	15	1	1	2	2	2		1		1	1							1		1	2	0.9306	0.8929	1.0103	0.9329	0.8773	1.0029
	20	1	1	2	2	1					1	2	1	3		1	2			1	2	0.9274	0.8582	1.0544	0.9348	0.8707	1.0709
	25		3	2	2	2		1			1	1	3		2	1	1	2		1	3	0.9243	0.8850	1.0837	0.9361	0.8771	1.0777
	7		1				1	1						1					1		2	0.9333	0.9571	1.0684	0.9506	0.9213	1.0419
		1	2	3	4	5	6	7	8	9	10	11	12	13	14	15	16	17	18	19	20	J1	J2	J3	J1	J2	J3
J2 Minimisation	5											1	1		1						2	0.9419	0.9103	1.0384	0.9385	0.9900	1.0563
	10		1				1			1	1	3	2			1						0.9523	0.8594	0.9974	0.9556	0.9479	1.0460
	15		1			2	1			1		2	2	1	1		1		1		2	0.9415	0.8287	1.0332	0.9429	0.8747	1.0617
	20		1			1	2	2		2	2	2	1	2	1	2		1			1	0.9431	0.8268	1.0282	0.9356	0.8807	1.0716
	25	1				3	2	2	2	3		1		3	2			1	1	1	3	0.9522	0.7985	1.0799	0.9518	0.9020	1.0758
	7							1	1	1					1				1		2	0.9473	0.8782	1.0436	0.9535	0.9380	1.0480
		1	2	3	4	5	6	7	8	9	10	11	12	13	14	15	16	17	18	19	20	J1	J2	J3	J1	J2	J3
J3 Minimisation	5			1		1	1				1	1										0.9605	0.9226	1.0040	0.9430	0.9835	1.0308
	10		1				1				2	2	3		1							0.9470	0.8847	0.9901	0.9385	0.9235	1.0286
	15	1	1			1	1				1	1	2	2	2				1		2	0.9378	0.8346	1.0113	0.9666	0.8660	1.0288
	20	2	2	1			1	1				3	3	1	1		1	1		2	1	0.9389	0.8536	0.9961	0.9432	0.8998	1.0328
	25	3	2	1			3				3	2	3		2	1		1		3	1	0.9452	0.8500	0.9883	0.9451	0.8182	1.0292
	7	1									1	1	2					2				0.9496	0.9148	1.0063	0.9576	0.9134	1.0539

Table 3-4. Optimal MR Damper Placements

		Optimal Assignment of Control Devices, (DESIGN 2 : MR Dampers)																				Semi-Active Structural Performance Using Optimal MR Damper Assignments			Semi-Active Structural Performance Using Optimal Actuator Assignments		
		1	2	3	4	5	6	7	8	9	10	11	12	13	14	15	16	17	18	19	20	J1	J2	J3	J1	J2	J3
Trade-Off	5						1			1				1	1	1						0.9551	0.9723	1.0152	1.0130	1.1180	1.0717
	10				1			1		3	1	1						1	1	1		0.9290	1.0072	1.0252	0.9627	1.2374	1.0108
	15	1	1			1		1		1	2	1	1	3		1	1			1		0.9245	0.9867	1.0337	0.9257	1.1121	1.0401
	20	1		3		1	2		2		1	2	1	2	1	2	1		1			0.9178	1.0141	1.0215	0.9069	1.0816	1.0442
	25	2	3		2		2	1		3	2	1	1	2	1	1		1	1	1	1	0.9165	0.9771	1.0404	0.8989	1.1196	1.0220
	7	1				1				1			1		1				1	1		0.9254	0.9830	1.0368	1.0031	1.2368	1.1292
		1	2	3	4	5	6	7	8	9	10	11	12	13	14	15	16	17	18	19	20	J1	J2	J3	J1	J2	J3
J1 Minimisation	5												1	1				1	1		1	0.9347	1.0950	1.0921	0.9428	1.1069	1.0683
	10	2		1						1	1	1		2					1	1		0.9188	0.9647	1.0880	0.9407	1.1455	1.0637
	15	2	1		1		1				2	2	3	1	1					1		0.9117	1.2101	1.0317	0.9318	1.2965	1.1148
	20	3		3	2	1		1		1	1		1			2	2		1	1	1	0.9049	1.0139	1.1522	0.9108	1.2186	1.0948
	25		2	3	1	3	1	1		2	1	1	1	1	1	1	1	3		1	1	0.9040	0.9987	1.0552	0.9083	1.1167	1.0740
	7												1	1	1	1		1	1		1	0.9227	1.0308	1.0840	1.1778	1.3715	1.1075
		1	2	3	4	5	6	7	8	9	10	11	12	13	14	15	16	17	18	19	20	J1	J2	J3	J1	J2	J3
J2 Minimisation	5				1			1								1		1		1		0.9861	0.9509	1.0665	1.0130	1.1180	1.0717
	10						1		1			2	1				1	2	1	1		0.9333	0.9240	1.0584	0.9399	1.1611	1.0005
	15	3			1	1	1	1		1	2				1		1	2			1	0.9206	0.9284	1.1471	0.9314	1.0974	1.0453
	20	2		1	1	2		2	1		1	1	2	1	1	1	2		2			0.9203	0.8954	1.1103	0.9275	1.2676	1.0159
	25	1	1	1	1	2		2	2	1	3	1	2	1	1	1	1	2	1	1		0.9335	0.9371	1.1108	1.0260	1.0193	1.0565
	7			1	1			1			2				1	1						0.9549	0.9573	1.0175	0.9340	0.9637	1.0338
		1	2	3	4	5	6	7	8	9	10	11	12	13	14	15	16	17	18	19	20	J1	J2	J3	J1	J2	J3
J3 Minimisation	5						1			1		1			1						1	0.9883	1.0524	1.0014	0.9579	0.9902	1.0355
	10		2				1			1	1	2			1			1		1		0.9574	0.9402	1.0125	0.9293	1.2582	1.0112
	15	1		1				1		1	1	2	2	1	1				1	1	2	1.0019	1.2567	1.0173	0.9127	1.1121	1.0401
	20	1			2		1			1	2	1		2	2	3		2	2		1	0.9200	1.4536	1.0127	0.9130	1.1912	1.0716
	25	1				1	2	2		2	3	3	1	2	3	2	1	1			1	0.9253	1.0727	1.0136	1.0096	1.0283	1.0590
						3	1						1	1		1						0.9702	1.1460	1.0085	0.9493	1.0160	1.1000

CHAPTER 4

OPTIMAL SEMI-ACTIVE CONTROL OF NONLINEAR MR DAMPER-BUILDING SYSTEMS

4.1 CHAPTER OUTLINE

Two novel semi-active control methods for a seismically excited nonlinear benchmark building equipped with magnetorheological dampers are presented and evaluated in this chapter. While a primary controller is designed to estimate the optimal control force of a MR damper, the required voltage input for the damper to produce such desired control force is achieved using two different methods. The first technique uses an optimal compact TSK fuzzy inverse model of MR damper to predict the required voltage to actuate the MR dampers (TSKFInv). The approach to train the proposed inverse model is explained in Chapter 2. Another semi-active voltage controller is also introduced here which works based on the maximum and minimum capacities of MR damper at each time-step. Using the response of structure at each time-step, the maximum (passive on) and minimum (passive off) forces that can be generated by an MR damper is obtained by a simple forward model. Then considering a linear relation between these two operating points, the required voltage to produce a desired force is estimated. The method is designated as MaxMin Optimal Controller. Both semi-active algorithms, developed here use acceleration feedback only. In case the acceleration is not available at some storeys, a Kalman Filter is designed to estimate the required unknown response. The primary controller designed in this study to be combined with

voltage controllers, is LQG. The results demonstrate that both TSKFInv and MaxMin algorithms are quite effective in seismic response reduction for wide range of motions from moderate to severe seismic events, compared with the passive systems and performs better than original and Modified clipped optimal controller systems, known as COC and MCOC.

The rest of this chapter is organised as follows: in the first section, a literature review is given on different MR damper semi-active control strategies. Then the control strategies will be explained and applied to a 20-storey nonlinear benchmark building subjected to 10 different earthquake signals. The numerical results will be shown and conclusion drawn at the end.

4.2 INTRODUCTION AND BACKGROUND

One of the challenging tasks for civil engineers is to mitigate the response of a structure subjected to dynamic loads in order to reduce the risks of damage and injuries caused by extreme hazards such as earthquakes and strong winds. Earthquake engineers, however, have a number of options to design buildings that can resist earthquake loading, e.g. structural elements can be stiffened, bracing can be introduced, the structure can be isolated from the ground (base isolation) or dampers can be used (Chopra 1995).

Magnetorheological (MR) dampers are semi-active damping devices first described in the context of civil engineering by Dyke et al. (Dyke et al. 1996b). They resemble conventional viscous dampers but are filled with MR fluid. As discussed earlier in Chapter 2, The main advantages of MR dampers are that they can generate relatively large controllable damping forces by tuning the magnetic field applied to the fluid (Carlson & Jolly 2000). They adapt with very fast response times over broad temperature ranges (–40 to 150C) while having low power requirements and a fail-safe performance in the case of power-cuts (Dyke et al. 1996b).

One of the challenges in the application of MR dampers is using an appropriate control algorithm to determine their command voltage. In developing the control laws, note that it is not possible to directly command the i^{th} MR damper to generate a specified force, f_i , because the response of the MR damper is dependent on the local motion of

the structure where the MR damper is attached. However, the force produced by the MR damper may increase or decrease by adjusting the value of the voltage applied to the current driver v_i. Based on this observation, the following guidelines are used in developing the control laws: i) the control voltage to the i^{th} device is restricted to the range $v_i = [0, V_{max}]$, and ii) for a fixed set of states, the magnitude of the applied force $|f_i|$ increases when v_i increases, and decreases when v_i decreases. Furthermore, the first order lag in the device model (representing the dynamics involved in the current driver and electromagnet) limits the rate at which the MR effect is realised. Thus, in developing the control laws, one must consider the fact that the force varies continuously even when a step command signal is applied.

4.2.1 Control Based on Lyapunov Stability Theory

Let the linear equations of motion of a structure be written in state-space form as:

$$\dot{z} = Az + Bf + E\ddot{x}_g \tag{4.1}$$

$$y = Cz + Df + v \tag{4.2}$$

where Z is the state vector, $\mathcal{Y}$ is the vector of measured outputs, and $\mathcal{V}$ is the measurement noise vector.

In some cases it is possible to employ Lyapunov's direct approach for stability analysis in the design of a feedback controller (Brogan). The approach requires the use of a Lyapunov function, denoted $V(z)$, which must be a positive definite function of the states of the system, Z. Let us assume that the origin is a stable equilibrium point. According to Lyapunov stability theory, if the rate of change of the Lyapunov function, $\dot{V}(z)$, is negative semi-definite, the origin is stable (in the sense of Lyapunov). Thus, in developing the control law, the goal is to choose control inputs for each device that will result in making $\dot{V}$ as negative as possible. An infinite number of Lyapunov functions may be selected, that may result in a variety of control laws.

Leitmann applied Lyapunov's direct approach for the design of a semi-active controller (Leitmann 1994). In this approach, a Lyapunov function is chosen of the form

$$V(z) = \frac{1}{2}\|z\|_P^2 \tag{4.3}$$

where $\|z\|_P$ is the P-norm of the states defined by

$$\|z\|_P = [z^T P z]^{1/2} \tag{4.4}$$

and P is a real, symmetric, positive definite matrix. In the case of a linear system, to ensure $\dot{V}$ is negative definite, the matrix P is found using the Lyapunov equation

$$A^T P + PA = -Q_P \tag{4.5}$$

for a positive definite matrix Q_p. The derivative of the Lyapunov function for solution of Equation. 4.1 is

$$\dot{V} = -\frac{1}{2} z^T Q_P z + z^T PBf + z^T PE\ddot{x}_g \tag{4.6}$$

The only term which can be directly affected by a change in the control voltage is the middle term which contains the force vector f. Thus, the control law which will minimise $\dot{V}$ is

$$v_i = V_{\max} H((-z)^T PB_i f_i) \tag{4.7}$$

where $H(.)$ is the Heaviside step function, f_i is the measured force produced by the i^{th} MR damper, and B_i is the i^{th} column of the B matrix in Equation. 4.1. Notice that this algorithm is classified as a bang-bang controller, and is dependent on the sign of the measured control force and the states of the system. To implement this algorithm, a Kalman filter can be used to estimate the states based on the available measurements (*i.e.*, device displacements, device forces, structural accelerations). Thus, in this algorithm, better performance is expected when full measurements of the structural responses are used. However, one challenge in the use of the Lyapunov algorithm is in the selection of an appropriate Q_p matrix.

4.2.2 Decentralised Bang-Bang Control

McClamroch and Gavin used a similar approach to develop the decentralised bang-

bang control law for use with an electrorheological damper (McClamroch & Gavin 1995). In this approach, the Lyapunov function was chosen to represent the total vibratory energy in the structure (kinetic plus potential energy), as in

$$V = \frac{1}{2} x^T K_s x + \frac{1}{2} (\dot{x} + \Gamma \dot{x}_g)^T M_s (\dot{x} + \Gamma \dot{x}_g) \tag{4.8}$$

The rate of change of the Lyapunov function is then

$$\dot{V} = \frac{1}{2} x^T K_s \dot{x} + (\dot{x} + \Gamma \dot{x}_g)^T (-C_s \dot{x} - K_s x + \Lambda f) \tag{4.9}$$

In this expression, the only way to directly effect $\dot{V}$ is through the last term containing the force vector f. To control this term and make $\dot{V}$ as large and negative as possible (maximising the rate at which energy is dissipated), the following control law is chosen

$$v_i = V_{\max} H(-(\dot{x} + \Gamma \dot{x}_g)^T \Lambda_i f_i) \tag{4.10}$$

where Λ_i is the i^{th} column of the Λ matrix. Note that, because the only non-zero terms in the Λ matrix are those corresponding to the location of the MR dampers, this control law requires only measurements of the floor velocities and applied forces. Interestingly, when any of the semi-active devices are located between the ground and first floor, the absolute velocity of the first floor is required. When the control device is located in the upper floors, the inter-storey velocity is needed. Therefore, to implement this control algorithm, one would approximate the absolute velocity (obtaining the pseudo velocity) by passing the measured accelerations through a second order filter with the following transfer function (Spencer, Dyke & Deoskar 1998)

$$T(s) = \frac{39.5s}{39.5s^2 + 8.89s + 1}. \tag{4.11}$$

4.2.3 Maximum Energy Dissipation

This control algorithm is presented as a variation of the decentralised bang-bang approach (McClamroch & Gavin 1995). In the decentralised bang-bang approach, the Lyapunov function was chosen to represent the total vibratory energy in the system. Let us, instead, consider a Lyapunov function which represents the relative vibratory

energy in the structure (*i.e.*, without including the velocity of the ground in the kinetic energy term), as in

$$V = \frac{1}{2} x^T K_s x + \frac{1}{2} x^T M_s \dot{x} \tag{4.12}$$

Using the same procedure applied to develop the decentralised bang-bang approach, the term which can be directly affected by changes in the control voltage is identified and the following control law is obtained

$$v_i = V_{\max} H(-\dot{x}^T \Lambda_i f_i) \tag{4.13}$$

where Λ_i is the i th column of the Λ matrix. Note that this equation is also a bang-bang control law. As in the decentralised bang-bang approach, only local measurements (*i.e.*, the velocity and control force) are required to implement this control law. Note that if the semi-active device is not located on the first floor of the structure, the resulting control law will be the same as in the decentralised bang-bang approach. However, if the control device is on the first floor, the control action depends on the relative velocity measurement rather than the absolute velocity which was used in the decentralised bang-bang approach. Both a numerical differentiation of the measured device displacements and a subtraction of the absolute velocities using Equation. 4.11 can be considered to determine the relative velocities.

Notice that the resulting control law will command the maximum voltage when the measured force and relative velocity are dissipating energy (producing large dissipative forces), and command the minimum voltage when energy is not being dissipated (producing small forces when the force is not dissipative). Thus, herein it is called the maximum energy dissipation algorithm.

4.2.4 Modulated Homogeneous Friction

Another semi-active control algorithm was originally proposed for use with a variable friction damper (Inaudi 1997). This algorithm is considered herein because there are strong similarities between the behaviour of a variable friction device and of the MR damper. In this approach, at every occurrence of a local extreme in the deformation of the device (*i.e.*, when the relative velocity between the ends of the semi-active device is zero), the normal force applied at the frictional interface is updated to a new value. The

normal force, $N_i(t)$, is chosen to be proportional to the absolute value of the deformation of the semi-active device. The control law is written as

$$N_i(t) = g_i \left| P[\Delta_i(t)] \right| \tag{4.14}$$

where g_i is a positive gain, and the operator $P[.]$ (referred to as the prior-local-peak operator) is defined as

$$P[\Delta_i(t)] = \Delta_i(t-s), \quad \text{where} \quad s = \{\min x \geq 0 : \dot{\Delta}_i(t-x) = 0\}, \tag{4.15}$$

defining $\Delta_i(t-s)$ as the most recent local extreme in the deformation of the i^{th} device.

Because this algorithm was developed for use with a variable friction device, the following modifications were necessary to apply it to the MR damper: i) there is no need to check if the force is greater than $\mu N_i(t)$, where μ is the coefficient of friction, because the MR damper is not subject to static friction, and ii) a force feedback loop was implemented to induce the MR damper to produce approximately the frictional force corresponding to the desired normal force. Thus, the goal is to generate a desired control force with a magnitude

$$f_{ni} = \mu g_i \left| P[\Delta_i(t)] \right| = g_{ni} \left| P[\Delta_i(t)] \right| \tag{4.16}$$

where the proportionality constant g_{ni} has units of stiffness (N/cm). For further clarification, Figure 4.1shows a plot of the typical desired control force produced by this algorithm as a function of the device displacement. $f_{ni} = g_{ni}\Delta_i$ is shown here as a dashed line because at each peak in the displacement, the magnitude of the desired control force is selected according to this relationship.

Because the force produced by the MR damper cannot be directly commanded, a force feedback loop is used. The measured force is compared to the desired force determined by Equation. 4.16, and the resulting control law is

$$v_i = V_{\max} H\left(f_{ni} - \left| f_i \right|\right) \tag{4.17}$$

An appropriate choice of g_{ni} will keep the force f_{ni} within the operating envelope of each MR damper for majority of the time, allowing the MR damper forces to closely

approximate the desired force of each device. However, the optimal value of g_{ni} is dependent on the amplitude of the ground excitation. Additionally, notice that this control law is quite straightforward to implement because it requires only measurements of applied force and the relative displacements of the control device.

4.2.5 Clipped-Optimal Control

As mentioned previously, MR devices are highly nonlinear. Often the most effective nonlinear control algorithm is dependent on the specific device which is to be implemented, and the measurements available. For civil structures these measurements are typically absolute accelerations, as well as device displacement and force applied by the device. The clipped-optimal method is very well adapted to these conditions, and is, therefore, a good choice for semi-active control of a civil structure. Essentially, it is an attempt to mimic optimal active control with semi-active devices.

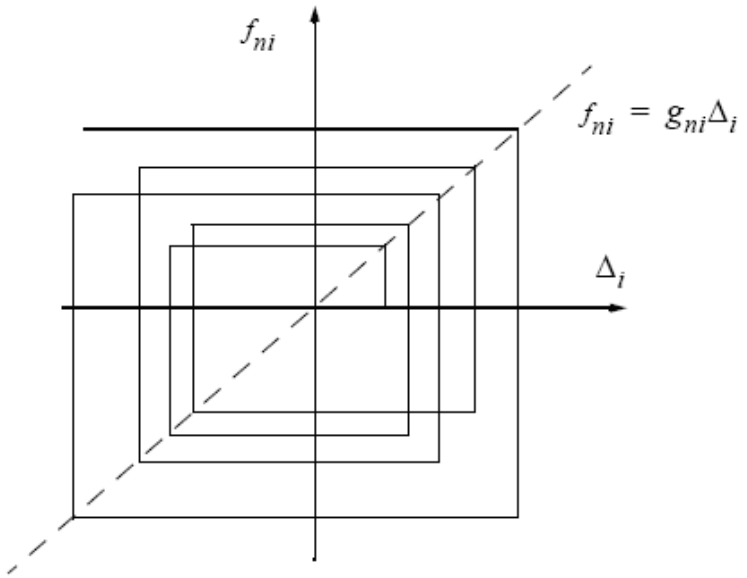

Figure 4.1. Typical desired control force produced with the Modulated Homogeneous Friction algorithm

For a system with *n* MR dampers, the approach utilised in the clipped-optimal control algorithm is to maintain *n* force feedback loops that induce each MR damper to produce approximately the desired control force. The desired control force of the i^{th} MR damper is denoted as f_{ci}.

Due to the fact that the forces generated in the MR dampers are dependent on the local

responses of the structural system, the desired optimal control force f_{ci} cannot always be developed in the MR damper. The control voltage v_i is the only variable which can be directly controlled to increase or decrease the force produced by the device. Therefore, a force feedback loop is introduced such that the forces produced by the MR damper will be approximately equal to the desired optimal control force f_{ci}.

The approximation of the desired optimal force is achieved in the following manner. The algorithm compares the magnitude and direction of the measured forces in the MR devices and the optimal forces output by the nominal optimal controller. This results in three classifications: i) the force commanded is larger in magnitude than the force applied; ii) the commanded force is smaller in magnitude than the applied force; iii) and the forces are of opposite sign. The first category results in the command of maximum voltage, whereas categories two and three result in the command of minimum voltage. The algorithm for selecting the command signal for the i^{th} MR damper is graphically represented in Figure 4.2 and can be stated as

$$v_i = V_{\max} H(\{f_{ci} - f_i\} f_i) \tag{4.19}$$

where $V_{\max}$ is the maximum voltage to the current driver, and $H(\,.\,)$ is the Heavyside step function. This cycle of maximum and minimum voltages commanded results in the force applied by the MR damper mimicking as best as possible the optimal force dictated by the primary controller.

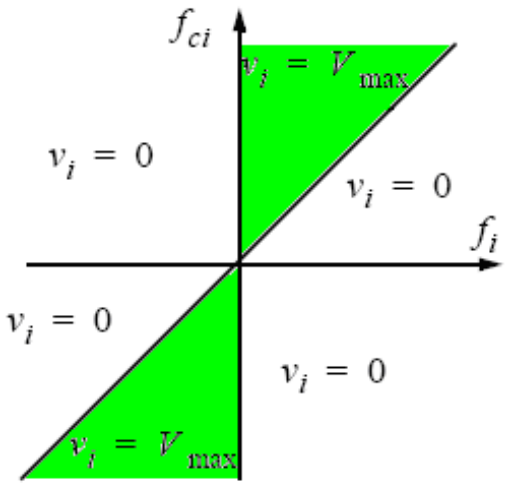

Figure 4.2. Graphical representation of clipped-optimal control algorithm.

4.2.6 Modified Clipped-Optimal Control

In the original clipped-optimal control algorithm, the command voltage takes on values of either zero or the maximum value. In some situations when the dominant frequencies of the system under control are low, large changes in the forces applied to the structure may result in high local acceleration values. Yoshida and Dyke proposed a modification to the original clipped-optimal control algorithm to reduce this effect (Yoshida & Dyke 2004). In the modified version of the algorithm, the control voltage can be any value between 0 and V_{max}. The control voltage is determined using a linear relationship between the applied voltage and the maximum force of MR damper. When the desired force is larger than the maximum force that the device can produce, the maximum voltage is applied. This modified clipped-optimal control algorithm is graphically represented in Figure 4.3, and can be given as follows:

$$v_i = V_{ci} H(\{f_{ci} - f_i\} f_i) \tag{4.20}$$

in which

$$V_{ci} = \begin{cases} \mu_i f_{ci} & for \quad f_{ci} \le f_{\max} \\ V_{\max} & for \quad f_{ci} > f_{\max} \end{cases} \tag{4.21}$$

where $\mu = V_{max}/f_{max}$ and f_{max} is the maximum force of the MR damper. They showed that the modified clipped-optimal control algorithm is typically able to achieve a significant reduction in the peak accelerations over that of the original clipped-optimal control algorithm (Yoshida & Dyke 2004).

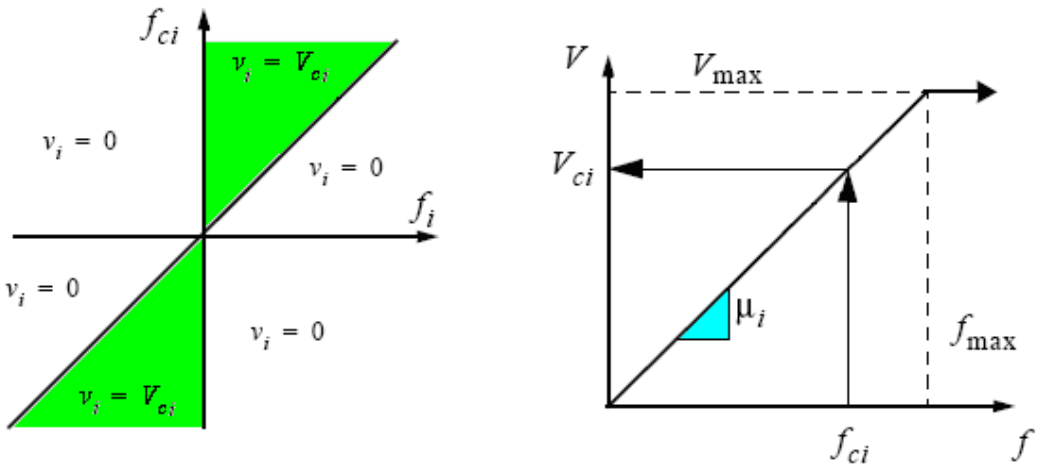

Figure 4.3.Graphycal representation of modified clipped-optimal control algorithm.

4.2.7 Signum Function Controller

This MR damper controller is based on signum function and can be expresses as:

$$v_{Sign} = v_{Sign}\,1 \times v_{Sign}\,2 \tag{4.22}$$

Where

$$v_{Sign}\,1 = \frac{V_{max}}{2N}\left\{\sum_{0\le j\le N-1}\{sgn\{[f_c-(1+Kj)f]f\}+1\}\right\}$$

$$v_{Sign}\,2 = 1-\left[\frac{sgn\left((V_{max}/2N)\{\sum_{0\le j\le N-1}\{sgn\{[f_c-(1+Kj)f]f\}+1\}\}-V_{max}\right)+1}{2}\right] \tag{4.23}$$

$$\cap\left[\frac{1-sgn(f\dot{f})}{2}\right]$$

which in, $\mathrm{sgn}(.)$ is the signum function; $\cap$ is the logical AND; f_c, f and V_{max} are defined as in Equation (4-19); N is an integer with $0 \le j \le N-1$; K is a small constant; and $\dot{f}$ is the time derivative of f.

In fact, Equation (4-22) alone can be used as a damper controller. The graphical illustration of $v_{Sign}\,1$, is shown in Figure 4.4, in which three cases including $f_c \gg f$, $f_c \approx f$ and $f_c \ll f$ are illustrated in Figure 4.4(a)-(c), respectively. In this figure, only the cases for $f > 0$ and $f_c > 0$ are shown. It can be illustrated in other cases too.

The graphical explanation of $v_{Sign}\,2$, is shown in Figure 4.5, when the condition $v_{Sign}\,2 \ge V_{max}$ is satisfied. When $v_{Sign}\,2 \ge V_{max}$ and $f\dot{f} < 0$, then $v_{Sign}\,2 = 0$ and $v_{Sign} = 0\ (= V_{min})$; othervise, $v_{Sign}\,2 = 1$ and $v_{Sign} = v_{Sign}\,1$. Thus $v_{Sign}\,2$ is a dimension-less quantity with two values of 0 and 1, and the conditions are shown in Figure 4.5.

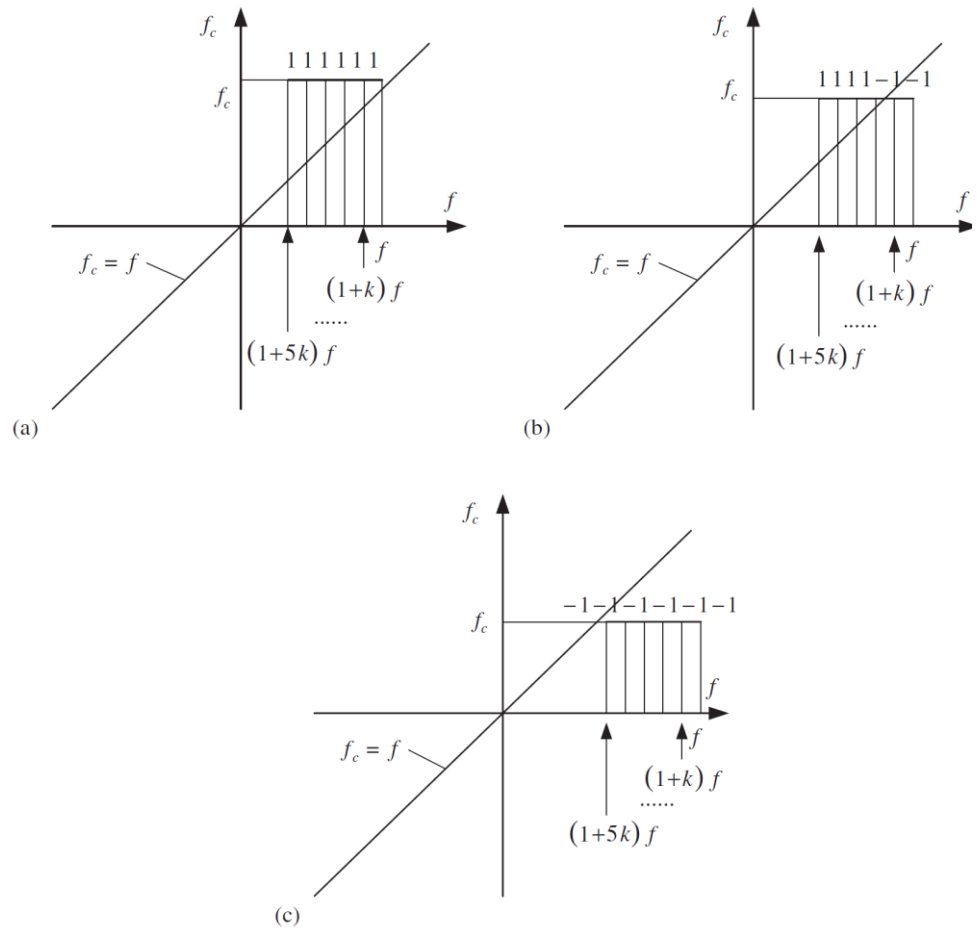

Figure 4.4.Graphical representation of $\boldsymbol{v_{Sign}1}$ *(*$\boldsymbol{N = 6}$, $\boldsymbol{k < 0}$, $\boldsymbol{f_c > 0}$, $\boldsymbol{f\ > 0}$*): (a)* $\boldsymbol{f_c \gg f}$ *and* $\boldsymbol{v_{Sign}1 = V_{max}}$*; (b)* $\boldsymbol{f_c \approx f}$ *and* $\boldsymbol{v_{Sign}1 = 2/3\,V_{max}}$*; and (c)* $\boldsymbol{f_c \ll f}$ *and* $\boldsymbol{v_{Sign}1 = 0}$.

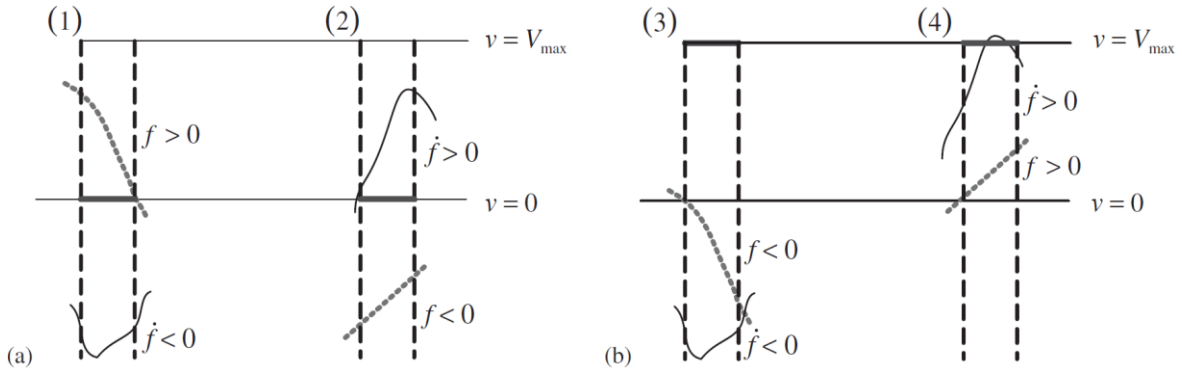

Figure 4.5. Graphical representation of $\boldsymbol{v_{Sign}2}$ *provided that the condition* $\boldsymbol{v_{Sign}1 \geq V_{max}}$ *is satisfied: (a) if* $\boldsymbol{f\dot{f} < 0}$*, then* $\boldsymbol{v_{Sign}2 = 0}$, $\boldsymbol{v_{Sign}2 = 0}$ *(=*$\boldsymbol{V_{min}}$*)and (b)if* $\boldsymbol{f\dot{f} > 0}$*, then* $\boldsymbol{v_{Sign}2 = 1}$, $\boldsymbol{v_{Sign} = v_{Sign}1}$.

4.2.8 Soft Computing Based Control

Extensive literature on the use of soft computing techniques for structural control can be found. Neural networks, fuzzy logic and genetic algorithms are examples of the methodologies most widely applied to semi-active modelling and control of MR dampers. For instance, Kim et al, conducted full-scale experiments on a single degree of freedom mass equipped with a hybrid base isolation system comprised of a friction pendulum system and a magnetorheological damper (Kim et al. 2006). The fuzzy logic controller takes the displacement and acceleration readings of the structure to calculate the appropriate signals to drive the MR damper. Both the friction pendulum and the MR damper were modelled by ANFIS approaches. This work was later improved by Kim and Roschke employing genetic algorithm to optimise the fuzzy models (Schurter & Roschke 2000). Many other researchers have also designed and used fuzzy/NN controller to command the MR dampers (Das, Datta & Madan 2012; Du et al. 2013; Wang & Liao 2005).

Soft computing methods can also be combined with model-based controllers to estimate the required voltage of MR dampers in order to produce desirable control force. This can be done through portraying the inverse behaviour of MR damper. This idea was first introduced by Chang (Chang & Zhou 2002). He trained a recurrent neural network (RNN) and used it in linear structures to estimate damper force based on the inputs of displacement, velocity and voltage. Many other techniques, based on artificial intelligence, have been reported to construct a proper inverse model of MR damper to be combined with the primary controller (Karamodin et al. 2009; Zong et al. 2012). The performance of such systems is dependent on the accuracy of the model. However, most of these works suffer from being complex or not accurate enough. They also need full state response, such as velocity and displacement of the two consecutive floors, where in between, the MR damper is installed.

In this chapter, two new semi-active approaches are proposed. The first one uses the method introduced in Chapter 2 to model the inverse behaviour of a 1,000kN MR damper using the acceleration feedback and desired force only. The proposed dynamic inverse model considers the generated force of MR damper at previous time step as an indication of the status of MR damper and produces a proper voltage at the current time step. Such force can directly come from the force sensors, however, a TSK forward

model of MR damper is designed here to estimate the proposed required force and, thus, avoid using load cells.

In the second approach, the maximum and minimum possible forces of MR damper at each time-step are found, using one of the available parametric or non-parametric forward models. Then, considering a linear relation between damper's voltage and force, the required voltage of MR damper to produce a desired force is obtained. The algorithm benefits from being simple, accurate and force-sensor-less. The latest feature is important as it is not always possible to install force sensors in certain large-scale applications due to mechanical or cost constraints. However, depending on which forward model is used, it may need extra sensors to measure the responses of the structure.

4.3 CASE STUDY: 3RD GENERATION 20-STOREY NONLINEAR BENCHMARK BUILDING

The case study that is considered here, is a benchmark building of 20-storeys designed for the Los Angeles region as defined by Ohtori in the problem definition (Ohtori et al. 2004). Based on the literature review, only few semi-active based controls have been reported to mitigate the seismic responses of this benchmark structure (Askari & Davaie-Markazi 2008; Askari, Li & Samali 2011; Bitaraf & Hurlebaus 2013; Karamodin et al. 2009).

Ten earthquake records are used in the simulation, using the original four earthquake records with different intensities. These records are the El Centro (1940) and Hachniohe (1968) earthquake records with 0.5, 1.0, and 1.5 intensity, and Northridge (1994) and Kobe (1995) earthquake records with 0.5 and 1.0 intensity.

25 MR dampers with capacity of 1,000 kN each are optimally placed throughout the stories of the 20-storey benchmark building as shown in Figure 4.6. This configuration is obtained using the optimisation algorithm introduced in Chapter 3. It should be noted that, the effects of two proposed semi-active voltage controllers in the optimisation of MR dampers layout have not been considered here. However, since the nominal controller of all two strategies is same, the optimal places of control devices would not be much different. The main aim here in this Chapter, is comparing the performances

of the aforementioned strategies based on a fixed configuration of control devices and the optimal configuration of MR dampers integrated with the proposed control strategies, can be studied in details in future.

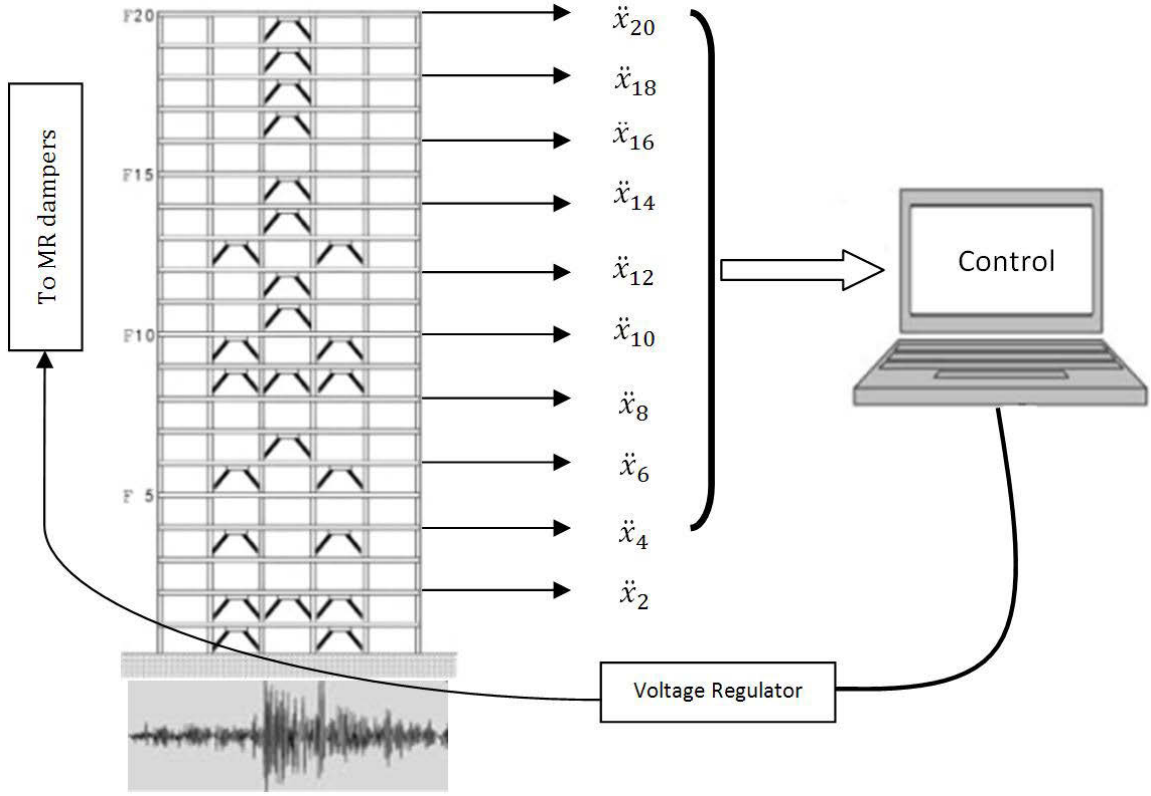

Figure 4.6. MR damper and accelerometer configurations

4.4 Proposed Control Strategies

The proposed controller for the MR damper is shown in Figure 4.7 and consists of two components which are the primary controller to produce the desired force and the voltage controller to convert desired force to the required voltage for MR dampers. There is basically no restriction on the type of control algorithm that calculates a desirable control force f_d based on response and/or excitation.

Both controllers use the acceleration feedback only as accelerometers are more convenient than LVDTs and GPS measurement tools, in terms of installation and cost. Therefore, ten sensors for acceleration measurements are used for feedback into the control system on the 2nd, 4th, 6th, 8th, 10th, 12th, 14th, 16th, 18th and 20th floors. In case the acceleration response of the structure at some levels is not available, a Kalman filter

observer is designed to estimate the acceleration of the proposed storeys based on the available measurements.

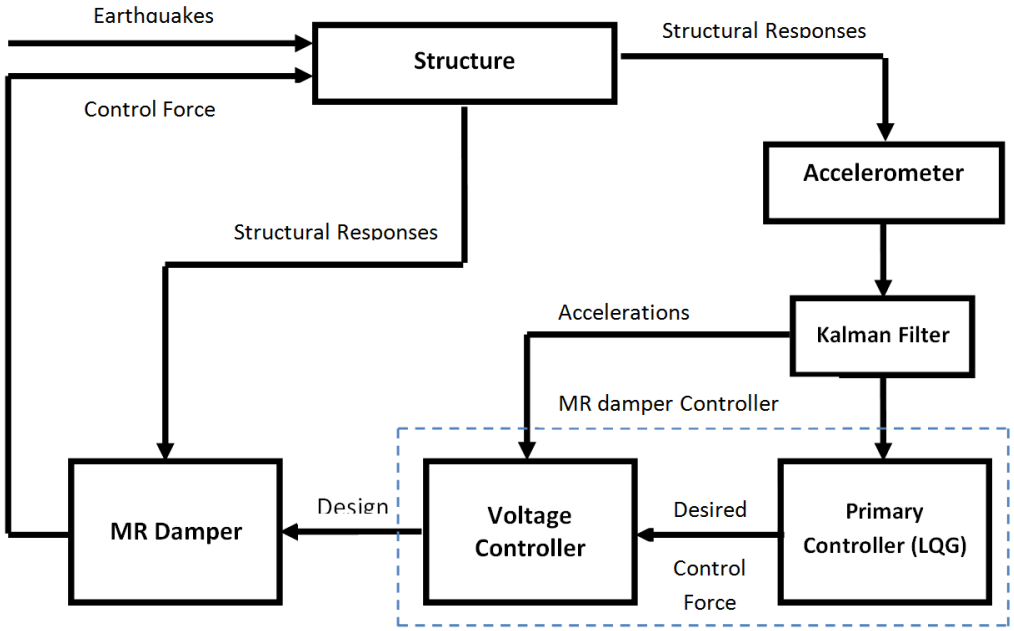

Figure 4.7. Block diagram of semi-active control strategy

4.4.1 Primary Controller and Kalman Filter Observer Design

Although there is no limitation on the type of controllers, as long as it measures the desired force based on the system response, a Linear Quadratic Gaussian (LQG) controller is designed in this study using the acceleration feedbacks (measured and estimated), to generate the desired control force to be passed to the inverse model of MR damper.

The force vector for control devices can be modelled as

$$\mathrm{f} = \mathrm{K_f u} \tag{4.24}$$

where K_f is a matrix that accounts for multiple actuators per level.

Because the benchmark building model is quite large, a reduced-order model of the system, designated as *the design model*, is developed for purposes of control design. The equations relevant to this 20-storey structure is given as

$$\begin{aligned}\dot{x}^d &= A_d x^d + B_d u + E_d \ddot{x}_g \\ y_{md} &= D_s(C_{md} x^d + D_{md} u + F_{md} \ddot{x}_g) + \upsilon \\ y_{ed} &= C_{ed} x^d + D_{ed} u + F_{ed} \ddot{x}_g\end{aligned} \tag{4.25}$$

where x^d is the design state vector, $y_{md} = [\ddot{x}_{a2}, \ddot{x}_{a4}, \ddot{x}_{a6}, \ddot{x}_{a8}, \ddot{x}_{a10}, \ddot{x}_{a12}, \ddot{x}_{a14}, \ddot{x}_{a16}, \ddot{x}_{a18}, \ddot{x}_{a20}]^T$ is the vector of measured responses , $y_{ed} = [\ddot{x}_{a1} \quad ... \quad \ddot{x}_{a20}]^T$ is the vector of the regulated responses (lateral acceleration at each floor), u is the control signal for the control force of the individual ideal actuators, and A_d, B_d, E_d, C_{md}, D_{md}, F_{md}, C_{ed}, D_{ed}, and F_{ed} are reduced-order coefficient matrices.

To simplify designing of the LQG controller, $\ddot{x}_g$ is taken to be a stationary white noise, and an infinite horizon performance index is chosen that weighs the accelerations of the floors, i.e.,

$$\hat{J} = \lim_{\tau \to \infty} \frac{1}{\tau} E[\int_0^{\tau} \{(C_{ed} x^d + D_{ed} u)^T Q (C_{ed} x^d + D_{ed} u) + R u^2\} dt] \tag{4.26}$$

where R=[16 × 16] matrix with equal weighting placed on each actuator force (i.e. R=(1/16)[I]) and the weighting matrix Q is chosen to be a [16 × 16] matrix with equal weighting placed on each of the level accelerations (i.e., Q=3 × 10^9[I]). Twenty five actuators are distributed over 16 levels of the proposed 20-storey building as shown in Figure 4.6. Further, the ground acceleration and measurement noises are assumed to be identically distributed, and the ratio of the power spectral densities is taken to be $S_{\ddot{x}_g \ddot{x}_g} / S_{\upsilon_i \upsilon_i} = \gamma_g = 25$.

The separation principle allows the control and estimation problems to be considered separately, yielding a control law of the form

$$u = -\underset{\sim}{K} \hat{x}^d \tag{4.27}$$

where $\hat{x}^d$ is the Kalman filter estimate of the state vector based on the reduced-order design model, including the actuator model. $\underset{\sim}{K}$ is the full state feedback gain matrix for the deterministic regulator problem given by

$$\underset{\sim}{K} = \tilde{R}^{-1}(\tilde{N} + B_d^T \underset{\sim}{P}) \tag{4.28}$$

where $\underset{\sim}{P}$ is the solution of the algebraic Riccati equation given by

$$\underset{\sim}{P}\tilde{A} + \tilde{A}^T \underset{\sim}{P} - \underset{\sim}{P} B_d \tilde{R}^{-1} B_d^T \underset{\sim}{P} + \tilde{Q} = 0 \tag{4.29}$$

and

$$\tilde{Q} = C_{ed}^T Q C_{ed} - \tilde{N}\tilde{R}^{-1}\tilde{N}^T \tag{4.30}$$

$$\tilde{N} = C_{ed}^T Q D_{ed} \tag{4.31}$$

$$\tilde{R} = R + D_{ed}^T Q D_{ed} \tag{4.32}$$

$$\tilde{A} = A_d - B_d \tilde{R}^{-1}\tilde{N}^T \tag{4.33}$$

Calculations to determine $\underset{\sim}{K}$ were done using the *MATLAB* routine *lqry.m* within the control toolbox.

The Kalman filter optimal estimator is given by

$$\dot{\hat{x}}^d = A_d \hat{x}^d + B_d u + L(y_s - C_{md}\hat{x}^d - D_{md}u) \tag{4.34}$$

$$L = [\underset{\sim}{R}^{-1}(\gamma_g F_{md} E_d^T + C_{md} S)]^T \tag{4.35}$$

Where S is the solution of the algebraic Riccati equation given by

$$S\underset{\sim}{A} + \underset{\sim}{A}^T S - S\underset{\sim}{G}S + \underset{\sim}{H} = 0 \tag{4.36}$$

and

$$\underset{\sim}{A} = A_d^T - C_{md}^T \underset{\sim}{R}^{-1}(\gamma_g F_{md} E_d^T) \tag{4.37}$$

$$\underset{\sim}{G} = C_{md}^T \underset{\sim}{R}^{-1} C_{md} \tag{4.38}$$

$$\underset{\sim}{H} = \gamma_g E_d E_d^T - \gamma_g^2 E_d F_{md}^T \underset{\sim}{R}^{-1} F_{md} E_d^T \tag{4.39}$$

$$\underset{\sim}{R} = I + \gamma_g F_{md} F_{md}^T \tag{4.40}$$

Calculations to determine L were done using the MATLAB routine lqe.m within the control toolbox.

4.4.2 Voltage Controller 1: Optimal TSK Fuzzy Inverse Controller (TSKFInv)

In this section, a voltage controller based on inverse model of MR damper is proposed. The controller is used to calculate voltage signals to be sent to the MR damper so that it can produce desired optimal control forces estimated by LQG control algorithm.

To design the inverse model of MR damper, it is important to know that, the model should be both accurate and concise to generate a quick and reliable response in real-time applications. Therefore, the algorithm introduced in Chapter 2 is employed here to select a small structure fuzzy inference system with acceptable accuracy. Since the inverse model uses the delayed force feedback of MR damper, a forward model can be considered to provide the force input in case load cells are not available. However, if use of force sensors is not an issue, the sensors' signal is preferable to use. A schematic of TSKFInv controller is shown in Figure 4.8. To build such forward model, any parametric or non-parametric model of MR damper can be used. In this study, in order to provide a quick, yet accurate response, a TSK fuzzy model is trained using a set of numerical data.

4.4.2.1 Forward Model of 1,000 kN MR Damper using Acceleration Feedback Only

The forward model describes the force characteristics of the MR damper which depends on the excitation signals when a constant voltage is applied. It can be constructed from many different models, such as modified Bouc–Wen, hyperbolic tangent or phenomenological model.

This research employs the optimal TSK fuzzy model proposed in Chapter 2, to derive a concise and precise forward model of a 1,000kN MR damper while the voltage is maintained at a maximum level of 10 V. The output of the forward model is then used as an input signal to the inverse model (Figure 4.8).

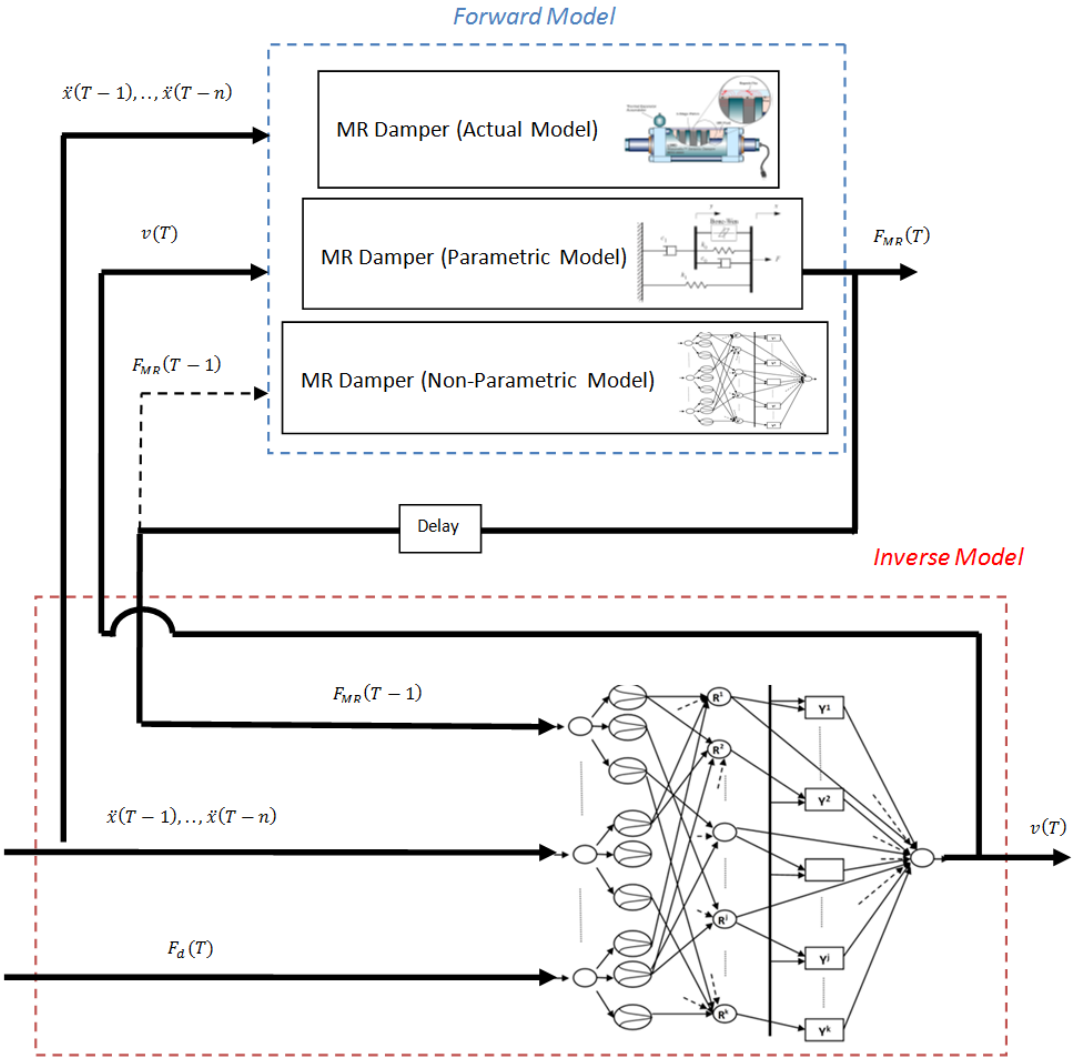

Figure 4.8. TSK Fuzzy inverse optimal controller

The dataset used for training process must include all possible ranges of excitation that may be applied to the MR damper during actual operation. Using the training data shown in Figure 2.8 in Chapter 2 and considering the candidate inputs to be current and past time histories of acceleration, i.e, $\ddot{x}(T-11), \ddot{x}(T-10), \ldots, \ddot{x}(T)$ as well as voltage, $v(T)$ signals, a Pareto front is obtained which helps to design a compact and accurate forward model of the MR damper (Figure 4.9). The proposed forward model, marked by red circle, uses $\ddot{x}(T-9)$, $\ddot{x}(T-8)$, $\ddot{x}(T-4)$, $\ddot{x}(T-2)$, $\ddot{x}(T)$, $v(T)$ as 6 inputs and has 18 fuzzy rules with RMS error of 8.35. The first 6,500 data-points are chosen for training while the last 3,500 are considered as testing data.

4.4.2.2 Inverse Model of 1,000 kN MR damper Model

The training process for designing the inverse model of MR damper is to capture the relationship between the applied voltage and the generated force. The training dataset to do so is the same as the dataset used in the previous section and has a 60 s time-span. The inputs of model will be optimally chosen from 16 candidates. The input candidates for the inverse model are floor accelerations; $\ddot{x}(T-14), \ddot{x}(T-13), \ldots, \ddot{x}(T)$, desired force; $F_d(T)$ and also the damper's force; $F_{MR}(T-1)$. The Pareto front achieved after running the optimisation program is shown in Figure 4.10 where the selected designing point is marked by a red star. The proposed designing point features an inverse fuzzy model with 7 inputs; $\ddot{x}(T-9)$, $\ddot{x}(T-6)$, $\ddot{x}(T-5)$, $\ddot{x}(T-4)$, $\ddot{x}(T-2)$, $F_d(T)$ and $F_{MR}(T-1)$, 19 rules and RMS error of 0.23. The predicted voltage is compared to the reference in Figure 4.11(Hann et al.). Also, Figure 4.11(bottom) shows the comparison between generated force by MR damper using the estimated voltage and the target force; F_d. This can also be considered as the validation of the developed forward model.

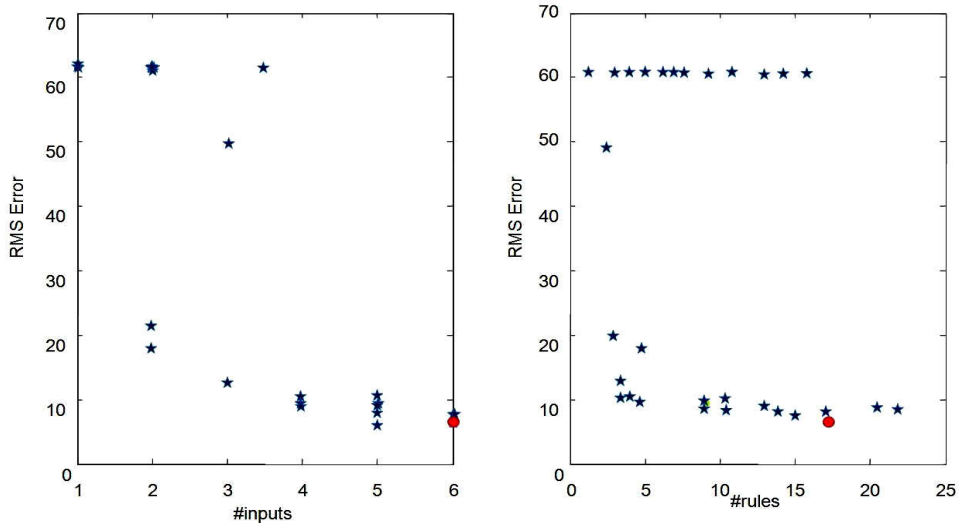

Figure 4.9. Pareto front of forward model of MR damper

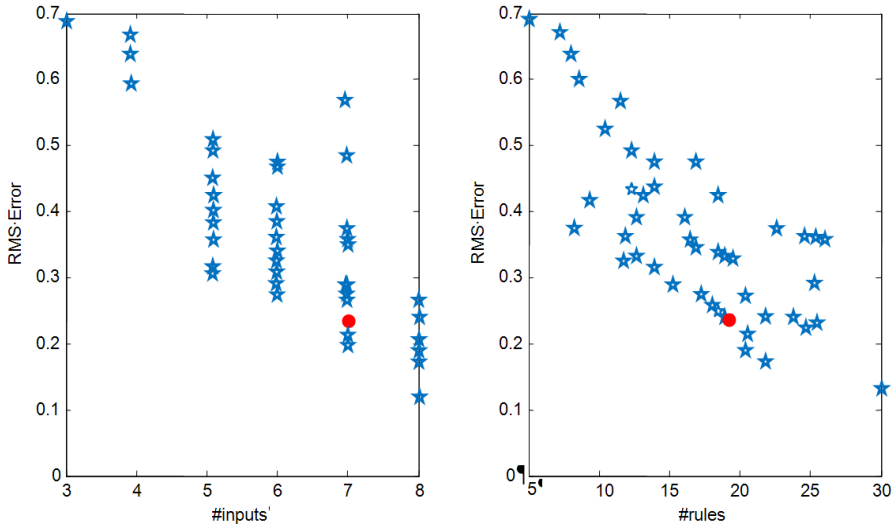

Figure 4.10. Pareto front of inverse model of MR damper

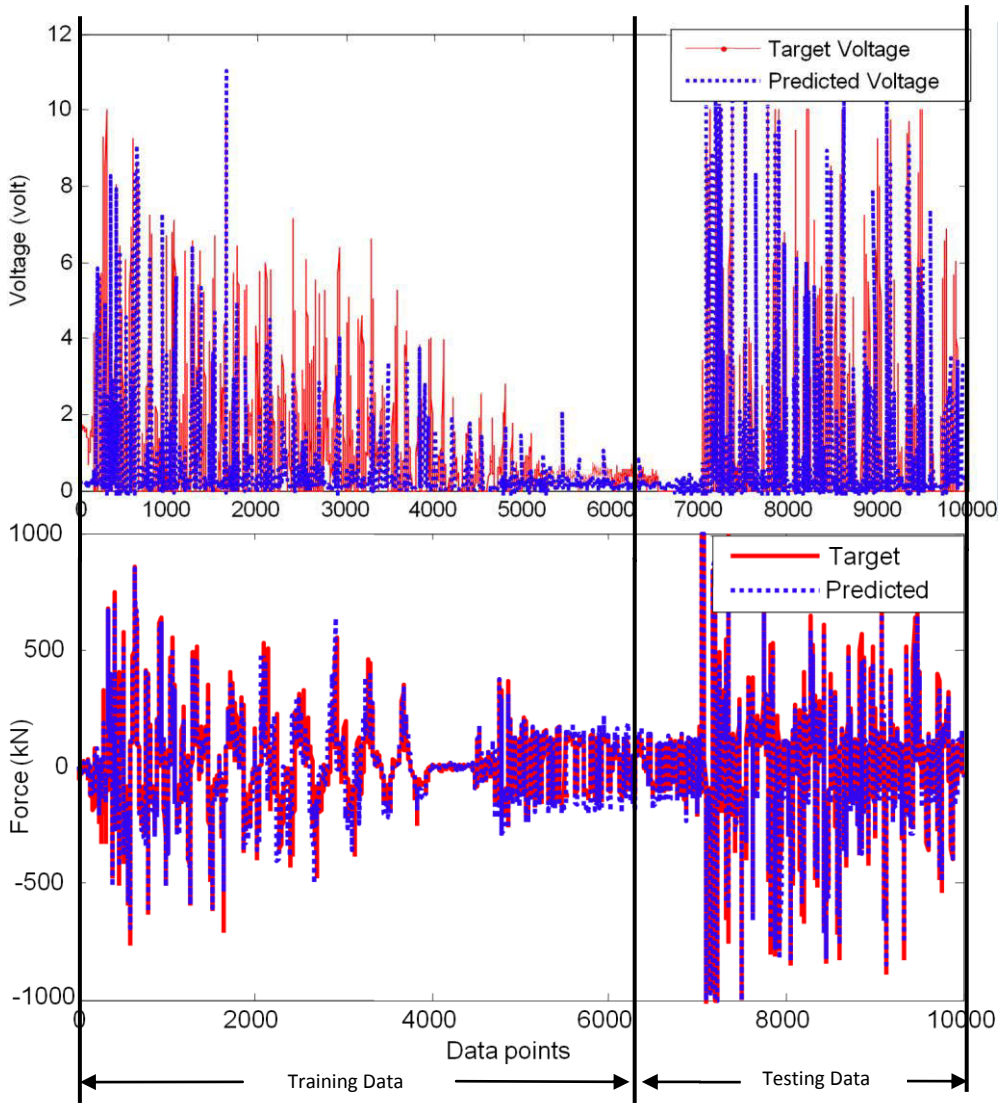

Figure 4.11. Comparison between target and predicted voltage (Hann et al.) and target and predicted force (bottom) using fuzzy inverse and forward models of MR damper

4.4.3 Voltage Controller 2: Max-Min Optimal Controller

Although inverse model of MR damper could estimate the voltage of MR damper to generate a specific desired force, the method needs force feedback which might not be available. Moreover, developing an inverse model is hard due to highly nonlinear behaviour of MR damper. Forward behaviour of MR dampers, on the other hand, is easy to model. Many parametric models are suggested by researchers, as discussed in Chapter 2, that can estimate the generated force of the MR damper in different states. Furthermore, they do not necessarily need force feedback to operate.

Here, a new semi-active control algorithm is proposed based on maximum and minimum generated forces of the MR damper at each time-step. The control law is as follows:

$$v_t = \begin{cases} v_{max} & if \quad |f_{d,t}| > |f_{max,t}| \\ v_{max}\left(\dfrac{|f_{d,t}| - |f_{min,t}|}{|f_{max,t}| - |f_{min,t}|}\right) & if \quad |f_{min,t}| < |f_{d,t}| < |f_{max,t}| \\ 0 & if \quad |f_{d,t}| < |f_{min,t}| \end{cases} \tag{4-41}$$

where, $f_{max,t}$ and $f_{min,t}$ are the maximum and minimum generated forces by the MR damper at time t which correspond to passive-on and passive-off forces. $f_{d,t}$ is also the desired force produced by nominal controller (LQG in this study) at time t. So, if the desired force is less than minimum capacity of the MR damper at time t, the voltage will be set to 0. Similarly, if the desired force is larger than maximum capacity of the MR damper; $f_{max,t}$, the voltage to be sent to the MR damper will be maximum; v_{max}, to produce a force to be as close as possible to the desired force. But, if the desired force is between the maximum and minimum forces of the MR damper, then the voltage takes a portion of maximum voltage. This portion is found by interpolation using a linear relationship between max/min voltage and max/min force of the MR damper. It is interesting to note that if we assume, $f_{min,t}$ and $f_{max,t}$ to be equal to 0 and the total capacity of the MR damper (which is 1,000kN in this study) respectively, then the proposed algorithm is similar to Modified Clipped Optimal Controller. However, this assumption is not correct as the maximum and minimum of the MR damper's forces at each time-step are functions of structural responses which are again functions of time. A schematic diagram for the controller is shown in Figure 4.12.

To find $f_{min,t}$ and $f_{max,t}$, one of the parametric forward models explained in Chapter 2 can be used. However, the complex ones, such as modified Bouc-Wen, are not very applicable to large real-time problems since they are time consuming and the simple ones, on the other hand, are not accurate enough. Therefore, the TSK fuzzy forward model, developed in previous section of this chapter, will be used to provide the maximum and minimum of damper force at each time-step using acceleration feedback.

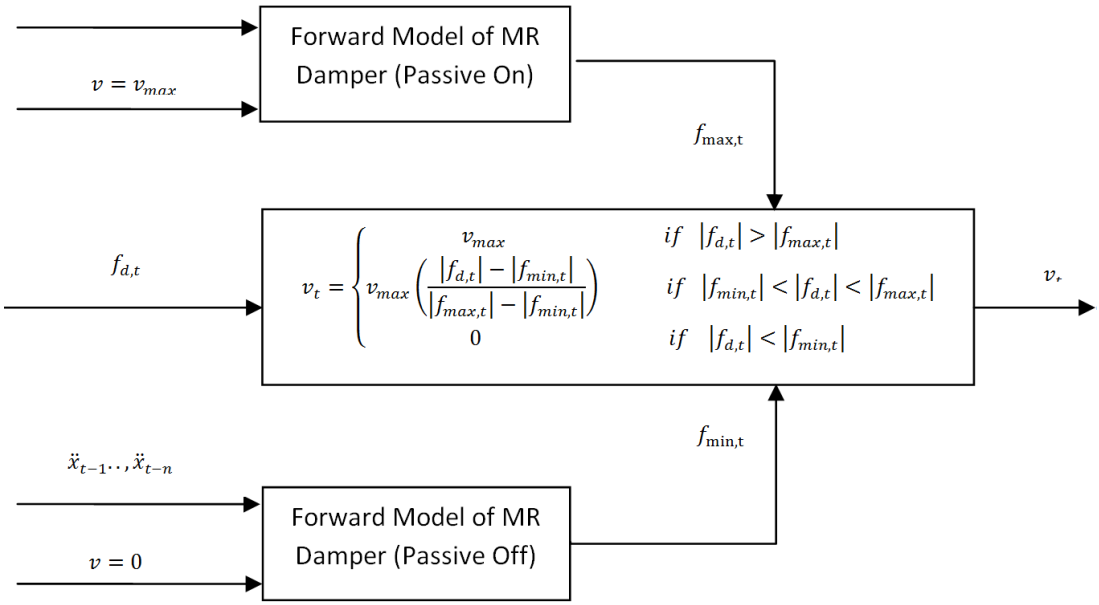

Figure 4.12. Schematic diagram of MaxMin optimal controller (proposed in this study)

4.5 NUMERICAL RESULTS

Two proposed semi-active strategies are validated through a highly nonlinear 20-storey benchmark building under 10 different ground accelerations. To make a comparison, an active control system, semi-active COC and Modified COC systems, together with two passive systems, passive off (POFF) and passive on (Ponsich et al.) are also designed. A *Simulink* model in MATLAB was used to implement the six different control strategies. For the passive control models the voltage is constant, whereas for the semi-active control models, the voltage is obtained through the respective control algorithms.

The comparison between the desired force developed by LQG and the MR damper's generated force using COC, MCOC, TSKFInv and MaxMin algorithms on the 20th floor, are depicted in Figure 4.13 to Figure 4.16 for 4 different earthquakes, each with intensity of 1. Also the required voltages of the MR damper to generate such forces,

using the aforementioned semi-active control approaches, are compared with each other in the same figures. For the sake of better observation and understanding, this comparison is done for a short period of time.

The force time history shown in these figures, illustrates the improvement introduced by MaxMin and TSKFInv algorithms compared to original COC and MCOC. The differences in MR damping forces are attributable to the voltage commanded by the different algorithms. For the MCOC, the voltage varies continuously between zero and a portion of maximum voltage ($v = \mu v_{max}$). This is in stark contrast to the original COC, for which the control voltage can only take two values, 0 and v_{max}. Unlike these two algorithms, both inverse and MaxMin models try to estimate the exact value of voltage which results in generating smooth and robust force signals being very close to the desired force. Consequently, the error between target and MR damper's forces generated by MaxMin and TSKFInv models are less than the original and modified versions of COC. These two methods can also successfully track the desired force while the generated force of COC and MCOC, in comparison, fluctuate a lot and produce many overshoots. As a consequence, the average force and voltage of COC is more than the other semi-active control algorithms. On the other hand, it can be seen that the absolute generated force of the MR damper using MCOC is, most of the time, smaller than the absolute force generated by the other three semi-active control strategies. This is because of the intention of MCOC to work with zero voltage in a wide range of situations, in particular when desired force is less than the damper's force while in reality the voltage is not zero as can be seen from the graphs of voltage history.

The comparison between performances of the two newly proposed semi-active control algorithms also shows that, although both are very effective in tracking the desired force signal, TSKFInv model performs slightly better as it is able to capture almost the exact inverse dynamics of the MR damper and, thus, command the MR damper better than MaxMin which uses a linear relationship between voltage and force of damper.

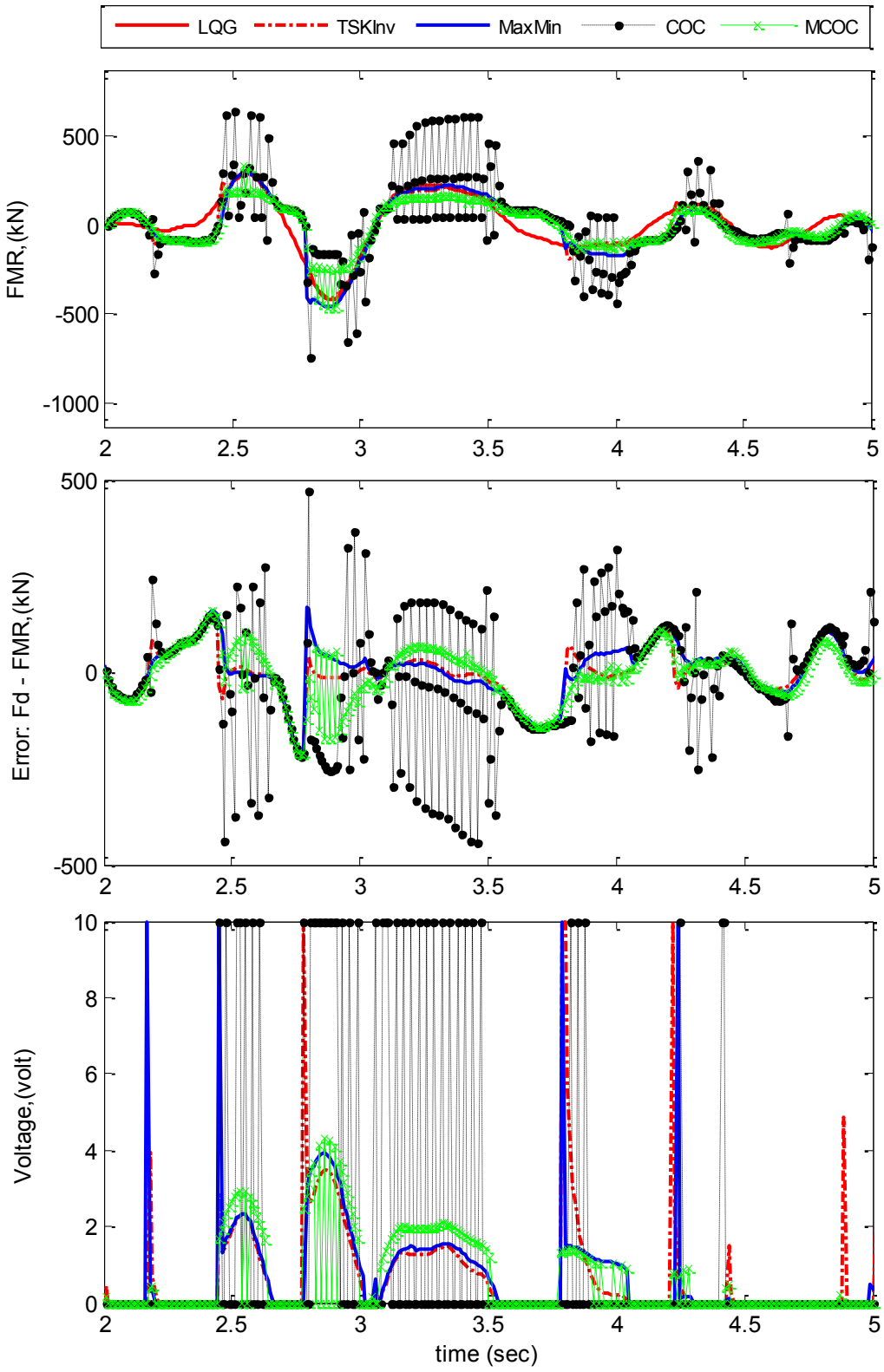

Figure 4.13. MR damper's force and voltage at 20th floor (El-Centro, intensity: 1.0)

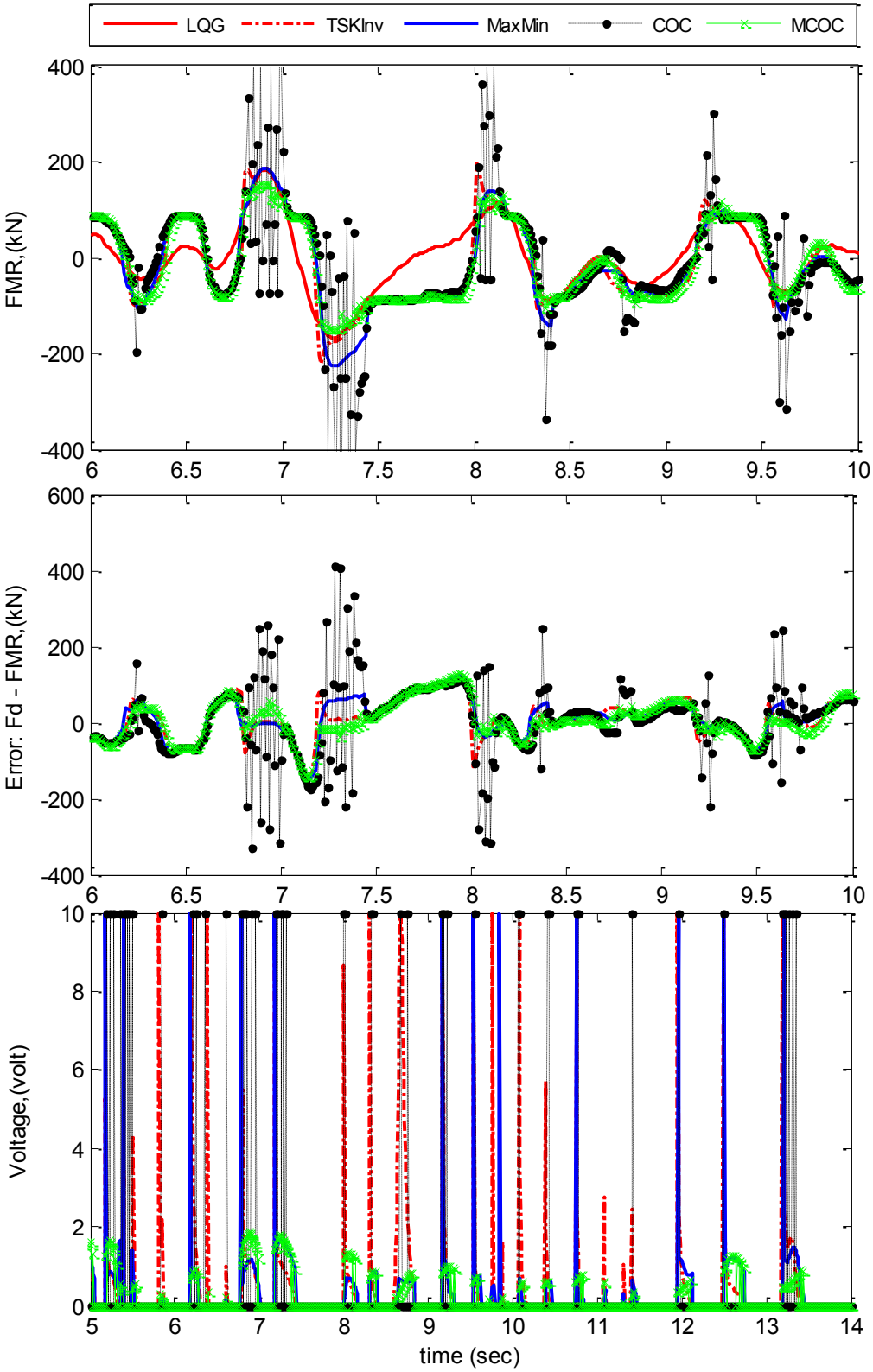

Figure 4.14. MR damper's force and voltage at 20th floor (Hachinohe, intensity:1.0)

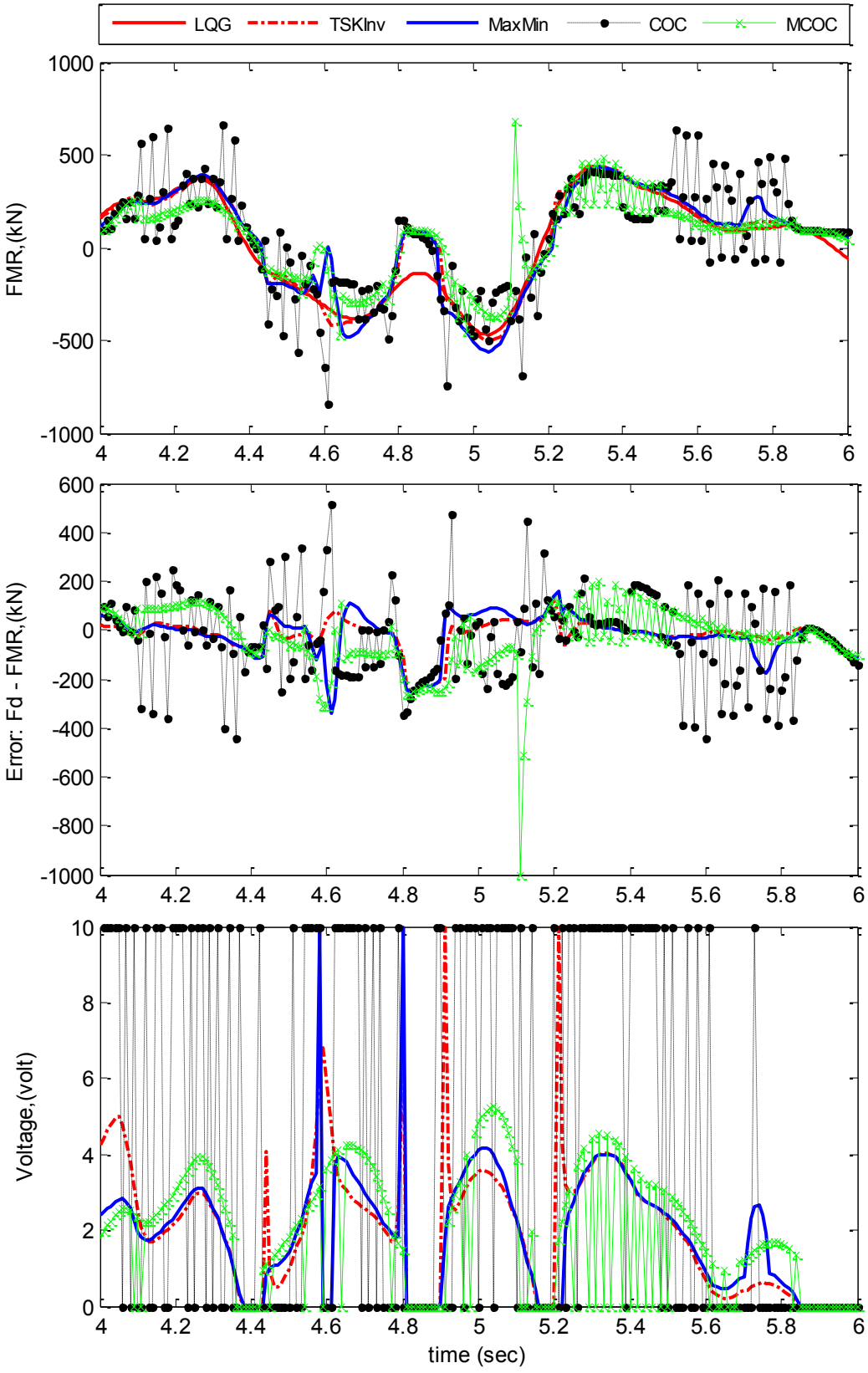

Figure 4.15. MR damper's force and voltage at 20th floor (Northridge, intensity:1.0)

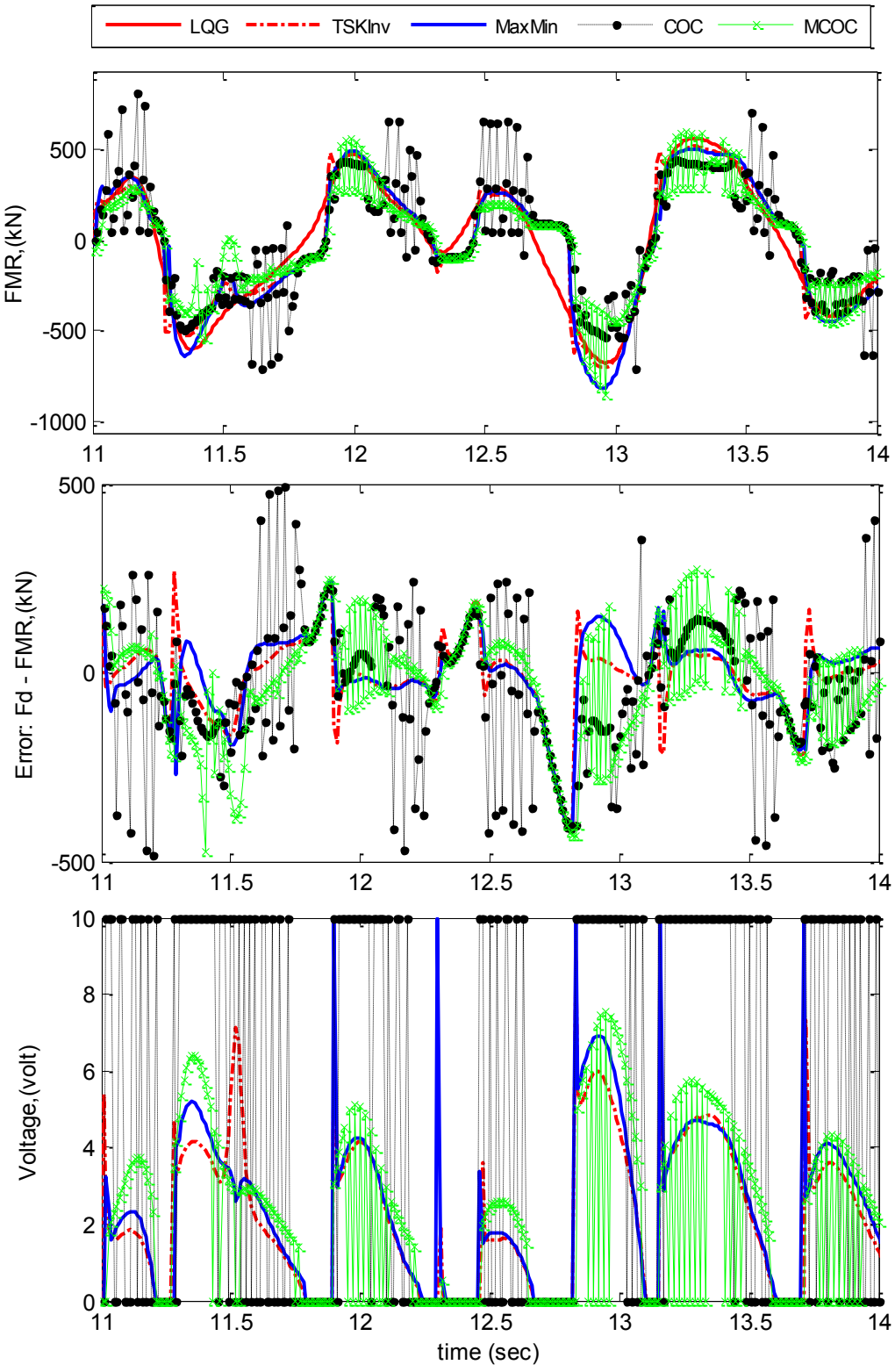

Figure 4.16. MR damper's force and voltage at 20th floor (Kobe, intensity:1.0)

To systematically evaluate the control performance of each controller, the seventeen evaluation criteria defined in the benchmark problem statement, namely, peak drift ratio J_1, peak acceleration J_2, peak base shear J_3, normalised drift ratio J_4, normalised acceleration J_5, normalised base shear J_6, ductility J_7, dissipated energy ratio J_8, plastic connection ratio J_9, normalised ductility J_{10}, control force ratio J_{11}, device stroke J_{12}, control power J_{13}, normalised control power J_{14}, number of control devices J_{15}, number of sensors J_{16} and computational resolution J_{17} are determined and presented in *Table* 4-1

Table 4-1. Structural evaluation criteria

	Controller	El-Centro			Hachinohe			Northridge		Kobe		Max
		0.5	1.0	1.5	0.5	1.0	1.5	0.5	1.0	0.5	1.0	
J_1	Active	0.742	0.743	0.742	0.867	0.871	0.887	0.840	0.947	0.784	0.678	0.947
	COC	0.751	0.717	0.720	0.870	0.862	0.897	0.824	0.916	0.705	0.835	0.916
	MCOC	0.764	0.752	0.744	0.899	0.898	0.916	0.867	0.914	0.790	0.923	0.923
	TSKFIN	0.756	0.731	0.735	0.880	0.874	0.899	0.844	0.914	0.736	0.730	0.914
	MaxMin	0.759	0.741	0.736	0.902	0.893	0.910	0.847	0.913	0.748	0.654	0.913
	P-ON	0.602	0.598	0.606	0.609	0.629	0.705	0.659	0.845	0.378	0.580	0.845
	P-OFF	0.772	0.811	0.989	0.909	0.921	0.957	0.921	0.937	0.909	0.896	0.957
J_2	Ac	0.639	0.635	0.652	0.710	0.705	0.796	0.777	0.844	0.665	0.842	0.844
	COC	0.800	0.820	0.750	0.932	0.849	0.898	0.869	0.977	0.722	0.938	0.977
	MCOC	0.693	0.692	0.720	0.913	0.845	0.924	0.931	0.923	0.718	0.886	0.931
	TSKFIN	0.626	0.613	0.624	0.841	0.756	0.836	0.906	0.835	0.668	0.828	0.906
	MaxMin	0.666	0.646	0.655	0.923	0.828	0.883	0.912	0.874	0.677	0.931	0.931
	P-ON	3.628	1.811	1.238	5.271	2.635	2.044	1.605	1.137	1.289	0.970	5.271
	P-OFF	0.790	0.839	1.055	0.943	0.955	1.061	1.015	1.144	0.848	1.004	1.144
J_3	Ac	0.760	0.763	0.888	0.973	0.977	0.995	0.885	0.983	0.921	1.024	1.024
	COC	0.767	0.840	0.924	1.015	0.984	1.013	0.877	0.993	0.938	1.040	1.040
	MCOC	0.772	0.784	0.908	0.995	0.981	1.009	0.880	0.985	0.981	1.072	1.072
	TSKFIN	0.767	0.786	0.914	0.995	0.981	1.008	0.880	0.985	0.962	1.039	1.039
	MaxMin	0.776	0.778	0.902	0.995	0.981	1.008	0.880	0.988	0.965	1.047	1.047
	P-ON	0.980	0.859	0.943	1.093	1.000	1.031	0.925	1.085	0.594	1.177	1.177
	P-OFF	0.772	0.812	0.948	0.996	0.982	1.008	0.930	0.986	1.017	1.034	1.034
J_4	Ac	0.681	0.680	0.686	0.885	0.884	0.905	0.768	0.998	0.672	0.225	0.998
	COC	0.589	0.605	0.624	0.836	0.844	0.865	0.651	0.923	0.544	0.276	0.923
	MCOC	0.613	0.638	0.663	0.840	0.848	0.871	0.695	0.933	0.629	0.278	0.933
	TSKFIN	0.605	0.625	0.644	0.838	0.846	0.869	0.670	0.951	0.571	0.200	0.951
	MaxMin	0.605	0.630	0.653	0.838	0.847	0.870	0.683	0.938	0.582	0.217	0.938
	P-ON	0.456	0.440	0.454	0.687	0.716	0.740	0.387	1.006	0.234	0.123	1.006
	P-OFF	0.621	0.659	0.700	0.840	0.852	0.881	0.811	0.869	0.706	0.588	0.881
J_5	Ac	0.556	0.554	0.572	0.648	0.644	0.654	0.614	0.646	0.586	0.713	0.713
	COC	0.513	0.497	0.520	0.626	0.613	0.621	0.546	0.615	0.531	0.694	0.694
	MCOC	0.573	0.572	0.595	0.661	0.666	0.678	0.615	0.662	0.613	0.764	0.764
	TSKFIN	0.548	0.538	0.554	0.644	0.641	0.650	0.574	0.626	0.564	0.698	0.698
	MaxMin	0.547	0.549	0.567	0.648	0.650	0.658	0.589	0.636	0.578	0.714	0.714
	P-ON	16.482	7.707	4.994	21.885	10.469	6.799	7.946	6.159	8.563	6.365	21.885
	P-OFF	0.597	0.627	0.688	0.672	0.708	0.742	0.712	0.767	0.732	0.885	0.885

Table 4-1. Earthquake evaluation criteria (continue)

	Controller	El-Centro			Hachinohe			Northridge		Kobe		Max
		0.5	1.0	1.5	0.5	1.0	1.5	0.5	1.0	0.5	1.0	
J_6	Ac	0.746	0.745	0.751	0.855	0.855	0.865	0.825	0.867	0.729	0.881	0.881
	COC	0.666	0.676	0.693	0.820	0.816	0.828	0.702	0.816	0.635	0.803	0.828
	MCOC	0.687	0.705	0.728	0.830	0.831	0.844	0.744	0.822	0.679	0.843	0.844
	TSKFIN	0.679	0.693	0.711	0.825	0.823	0.836	0.720	0.818	0.653	0.815	0.836
	MaxMin	0.677	0.697	0.718	0.826	0.827	0.840	0.734	0.823	0.666	0.820	0.840
	P-ON	0.685	0.605	0.581	0.950	0.873	0.826	0.441	0.705	0.352	0.590	0.950
	P-OFF	0.694	0.725	0.764	0.833	0.843	0.862	0.783	0.845	0.748	0.892	0.892
J_7	Ac	0.776	0.776	0.724	0.958	0.962	0.942	0.742	0.980	0.729	0.698	0.980
	COC	0.732	0.742	0.686	0.944	0.949	0.916	0.680	0.946	0.677	0.711	0.949
	MCOC	0.757	0.768	0.735	0.952	0.955	0.928	0.731	0.945	0.782	0.802	0.955
	TSKFIN	0.747	0.752	0.708	0.949	0.952	0.925	0.693	0.947	0.716	0.697	0.952
	MaxMin	0.748	0.760	0.717	0.947	0.951	0.922	0.706	0.946	0.728	0.690	0.951
	P-ON	0.659	0.652	0.597	0.677	0.730	0.690	0.596	0.846	0.297	0.533	0.846
	P-OFF	0.768	0.808	0.833	0.953	0.956	0.929	0.839	0.945	0.929	0.764	0.956
J_8	Ac	0.000	0.000	0.047	0.000	0.000	0.639	0.267	0.572	0.222	0.307	0.639
	COC	0.000	0.000	0.002	0.000	0.000	0.600	0.092	0.508	0.172	0.321	0.600
	MCOC	0.000	0.000	0.063	0.000	0.000	0.661	0.157	0.572	0.332	0.565	0.661
	TSKFIN	0.000	0.000	0.018	0.000	0.000	0.633	0.109	0.509	0.235	0.233	0.633
	MaxMin	0.000	0.000	0.033	0.000	0.000	0.633	0.127	0.517	0.260	0.238	0.633
	P-ON	0.000	0.000	0.000	0.000	0.000	0.002	0.000	0.310	0.000	0.048	0.310
	P-OFF	0.000	0.000	0.325	0.000	0.000	0.697	0.332	0.853	0.604	0.751	0.853
J_9	Ac	0.000	0.000	0.465	0.000	0.000	0.698	0.542	0.906	0.308	0.833	0.906
	COC	0.000	0.000	0.209	0.000	0.000	0.581	0.333	0.906	0.308	0.857	0.906
	MCOC	0.000	0.000	0.581	0.000	0.000	0.721	0.563	0.917	0.333	0.940	0.940
	TSKFIN	0.000	0.000	0.419	0.000	0.000	0.628	0.354	0.896	0.308	0.845	0.896
	MaxMin	0.000	0.000	0.419	0.000	0.000	0.698	0.396	0.896	0.308	0.857	0.896
	P-ON	0.000	0.000	0.000	0.000	0.000	0.000	0.000	0.823	0.000	0.536	0.823
	P-OFF	0.000	0.000	0.860	0.000	0.000	0.814	0.875	1.000	0.667	1.000	1.000
J_{10}	Ac	0.764	0.763	0.682	0.860	0.860	0.932	0.663	1.014	0.841	0.238	1.014
	COC	0.645	0.669	0.614	0.814	0.818	0.891	0.549	0.927	0.562	0.238	0.927
	MCOC	0.664	0.698	0.645	0.822	0.829	0.896	0.615	0.952	0.831	0.492	0.952
	TSKFIN	0.658	0.687	0.630	0.818	0.824	0.902	0.576	0.958	0.723	0.207	0.958
	MaxMin	0.658	0.692	0.638	0.819	0.826	0.898	0.591	0.944	0.744	0.250	0.944
	P-ON	0.449	0.455	0.422	0.651	0.699	0.715	0.294	1.013	0.211	0.139	1.013
	P-OFF	0.671	0.717	0.689	0.824	0.841	0.861	0.779	0.901	0.762	0.723	0.901
J_{11}	Ac	0.00204	0.00405	0.00605	0.00173	0.00322	0.00458	0.00642	0.00770	0.00584	0.00920	0.00920
	COC	0.00557	0.00682	0.00760	0.00518	0.00666	0.00738	0.00803	0.00807	0.00718	0.00920	0.00920
	MCOC	0.00159	0.00468	0.00725	0.00144	0.00363	0.00507	0.00667	0.00856	0.00666	0.00920	0.00920
	TSKFIN	0.00251	0.00449	0.00700	0.00219	0.00351	0.00494	0.00677	0.00911	0.00623	0.00920	0.00920
	MaxMin	0.00271	0.00401	0.00601	0.00170	0.00321	0.00454	0.00605	0.00795	0.00578	0.00920	0.00920
	P-ON	0.00816	0.00898	0.00920	0.00799	0.00886	0.00920	0.00920	0.00920	0.00920	0.00920	0.00920
	P-OFF	0.00088	0.00101	0.00920	0.00084	0.00092	0.00098	0.00109	0.00920	0.00107	0.00920	0.00920
J_{12}	Ac	0.074	0.074	0.074	0.076	0.07	0.081	0.079	0.102	0.131	0.106	0.131
	COC	0.073	0.073	0.073	0.074	0.075	0.080	0.074	0.099	0.127	0.131	0.131
	MCOC	0.073	0.076	0.076	0.073	0.074	0.080	0.078	0.099	0.139	0.145	0.145
	TSKFIN	0.073	0.074	0.075	0.073	0.074	0.080	0.075	0.099	0.133	0.115	0.133
	MaxMin	0.073	0.075	0.075	0.073	0.074	0.080	0.076	0.099	0.134	0.104	0.134
	P-ON	0.056	0.055	0.059	0.045	0.055	0.065	0.064	0.089	0.052	0.096	0.096
	P-OFF	0.073	0.078	0.092	0.073	0.074	0.079	0.086	0.099	0.156	0.141	0.156

Table 4-1. Earthquake evaluation criteria (continue)

	Controller	El-Centro			Hachinohe			Northridge		Kobe		Max
		0.5	1.0	1.5	0.5	1.0	1.5	0.5	1.0	0.5	1.0	
J_{13}	Ac	0.00129	0.00254	0.00400	0.00058	0.00117	0.00174	0.00308	0.00502	0.00363	0.00797	0.00797
	COC	0.00223	0.00320	0.00410	0.00149	0.00295	0.00411	0.00354	0.00480	0.00480	0.00855	0.00855
	MCOC	0.00137	0.00292	0.00439	0.00088	0.00121	0.00166	0.00295	0.00486	0.00326	0.00746	0.00746
	TSKFIN	0.00170	0.00281	0.00436	0.00107	0.00170	0.00232	0.00335	0.00568	0.00362	0.00845	0.00845
	MaxMin	0.00143	0.00257	0.00396	0.00096	0.00138	0.00198	0.00293	0.00511	0.00340	0.00779	0.00779
	P-ON	0.00908	0.00775	0.00904	0.00879	0.00737	0.00883	0.00635	0.00933	0.00931	0.01543	0.01543
	P-OFF	0.00113	0.00141	0.00616	0.00081	0.00093	0.00100	0.00103	0.00480	0.00159	0.00773	0.00773
J_{14}	Ac	0.00005	0.00009	0.00015	0.00003	0.00006	0.00010	0.00007	0.00011	0.00007	0.00013	0.00015
	COC	0.00008	0.00014	0.00020	0.00007	0.00011	0.00016	0.00009	0.00013	0.00008	0.00015	0.00020
	MCOC	0.00007	0.00011	0.00016	0.00006	0.00009	0.00012	0.00008	0.00011	0.00007	0.00013	0.00013
	TSKFIN	0.00007	0.00012	0.00018	0.00006	0.00010	0.00014	0.00008	0.00013	0.00008	0.00015	0.00015
	MaxMin	0.00007	0.00012	0.00017	0.00006	0.00009	0.00013	0.00008	0.00012	0.00008	0.00014	0.00014
	P-ON	0.00347	0.00177	0.00125	0.00135	0.00183	0.00148	0.00105	0.00101	0.00127	0.00105	0.00347
	P-OFF	0.00007	0.00011	0.00014	0.00006	0.00009	0.00011	0.00006	0.00008	0.00006	0.00009	0.00011
J_{15}	Ac COC MCOC TSKFIN MaxMin P-ON P-OFF	25										25
J_{16}	Ac	10.0										21
	COC	16+5.0										
	MCOC	16+5.0										
	TSKFIN	10.0										
	MaxMin	10.0										
	P-ON	0										
	P-OFF	0										
J_{17}	Ac COC MCOC TSKFIN MaxMin P-ON P-OFF	20										20

To more easily verify the effectiveness of each control algorithm, the results of each algorithm are also compared with those of the original and modified clipped optimal control algorithms (Table 4-1). However, it is noted that the original and modified clipped-optimal and TSKInv (without combining with forward model) controllers require the use of force feedback through either sensor measurements or a non-parametric forward model to achieve this level of performance.

The idea of developing a voltage controller is to make the MR damper generate the closest force to the desired one produced by nominal controller (LQG in this study). In other words, an ideal semi-active voltage controller is the one that can track the

performance of the designed active controller. From Table 4-1, it is seen that compared with COC and MCOC, active controller, in most cases, performs better in terms of reduction of objective indices. For these cases, J values of TSKFInv and Max-Min algorithms are either better than active controller or between active controller and COC. On the other hand, in some cases such as drift related indices, i.e. J_1 and J_4, COC and MCOC suppress the norm acceleration more than active system and, therefore, the objective values of TSKFInv and Max-Min algorithms, which are better controllers in tracking the desired force, are closer to active one and, therefore, more than COC and MCOC.

Results also show that both new proposed semi-active algorithms have very similar performances, although TSKInv is slightly better. In particular, these two algorithms are able to reduce the peak drift ratio and peak floor acceleration for all ten earthquakes by up to 35% and 38%, respectively, noting that a reduction in acceleration response of individual floors can be directly related to forces and, hence, to the mass and amount of material needed in each floor to resist the earthquake loads. This is while COC can only reduce the peak floor acceleration by 25%. The other performance indices which are important to reduce are the control force and power. Due to the fact that COC algorithm operates by switching the voltage of the MR dampers between two extremes, i.e. passive-on (v=10) and passive-off (v=0), it works with the maximum load on many occasions unnecessarily and often causes force overshoots as shown in Figure 4.13 to Figure 4.16. As a consequence, the maximum control force and power indices, i.e. J_{11} and J_{13} of COC are more than the other semi-active control algorithms considered in this study. MCOC, in contrast, has the least control power consumption as it works with zero or a small portion of voltage during the earthquake. However, at some point, due to inaccurate dynamic mapping of the MR damper, it also produces unnecessary forces, even though compared to COC, these forces are much less. MaxMin and TSKInv on the other hand, make a trade-off on reduction of structural responses and control force and power. Graphical comparisons of control force and power indices between the four aforementioned semi-active algorithms are shown in Figure 4.17. It shows that, in terms of peak control force reduction (J_{11}), MaxMin, TSKInv, MCOC and COC have the best performances while the least control power consumption belongs to MCOC, MaxMin, TSKInv and COC, respectively.

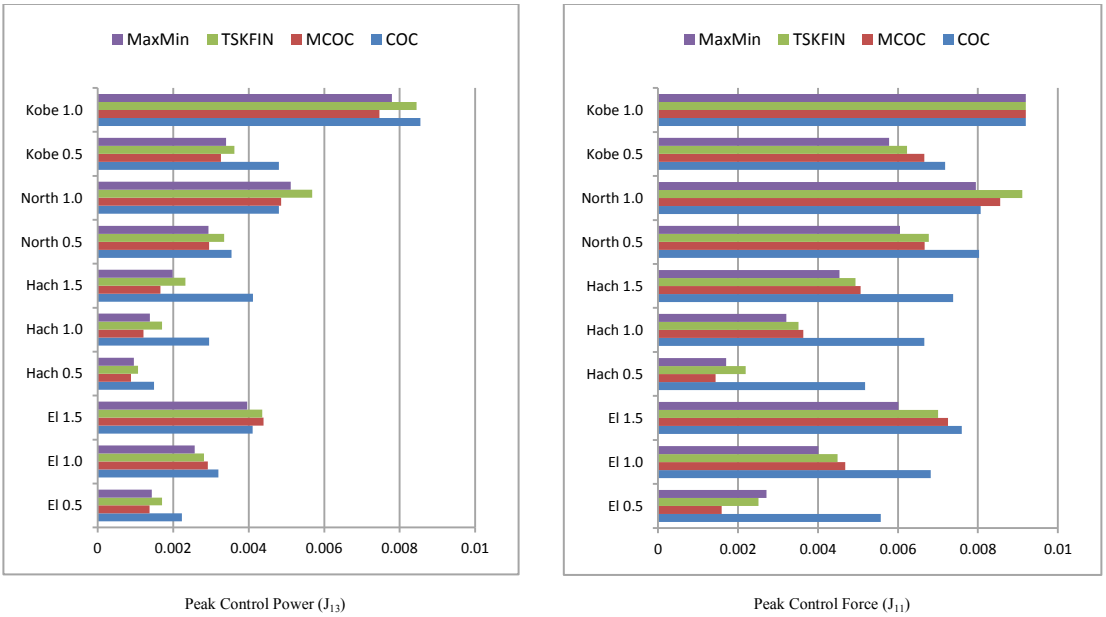

Figure 4.17. Structural control force and power comparison between different semi-active control algorithms

The last column of Table 4-1 indicates the maximum values of objective indices of the structure under 10 earthquake signals (the maximum of each row). This is called the worst case scenario as defined in the benchmark problem. The first six performance criteria of these objective indices are compared with each other for different control algorithms in Figure 4.18. It can be observed that both TSKFInv and MaxMin algorithms are able to track the performance of active controller closely which proves their superiority over COC and MCOC. Moreover, as can be seen, passive-on algorithm is the best in suppression of the peak drift ratio while it is the worse one in reduction of peak values of the acceleration, peak and normalised base shear, peak and normalised level acceleration and normalised drift ratio. The reason is due to working with maximum load and hence exerting too much resisting force which causes an overshoot in the response of structure.

In order to compare the computational effort of the algorithms under study, the simulation running time of each semi-active algorithm for 20 seconds of El-Centro earthquake with intensity of 1 is presented in Table 4-2. The MATLAB codes were ran on an "Intel Pentium, Core 2Duo, CPU E8500, 3.16 GHz, 3.25 GB of RAM" with time step of 0.01s as defined in the benchmark problem. The other features of four aforementioned algorithms are also compared with each other in the same table. The numerical model of the MR damper used in the *SIMULINK* is the modified Bouc-Wen model which is highly nonlinear and computationally expensive. Therefore, the running

time of the semi-active controllers, which use MR dampers, are numerically large where COC and MCOC provide the quickest response as they work with simple control laws and MaxMin method has the largest running time since it uses two fuzzy models to estimate the maximum and minimum capacities of the MR damper. In this study, a forward model of the MR damper is trained, using acceleration feedback to provide the required force feedback to TSKInv model. However, depending on the complexity of the model and availability of force sensors, one can directly use the actual force measurements. Moreover, instead of using the acceleration response of the structure to build and train the forward and inverse models of MR damper, other states of the structure can be employed.

Table 4-2. Computational effort comparison between different control algorithms for 20 seconds of El-Centro earthquake with intensity of 1

	Active (LQG)	**COC**	**MCOC**	**TSKInv**	**MaxMin**
Running Time	16.8 s	207.1	208.4 s	227.8 s	235.1 s
Force Feedback	-	Yes*	Yes*	Yes*	Yes*
Structural response feedback	Acc	-	-	Acc	Acc (+velocity)

- The force feedback is needed for all aforementioned semi-active control algorithms, however in case sensors are not avalbale or damaged, it can be replaced by a simple parametric/non-parametric model as explained in this chapter.

The top floor absolute acceleration and the inter-storey drift between the 19th and 20th floors of uncontrolled, TSKFInv and MaxMin controlled, in time domain, are shown in Figure 4.19 to Figure 4.28 for different earthquakes. For the other floors, similar observations can be made. Maximum acceleration and inter-storey drift ratio response profiles are also provided for all floors of the building.

According to these time history results, the peak relative acceleration and inter-storey drift are reduced using both semi-active control algorithms. The response profiles show the reduction in peak drift ratio as well as acceleration in almost all floors. Moreover, the figures show that both newly developed voltage regulating algorithms perform very similar to each other. However, MaxMin method performs slightly better.

4.6 SUMMARY

In this chapter, new technologies for improving structural resistance to earthquake loading were investigated. Two new semi-active control algorithms, named TSKInv

and MaxMin, were devised to convert the force generated by the nominal controller (LQG here) to the required voltage for MR dampers.

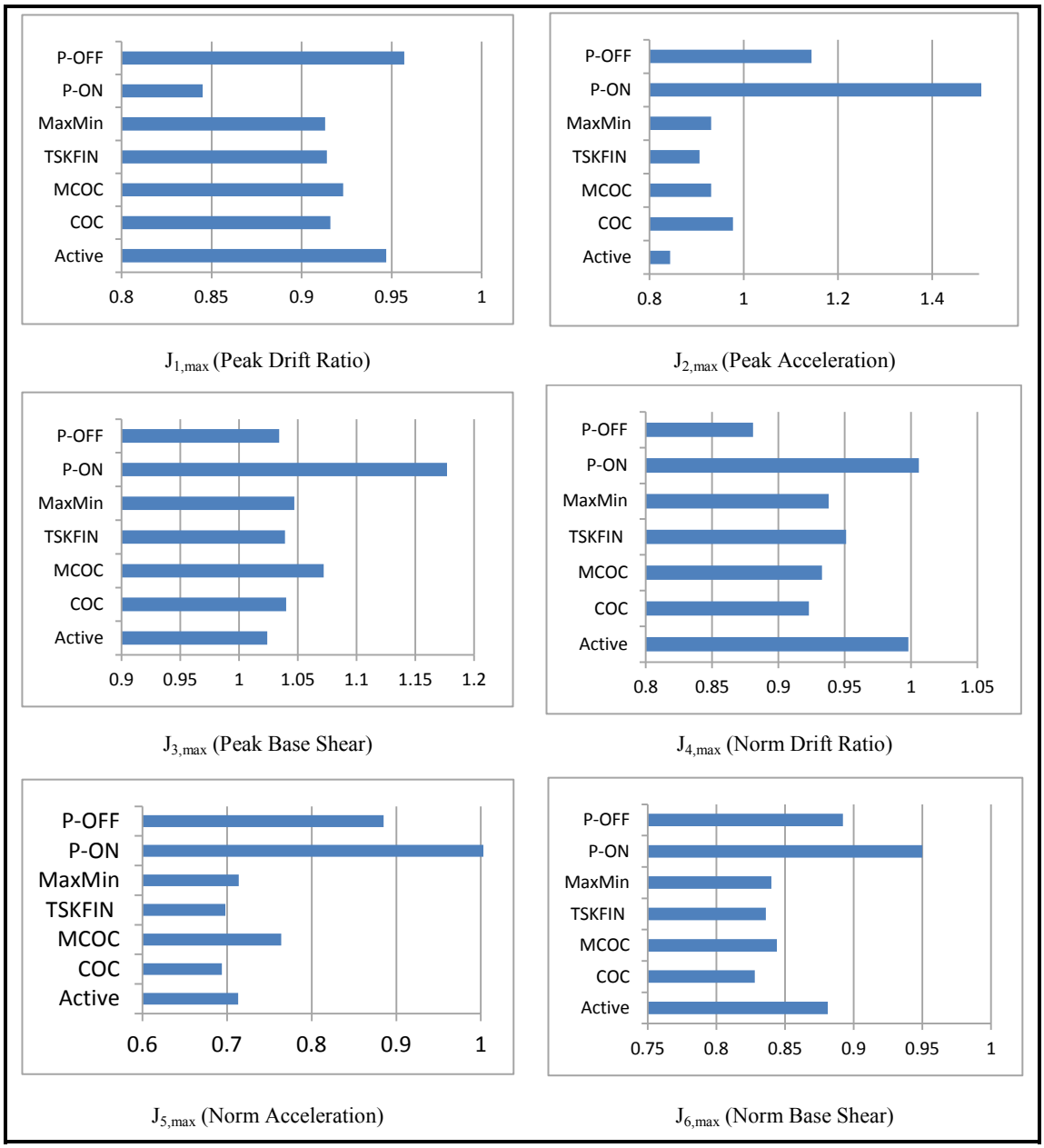

Figure 4.18. Performance criteria (worse case scenario)

TSKInv algorithm was developed by modelling the inverse dynamics of MR damper using TSK fuzzy inference systems. The structure of model was optimised to select the best minimal inputs and fuzzy rules which lead to an accurate model. To provide the force feedback to the inverse model, another fuzzy model was trained to capture the forward dynamics of the MR damper. The second algorithm was designed based on the maximum ($v = v_{max}$) and minimum ($v = v_{min}$) load of the MR damper at each time-step. Then, assuming a linear relationship between damper's voltage and force, a

decision is made for voltage regulation in order to generate a specific desired force. Both methods use only the acceleration feedback.

The models were critically evaluated against passive damping as well as the original and modified clipped optimal controller through a highly nonlinear 20-storey benchmark building. Evaluation was further conducted on the basis of performance criteria to show the effectiveness on reduction of quake-induced vibrations of the building structure via a set of ratios (indices) for the controlled and uncontrolled cases, respectively.

Results illustrate that the proposed new control algorithms can effectively track the desired control force and perform much better than COC and MCOC in terms of structural response reduction using less control force and power. Also, the comparison between MaxMin and TSKInv shows that MaxMin model uses less control power while TSKInv decreases the structural response more. However, MaxMin is easier to use, although computationally is slightly more expensive than TSKFInv. Ability to operate without force measurement is the other benefit of MaxMin model.

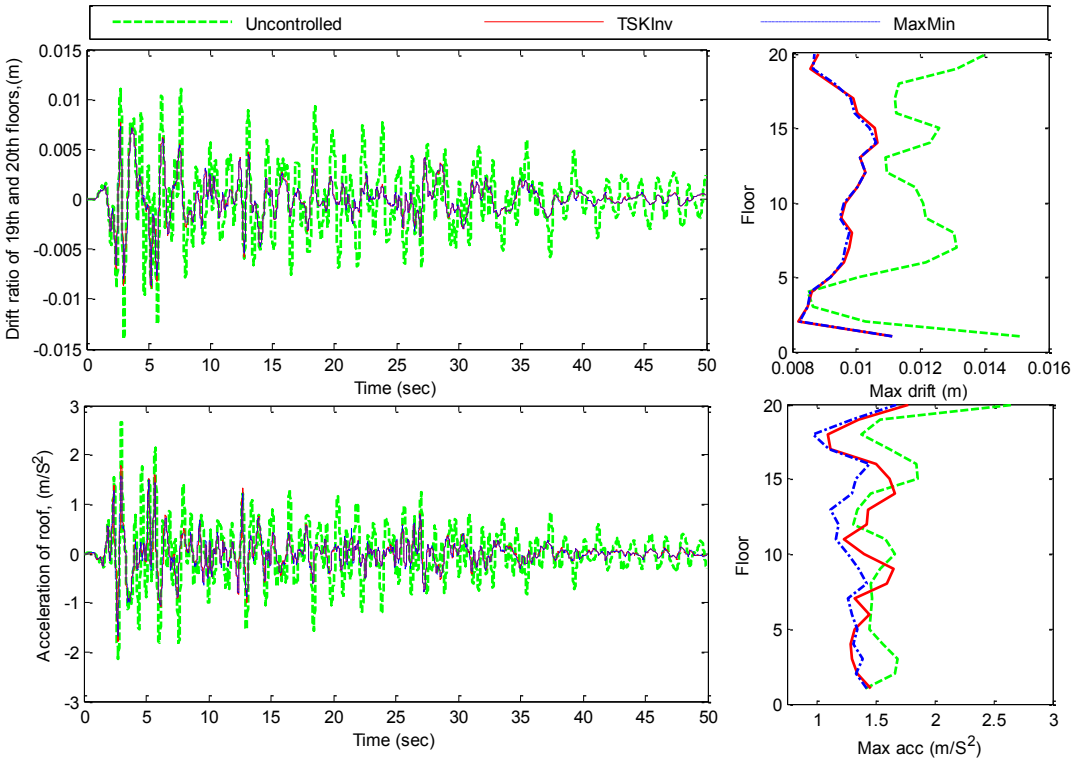

Figure 4.19. Structural Response (El-Centro, 0.5)

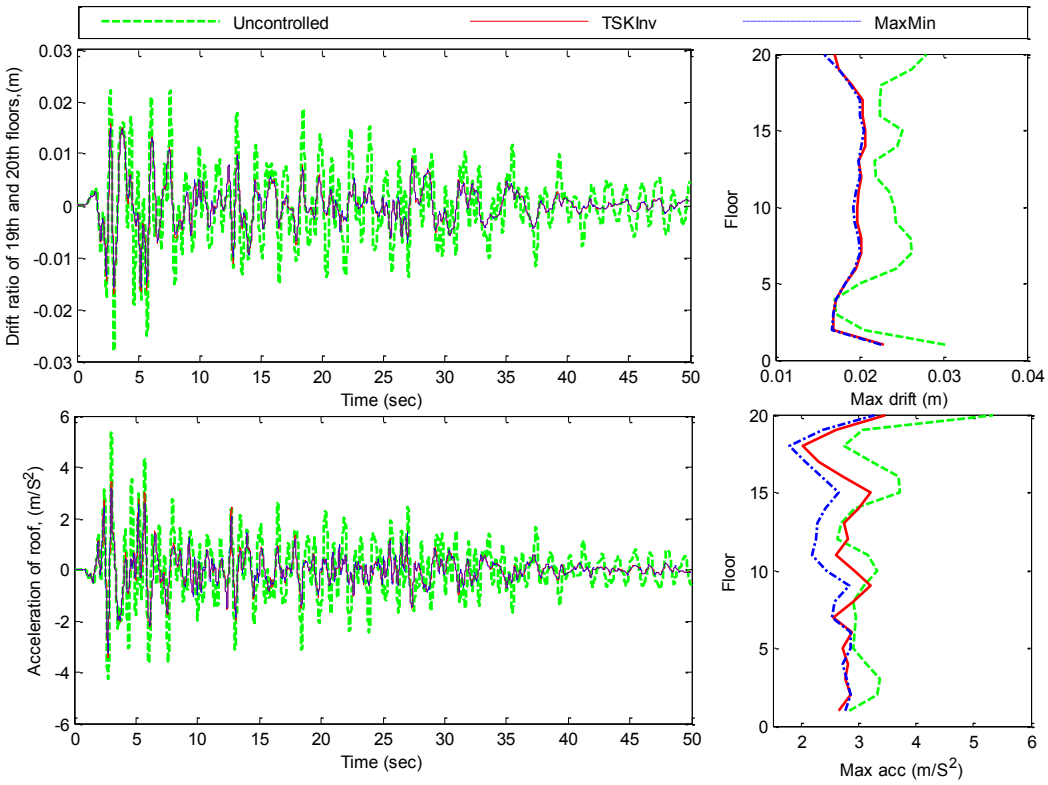

Figure 4.20. Structural Response (El-Centro, 1.0)

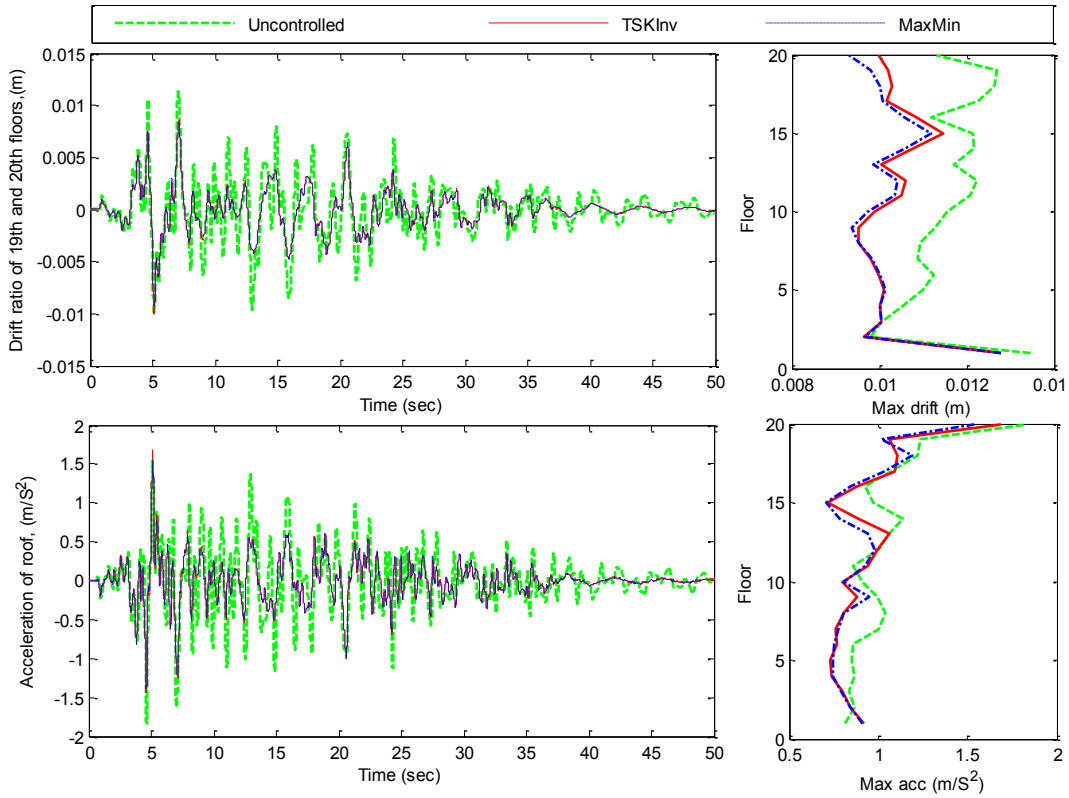

Figure 4.21. Structural Response (El-Centro, 1.5)

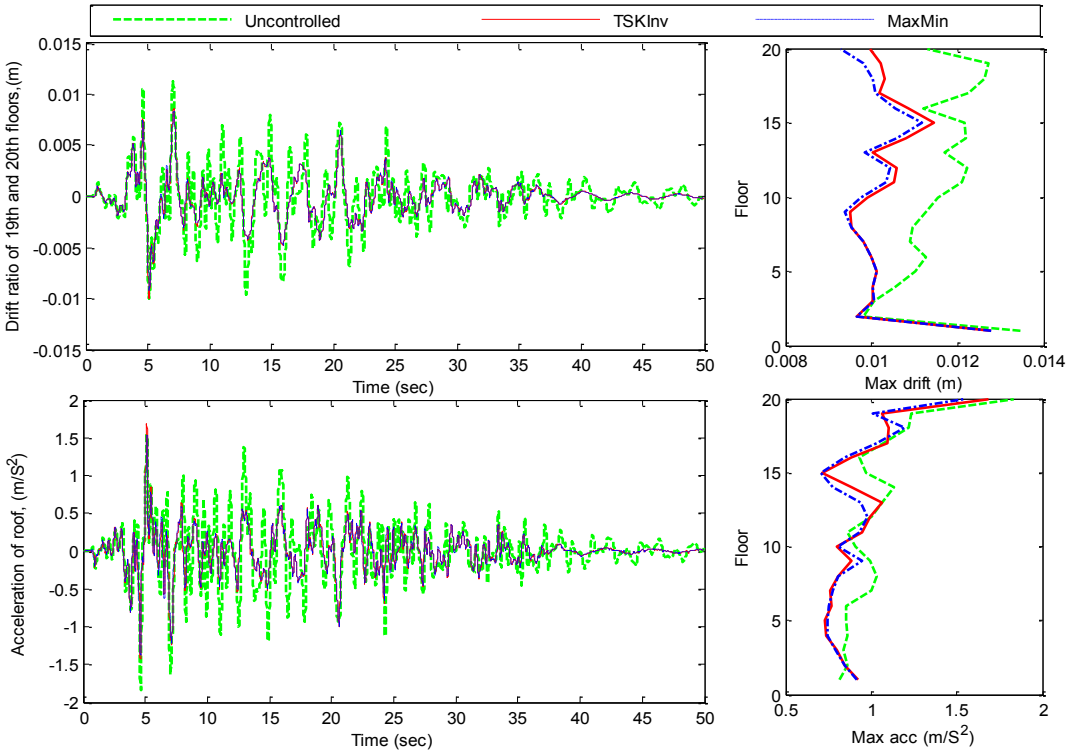

Figure 4.22. Structural Response (Hachinohe, 0.5)

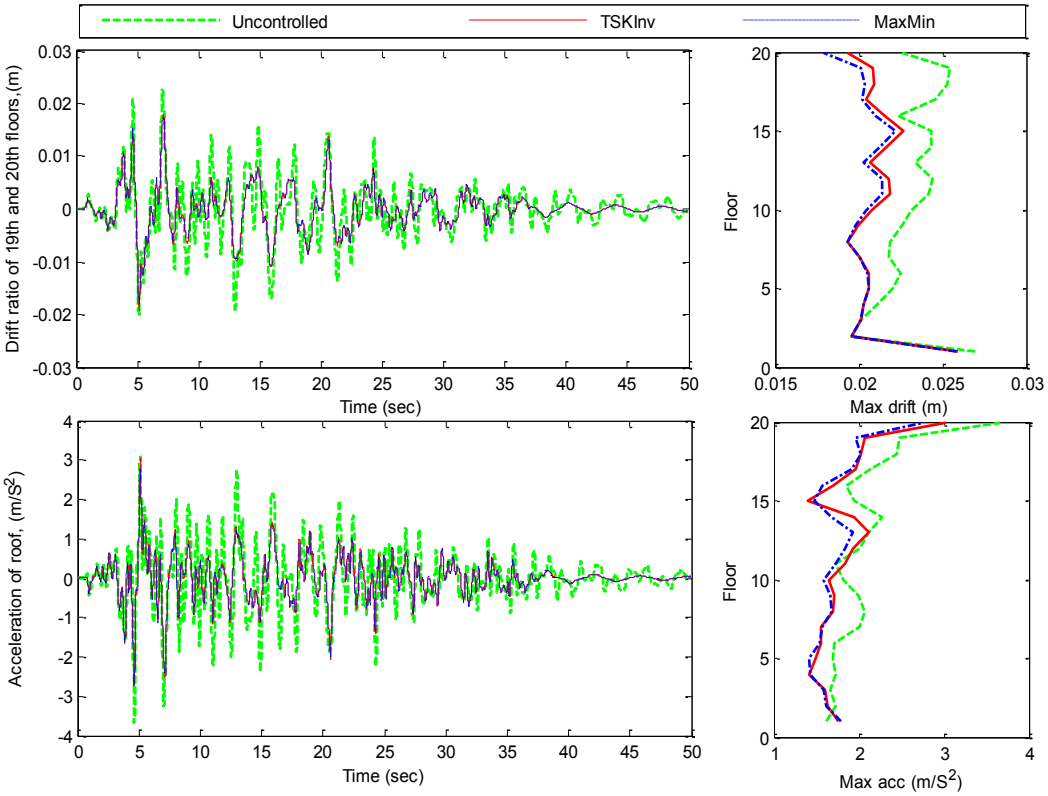

Figure 4.23. Structural Response (Hachinohe, 1.0)

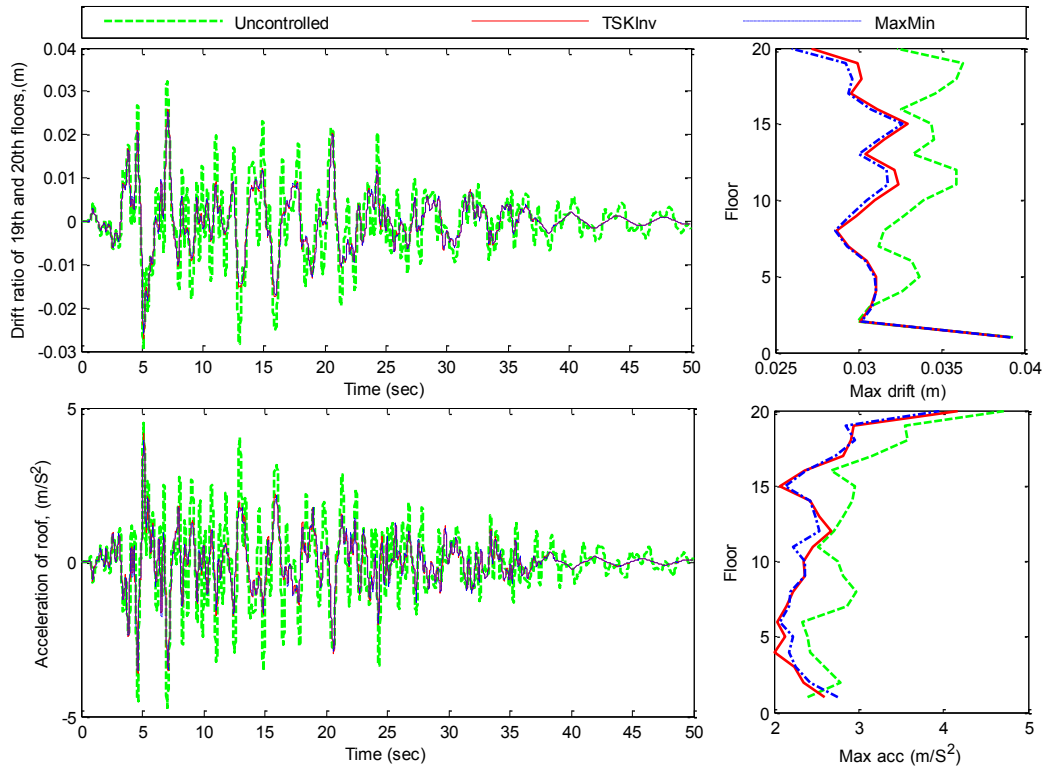

Figure 4.24. Structural Response (Hachinohe, 1.5)

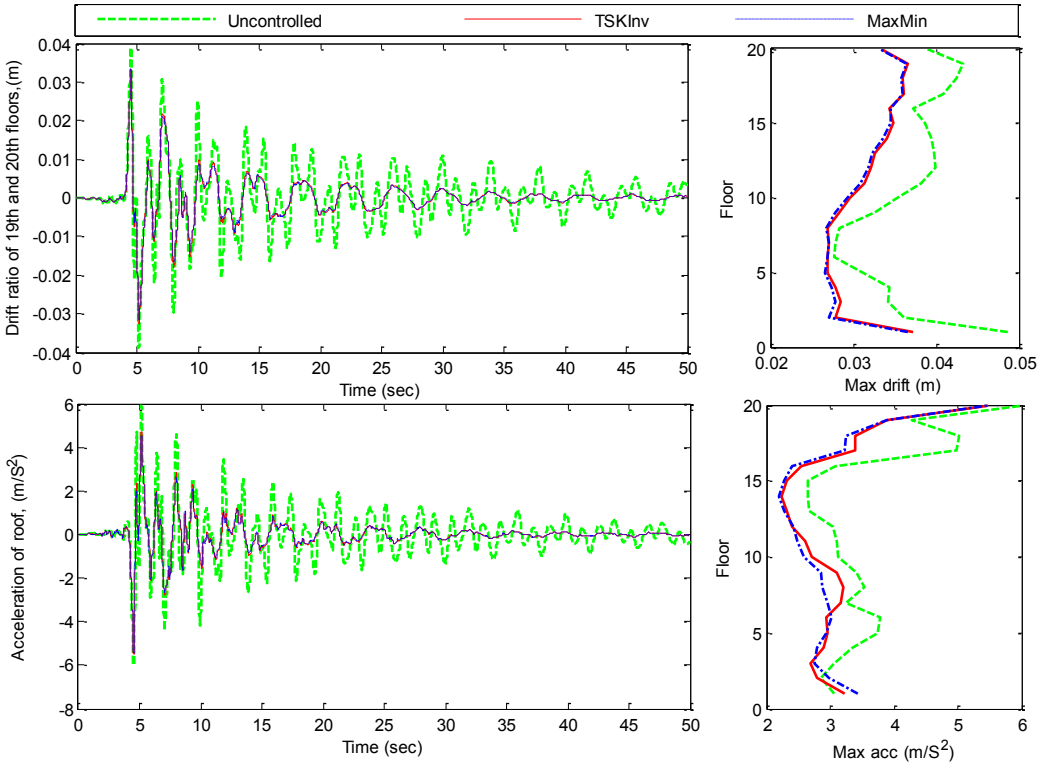

*Figure 4.25. Structural Response (*Northridge*, 0.5)*

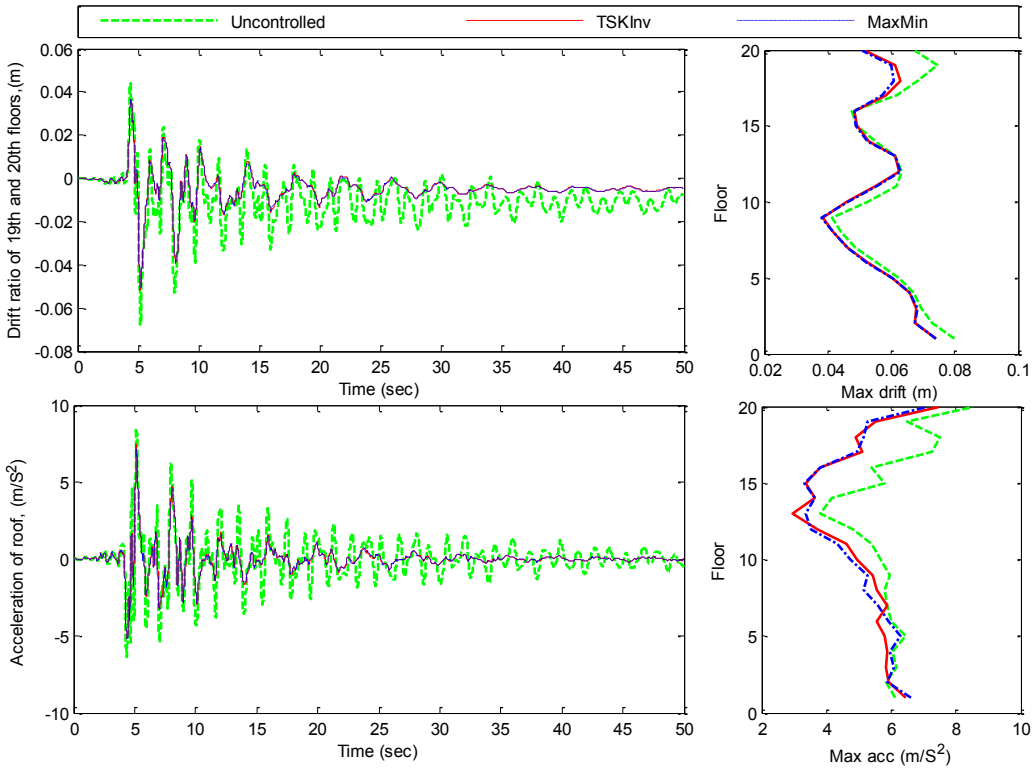

*Figure 4.26. Structural Response (*Northridge*, 1.0)*

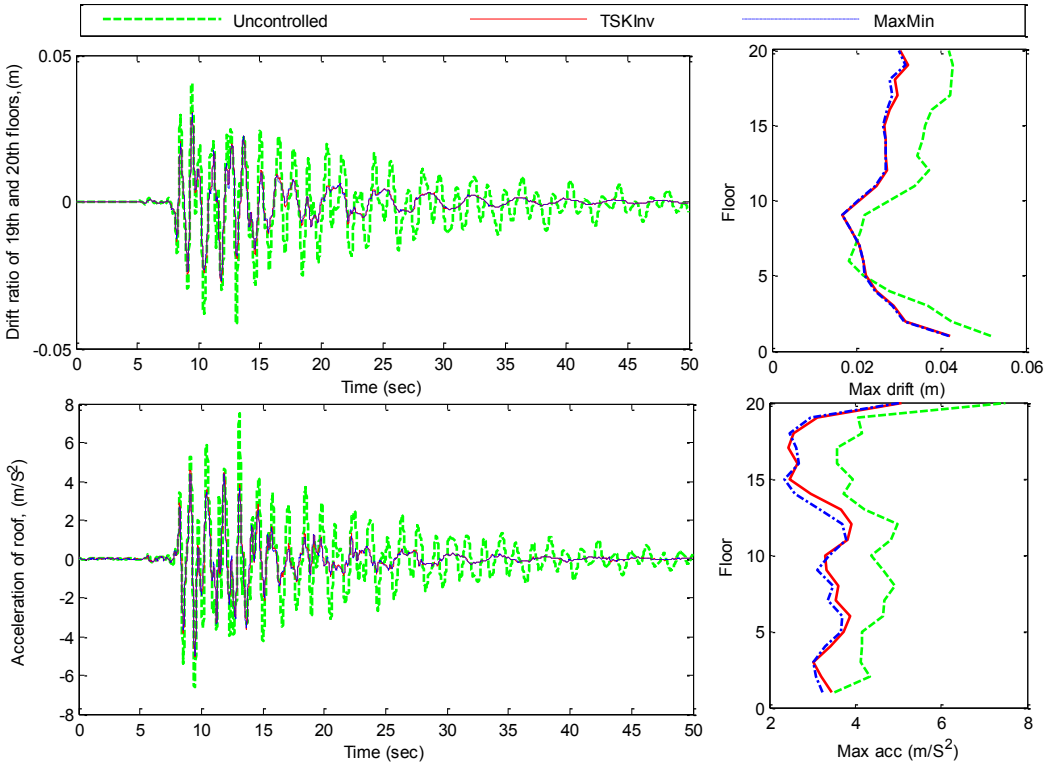

Figure 4.27. Structural Response (Kobe, 0.5)

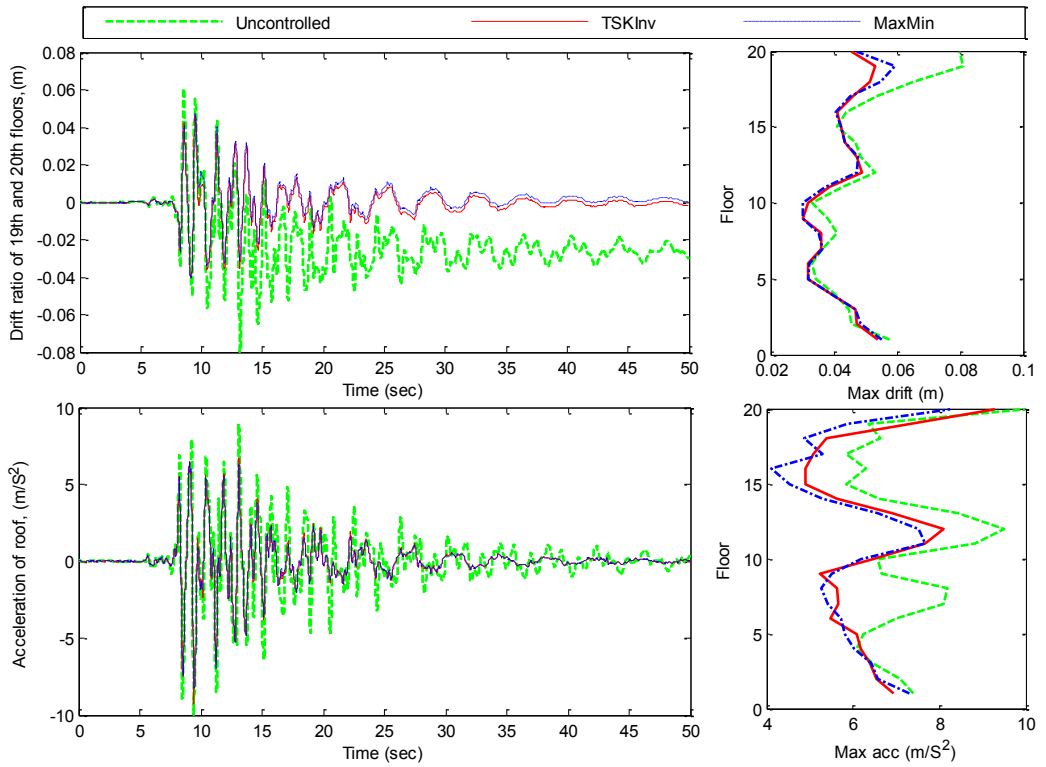

Figure 4.28. Structural Response (Kobe, 1.0)

CHAPTER 5

ONLINE REAL-TIME STRUCTURAL IDENTIFICATION

5.1 CHAPTER OUTLINE

System identification refers to any systematic way of deriving or improving models of dynamical systems through the use of experimental and field testing input–output data. In the field of civil engineering, identification of the state of a structure during service condition under dynamic loading, such as earthquake, in order to detect any damage as it occurs, has posed a great challenge to the research community. Therefore, online and real-time structural identification has attracted a great deal of attention and interest in the structural engineering research community over the past decades, especially when input-output measurement data are contaminated by high-level noise.

In this chapter, a literature review on different structural health monitoring methods is conducted first, stating the state-of-the-art in Structural Health Monitoring (SHM). Then an investigation is carried out on some recently developed Kalman filtering methods for their effectiveness and efficiency through a highly nonlinear SDOF structure as well as a two-storey linear structure. In the next section, a new self-adaptive recursive least square (RLS) based method is introduced which can track any abrupt change in structural parameters during excitation and has the ability to work

with unknown inputs. The efficiency of this method is validated using various numerical examples.

5.2 INTRODUCTION AND BACKGROUND

Our communities and infrastructures are vulnerable and susceptible to natural or man-made hazards. It has, therefore, created both motivation and challenge for governments and the engineering community, all over the world, to find a solution for the protection of civil infrastructure, hence, safe guarding the community from hazards such as major seismic events, strong winds, as well as ageing, deterioration, misuse and poor quality construction. In the past few decades, much research have been reported on finding realistic solutions to this problem which has led to two main areas of research, i.e. structural control (SC) and structural health monitoring (SHM).

Structural Health Monitoring (SHM) is defined as the process of comparing the current state of a structure's condition relative to a healthy baseline state to detect the existence, location, and degree of likely damage after a damaging input, such as an earthquake. SHM can simplify and improve typical visual or localised experimental based approaches, as it does not require subjective visual inspection of the structure. It can, thus, provide valuable data for post-event safety assessments to help optimise recovery planning.

Farrar et.al describe SHM as a four-part process (Farrar & Worden 2007):

1. Operational Evaluation

2. Data Acquisition, Fusion, and Cleansing

3. Feature Extraction and Information Condensation, and

4. Statistical Model Development for Feature Discrimination.

Operational evaluation determines economic and/or life safety issues, damage definitions, conditions, both operational and environmental, under which the system functions, and, finally, limitations on data acquisition in the operational environment. Data acquisition covers topics such as determination of the quantities to be measured,

the sensors type, location, number, resolution, and bandwidth, the data acquisition/storage/transmittal hardware, and how often the data should be collected.

The third step in the process is feature extraction, which is the process of identifying damage-sensitive properties from measured vibration responses to determine existence, location, type, and the extent of damage. Finally, statistical models are used to determine whether the changes observed in the selected features used to identify damage are statistically significant (diagnosis). Similar models are also used to estimate the remaining useful life of the structure (prognosis). Most traditional identification techniques, however, require measurements of excitation (input) and response (output) in order to produce the required data for model identification. In order to obtain such measurement data, controlled tests are needed to be conducted on the structure under investigation. For instance, in multi-input-multi-output (MIMO) modal testing, it is a common practice to excite a testing structure by applying measurable excitations at several points, and then collect response data at the sensor locations (Loh & Lin 1996). However, for many civil engineering structures it may be difficult or unfeasible to provide such artificial excitations due to their sheer size, geometry and location or simply due to interruption to normal service such as in case of bridges. Equally, the requirement on the amount of external energy to excite an entire large civil structure to gain a desired level of vibration may not be practical.

On the other hand, civil structures in their operational condition inevitably experience various unmeasurable dynamic loadings (wind, waves and traffic for example). Measurements of structural responses under such loadings can be used for identification of structural parameters or structural models. Some identification algorithms have been developed based on such output (response measurements) only vibration data, due to ambient and environmental forces, i.e. traffic, wind, etc.

If such identification is carried out after the entire data sets have been collected, the identification method is called off-line method which can be used when the final state of the structural parameters at the end of loading is of interest. Some of the off-line structural identification methods can be found in the literature (Caravani, Watson & Thomson 1977; Loh, Lin & Huang 2000; Lus, Betti & Longman 1999). However, in some cases, real-time system identification is absolutely necessary. For example, in structural control, during severe loading such as earthquakes, access to the updated

structural model in order to produce optimal control actions requires real-time structural identification.

The main focus of this chapter is on the third part of the SHM process, namely, developing novel feature extraction techniques, with the aim of resolving problems of existing feature extraction algorithms to provide better resolution, accuracy and relevance. A major drawback of many existing approaches, which will be reviewed in this chapter, is their inability to be implemented in real-time, on a sample-to-sample basis as the event occurs. Hence, these methods are not suitable for real-time structural control for damage mitigation purposes, and their results would not be immediately available after an event.

Among many proposed SHM techniques in the literature, only a very few, such as adaptive fading Kalman filters (Loh, Lin & Huang 2000; Sato & Takei 1997), adaptive H∞ filter techniques (Sato & Qi 1998), bootstrap filtering approaches (Li, Suzuki & Noori 2004), Artificial Neural Networks (ANNs) based methods (Masri et al. 2000; Zang, Friswell & Imregun 2004; Zapico, Worden & Molina 2001), or wavelet approaches (Kim & Melhem 2004), can achieve real-time or near real-time results. However, they are associated with significant computational cost and complexity, or are incapable of locating and quantifying the damage detected. Therefore, developing on-line SHM techniques with simpler and more suitable algorithms is still a challenge.

This thesis proposes real-time SHM algorithms for linear and nonlinear hysteretic structures using simpler and more suitable techniques for on-line SHM of such structures than the existing methods in the literature. It uses an Iterated Extended Kalman Filter, Iterated Unscented Kalman Filter and an adaptive Recursive Least Squares based techniques.

The following sections present a brief review of the existing literature on the third step of the SHM process, covering a range of SHM algorithms.

Existing SHM algorithms in the literature can be categorised into two main groups: parametric and non-parametric methods. In parametric SHM, the mathematical model, governing the structural behaviour, is known and the aim is to identify likely changes in the structural parameters with respect to a baseline model to detect and locate damage. In contrast, non-parametric methods map the inputs to the structure to its outputs,

without any knowledge of the internal structural model. Damage is then detected by identifying changes in the parameters of the generic or non-physical model created. Nevertheless, non-parametric models cannot locate the damage detected unless a priori knowledge from all possible damage cases and the corresponding structural responses is available. However, a significant advantage of non-parametric SHM methods over the parametric approaches is their capability to capture the full dynamics of the structure including un-modelled or simplified dynamics.

5.2.1 Parametric Methods

Many current vibration-based SHM methods are based on the idea that changes in modal parameters: frequencies, mode shapes, and modal damping, are a result of damage or decay (Doebling et al. 1996). The idea was first proposed by (Chen, Czarnecki & Scholl 1976), who found longer time period, higher damping, and some mode shape discontinuity for the damaged structure in a forced vibration test on a full-scale four-storey concrete model building. However, modal properties are not robust in the presence of noise and are not sensitive to small amounts of damage (Farrar et al. 1994). Moreover, sometimes damage at two different locations result in exactly the same shifts in the natural frequencies, and the damage cannot be uniquely localised. Further, modal-based methods are typically more applicable to steel-frame and bridge structures where vibration response is highly linear (Doebling et al. 1996; Geoffrey Chase et al. 2005).

The most common method for identification of modal parameters in civil structures is the Eigen-system Realisation Algorithm (Hera & Hou), using time domain free vibration response data (Juang & Pappa 1985). In ERA, a discrete Hankel matrix is formed, the state and output matrices determined, and a continuous time system model created. The natural frequencies and mode shapes are then found by determining the eigenvalues of this continuous time system. Dyke, et al. (Dyke, Caicedo & Johnson 2000) used cross-correlation functions in conjunction with the ERA method for identification of the modal parameters, which are used to identify frequency and damping parameters. Caicedo et al. introduced SHM methods based on changes in the component transfer functions of the structure, or transfer functions between the floors of a structure, and used the ERA to identify the natural frequencies of each component

transfer function (Caicedo, Dyke & Johnson 2000). They also presented ERA-based methods to identify modal parameters before using least squares optimisation to locate and identify damage (Caicedo, Dyke & Johnson 2003). Lus et al. presented ERA methods using a Kalman filter estimator to identify a baseline model and the ERA method for modal parameters before using least squares optimisation to locate and identify damage. Lus and Betti also proposed a damage identification method based on ERA with a Data Correlation and Kalman Observer (Lus, Betti, et al. 2003). Bernal and Gunes, also used ERA with a Kalman Observer for identifying modal characteristics when the input is known, and used a subspace identification algorithm when the input cannot be measured (Bernal & Gunes 2003). A novel modal identification based approach was also presented by Barroso and Rodriguez who employed a damage index method to identify changes in stiffness mass ratios for the IASC-ASCE (International Association for Structural Control-American Society of Civil Engineers) benchmark structure (Barroso & Rodriguez 2004).

Flexibility-based methods are generally more sensitive to changes in the first few natural modes, which also dominate the response of many typical civil structures, than the modal-based techniques. Lin used the cross-unity check between the flexibility matrix obtained from measured data and the analytical stiffness matrix to locate damage (Lin 1990). Bernal and Gunes, presented a flexibility-based method that involved sub-matrix inverses and the full data record to perform models identification (Bernal & Gunes 2003). Bernal and Marin, also introduced Dynamic Damage Locating Vectors (DDLVs) approach for structural damage detection and localisation (Bernal 2007; Marin et al. 2013). DDLVs lie in the null space of the change in the transfer matrix and provide Laplace transform of dynamic loads, and thus, result in zero stress fields over the damaged region.

The problem of damage detection can also be seen as an inverse problem. Using measured input-output vibration data, analytical model of the structure can be updated to reproduce the measured data. Minimising the error between the reproduced and measured responses by iteratively refining the stiffness and mass matrices yields the damaged structure's parameters (Lus, Betti, et al. 2003; Lus, De Angelis, et al. 2003). Some recently published methods also include Bayesian statistical approaches using one or two stages to identify modal parameters and then damage (Ji et al. 2010; Lam,

Katafygiotis & Mickleborough 2003; Yuen, Au & Beck 2003).

The reviewed parametric SHM methods are used mainly as off-line techniques because post processing of measured time history data is required to extract the necessary diagnostic information. However, the inability of off-line SHM techniques to be implemented in real-time, on a sample-to-sample basis as the event occurs, makes them unsuitable for real-time structural control for damage reduction purposes upon detecting damage. Equally, their outcomes may not be available immediately after an event, perhaps reducing their potential and positive impact on immediate earthquake response. In contrast, on-line/real-time methods provide all the necessary information to plan damage mitigation measures in advance, and thus, avoid catastrophic failures, as well as aiding immediate post-event response.

Adaptive fading Kalman filters (Loh, Lin & Huang 2000; Sato & Takei 1997), adaptive H∞ filter techniques (Sato & Qi 1998), and bootstrap filtering approaches (Li, Suzuki & Noori 2004), can achieve real-time or near real-time results and provide structural parameter identification. However, they have significant computational cost and complexity which makes the implementation of such methods for on-line SHM difficult.

Simpler algorithms for on-line SHM make the use of adaptive Least Squares Estimation (LSE). Chassiakos et al. used adaptive least squares approach for on-line identification of hysteretic systems through reliable estimates of the hysteretic restoring force parameters using acceleration data (Chassiakos et al. 1998). This work was extended by Smyth et al. to handle the general case when no information is available on the system parameters (Smyth et al. 1999).

Lin et al. presented a Recursive Least Squares based algorithm that upgrades the diagonal elements of the adaptation gain matrix sample-to-sample by comparing the values of estimated parameters between two consecutive time steps (Lin et al. 2001). The method requires full-state structural response measurement and is not able to identify the different abrupt changes in the parameters. Yang et al. also proposed an on-line adaptive least-square tracking technique that uses only acceleration data to identify abrupt changes in the parameters of hysteretic structures, from which structural damage can be determined (Yang & Lin 2004). This method, however, is computationally very

expensive.

MX Least Mean Squares (MX-LMS) filters, named after their modular cross-coupled structure, were also used by Kaiser et al. to identify modal parameters in the health monitoring of adaptive aerospace structures (Kaiser et al. 1999). The changes of these parameters are then related to the location and extent of damage.

Model-based methods, combined with adaptive LMS filtering theory, were also used to identify structural stiffness changes in real-time in a computationally efficient and robust fashion. Adaptive LMS filters approximate gradient optimisation and convergence in real-time from sample-to-sample. In contrast, least squares structural optimisation methods use the full data record and multiple computational analyses to converge to a solution.

LMS-based SHM has been used for a benchmark problem (Geoffrey Chase et al. 2005), and also for a highly nonlinear rocking structure (Chase et al. 2005), to directly identify changes in structural stiffness only. Similar RLS methods have also been applied to the same problem (Chase, Begoc & Barroso 2005). All these methods directly identify changes in structural stiffness over time by comparing the stiffness matrix of a structure with the undamaged model matrix. These model-based adaptive filtering methods are robust with fast convergence and low computational cost. However, they do not identify plastic and permanent deformations, and require full-state structural response measurements. Most importantly, the algorithm needs priory knowledge on the changing rate of structural parameters. Moreover, the algorithm should be tuned by trial and error for a specific structure and damage pattern.

Hann et al. proposed a SHM method for nonlinear hysteretic dynamics identification using convex integral-based fitting methods and Piecewise Linear Least Squares (PLLSQ) fitting (Hann et al. 2009). The method uses only acceleration measurements and infrequently measured displacements motivated by global positioning system (GPS), and is also capable of identifying plastic and permanent deformations in real-time. The identified permanent displacement is a particularly useful damage measure for the construction of probabilistic fragility functions.

5.2.2 Non-parametric Methods

Artificial Neural Networks (ANNs) are one of the common non-parametric SHM methods. A neural network is composed of many layers with weight factors and a bias value. Outputs of one layer are multiplied by its weights and shifted by the layer's bias value and then used as inputs to the next layer. The weights and biases are adjusted during the training phase of the ANN to minimise error between measured and predicted outputs of the structure. When damage occurs, the weights change to compensate for changes in the outputs of the structure due to the damage. However, the non-uniqueness of the set of the network weights calculated for a particular type or form of damage makes it difficult to relate changes in the weights to the location and severity of the damage occurred. Equally, training sets may not generalise well to actual damage, or remain relevant over time.

Masri et al. proposed an ANN-based method that can detect changes in an unknown system's nonlinear dynamic behaviour based on the level of output prediction error when measured responses of a damaged system are passed through the network trained to predict the undamaged state responses (Masri et al. 2000). However, it is difficult to relate this information to locate or quantify the damage detected.

In another study, Zapico et al. proposed a procedure based on a Multi Layer Perception (MLP) for damage assessment in a two-storey steel frame with steel-concrete composite floors (Zapico, Worden & Molina 2001). The MLPs were trained using a simplified finite element model through the error back-propagation algorithm. The two longitudinal bending natural frequencies were used as inputs to the MLPs to determine damage at floor levels. Nevertheless, more knowledge of the damage level at each floor, for example through analysing the experimental frequency response functions of the damaged structure, is needed to validate the results.

Zang et al. also presented an approach to detect structural damage based on a combination of Independent Component Analysis (ICA) extraction of time domain data and ANN to detect damage in a truss structure and also in a three-storey bookshelf-type model building (Zang, Friswell & Imregun 2004). The proposed ICA technique captures the essential structure of a large volume of the measured vibration data to be used in the ANN training phase.

Discrete and continuous wavelet analyses have also been used in SHM. A good review of the research on damage detection using wavelet analysis can be found in (Kim & Melhem 2004). One example of wavelet-based approaches is a statistical pattern classification method, developed by Sun and Chang, based on Wavelet Packet Transform (WPT) (Sun & Chang 2004). This method uses acceleration responses of the free end of a steel cantilever I-beam excited by a pulse load to detect induced damage in the beam in the form of line cuts of different severities in the flange. The responses are decomposed into wavelet packet components, and dominant signal energies of the wavelet packet components are then used as the Wavelet Packet Signature (WPS) for damage detection.

Two damage indicators were formulated by Sun and Chang to lump the discriminate information from the extracted WPS with thresholds set based on the statistical properties and successive measurements.

Wavelet-based methods determine the time at which damage occurred (Hera & Hou 2003; Hou, Noori & Amand 2000). Damage, and the moment when the damage occurs, can be detected by a spike or an impulse in the plots of higher resolution details from wavelet decomposition of the acceleration response data. Hera and Hou, also used the spatial distribution pattern of the observed spikes to determine the region in which the damage occurred.

Empirical Mode Decomposition (EMD) has also been used for damage detection. Yang et al. used EMD to extract sudden stiffness damage time instants and locations over the full measured record (Yang et al. 2003). They also used EMD and Hilbert–Huang linear transforms to identify damage time instants, as well as natural frequencies and damping ratios of the structure before and after damage, using measured data. However, these methods are complex, and require the full record and sometimes operator input to arrive at a final diagnosis, therefore, they are neither on-line nor automated.

5.2.3 Final Statements on the literature

The SHM field is too large to present a complete literature review here. Similar approaches can be found in excellent reviews by (Fan & Qiao 2011), (Montalvao, Maia

& Ribeiro 2006), and (Dharap 2006).

Overall, despite the extensive efforts made by the SHM community, it can be seen that there is still a great need for further developments in the following areas:

• Many existing SHM algorithms cannot be implemented in real time. Therefore, their results would not be available during or immediately after an event for urgent post-event response. Further, these off-line techniques are not capable of providing the input information required for structural control systems for damage mitigation. On-line SHM methods resolve these issues. However, existing on-line SHM approaches have significant computational complexity. Therefore, developing computationally-efficient and more suitable algorithms for RT-SHM is crucial in developing damage-free structures, providing more reliable information for post-event decision making and consequently more resilient communities to devastating earthquakes.

• Many existing off-line or on-line SHM methods require full structural response measurements, including velocities, displacements and external excitations that are typically difficult to measure. Novel displacement and velocity sensors would provide the inputs required for many SHM algorithms and make their implementation by the profession possible.

• Parametric SHM methods are generally more suitable for SHM because of their ability to determine type and location of damage over the non-parametric approaches. However, many parametric SHM techniques use linear baseline models that do not provide enough information about the structure. More comprehensive nonlinear baseline models offer further structural parameters to be monitored and consequently more useful information on safety and serviceability of structures after an event.

5.3 KALMAN FILTERING METHODS

As discussed earlier, the state-space model is another commonly used model especially for multivariable input/output systems to model the dynamic behaviour of structures. A variety of methods, such as extended Kalman filter, unscented Kalman filter, ensemble Kalman filter etc., have been proposed to estimate the state space response of the model as well as the parameters of the model (Wu & Smyth 2007).

Hoshiya et al. utilised extended Kalman filter (EKF) to perform system identification of seismic structural systems (Hoshiya & Saito 1984). To obtain the stable and convergent solutions, a weighted global iteration procedure with an objective function was incorporated into the extended Kalman filter algorithm for stable estimation. The effectiveness of this method was verified on multiple degree-of-freedom linear systems, bilinear hysteretic systems, and equivalent liberalisation of bilinear hysteretic systems.

Yang et al. proposed an EKF approach with unknown inputs (EKF-UI) to identify the structural parameters, such as the stiffness, damping and other nonlinear parameters, as well as the unmeasured excitations (Yang, Pan & Huang 2007). An analytical solution for the proposed EKF-UI approach was derived and presented. An adaptive tracking technique was also implemented in the proposed EKF-UI approach to track the variations of structural parameters due to damage. Simulation results for linear and nonlinear structures demonstrated that the proposed approach was capable of identifying the structural parameters and their variations due to damage and unknown excitations.

Ghanem et al. pointed out that the accuracy of EKF relies on the simple structure of linear dynamical systems excited by Gaussian noise (Ghanem & Ferro 2006). In situations where either the noise is significantly non-Gaussian or the dynamics is highly non-linear, the accuracy associated with filtering the linearised system may not be acceptable. To tackle the above challenges, they presented a combination of the ensemble Kalman filter (EnKF) and non-parametric modelling techniques. EnKF relies on the traditional corrector equation of the standard Kalman filter, except that the gain is calculated from the error covariance provided by the ensemble of model states. Both location and time of occurrence of damage were accurately detected in spite of measurement and modelling noise. A comparison between ensemble and extended Kalman filters was also presented, highlighting the benefits of the approach.

Another technique to handle the difficulty of EKF in dealing with strong nonlinear system is Unscented Kalman Filter (UKF) which is introduced by Julier and utilises a deterministic “sampling” approach to calculate mean and covariance terms (Julier & Uhlmann 1997). Essentially 2L+1 sigma points (L is the state dimension), are chosen based on a square-root decomposition of the prior covariance. These sigma points are

propagated through the true nonlinearity, without approximation, and then a weighted mean and covariance is taken. A simple illustration of the approach is shown in Figure 5.1 for a 2-dimensional system and will be explained in details later. The UKF uses a deterministic sampling technique known as the unscented transform to pick a minimal set of sample points (called sigma points) around the mean. These sigma points are then propagated through the non-linear functions, from which the mean and covariance of the estimate are then recovered. Compared with EKF, UKF more accurately captures the true mean and covariance of the estimation. In addition, UKF removes the requirement to explicitly calculate Jacobian, which for complex functions can be a difficult task in itself. Wu et al. compared EKF and UKF in estimating the dynamic responses of nonlinear structures, whose results show that the UKF produces better state estimation and parameter identification than the EKF and is also more robust to measurement noise levels (Wu, Hu & Hu 2007).

The iterated forms of EKF and UKF (IEKF, IUKF), which are recently developed, can be thought as an estimator of the conditional mode that employs an approximate Newton–Raphson iterative scheme to solve the maximisation of the conditional probability density function (Ungarala 2012).

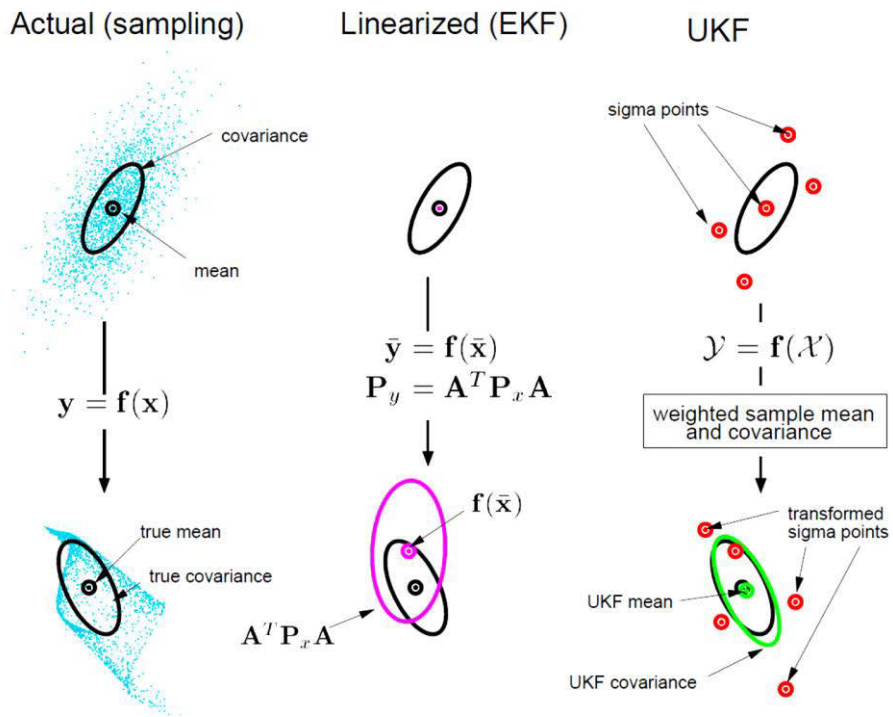

Figure 5.1. Example of mean and covariance propagation (Julier & Uhlmann 1997).

In the next section, the capability of four proposed algorithms, i.e. EKF, IEKF, UKF and IUKF in identifying the structural parameters, are compared, based on numerical examples, including one highly nonlinear structure whose Jacobian matrix is quite complex. The robustness and sensitivity of the methods to the measurement noise level and initial guesses of state vector will also be examined. To the authors' best knowledge, such investigation has not been reported in published literature.

5.3.1 Principles of EKF, IEKF, UKF and IUKF

Consider the general dynamical system described by the following nonlinear continuous state space equation with added noise:

$$\dot{x} = f\big(x(t)\big) + \nu(t) \tag{5-1}$$

and the nonlinear observation equation at time $t = k\Delta t$:

$$y_k = h(x_k) + \eta_k \tag{5-2}$$

where $\nu(t)$ and η_k denote the process and measurement noise with corresponding covariance matrices Q(t) and R_k, respectively. In discrete time, equation (5-1) can be rewritten as follows and we obtain a discrete nonlinear state space equation:

$$\begin{aligned} x_{k+1} &= F(x_{k0}) + \nu_k \\ y_k &= h(x_k) + \eta_k \end{aligned} \tag{5-3}$$

where ν_k is the process noise vector with covariance matrix Q_k, and function F is obtained from equation (5-1) via integration:

$$F(x_k) = x_k + \int_{k\Delta t}^{(k+1)\Delta t} f(x(t))dt \tag{5-4}$$

A recursive estimation of x_k can be obtained from one of the algorithms described below.

5.3.1.1 Extended Kalman Filter (EKF)

In the extended Kalman filter method, a new priori estimate of the state vector is first predicted using the system model ('time update' step) and then the predicted estimate is

improved using available measurements ('measurement update' step). The state prediction $\hat{x}_k^-$ and corresponding covariance can be calculated as:

$$\hat{x}_k^- = \hat{x}_{k-1} + \int_{(k-1)\Delta t}^{(k)\Delta t} f(x(t))dt \tag{5-5}$$

$$P_k^- = \emptyset_k P_{k-1} \emptyset_k{}^T + Q_{k-1} \tag{5-6}$$

In equation (5-6), $\emptyset_k$ is the state transition matrix which can be obtained as:

$$\emptyset_k = I + \Delta t \left[\frac{\partial f(x(t))}{\partial x(t)}\right]_{x(t)=\hat{x}_{k-1}} \tag{5-7}$$

The predicted measurement is estimated as

$$\hat{Y}_k = h(\hat{x}_k^-) \tag{5-8}$$

Thus, in the measurement update step,

$$\hat{x}_k = \hat{x}_k^- + K_k(Y_k - \hat{Y}_k)$$

$$P_k = [I - K_k H_k]P_k^-[I - K_k H_k]^T + K_k R_k K_k{}^T \tag{5-9}$$

$$K_k = P_k^- H_k{}^T [H_k P_k^- H_k^T + R_k]^{-1}$$

where K_k is the Kalman gain matrix at time step k and H_k is the linearised coefficient matrix of the observation equation given as:

$$H_k = \left[\frac{\partial \mathrm{h(x)}}{\partial x}\right]_{x=\hat{x}_k^-} \tag{5-10}$$

5.3.1.2 Iterated Extended Kalman Filter (IEKF)

The main difference between IEKF and EKF is in the measurement updates. In IEKF, once the state prediction $\hat{x}_k^-$ and the corresponding covariance are estimated, the following iterations will be done recursively:

$$\hat{x}_{k,0} = \hat{x}_k^-, \quad P_{k,0} = P_k^-$$

$$\hat{x}_{k,j+1} = \hat{x}_k^- + K_{k,j}[y_k - h(\hat{x}_{k,j}) - H_{k,j}(\hat{x}_k^- - \hat{x}_{k,j})] \tag{5-11}$$

$P_{k,j} = (I - K_{k,j}H_{k,j})P_k^-$,

where

$$H_{k,j} = \frac{\partial h(x)}{\partial x}|_{x=\hat{x}_{k,j}}$$
$$K_{k,j} = P_k^- H_{k,j}^T (H_{k,j}P_k^- H_{k,j}^T + R_k)^{-1}. \quad (5\text{-}12)$$

This process will be stopped if a certain condition is met. A common termination condition is that the inequality $\left\|\hat{x}_{k,j+1} - \hat{x}_{k,j}\right\| \leq V_{th}$ is satisfied, where V_{th} is the predetermined threshold. After N iterations, the ultimate state estimate and corresponding covariance matrix are:

$$\hat{x}_k = \hat{x}_{k,N}, \qquad P_k = P_{k,N} \quad (5\text{-}13)$$

5.3.1.3 Unscented Kalman Filter (UKF)

The UKF has the same level of computational complexity as that of EKF. However, it does not need to calculate Jacobians or Hessians, and can achieve second-order accuracy, whereas the accuracy of the EKF is of the first order. The UKF estimation can be expressed, as explained in the following steps:

Step 1: Sigma Point Calculation

At instant k-1, a set of deterministic sample points with associated weights are generated as;

$$\chi_{0,k-1} = \overline{x}_{k-1}$$
$$\chi_{i,k-1} = \overline{x}_{k-1} + (\sqrt{(L+\gamma)P_{k-1}})_i, \qquad i = 1,2,..,L \quad (5\text{-}14)$$
$$\chi_{i,k-1} = \overline{x}_{k-1} - (\sqrt{(L+\gamma)P_{k-1}})_{i-L}, \qquad i = L+1, L+2, \ldots, 2L$$

$$w_0^{(m)} = {\gamma}/{(L+\gamma)}$$

$$w_0^{(c)} = {\gamma}/{(L+\gamma)} + (1-\alpha^2+\beta) \tag{5-15}$$

$$w_i^{(m)} = w_i^{(c)} = {1}/{\{2(L+\gamma)\}}, \quad i = 1,2,\dots,2L$$

where χ_i and w_i represent sigma point and corresponding weight, respectively; L is the dimension of x; $\gamma = \alpha^2(L+\kappa) - L$ is a scaling parameter; α determines the spread of the sigma points around $\bar{x}$, and is usually a small positive value (0.0001≤ α ≤ 1); κ is a secondary scaling parameter which is usually set to 0; β is used to incorporate the prior distribution of x (for a Gaussian distribution β =2 is optimal); $(\sqrt{P})_i$ denotes the i[th] row of the matrix square root.

Step 2: Time Update

After the sample points are propagated through the nonlinear equations, the predicted mean and covariance are computed as:

$$\chi_{k|k-1} = f(\chi_{k-1})$$

$$\hat{x}_k^- = \sum_{i=0}^{2L} w_i^{(c)} \chi_{i,k|k-1}$$

$$P_k^- = \sum_{i=0}^{2L} w_i^{(c)} \left[\chi_{i,k|k-1} - \hat{x}_k^-\right]\left[\chi_{i,k|k-1} - \hat{x}_k^-\right]^T + Q_k$$

$$\chi_{k|k-1}^* = \left[\chi_{0:2L,k|k-1}, \quad \chi_{0,k|k-1} + \nu\sqrt{Q_k}, \quad \chi_{0,k|k-1} - \nu\sqrt{Q_k}\right] \tag{5-16}$$

$$Y_{k|k-1}^* = h\left(\chi_{k|k-1}^*\right)$$

$$\hat{y}_k^- = \sum_{i=0}^{2L^\alpha} w_i^{*(m)} Y_{i,k|k-1}^*$$

$$P_{yy,k} = \sum_{i=0}^{2L^\alpha} w_i^{*(c)} \left[Y_{i,k|k-1}^* - \hat{y}_k^-\right]\left[Y_{i,k|k-1}^* - \hat{y}_k^-\right]^T + R_k$$

$$P_{xy,k} = \sum_{i=0}^{2L^\alpha} w_i^{*(c)} \left[\chi_{i,k|k-1}^* - \hat{x}_k^-\right]\left[Y_{i,k|k-1}^* - \hat{y}_k^-\right]^T,$$

where L^{α} =2L, $\nu = \sqrt{L + \gamma}$; $w_i^{*(c)}i$ and $w_i^{*(m)}$are calculated in the same way as equation (5-15) with the replacement of L by L^{α}. Note that in (5-16), the sigma points are augmented with additional points derived from the matrix square root of the process noise covariance Q. The main purpose is to incorporate the effect of the process noise on the observed sigma points *Y*. For more details, refer to (Van Der Merwe 2004).

Step 3: Measurement Update

The Kalman gain is calculated to update the state and covariance.

$$K_k = P_{xy,k} P_{yy,k}^{-1}$$

$$\hat{x}_k = \hat{x}_k^- + K_k(y_k - \hat{y}_k^-) \quad (5\text{-}17)$$

$$P_k = P_k^- - K_k P_{yy,k} K_k^T$$

The above three steps, provide a general summary of the UKF algorithm. Given the initial condition $\bar{x}_0 = E[x_0]$ and $P_0 = E[(x_0 - \bar{x}_0)(x_0 - \bar{x}_0)^T]$, the filtering procedure can be recursively implemented.

5.3.1.4 Iterated Unscented Kalman Filter (IUKF)

Enlightened by the development of iterated extended Kalman filter (IEKF), as well as the superiority of UKF, a natural idea is that improved performance may be expected if the iterations are implemented in UKF. However in view of the potential problems exhibited by the IEKF, special steps should be taken to make the iterated filter perform as good as possible. In what follows, an iterated unscented Kalman filter (IUKF) will be developed to address this problem, using a different iteration strategy. The procedure for IUKF is summarised as follows:

Step 1: for each instant, when $k \geq 1$, evaluate the state estimate $\hat{x}_k$, and corresponding covariance matrix P_k through equations (5-14 to 5-17),

Step 2: Let $\hat{x}_{k,0} = \hat{x}_k^-$, $P_{k,0} = P_k^-$ and $\hat{x}_{k,1} = \hat{x}_k$, $P_{k,1} = P_k$. Also let g=1 and j=2.

Step 3: Generate new sigma points:

$$\chi_{i,j} = \left[\hat{x}_{k,j-1}\,, \quad \hat{x}_{k,j-1} + \sqrt{(L+\gamma)P_{k,j-1}}, \quad \hat{x}_{k,j-1} - \sqrt{(L+\gamma)P_{k,j-1}}\right]_i \tag{5-18}$$

Step 4: Recalculate equations (5-16 to 5-17) as follows:

$$\hat{x}_{k,j}^{-} = \sum_{i=0}^{2L} w_i^{(m)}\, \chi_{i,j}$$

$$Y_{i,j} = h(\chi_{i,j})$$

$$\hat{y}_{k,j}^{-} = \sum_{i=0}^{2L} w_i^{(m)}\, Y_{i,j}$$

$$P_{yy,k,j} = \sum_{i=0}^{2L} w_i^{(c)} \left[Y_{i,j} - \hat{y}_{k,j}^{-}\right]\left[Y_{i,j} - \hat{y}_{k,j}^{-}\right]^T + R_k \tag{5-19}$$

$$P_{xy,k,j} = \sum_{i=0}^{2L} w_i^{(c)} \left[\chi_{i,j} - \hat{x}_{k,j}^{-}\right]\left[Y_{i,j} - \hat{y}_{k,j}^{-}\right]^T$$

$$K_{k,j} = P_{xy,k,j} P_{yy,k,j}^{-1}$$

$$\hat{x}_{k,j} = \hat{x}_{k,j}^{-} + g.K_{k,j}(y_k - \hat{y}_{k,j}^{-})$$

$$P_{k,j} = P_{k,j-1}^{-} - K_{k,j} P_{yy,k,j} K_{k,j}^T$$

where the subscript j denotes the jth iteration; $Y_{i,j}$ represents the ith component of Y_j.

Step 5: Define the following three equations:

(i) $\hat{y}_{k,j} = h(\hat{x}_{k,j})$

(ii) $\tilde{x}_{k,j} = \hat{x}_{k,j} - \hat{x}_{k,j-1}$

(iii) $\tilde{y}_{k,j} = y_k - \hat{y}_{k,j}$

Step 6: if the following inequality holds:

$$\tilde{x}_{k,j}^T P_{k,j-1}^{-1} \tilde{x}_{k,j} + \tilde{y}_{k,j}^T R_k^{-1} \tilde{y}_{k,j} < \tilde{y}_{k,j-1}^T R_k^{-1} \tilde{y}_{k,j-1}, \tag{5-20}$$

and if $j \leq N$, then set $g = \eta . g\ , j = j + 1$ and return to step 3; otherwise, continue to step 7.

Step 7: stop if the inequality (5-20) is not satisfied or if j is too large (j>N) and set $\hat{x}_k = \hat{x}_{k,j}\ , P_k = P_{k,j}$.

Now, to explain why the iterations converge to a solution, we first come back to the last equation of (5-19). For the positive definite matrices $P_{k,j}$, $P_{k,j-1}$ and $P_{yy,k,j}$ assume that $\lim_{j\to\infty} K_{k,j} \neq 0$, then according to (5-19), we have $P_{k,j} < P_{k,j-1}$ for any $j = 1,2,.. < \infty$. Based on the fact that each element of the matrix $P_{k,j}$ is bounded, it is easy to know that $\lim_{j\to\infty} P_{k,j} = \lim_{j\to\infty} P_{k,j-1}$. With this premise, it can be inferred from (5-19) that $\lim_{j\to\infty} K_{k,j} = 0$, which violates the assumption that $\lim_{j\to\infty} K_{k,j} \neq 0$. Obviously, the assumption does not hold and only possibility is that $\lim_{j\to\infty} K_{k,j} = 0$. Now suppose that $K_{k,j} \to 0$ when $j > N$, then from (5-19), we have $\hat{x}_{k,j} \to \hat{x}_{k,j}^- = \hat{x}_{k,j-1}$ and $P_{k,j} \to P_{k,j-1}$, which means that convergence is guaranteed as the iteration process proceeds.

According to (5-19), the result of N iterations is $\hat{x}_{k,N} = \hat{x}_{k,N}^- + \eta^{N-1} K_{k,n}(y_k - \hat{y}_{k,N}^-)$. Now if the decaying factor η is chosen as $0 < \eta < 1$ and N is large enough, then we have $\hat{x}_{k,N} \to \hat{x}_{k,N}^- = \hat{x}_{k,N-1}$ because $\eta^{N-1} \to 0$ for a large N. From this assumption, it can also be concluded that iteration process will converge to a solution; meanwhile, the convergence speed is affected by the factor η.

Compared with the standard UKF, the IUKF can adjust the state estimate to adaptively approach the true value through corrections of the measurement, so after the iteration terminates, a lower state error can be expected. In addition, the proposed filter can respond to new measurements as quickly as possible with the adjustment of state and covariance matrix, making a faster convergence speed possible in situations where the initial error is large (Chatzi & Smyth 2009; Xie & Feng 2012).

5.3.2 Numerical Simulations

5.3.2.1 SDOF nonlinear hysteretic system

Consider a single degree of freedom (SDOF) nonlinear hysteretic Bouc-Wen system

subjected to earthquake acceleration $\ddot{x}_g$ (Figure 5.2). The governing equation of motion is:

$$m\ddot{x}(t) + c\dot{x} + kr(t) = -m\ddot{x}_g(t) \tag{5-21}$$

The Bouc-Wen model that will be used for $r(\dot{x}, x)$ is as follows:

$$\dot{r} = \dot{x} - \beta|\dot{x}||r|^{\alpha-1}r - \gamma\dot{x}|r|^{\alpha} \tag{5-22}$$

where, c is the damping coefficient, k is the stiffness, and β, γ and α are hysteretic parameters. The following parametric values are used for the simulation study: m=1 kg, c=0.3 Ns/m, k=9 N/m, β=2, $\gamma = 1$, $\alpha = 2$ and $\ddot{x}_g$ is the El-Centro earthquake of 1940 with a peak ground acceleration of 0.15 g (PGA=0.15g). The acceleration of the mass, $\ddot{x}$, and ground, $\ddot{x}_g$, is measured using the installed sensors and the unknown parameters are taken as c, k, β, α and γ. For the purpose of exploring the identification robustness to noise, a white noise process with different root mean square (RMS) noise-to-signal ratios is superimposed to both the simulated acceleration response and the earthquake ground acceleration. The system responses of the displacement, velocity, and acceleration were obtained by solving differential equation (5-21) using the fourth-order Runge–Kutta integration method.

The objective is to estimate the unknown parameters as well as the displacement, velocity and r(t) signals. Therefore, the state vector to be estimated is defined as:

$$X = [x_1,\ x_2,\ x_3,\ x_4,\ x_5,\ x_6,\ x_7,\ x_8\ ]^T = [x, \dot{x}, r, c, k, \beta, \gamma, \alpha]$$

Equations (5-21) and (5-22) can be rewritten in the form of state space as follows:

$$f\big(X(t), u(t)\big) = \begin{bmatrix} x_2 \\ -\ddot{x}_g - \dfrac{x_2x_4 + x_3x_5}{m} \\ x_2 - x_6|x_2||x_3|^{x_8-1}x_3 - x_7x_2|x_3|^{x_8} \\ 0 \\ 0 \\ 0 \\ 0 \\ 0 \end{bmatrix} \tag{5-23}$$

The system equation (5-23), clearly exhibits a very strong nonlinear behaviour. If the

acceleration response and excitation are measured, the observation equation, which is the absolute acceleration of the mass m, can be expressed as:

$$y = \ddot{x} + \ddot{x}_g + v = -\frac{c\dot{x} + r}{m + v} = -\frac{x_2 x_4 + x_3 x_5}{m} + v \tag{5-24}$$

The simulation is carried out using 2% added root mean square (RMS) noise-to-signal ratio and initial guesses of $X_0 = [0, 0, 0, 0.2, 5, 0, 0.5, 1]$. The identification of the parameters during the earthquake is depicted in Figure 5.3 while the estimated hysteretic loops between 4 to 8 seconds, using the four aforementioned algorithms are shown in Figure 5.4.

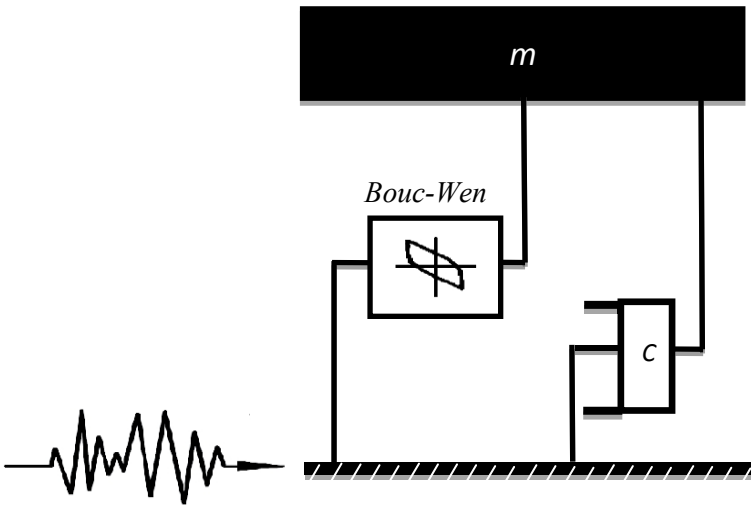

Figure 5.2. SDOF nonlinear hysteretic system

As can be observed from Figure 5.3, the IEKF and IUKF have better convergence speed and accuracy compared to their standard forms where IUKF shows the best performance among all methods in terms of both accuracy and convergence speed. It is worth noting that the former (IEKF) has not been applied to structural parameters identification before.

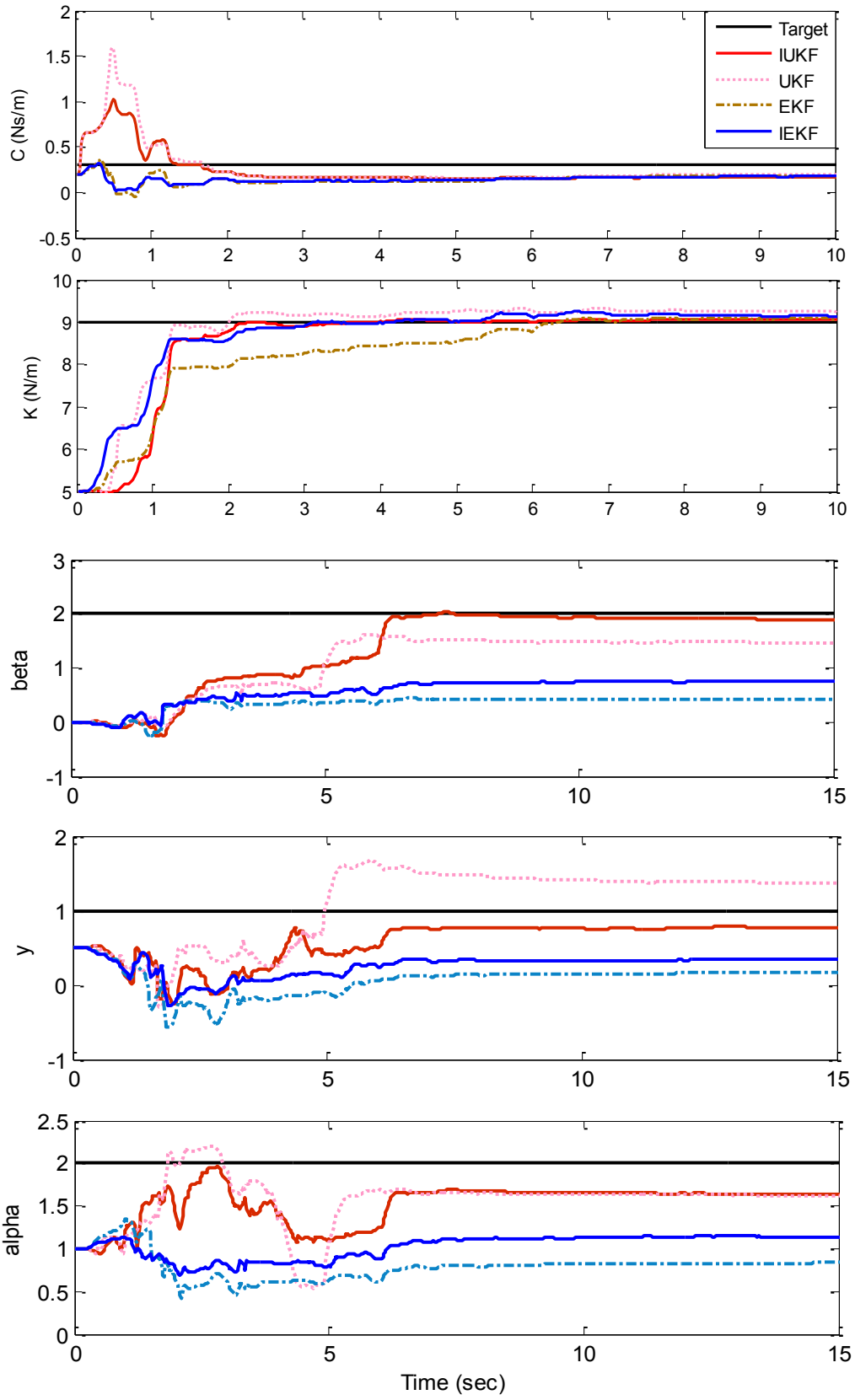

Figure 5.3. Parameters estimation for SDOF nonlinear system, noise level 2% RMS.

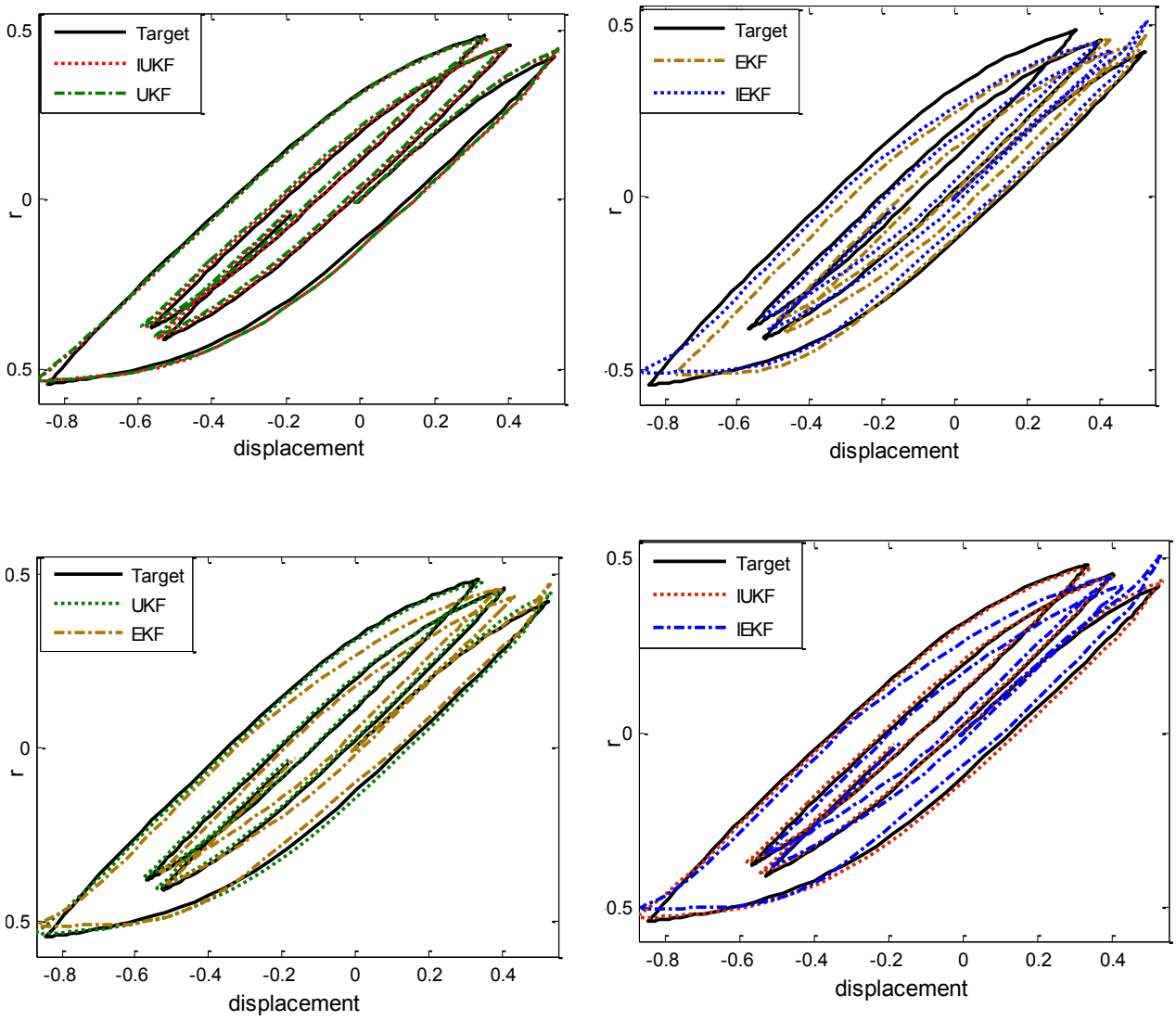

Figure 5.4. Estimated hysteretic loops for the Bouc–Wen system, noise level 2% RMS

5.3.2.2 2DOF linear structural system

As another application of the proposed identification algorithms, a two-degree of freedom structural system subjected to an earthquake excitation is considered (Figure 5.5). The governing equations of motion are as follows:

$$m_1\ddot{x}_1 + c_1\dot{x}_1 + c_2(\dot{x}_1 - \dot{x}_2) + k_1x_1 + k_2(x_1 - x_2) = -m_1\ddot{x}_g$$
$$m_2\ddot{x}_2 + c_2(\dot{x}_2 - \dot{x}_1) + k_2(x_2 - x_1) = -m_2\ddot{x}_g, \quad (5\text{-}25)$$

in which $m_1 = m_2 = 1\ kg$, $c_1 = 0.6\ Ns/m$, $c_2 = 0.5\ Ns/m$, $k_1 = 12\ N/m$, and $k_2 = 10\ N/m$. The system is linear; however, the estimation of the unknown parameters jointly with the state is a nonlinear estimation problem. The same

earthquake as in the previous case study is used as the excitation to the structure. The acceleration response and the earthquake excitation are assumed to be measurable. The purpose here is to also predict the stiffness and damping of different storeys and estimate the velocity and displacement signals of different floors. Thus, the state vector to be tracked is defined as:

$$X = [X_1, X_2, X_3, X_4, X_5, X_6, X_7, X_8\ ]^T = [x_1, \dot{x}_1, x_2, \dot{x}_2, k_1, k_2, c_1, c_2].$$

As mentioned, although the system is linear, the estimation of unknown parameters together with the states, is a nonlinear estimation problem.

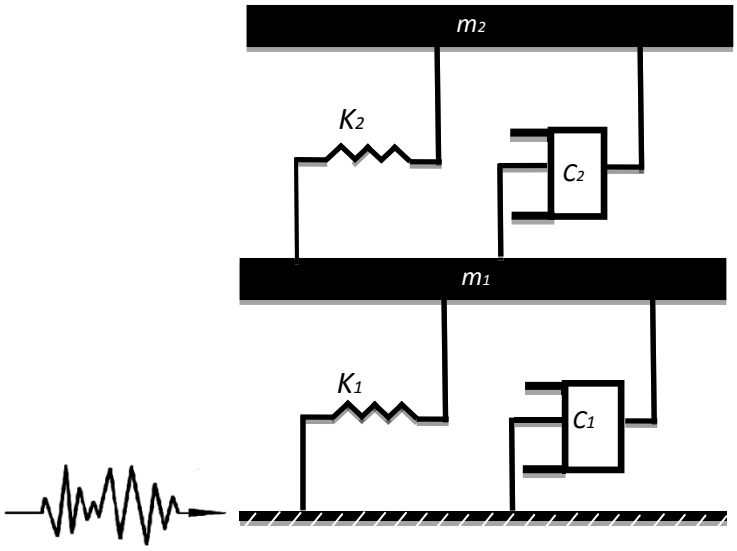

Figure 5.5. 2DOF linear system

In the first run, a noise level of 1% RMS is added to both measured signals and ground acceleration. The initial state vector is also thought to be$X_0 = [0.0001, 0.0001, 0.0001, 0.0001, 5, 5, 0.3, 0.3]$. The identified parameters during the first 8 seconds of the earthquake are illustrated in Figure 5.6. As can be seen, UKF and IUKF have better performances than EKF and IEKF in the beginning of the process. However, all the methods converge to almost the same values after four seconds. It is interesting to note that although the performance of IEKF was expected to be always better than EKF, the results show that EKF can track the damping values with less fluctuation than IEKF. The reason is that although theoretically the IEKF is superior to EKF (Bell & Cathey 1993), this theory is only valid when the local

linearisation condition is unconditionally met (Fucheng, Zhongkang & Kan 2003; Xiangyi 2004), i.e., the state estimate is close enough to the true value. However, in many applications, this assumption is not always true because the initial estimate errors may be large. The other reason is that, from the update equations, it is clear that the state correction in each iteration, is realised through measurement, while the measurement error cannot be zero as ideal cases. Therefore, the convergence property of iterations depends on the precision of measurements. Additionally, the threshold V_{th} is crucial to successfully using the iterated algorithm, but a proper choice of V_{th} is not easy. In this study, a threshold of 0.08 has been used to simulate the IEKF.

To examine the robustness and sensitivity of the algorithms to the noise level and the initial state vector, a second simulation is performed using a noise level of 5% RMS and initial state vector of $X_0 = [0.0001, 0.0001, 0.0001, 0.0001, 2.8, 2.8, 0.15, 0.15]$. Results are shown in Figure 5.7 in which, the performance of four proposed identification techniques are compared to each other.

As can be found from Figure 5.7, although IEKF is an improved version of EKF, it still cannot perform well when the initial values of the unknown parameters are far from the real ones. IUKF, on the other hand, tracks the parameters with good accuracy, which is even better than UKF.

Table 5-1, also shows the final identified parameters of the proposed structure with different noise levels and initial state vector. The best result in each section is bolded. The superiority of IUKF over other methods is clearer when more noise level is superimposed to the signals and the initial state vector is far from the real values.

The UKF method, on the other hand, has proven to be far superior to standard EKF and IEKF in the structural identification applications, while, when the structure is highly nonlinear or the initial guesses for the unknown variables are not close to real values, or the measurement signals are contaminated with high noise level, IUKF is even better than UKF in robustness, convergence speed and tracking accuracy. It is also worth noting that no publication has been found in the literature, on the application of IEKF to structural parameters identification. Also, such comparison between these four aforementioned algorithms in finding the structural parameters has not been undertaken before.

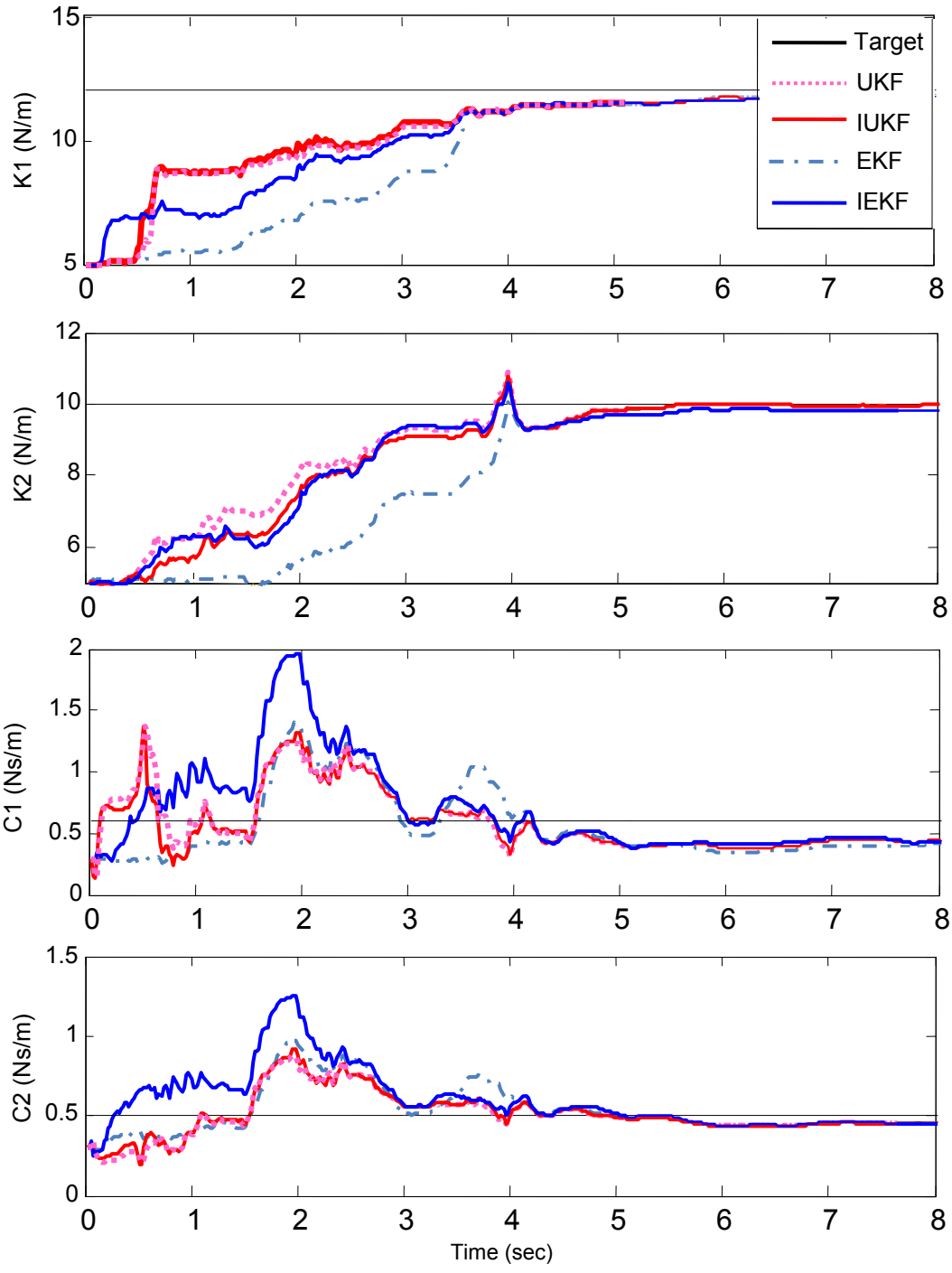

Figure 5.6. Parameters estimation for 2-DOF linear system, noise level 1% RMS and $X_0 = [0.0001,0.0001,0.0001,0.0001,5,5,0.3,0.3]$.

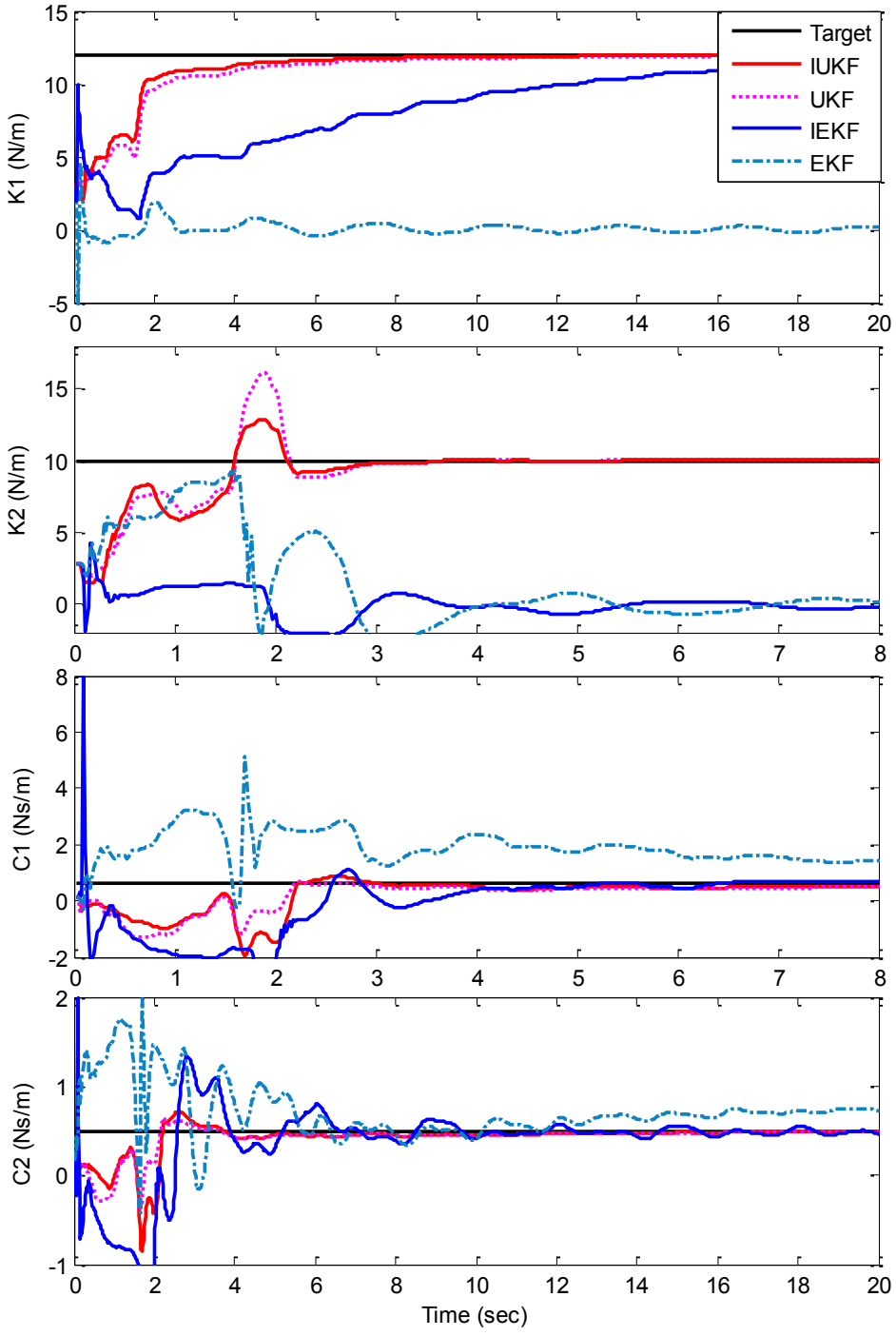

Figure 5.7. Parameters estimation for 2-DOF linear system, noise level 5% RMS, and $X_0 = [0.0001, 0.0001, 0.0001, 0.0001, 2.8, 2.8, 0.15, 0.15]$.

Table 5-1. Estimation results for the 2DOF linear system.

Starting Point	Noise Level	Identification Method		K_1(N/m)	K_2(N/m)	C_1(N s/m)	C_2 (N s/m)
			Exact:	12	10	0.6	0.5
X_0 = [0.0001,0.0001,0.0001,0.0001,5,5,0.3,0.3].	1%	EKF	Estimated:	11.9553	10.0033	0.5595	0.4912
			Error (%):	0.37	0.03	6.75	1.76
		IEKF	Estimated:	11.9688	9.9974	0.5855	0.4852
			Error (%):	0.26	0.026	**2.42**	2.96
		UKF	Estimated:	11.9916	10.0010	0.5808	0.4900
			Error (%):	0.07	**0.01**	3.2	2
		IUKF	Estimated:	11.9917	10.0024	0.5812	0.4914
			Error (%):	**0.069**	0.024	3.13	**1.74**
X_0 = [0.0001,0.0001,0.0001,0.0001,2.8,2.8,0.15,0.1	5%	EKF	Estimated 1:	0.159	-0.1226	1.18	0.73
			Error (%):	98.66	101	96.67	46.00
		IEKF	Estimated:	11.518	0.123	0.76	0.458
			Error (%):	4.017	98.77	26.67	8.4
		UKF	Estimated:	11.957	10.049	0.581	0.490
			Error (%):	0.358	0.49	3.16	**2**
		IUKF	Estimated:	11.977	10.047	0.592	0.485
			Error (%):	**0.192**	**0.47**	**1.33**	3

5.4 Recursive Least Square Based Methods

For on-line structural damage detection methods, time domain analysis, including the recursive least square (RLS) based approaches, has been used successfully in the last decades (Caravani, Watson & Thomson 1977; Tang et al.). However, when a priori knowledge on the changing rate of each parameter is not available, these methods cannot perform well. To overcome this drawback, Yang et.al, proposed some adaptive algorithms which are able to track any abrupt changes in the parameters of structures (Yang, Huang & Lin 2006; Yang & Lin 2004). Although the methods were successfully applied to different type of structures with various damage scenarios, the

authors believe that these methods are computationally inefficient and cannot be used in real-time applications such as integration of control and SHM, where real-time parameter identification is required.

Recently, a new RLS based method, using the forgetting factor, is introduced by Vahidi and applied to identification of vehicle mass and road grade which dramatically decreases the computational effort (Vahidi, Stefanopoulou & Peng 2005). In the next section, we will improve on the aforementioned algorithm by defining an adaptive rule for the forgetting factors and apply that to several structural identification examples, including both linear and highly nonlinear structures. The robustness of the technique will also be examined to the measurement noise level.

5.4.1 Recursive least square with adaptive multiple forgetting factor and known inputs (AMFF-RLS)

Consider a dynamic system with additive noise described as:

$$y_k = \emptyset_k^{'}\theta_k + v_k \tag{5-26}$$

where y_k, at a generic time step k, is the noisy measurement vector, of order m, while $\emptyset_k^{'}$ is the observation matrix of dimension $m \times n$, containing the available values of the system's responses obtained from measurements or data analysis. The vector θ_k, is a vector of n unknown system's parameters that need to be identified, and v_k is the noise component. In least square estimation, unknown parameters of a linear model are chosen in such a way that the sum of the squares of the error between the actual output and computed values is a minimum. For the linear system shown in equation (5-26), this turns into finding the parameter(s) that minimises the following objective function:

$$V(\hat{\theta}, k) = \frac{1}{2}\sum_{i=1}^{k}(y_i - \emptyset_i^{'}\hat{\theta}_i)^2 \tag{5-27}$$

A recursive least-square solution for the estimated parameter $\hat{\theta}_k$is as follows:

$$\hat{\theta}_k = \hat{\theta}_{k-1} + L_k(y_k - \emptyset_k^{'}\hat{\theta}_{k-1}) \tag{5-28}$$

$$L_k = P_k\emptyset_k = P_{k-1}\emptyset_k(I_n + \emptyset_k^{'}P_{k-1}\emptyset_k)^{-1} \tag{5-29}$$

$$P_k = (I_n - L_k \emptyset_k') P_{k-1} \tag{5-30}$$

with I_n being the identity matrix of order n and P_k is called the covariance matrix of order $n \times n$. Since, there is no priori information about the system's unknown parameters, large initial values of the covariance matrix will be required for fast convergence. In fact, large values of P_0, will reflect in large values of L_1 which, in turn, will induce large values of $\hat{\theta}_1$, and improve the convergence rate of the identified parameters. As time progresses, the elements of matrix P_k, will be updated and decreased and consequently, the identified parameters do not fluctuate anymore. This, however, causes a deficiency when an abrupt change occurs in some parameters and, therefore, a boost-up in covariance matrix is needed. To overcome this problem, the RLS algorithm is modified by including an adaptive forgetting factor.

In the least square method, forgetting factor can be thought as giving more weight to recent data and less weight to older ones. The objective function is then modified as follows:

$$V(\hat{\theta}, k) = \frac{1}{2} \sum_{i=1}^{k} \lambda^{k-i} (y_i - \emptyset_i' \hat{\theta}_i)^2 \tag{5-31}$$

where λ is called the forgetting factor and is usually a number between 0.5 and 1. The updates for the expression of P_k and L_k are as follows:

$$L_k = P_{k-1} \emptyset_k (\lambda I_n + \emptyset_k' P_{k-1} \emptyset_k)^{-1} \tag{5-32}$$

$$P_k = \frac{1}{\lambda} (I_n - L_k \emptyset_k') P_{k-1} \tag{5-33}$$

In equation (5-33), the covariance matrix is divided by λ at each update, which slows down fading out of the covariance matrix, and therefore, makes it capable of keeping track of changes in the parameters.

The RLS with single forgetting factor (RLS-SFF) has widely been used in identification and tracking of time-varying parameters in various fields of engineering. However, in many cases, the variation rate of various parameters is different and RLS-SFF cannot perform well. Therefore, it is desirable to assign one forgetting factor to each of the parameters. A solution to this problem is using a diagonal matrix of

forgetting factors and scaling down the covariance matrix using the proposed matrix. The method is called RLS with vector forgetting factor (Lin et al. 2001), which in the update of the covariance matrix is as follows:

$$P_k = \Lambda^{-1}\left(I_n - L_k \emptyset_k^{'}\right) P_{k-1} \Lambda^{-1} \tag{5-34}$$

$$\Lambda = diag[\lambda_1, \lambda_2, \dots, \lambda_n] \tag{5-35}$$

where λ_i is the forgetting factor reflecting the variation rate of the ith parameter. This method is very effective in tracking the time-varying parameters. However, for large number of unknown parameters, n, the identification becomes very slow since $n \times n$ elements of covariance matrix should be calculated at each update.

Recently, another RLS algorithm with multiple forgetting factors (RLS-MFF) was introduced by Vahidi et.al (Vahidi, Stefanopoulou & Peng 2005), which effectively reduces the computational efforts. In this approach, the objective function is defined based on the decomposition of error due to different parameters and, therefore, assigning a suitable forgetting factor to each. Let the number of unknown parameters be n. Then the objective function is as follows:

$$V\left(\hat{\theta}_1, \hat{\theta}_2, .. \hat{\theta}_n, k\right) = \frac{1}{2}\sum_{i=1}^{k} \lambda_1^{k-i}\left(y_i - \emptyset_{1,i}^{'}\hat{\theta}_{1,i} - \emptyset_{2,i}^{'}\theta_{2,i} - \cdots - \emptyset_{n,i}^{'}\theta_{n,i}\right)^2 +$$

$$\frac{1}{2}\sum_{i=1}^{k} \lambda_2^{k-i}\left(y_i - \emptyset_{1,i}^{'}\theta_{1,i} - \emptyset_{2,i}^{'}\hat{\theta}_{2,i} - \cdots - \emptyset_{n,i}^{'}\theta_{n,i}\right)^2 + \dots + \tag{5-36}$$

$$\frac{1}{2}\sum_{i=1}^{k} \lambda_n^{k-i}\left(y_i - \emptyset_{1,i}'\theta_{1,i} - \emptyset_{2,i}'\theta_{2,i} - \cdots - \emptyset_{n,i}'\hat{\theta}_{n,i}\right)^2$$

The optimal estimates for θ are those that minimise the objective function and are obtained as follows:

$$\hat{\theta}_{1,k} = \hat{\theta}_{1,k-1} + L_{1,k}(y_k - \emptyset_{1,k}^{'}\hat{\theta}_{1,k-1} - \emptyset_{2,k}^{'}\theta_{2,k-1} - \cdots - \emptyset_{n,k}^{'}\theta_{n,k-1}) \tag{5-37}$$

where

$$L_{1,k} = P_{1,k-1}\emptyset_{1,k}(\lambda_1 + \emptyset_{1,k}^{'}P_{1,k-1}\emptyset_{1,k})^{-1} \tag{5-38}$$

$$P_{1,k} = \frac{1}{\lambda_1}\left(1 - L_{1,k}\emptyset'_{1,k}\right)P_{1,k-1}$$

and similarly,

$$\begin{aligned}
\hat{\theta}_{2,k} &= \hat{\theta}_{2,k-1} + L_{2,k}(y_k - \emptyset'_{1,k}\theta_{1,k-1} - \emptyset'_{2,k}\hat{\theta}_{2,k-1} - \cdots - \emptyset'_{n,k}\theta_{n,k-1}) \\
L_{2,k} &= P_{2,k-1}\emptyset_{2,k}(\lambda_2 + \emptyset'_{2,k}P_{2,k-1}\emptyset_{2,k})^{-1} \\
P_{2,k} &= \frac{1}{\lambda_2}\left(1 - L_{2,k}\emptyset'_{2,k}\right)P_{2,k-1}
\end{aligned} \tag{5-39}$$

and

$$\begin{aligned}
\hat{\theta}_{n,k} &= \hat{\theta}_{n,k-1} + L_{n,k}(y_k - \emptyset'_{1,k}\hat{\theta}_{1,k-1} - \emptyset'_{2,k}\hat{\theta}_{2,k-1} - \cdots - \emptyset'_{n,k}\hat{\theta}_{n,k-1}) \\
L_{n,k} &= P_{n,k-1}\emptyset_{n,k}(\lambda_n + \emptyset'_{n,k}P_{n,k-1}\emptyset_{n,k})^{-1} \\
P_{n,k} &= \frac{1}{\lambda_n}\left(1 - L_{n,k}\emptyset'_{n,k}\right)P_{n,k-1}
\end{aligned} \tag{5-40}$$

With some more mathematical manipulations, the unknown parameters can be estimated in the form of:

$$\hat{\theta}_k = \hat{\theta}_{k-1} + L_k{}^*(y_k - \emptyset'_k\hat{\theta}_{k-1}), \tag{5-41}$$

where:

$$L_k{}^* = \frac{1}{1 + \sum_{i=1}^{n}\frac{P_{i,k-1}\emptyset_{i,k}{}^2}{\lambda_i}}\begin{bmatrix} \frac{P_{1,k-1}\emptyset_{1,k}}{\lambda_1} \\ \frac{P_{2,k-1}\emptyset_{2,k}}{\lambda_2} \\ \vdots \\ \frac{P_{n,k-1}\emptyset_{n,k}}{\lambda_n} \end{bmatrix} \tag{5-42}$$

As can be found from equations (5-38 to 5-41), the size of covariance matrix is only $n \times 1$, which compared to the size of covariance matrix in the vector type RLS-FF, is n times less and, therefore, makes the real-time identification of time-varying parameters possible. This algorithm has originally been used to identify the vehicle mass and road grade. In this study, we are going to apply this method for structural parameters

identification. However, since in the original form of this algorithm the forgetting factors have been adjusted by trial and error, an improvement needs to be done in order to make the algorithm self-adaptive.

To make the forgetting factors adaptive, some ideas and approaches have been introduced and applied to RLS-SFF (Lin et al. 2001). Here we use an adaptive rule defined by Lin and reform it to apply to the aforementioned RLS-MFF algorithm. The proposed modified adaptive forgetting factor is expressed as follows:

$$\lambda_{n,k+1} = 1 - \frac{e_k^2}{\xi}\left(1 - \frac{\emptyset_{n,k}^{'} P_{n,k-1} \emptyset_{n,k}}{\lambda_{n,k} + \emptyset_{n,k}^{'} P_{n,k-1} \emptyset_{n,k}}\right) \tag{5-43}$$

where e_k is the error of identification at update k. ξ is also a scalar which is usually thought as the initial error of the identification based on the initial guess for the to-be-identified parameters. It should be mentioned that, if a priori knowledge is available on the variation rate of a parameter, it is better to be applied before the algorithm starts. For example, if it is known that a parameter would not change with time, its corresponding forgetting factor should be set to 1.

The features of proposed algorithm, compared to others, are outlined in

Table 5-2.

5.4.2 Recursive least square with adaptive multiple forgetting factor and unknown inputs (AMFF-RLS-UI)

When some external excitations are not measured or not available, then the equation (5-26) can be rewritten as:

$$\emptyset_k' \theta_k + v_k = y_k + \eta^* {f^*}_k \tag{5-44}$$

in which f^* is the r-unknown excitation vector and $\eta^* = (\mathrm{m} \times \mathrm{r})$ is the known excitation influence matrix associated with ${f^*}_k$. Equation (5-44) can be rewritten as follows:

$$\emptyset_k' \theta_k - \eta^* {f^*}_k + v_k = y_k \tag{5-45}$$

Table 5-2. RLS based method feature comparison

	Off-Line	Online	Real-Time	Time-Varying Parameters	Priory Knowledge	Complexity
Least Square	☑	☒	☒	☒☒☒	☑☑	☑
Recursive Least Square(Caravanil, 1977)		☑	☑	☒☒☒	☑☑	☑
Recursive Least Square with Adaptive Single Forgetting Factor (Lin, 2001)		☑	☑	☑☒☒	☑☑	☑
Recursive Least Square with Constant Vector Forgetting Factor (Yang, 2003)		☑	☑	☑☑☒	☒☒	☑
Recursive Least Square with Constant Multiple Forgetting Factor (Vahidi, Stefanopoulou & Peng 2005)		☑	☑	☑☑☒	☒☒	☑
Recursive Least Square with Adaptive Vector Forgetting Factor (Yang, Pan & Huang 2007)		☑	☒	☑☑☑	☑☑	☒
Recursive Least Square with Adaptive Multiple Forgetting Factors (proposed in this study)		☑	☑	☑☑☑	☑☒	☑

Now, let us define an extended unknown vector $\theta_{e,k}$ and an extended observation matrix $\emptyset'_{e,k}$ at $t = k\Delta t$, i.e.

$$\theta_{e,k} = \begin{bmatrix} \theta_k \\ f^*{}_k \end{bmatrix}; \tag{5-46}$$

$$\emptyset'_{e,k} = [\emptyset'_k \ -\eta^*], \tag{5-47}$$

in which $\theta_{e,k}$ is a (n+r)-unknown vector. Then equation (5-45) can be expressed as:

$$\emptyset'_{e,k}\theta_{e,k} + v_k = y_k \tag{5-48}$$

Considering an objective function to be minimised;

$$\begin{aligned} V\left(\hat{\theta}_{e,1}, \hat{\theta}_{e,2}, .. \hat{\theta}_{e,n}, k\right) = {} & \frac{1}{2}\sum_{i=1}^{k} \lambda_1^{k-i}\left(y_i - \emptyset'_{e,1,i}\hat{\theta}_{e,1,i} - \emptyset'_{e,2,i}\theta_{e,2,i} - \right. \\ & \left. \cdots - \emptyset'_{e,n,i}\theta_{e,n,i}\right)^2 + \frac{1}{2}\sum_{i=1}^{k} \lambda_2^{k-i}\left(y_i - \emptyset'_{e,1,i}\theta_{e,1,i} - \emptyset'_{e,2,i}\hat{\theta}_{e,2,i} - \cdots - \right. \\ & \left. \emptyset'_{e,n,i}\theta_{e,n,i}\right)^2 + \ldots + \frac{1}{2}\sum_{i=1}^{k} \lambda_2^{k-i}\left(y_i - \emptyset'_{e,1,i}\theta_{e,1,i} - \emptyset'_{e,2,i}\theta_{e,2,i} - \cdots - \right. \\ & \left. \emptyset'_{e,n,i}\hat{\theta}_{e,n,i}\right)^2, \end{aligned} \tag{5-49}$$

one can estimate the unknown parameters, θ_k, and the unknown excitation, $f^*{}_k$ at time $t = k\Delta t$ under the conditions: (i) the number of output measurements is greater than that of the unknown excitations and (ii) measurements (sensors) are available at all DOFs where the unknown excitations, $f^*{}_k$, act; that is, matrix η^* is nonzero; as follows:

$$\begin{aligned} \hat{\theta}_k &= \hat{\theta}_{k-1} + L_k{}^*(y_k - \emptyset'_k\hat{\theta}_{k-1} + \eta^*\hat{f}^*{}_k) \\ \hat{f}^*{}_k &= (\eta^{*\mathrm{T}}\,\eta^*)^{-1}\,\eta^*\,(y_k - \emptyset'_k\hat{\theta}_{k-1}) \end{aligned} \tag{5-50}$$

in which,

$$L_k{}^* = \frac{1}{1 + \sum_{i=1}^{n} \frac{P_{i,k-1}\emptyset_{i,k}{}^2}{\lambda_i}} \begin{bmatrix} \frac{P_{1,k-1}\emptyset_{1,k}}{\lambda_1} \\ \frac{P_{2,k-1}\emptyset_{2,k}}{\lambda_2} \\ \vdots \\ \frac{P_{n,k-1}\emptyset_{n,k}}{\lambda_n} \end{bmatrix} \tag{5-51}$$

The covariance matrix $P_{n,k}$, is also updated using the following equations:

$$P_{n,k} = \frac{1}{\lambda_n}(1 + L_{n,k}\,\eta^*\,\mathrm{S_{n,k}}\,\eta^{*\mathrm{T}}\,\emptyset_{n,k}) * \left(1 - L_{n,k}\emptyset'_{n,k}\right)P_{n,k-1} \tag{5-52}$$

where,

$$\mathrm{S_{n,k}} = (\eta^*\,(\mathrm{I} - \emptyset'_{n,k}L_{n,k}\,\eta^*))^{-1} \tag{5-53}$$

and the adaptive forgetting factor, λ_n, can still be found from equation (5-43). To verify the effectiveness of the proposed real-time adaptive identification algorithm, different types of structures with different damage scenarios are considered in the next section.

5.4.3 Numerical Simulations

5.4.3.1 SDOF nonlinear hysteretic system

Consider a single degree of freedom (SDOF) nonlinear hysteretic Bouc-Wen system subjected to earthquake acceleration $\ddot{x}_g$, with the following governing equation of motion,

$$m\ddot{x}(t) + r(\dot{x}, x) = -m\ddot{x}_g(t) \tag{5-54}$$

The Bouc-Wen model that will be used for $r(\dot{x}, x)$ is as follows:

$$\dot{r} = c\ddot{x} + k\dot{x} - \beta|\dot{x}||r|^{\alpha-1}r - \gamma\dot{x}|r|^{\alpha} \tag{5-55}$$

where, c is the damping coefficient, k is the stiffness, and β, γ and α are hysteretic parameters. The following parametric values are used for the simulation study (Lin et al. 2001): m=125.53 kg, c=0.31kNs/m, k=24.2 kN/m, β=2 s/(m kN), $\gamma = 1\ \mathrm{s/(m\,kN)}$, $\alpha = 2$ and $\ddot{\mathrm{x}}_{\mathrm{g}}$ is the El-Centro (1940) earthquake with a scaled peak ground acceleration of 0.15 g (PGA=0.15g). The unknown parameters are taken as c, k, β and γ. For the purpose of examining the identification robustness to noise level, a white noise with 2% RMS is added to both the simulated response and the earthquake ground acceleration. The accelerations of the system as well as the ground acceleration are measured by the accelerometers while system response of the velocity is obtained online, using the numerical integrator.

From equation (5-54),

$$r_k = -m(\ddot{x}_{g,k} + \ddot{x}_k), \tag{5-56}$$

where index k refers to time at $t_k = k\Delta t$. Based on a third-order corrector method, r_k can be expressed as:

$$r_k - r_{k-1} = \left(\frac{\Delta t}{12}\right)(5\dot{r}_k + 8\dot{r}_{k-1} - \dot{r}_{k-2}) \tag{5-57}$$

If the measured vector is defined as $y_k = \left(\frac{12}{\Delta t}\right)(r_k - r_{k-1})$, then:

$$y_k = 5\dot{r}_k + 8\dot{r}_{k-1} - \dot{r}_{k-2} = \left(-\frac{12m}{\Delta t}\right)(\ddot{x}_k - \ddot{x}_{k-1} + \ddot{x}_{g,k} - \ddot{x}_{g,k-1}) \tag{5-58}$$

The unknown parameters are defined as a vector of $\theta_k = [c, k, \beta, \gamma]^T$ and the observation matrix is also $\emptyset_k = \left[\emptyset_{k,1}\ ,\ \emptyset_{k,2}\ ,\ \emptyset_{k,3}\ ,\emptyset_{k,4}\right]^T$. It can be found that the components of observation matrix are as follows:

$$\emptyset_{k,1} = 5\ddot{x}_k + 8\ddot{x}_{k-1} - \ddot{x}_{k-2},$$

$$\emptyset_{k,2} = 5\dot{x}_k + 8\dot{x}_{k-1} - \dot{x}_{k-2},$$

$$\begin{aligned}\emptyset_{k,3} = {} & 5|\dot{x}_k|\left|m\left(\ddot{x}_k + \ddot{x}_{g,k}\right)\right|^{\alpha-1} m\left(\ddot{x}_k + \ddot{x}_{g,k}\right) \\ & +8|\dot{x}_{k-1}|\left|m\left(\ddot{x}_{k-1} + \ddot{x}_{g,k-1}\right)\right|^{\alpha-1} m\left(\ddot{x}_{k-1} + \ddot{x}_{g,k-1}\right) \\ & -|\dot{x}_{k-2}|\left|m\left(\ddot{x}_{k-2} + \ddot{x}_{g,k-2}\right)\right|^{\alpha-1} m\left(\ddot{x}_{k-2} + \ddot{x}_{g,k-2}\right),\end{aligned} \tag{5-59}$$

$$\begin{aligned}\emptyset_{k,4} = {} & -5\dot{x}_k\left|m\left(\ddot{x}_k + \ddot{x}_{g,k}\right)\right|^{\alpha} - 8\dot{x}_{k-1}\left|m\left(\ddot{x}_{k-1} + \ddot{x}_{g,k-1}\right)\right|^{\alpha} \\ & - \dot{x}_{k-2}\left|m\left(\ddot{x}_{k-2} + \ddot{x}_{g,k-2}\right)\right|^{\alpha}.\end{aligned}$$

Two damage scenarios will be considered here. For case 1, suppose a damage occurs at t=15s, where stiffness k, is abruptly reduced from 24.2 to 15 kN/m. With initial estimates of $\theta_0 = [0.1, 10, 0, 0]^T$, and $P_{n,0} = 10^8$, the identified structural parameters are shown in Figure 5.8. We also assumed we knew that damping is not going to change much and hence the corresponding forgetting factor is set as 1. The identified values of unknown parameters are depicted in Figure 5.8 as dashed curves. The solid curves show the theoretical results for comparison.

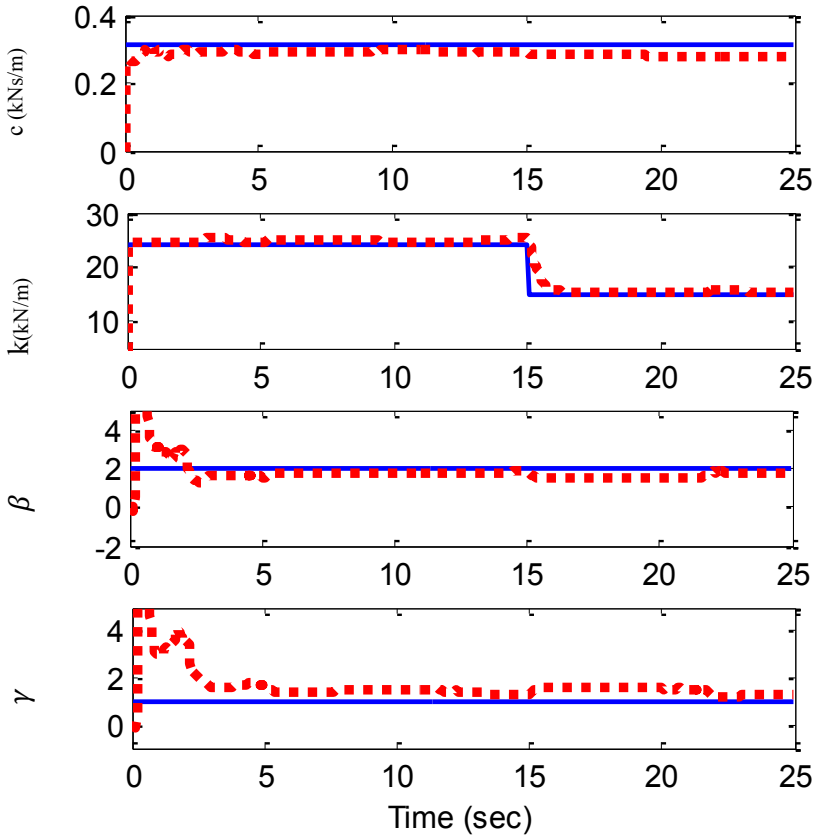

Figure 5.8. Identified results for an SDOF system (case 1)

Another damage scenario is then defined as an abrupt change in both damping and stiffness at time t=15s, where k and c drop to 15kN/m and 0.15kNs/m from 24.2 kN/m and 0.31kNs/m, respectively. With the same initial guesses as the previous case, the identified parameters are presented in Figure 5.9. Here, no a priori information is available on the changing rate of the parameters.

The identified earthquake ground acceleration for Damage Case 1 is presented in Figure 5.10 as a dashed curve, whereas the solid curve is the theoretical result for comparison. Instead of presenting the entire earthquake ground acceleration for 30 seconds, only a small segment from 11 to 15 sec is presented in Figure 5.10. The difference between the solid curve and the dashed curve is about the same as in the other segments. Further, the prediction of ground acceleration for Damage Pattern 2 is almost identical to that for Damage Pattern 1 shown in Figure 5.10, and hence, it is not presented. It is observed from Figure 5.10 that the proposed AMFF-RLS-UI approach is capable of tracking the unknown earthquake excitation, structural parameters, and their variations due to damage very well.

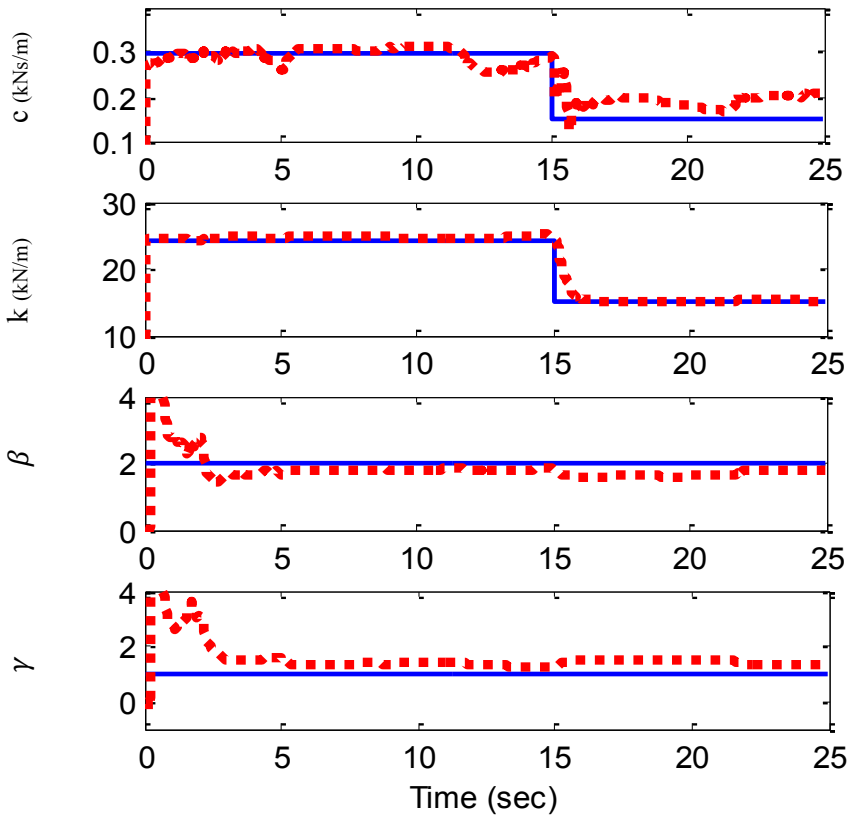

Figure 5.9. Identified results for a SDOF system (case 2)

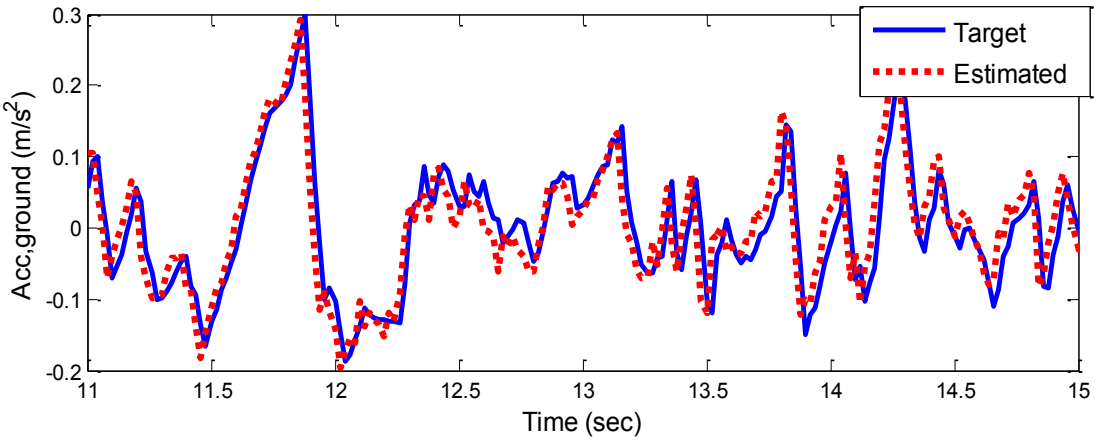

Figure 5.10. Identified unknown earthquake acceleration for the SDOF system (case 2)

5.4.3.2 2DOF linear structural system

As another application of the proposed identification algorithm, a two-degree of freedom structural system subjected to El-Centro (1940) excitation with intensity of 0.5 is considered.

$$\begin{aligned} &m_1\ddot{x}_1 + c_1\dot{x}_1 + c_2(\dot{x}_1 - \dot{x}_2) + k_1x_1 + k_2(x_1 - x_2) = -m_1\ddot{x}_g \\ &m_2\ddot{x}_2 + c_2(\dot{x}_2 - \dot{x}_1) + k_2(x_2 - x_1) = -m_2\ddot{x}_g, \end{aligned} \tag{5-60}$$

in which $m_1 = m_2 = 1\ kg$, $c_1 = 0.6$ Ns/m, $c_2 = 0.5$ Ns/m, $k_1 = 12$ N/m, and $k_2 = 10$ N/m. The acceleration response of the structure is assumed to be measurable. A noise level with 5% RMS white noise is also added to measured responses.

As the first damage case, it is assumed that the stiffness of the second storey changes to 5 at time $t = 5s$. The initial guesses are taken as $c_{1,0} = c_{2,0} = 0.2$ Ns/m, $k_1 = k_2 = 5$ N/m and $P_{n,0} = 10^{10}$. Here, it is known that the dampings would not change very much and, therefore, the forgetting factors for the damping of first and second storeys are bounded to $0.97 \leq [\lambda_1, \lambda_2] \leq 1$. Tracking the structural parameters with known earthquake measurement is shown in Figure 5.11 where rapid convergence of identified values to true ones can be seen. In the second attempt, the unknown parameters are identified together with the unknown earthquake measurement, and the results are shown in Figure 5.12Figure 5.13. As can be found, the unknown parameters can be identified well although the convergence is slower than when the input, i.e earthquake signal, is known. It can also be observed from the results that when a change occurs in some parameters, there would be an undesirable fluctuation in the invariant parameters as well. This is because of the fact that their forgetting factors are also affected by the total error of identification.

To show the effectiveness of the proposed algorithm, a single forgetting factor-RLS was also designed carefully and applied with trial and error to track the stiffness of the second storey for the same damage scenario. It was found that the time invariant parameters will overshoot a lot, at the time the damage occurs (Figure 5.14). These jumps are minimised in the proposed algorithm of this study (Figure 5.11).

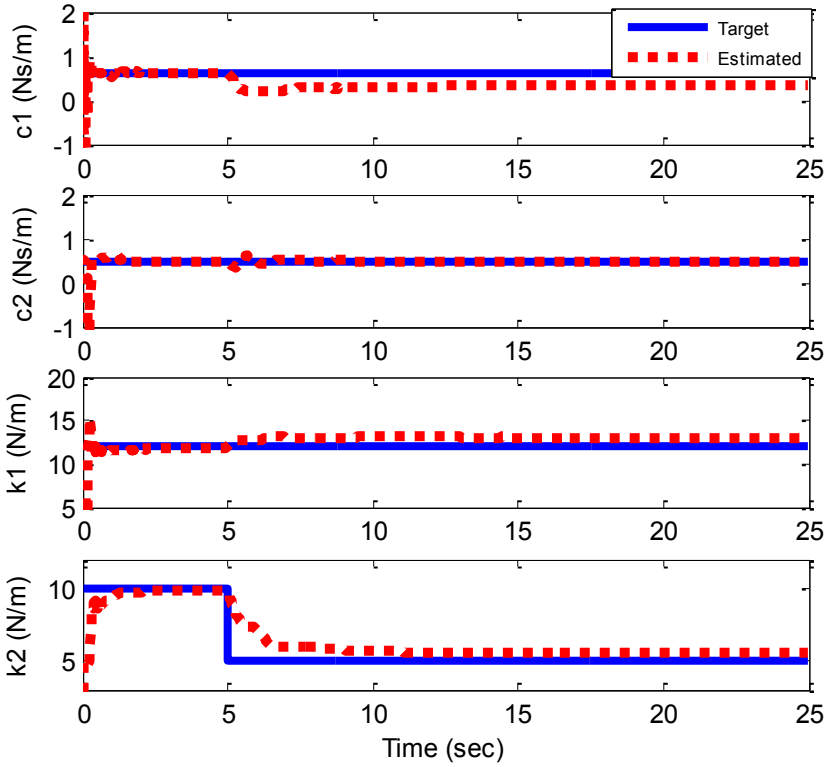

Figure 5.11. Identified parameters for 2DOF system with known input (case 1)

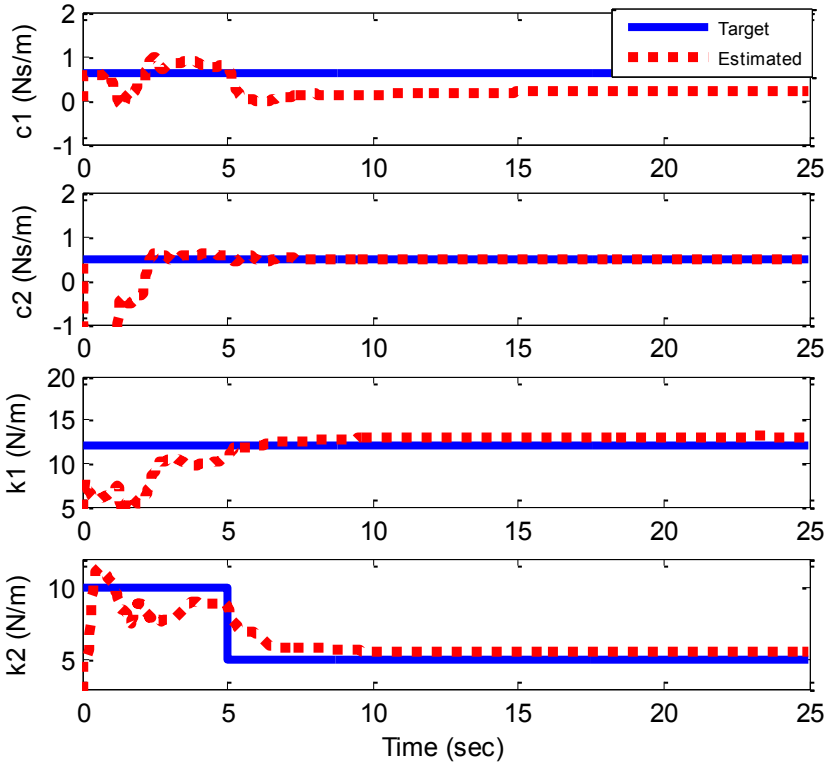

Figure 5.12. Identified parameters for 2DOF system with unknown input (case 1)

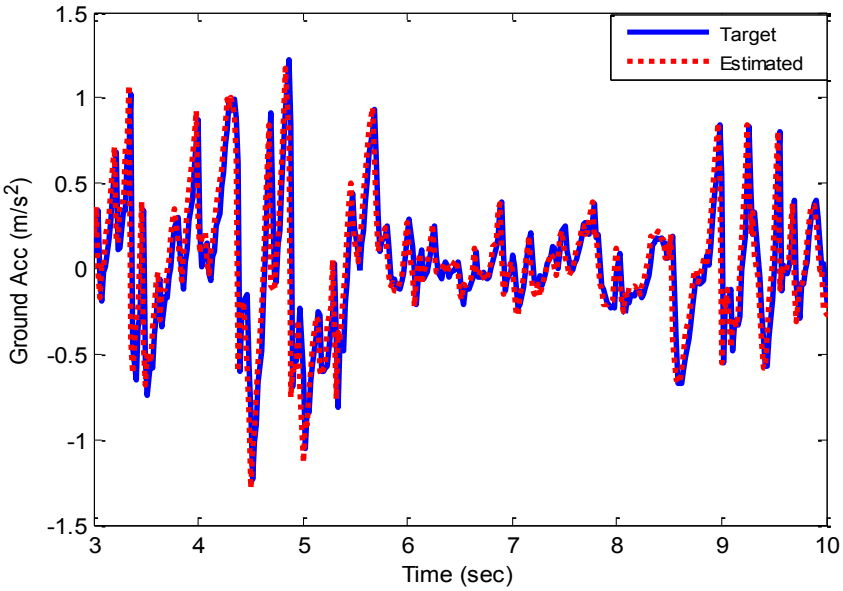

Figure 5.13. Identified unknown earthquake acceleration for the 2DOF system (case 1)

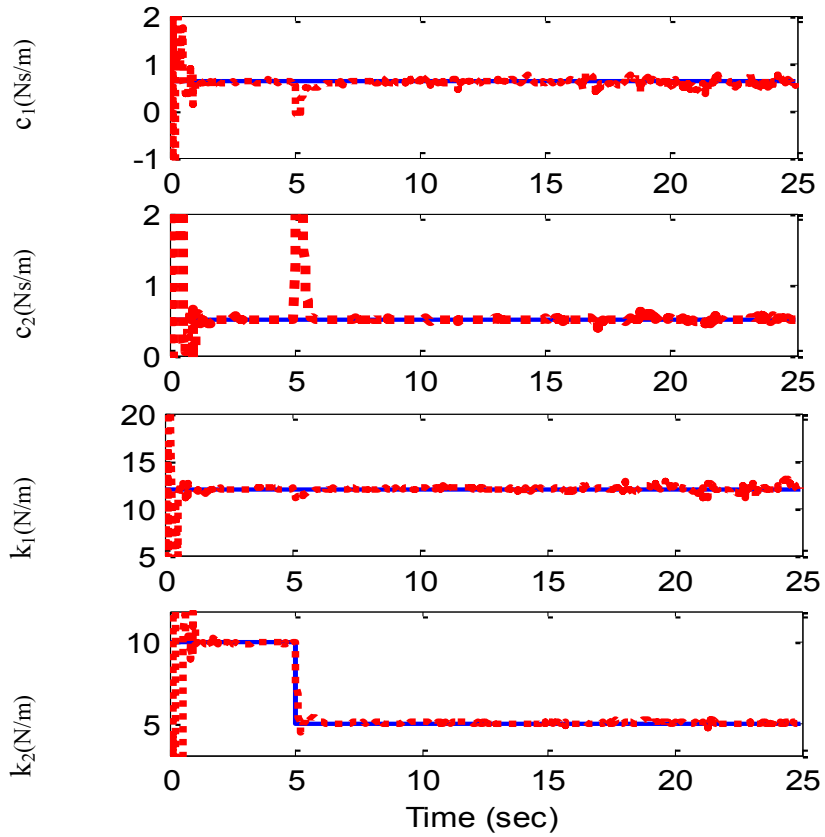

Figure 5.14. Identified results for a 2DOF system with known input, using RLS with single forgetting factor of 0.95 (case 1)

The time-varying forgetting factor obtained for the stiffness of the second storey is plotted in Figure 5.15. It shows that, whenever an error is seen in the identification, i.e. at the beginning of identification or when damage occurs, the forgetting factor value will be decreased to amplify the covariance matrix. However, when the identified parameters are converging to the actual ones, the forgetting factors approach 1.

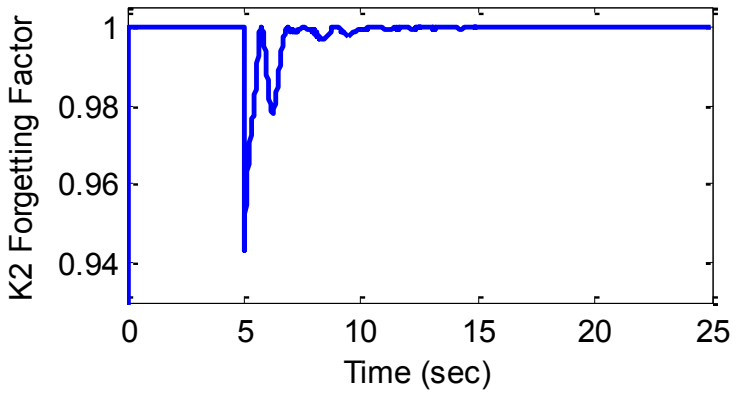

Figure 5.15. The forgetting factor obtained for the stiffness of the second storey (Case 1)

A more complicated damage scenario which is considered here in order to test the proposed identification algorithm is as follows; a damage occurs in the first storey at time t=10s where the stiffness drops to 10N/m. Another damage also occurs in the second storey and the stiffness abruptly changes to 9N/m at t=5s and linearly reduces to 7N/m and then drops to 6N/m at t=10s. The identification results are plotted in Figure 5.16.

The results show that, although damping coefficients together with the stiffness of the first storey are identified well, the proposed algorithm cannot fully track the change of the stiffness of the second storey due to multi-stage damage. This might be because of the fact that the excitation along with structural responses become small as time progresses and, therefore, the identification error will be small which cannot boost the covariance, and as a consequence, the convergence becomes very slow. In other words, in structural identification, the external excitation needs to be large enough in order to make the response of structure large and as a consequence, make the difference between estimated values, $\emptyset_k^{'}\hat{\theta}_{k-1}$ and the measured value, y_k, visible. Otherwise, the parameters of the structure do not show their impact on the response, and identification fails. As can be seen in Figure 5.17, even though the stiffness of second storey could not be estimated very well, the unknown excitation, i.e. the El-Centro earthquake, is

still estimated perfectly as the difference between the estimated value of proposed stiffness after t=10s, i.e. $\hat{k}_2 = 8\ \mathrm{N/m}$ and the target one, does not make that much difference in the response of the structure.

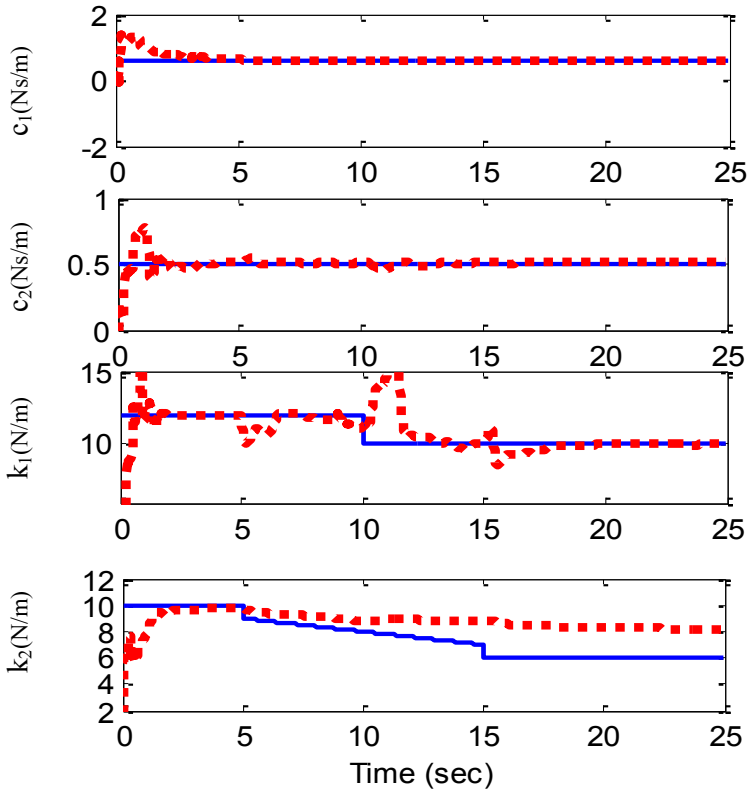

Figure 5.16. Identified results for a 2DOF system (case 2)

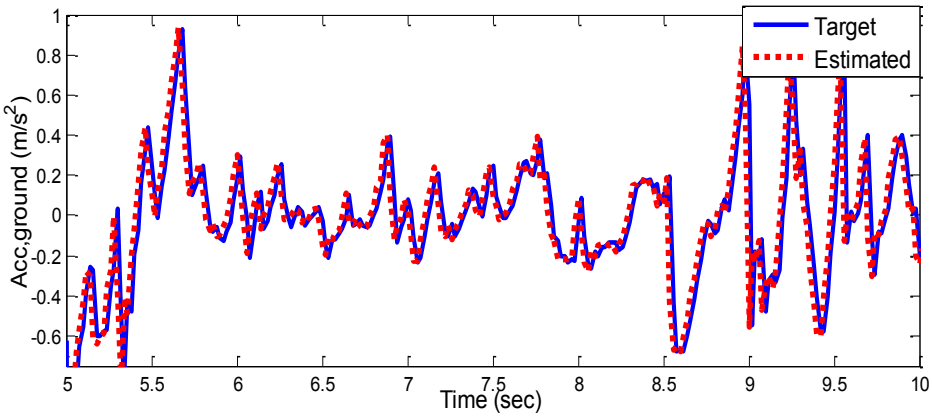

Figure 5.17. Identified unknown earthquake acceleration for a 2DOF system (case 2)

5.4.3.3 3DOF linear structural system with unknown excitation on top floor

Consider a three-storey linear structure with unknown excitation on top floor as another case study to be identified. The masses of all floors are $\mathrm{m_1 = m_2 = m_3 = 98.3\ kg}$.

The other properties of the building model are $c_1 = 125$ Ns/m, $c_2 = c_3 = 50$ Ns/m, $k_1 = 5.16 \times 10^5$ N/m, $k_2 = k_3 = 6.84 \times 10^5$ N/m. A sinusoidal load with the amplitude of 3 m/s^2 and frequency of 6 rad/sec is applied to top floor as an external excitation.

Sensors are installed to measure the accelerations of all stories. These measured accelerations are simulated by superimposing the theoretically computed responses with their respective 2% RMS noises. The RMS of a particular signal, say $x_1(t)$, is computed from the temporal average over 25 s. Then, the corresponding stationary noise process is generated using 2% RMS. The velocity and displacement of stories are obtained from the measured noise-polluted acceleration signal by numerical integrations.

A damage is considered to have occurred in the first storey at t = 5 s, at which time the stiffness k_1 and damping c_1 are reduced abruptly from 5.16×10^5 N/m to 2.16×10^5 N/m and from 125 Ns/m to 40 Ns/m, respectively. Unknown parameters to be identified are stiffness and damping of all floors whereas the unknown excitation on roof will also be estimated.

The initial estimates of unknown parameters and P_n are assumed as follows: $c_{i,0} = 20\ Ns/m$, $k_{i,0} = 1.20 \times 10^2 N/m$, $P_n = 10^{20}$. The identification results of the proposed algorithm are shown in Figure 5.18. The identified sinusoidal load on the top floor is also shown in Figure 5.19. As can be seen, even though the initial estimates of unknown parameters are far from the target ones, yet the proposed algorithm works well. However, in the beginning and at time $t = 5\ s$, the dashed line, i.e. the estimated values, fluctuate when identifying and tracking the structural parameters. The external excitation, as a consequence, cannot be tracked in the beginning. For the same reason, the forgetting factor for the stiffness of the first storey, which is shown in Figure 5.20, is highly oscillatory in the first few seconds as well as at the time damage occurs. However, since after $t = 5\ s$, the structural parameters are identified and do not change anymore, the proposed forgetting factor stays almost constant and close to 1.

5.5 SUMMARY

In this chapter, an investigation on different Kalman filtering algorithms used in system identification was carried out, in which EKF, IEKF, UKF and IUKF have been applied to estimate the parameters of targeted structures in real-time using acceleration responses only. In both numerical examples, the measurement equation was nonlinear and in one of the cases, the structure also exhibited hysterical structural nonlinearity. It is observed that in most cases, the results of EKF and UKF are improved using their corresponding iterated versions, i.e. IEKF and IUKF. However, it is seen that IEKF, in some cases, shows a weaker performance than EKF, which can be because of its sensitivity to the measurement error and noise level. It is also shown that, IUKF, among the four studied algorithms, produces better results on state estimation and parameter identification. IUKF is also more robust to measurement noise levels and initial estimates of unknown parameters, compared to the other approaches.

Then, a RLS based method with adaptive multiple forgetting factor was proposed and applied to different structural identification problems with unknown excitations. The covariance matrix in this method had the same size as the unknown parameters, which makes the proposed algorithm compact and capable of real-time tracking of the unknown system's parameters. It is found from the results that the proposed algorithm can effectively identify the time-varying parameters with high computational efficiency as well as the unknown inputs to the structure. However, when damage occurs while the excitation is small, the measurements become very small and thus, the identification error remains in a small value range, and therefore, covariance cannot be amplified. This basically makes the algorithm very slow, which justifies the continuation of the current research. Moreover, another challenge is that, the expected level of model errors should be estimated reasonably well in order to select a good ξ in equation (5-43). Also, it should be mentioned that, errors exist in the numerical integration results of velocity and displacement from the measured noise-polluted acceleration responses, especially the displacement responses obtained through double numerical integrations may involve significant drifts, which is hard to be removed on-line in real time. This is one of the drawbacks of LSE methods needs to be studied in future.

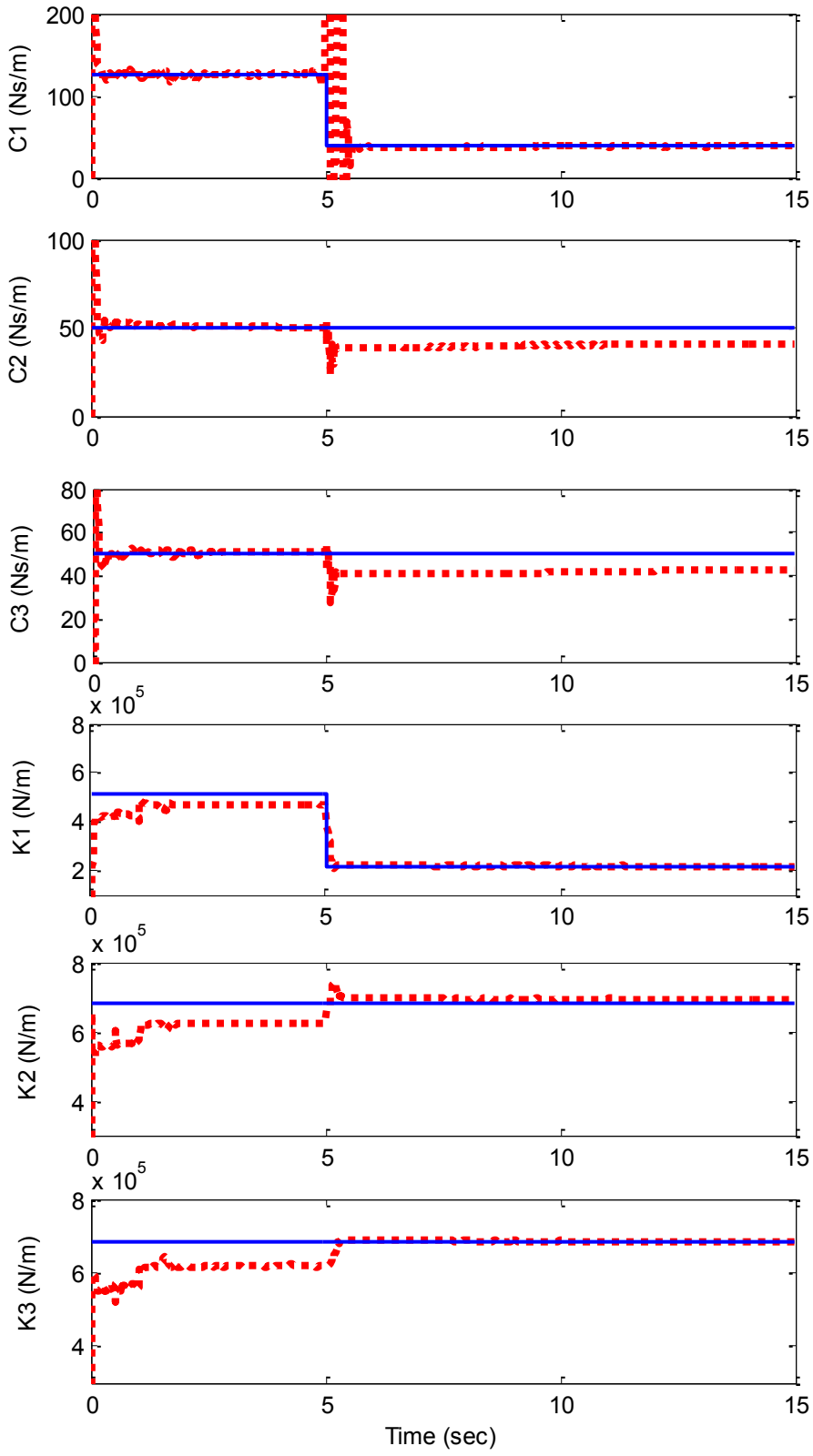

Figure 5.18. Identified parameters for 3DOF system

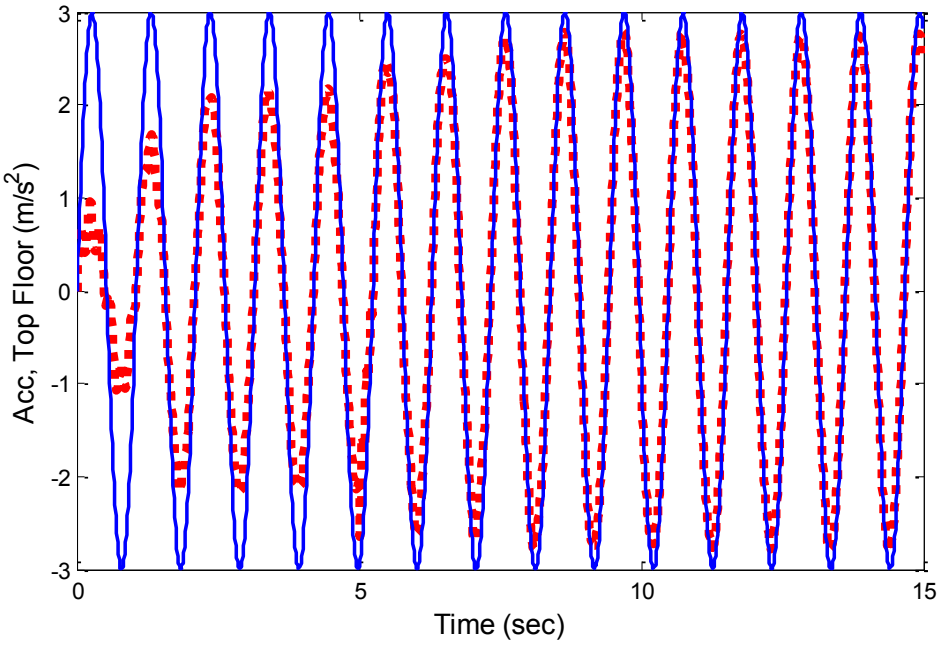

Figure 5.19. Identified external input, on top floor for 3DOF system

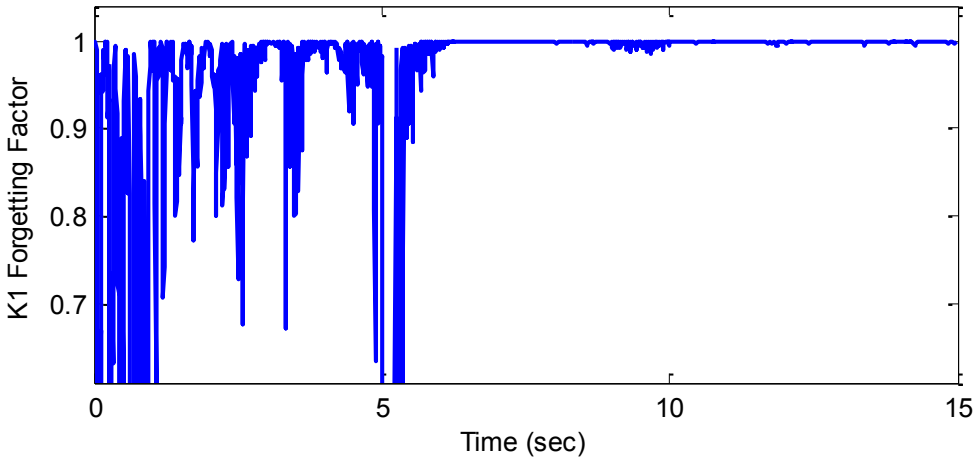

Figure 5.20. The forgetting factor obtained for the stiffness of the first storey

CHAPTER 6

CONCLUSIONS AND FUTURE RESEARCH

The main aim of the project was to develop new techniques in the field of structural control and health monitoring to prepare a platform for real-time structural integrity assessment of civil infrastructures, during or after earthquakes. The major achievements of this study are summarised in the following sections.

6.1 MR DAMPER MODELLING

Semi-active dampers are often considered to be a desirable compromise between fail-safe passive damping and effective active control. They require little power for operation and are thus able to run for instance on battery power. Besides, they do not add energy to the system, whereby the stability due to the damper cannot be compromised because control forces are developed through proper adjustment of damping and stiffness components of controller. One of the most common types of semi-active dampers for engineering applications is magnetorheological (MR) dampers which are currently being developed for a number of applications, particularly for controlling the dynamic responses of civil structures.

In Chapter 2 of this dissertation, a new encoding scheme was presented for a fuzzy-based nonlinear system identification methodology, using subtractive Fuzzy C-Mean clustering and non-dominated sorting genetic algorithm. The method was able to

automatically select the best inputs as well as the structure of the fuzzy model such as rules and membership functions. Moreover, three objective functions were considered to satisfy both accuracy and compactness of the model. The proposed method was then employed to identify the forward and inverse models of a MR damper. Numerical and Experimental results showed that the developed evolving TSK fuzzy model can identify and grasp the nonlinear dynamics of both forward and inverse systems very well, while a small number of inputs and fuzzy rules are required for this purpose.

6.2 Multi-Objective Optimal Placement of Structural Control Devices

The optimal design and placement of control devices, is an important problem that affects the control of civil engineering structures. In Chapter 3 of this thesis, a comprehensive study on methods and approaches used by other researchers in order to obtain the optimum locations of control devices, in particular actuators and MR dampers, were carried out. As discussed, most of the reported works in this area have focused on optimal assignments of active control devices. Also they have only considered one or two structural indices as the objective functions to be minimised through the optimisation process. Moreover, they use simple single objective optimisation algorithms which lead to only one final design. Application of these algorithms to high-rise nonlinear buildings also has not been reported. However, it is necessary to do a comparative study between optimal locations of actuators and MR dampers and show the differences. Also, it is more beneficial if the optimisation is carried out with consideration of more structural performance indices as objective functions. Moreover, since optimal placement of control devices in a structure deals with integer adjustable parameters (each actuator/damper can be assigned to an integer value which is the floor number), an advanced and accurate integer coded optimisation algorithm is needed. In addition, a set of Pareto fronts, as the final result of optimisation, gives more flexibility to the user to choose one's own design based on one's own criteria. Finally, it is important to apply the method to a high-rise nonlinear building in order to validate the performance of algorithm.

To this end, a modified integer coded version of non-dominated sorting genetic algorithm II (MI-NSGAII) was introduced in this research study and applied to find

optimal places of actuators and MR dampers in a nonlinear 20-storey benchmark building. The method uses the best features of a recently developed integer coded algorithm named MI-LXPM into the framework of NSGAII. Using the proposed approach, a Pareto front can be generated using three considered objective indices, i.e. peak inter-storey drift ratio (J1), peak acceleration (J2) and peak base shear force (J3). These objective functions were selected in such a way that both human comfort (J2) and safety (J1, J3) of the structure is guaranteed. By choosing a pre-defined level of performance on dynamic responses of a structure, the designer can decide on decreasing or increasing the number of control devices. In other words, both control cost and dynamic performance is considered in this optimisation problem to be minimised. For an active control system, an LQG algorithm was proposed and 1,000kN hydraulic actuators together with accelerometers were installed in the building. For the semi-active case on the other hand, an LQG-COC algorithm was designed and 1,000kN MR dampers and accelerometers were placed within the structure.

The results of optimal placement of active actuators were compared to the benchmark problem definition(Ohtori et al. 2004) in which 25 actuators have been located in non-optimal locations. Results showed the effect of proposed strategy where the same level of structural performance, in terms of proposed objective functions, was obtained by use of only 7 actuators in an optimal layout. However, some indices were slightly increased compared to the original work. This shortcoming can be solved by using more control devices or taking more performance indices into account during the optimisation. Also, the proposed algorithm can lead to a cost effective distribution of control devices.

The optimal configuration of different number of MR dampers in the same nonlinear benchmark building was also studied in this dissertation work. As mentioned, due to highly nonlinear behaviour of these devices, and thus complexity of the problem, few reported studies have been conducted in this area. Results showed that optimal places of actuators and MR dampers are totally different. It should be mentioned that using different Pareto fronts, design engineers can select the number and arrangement of devices based on the level of performance that is acceptable. It also demonstrated the superiority of optimally assigned MR dampers on actuators in reduction of structural peak inter-storey drift. On the other hand, optimally located actuators performed better

than MR dampers in reducing the peak floor acceleration as well as peak base shear force.

6.3 SEMI-ACTIVE CONTROL OF MR DAMPER BUILDING SYSTEMS

One of the challenges in the application of MR dampers is using an appropriate control algorithm to determine their command voltage. In developing the control laws, note that it is not possible to directly command the i^{th} MR damper to generate a specified force,f_i , because the response of the MR damper is dependent on the local motion of the structure where the MR damper is attached. However, the force produced by the MR damper may increase or decrease by adjusting the value of the voltage applied to the current driverv_i. Based on this observation, in the model, the following guidelines are used in developing the control laws: i) the control voltage to theith device is restricted to the range$v_i = [0, V_{max}]$, and ii) for a fixed set of states, the magnitude of the applied force$|f_i|$ increases when $v_i$increases, and decreases when $v_i$decreases. Furthermore, the first order lag in the device model (representing the dynamics involved in the current driver and electromagnet) limits the rate at which the MR effect is realised. Thus, in developing the control laws, one must consider the fact that the force varies continuously even when a step command signal is applied.

In this thesis, following an investigation on current available semi-active control algorithms, two new semi-active control strategies were introduced to regulate the voltage of control devices such as MR dampers to get a desirable force generated by an optimal controller such as LQG.

The first technique, designated as TSKInv, was developed by modelling the inverse dynamics of MR damper using TSK fuzzy inference systems. The structure of model was optimised to select the best minimal inputs and fuzzy rules which lead to an accurate model. To provide the force feedback required for inverse model, another fuzzy model was trained to capture the forward dynamics of MR damper. The second algorithm, referred to as MaxMin, was designed based on the maximum ($v = v_{max}$) and minimum ($v = v_{min}$) load of MR damper at each time-step. Then assuming a linear

relationship between damper's voltage and force, a decision is made for voltage regulation in order to generate a specific desired force.

Using 25 optimally placed MR dampers, each with capacity of 1,000 kN, incorporated into a 20-storey nonlinear benchmark building, the performance of proposed algorithms were validated and compared to other passive and semi-active control approaches. Both controllers used the acceleration feedback only as accelerometers are more convenient than LVDTs and GPS measurement tools, in terms of installation and cost. Therefore, ten sensors for acceleration measurements were used for feedback in the control system on the 2^{nd}, 4^{th}, 6^{th}, 8^{th}, 10^{th}, 12^{th}, 14^{th}, 16^{th}, 18^{th} and 20^{th} floors. For those floors whose acceleration response was not measured, a Kalman filter observer was designed to estimate the corresponding acceleration signal based on the available measurements. An LQG controller was also considered as the primary controller.

Results illustrated that the proposed new control algorithms can effectively track the desired control force and perform much better than the original and modified versions of clipped optimal controllers (COC and MCOC) in terms of structural response reduction with less control force and power. However, in some cases they produce larger performance indices than COC and MCOC. The reason is the claim that TSKInv and MaxMin are better algorithms in imitating the designed target controller compared to COC and MCOC. In other words, if a better active controller is designed and used as the target, TSKInv and MAxMin will definitely produce better performances as semi-active control algorithms. In this study, the primary controller (LQG) is an efficient method for linear systems while the proposed 20-storey benchmark building is a nonlinear system. In addition, the designed active control strategy uses only accelerometers for the control feedback. Therefore, the desired force produced by LQG is compromised in terms of its effectiveness. In the meantime, as part of the inherent stability of any semi-active system, an installed MR damper between two adjacent storeys, automatically acts to resist the movements of two floors in a passive fashion. Blindly switching of voltage between two extremes using COC, produces maximum damping resistance at some occasions to the inter-storey drifts (at the cost of large power consumption) somehow produces better performance. As a result, although the main objective of both clipped optimal algorithms and newly proposed ones are tracing the active control performance, but in some cases, the more successful strategy

(TSKInv and MaxMin) for this purpose leads to larger performance indices in comparison with COC algorithms. Also, the comparison between MaxMin and TSKInv showed that, MaxMin model used less control power while TSKInv decreased the structural response more. However, MaxMin is easier to use although computationally is a bit more expensive than TSKFInv as it needs to evaluate two parametric/nonparametric models at each time step. Operation without force measurement is another benefit of MaxMin model. Furthermore, as mentioned earlier, in this study, a fuzzy forward model of MR damper was designed and combined with TSKInv to provide an estimation of MR damper's force feedback. However, if the force measurements are available, they are preferred to be used.

6.4 ONLINE REAL-TIME STRUCTURAL IDENTIFICATION

Structural Identification and Damage prognosis is the prediction in near real time of the remaining useful life of an engineered system, given the measurement and assessment of its current structural state and accompanying predicted performance in anticipated future loading environments.

An important objective of health monitoring systems for civil infrastructures is to identify the state of the structure and to evaluate its possible damage. Frequently, damage can be inferred from the changes of structural parameters, such as the stiffness and damping coefficients. System identification and damage detection, based on vibration data measured from the structural health monitoring system, have received considerable attention recently including many popular techniques, such as the frequency domain analysis, time domain analysis and others.

Among real-time identification methods, one of the most successful and widely used methods for estimation of states and parameters is the Kalman filter and its various nonlinear extensions like Extended Kalman Filter (EKF) and iterated Extended Kalman Filter (IEKF). However, these methods are not effective in the case of highly nonlinear problems. To overcome the problem, two filtering techniques, namely, unscented Kalman filter (UKF) and iterated unscented Kalman filter (IUKF), have been recently developed to handle any functional nonlinearity. In this study, an investigation was

carried out on the aforementioned methods for their effectiveness and efficiencies through a highly nonlinear SDOF structure as well as a two-storey linear structure. In both applications, the measurement equation was nonlinear and in one of the cases the structure also exhibited hysterical structural nonlinearity. It is observed that in most cases, the results of EKF and UKF were improved by their corresponding iterated versions, i.e. IEKF and IUKF. However, it was seen that IEKF, in some cases, showed a weaker performance than EKF which can be because of its sensitivity to the measurement error and noise level. The UKF method, on the other hand, has proven to be far superior to standard EKF and IEKF in the structural identification applications, while in nonlinear structures with noise contaminated measurements, IUKF performed even better than UKF in terms of robustness, convergence speed and tracking accuracy. It is also worth noting that no publication has been found on the application of IEKF to structural identification. Moreover, to date, no such comparison has been done before.

The Recursive Least Square (RLS) based methods are also another category of identification approaches which have been used widely in estimation of structural system parameters. For the purpose of damage detection, RLS has been combined with single forgetting factor to track the time-varying parameters in the fields of electrical and mechanical engineering. However, when there are multiple parameters that each (or some) varies with a different rate, this method cannot perform well. On the other hand, a priori information on the changing rate of the parameters might not be available, and the forgetting factors must be updated adaptively. In this research, a new adaptive tracking technique, based on RLS with adaptive multiple forgetting factors (AMFF-RLS), was presented which can estimate the unknown structural parameters as well as unknown input, e.g. earthquake signal. The proposed method considers an adaptive rule for each of the forgetting factors assigned to each of the parameters and thus, enables simultaneous estimation of the time-varying stiffness and damping of the storeys of the structure. The covariance matrix in this method has the same size as the unknown parameters, which makes the proposed algorithm compact and capable of real-time tracking of the unknown system's parameters. The method was applied to different structures, with different excitations and damage scenarios. It is found from the results that the proposed algorithm can effectively identify the time-varying parameters such as damping, stiffness, as well as unknown excitations with high computational efficiency, even when the observed data were contaminated with

different types and significant levels of noise. However, when damage occurs while the excitation is small, the measurements become very small and thus, the identification error remains at a small range, and therefore, covariance cannot be amplified. This basically makes the algorithm very slow, which justifies the continuation of the current research.

6.5 FUTURE RESEARCH

Although significant achievements have been attained during this study toward the ultimate goal of designing accurate and efficient online and real-time Structural control and health monitoring systems for real building structures, there are still a lot of challenges ahead. Here are some critical areas needing further investigation.

- In this study, the places of sensors are chosen first and then the optimal number and places of control devices have been found. However, as location of sensors also play an important role in structural control, further study is needed to find the best location of sensors.

- The new proposed semi-active control algorithms will be experimentally validated using UTS 5-storey benchmark building and shake-table.

- The RLS based damage detection method introduced in Chapter 5, needs full state of the structure which might not be available all the time. Therefore, modification of the proposed method to work with incomplete measurements needs to be studied in the future.

- Substructure identification methods provide an effective means for SHM systems to tackle the difficulty of identifying complex real structures. A substructure identification method, applying a “divide and conquer” strategy, divides a large complex structure into many simple substructures and carries out system identification and damage detection for each substructure as an independent structure. Since the identification problem of each substructure is much simpler than that of the whole structure, the convergence and ill-conditioning problems frequently encountered in global SHM methods are alleviated and more accurate damage detection and localisation can be achieved. In addition to the improvement

of identification accuracy, substructure identification methods have many other promising features.

- The identification of one substructure generally does not require measuring the excitation forces applied outside this substructure; thus, substructure identification methods partially solve the common difficulty facing many SHM methods which is: how to perform the identification without excitation information.
- Each identification step in a substructure identification method only utilises the structural responses related to one substructure and can be carried out almost independently. Consequently, substructure identification methods do not need to simultaneously measure all structural responses of a large structure, which may greatly reduce the cost of SHM systems, especially when power-limited wireless sensors are used to collect and transmit the measured data.
- Since structural damage inside one substructure usually only affects the identified parameters of that substructure, substructure identification methods make it easier to detect structural damage at the substructure level.

Since the new developed RLS based damage identification method (AMFF-RLS) is able of estimating both structural parameters and unknown excitation, it might be useful for the substructure based approaches, where the focus of damage detection is only on some floors of the structure (Figure 6.1). Therefore, its feasibility can be studied as part of a future research.

- The forgetting factors incorporated into RLS based methods may be considered as fuzzy parameters. Therefore, a set of fuzzy rules and membership functions can be defined to adjust and update the parameters during the earthquake.
- Some more numerical studies can be performed on online damage identification of structures subjected to wind load while wind is considered as an unknown input.
- All the techniques studied in Chapter 5, including Kalman filtering methods and RLS based methods, can be experimentally verified.

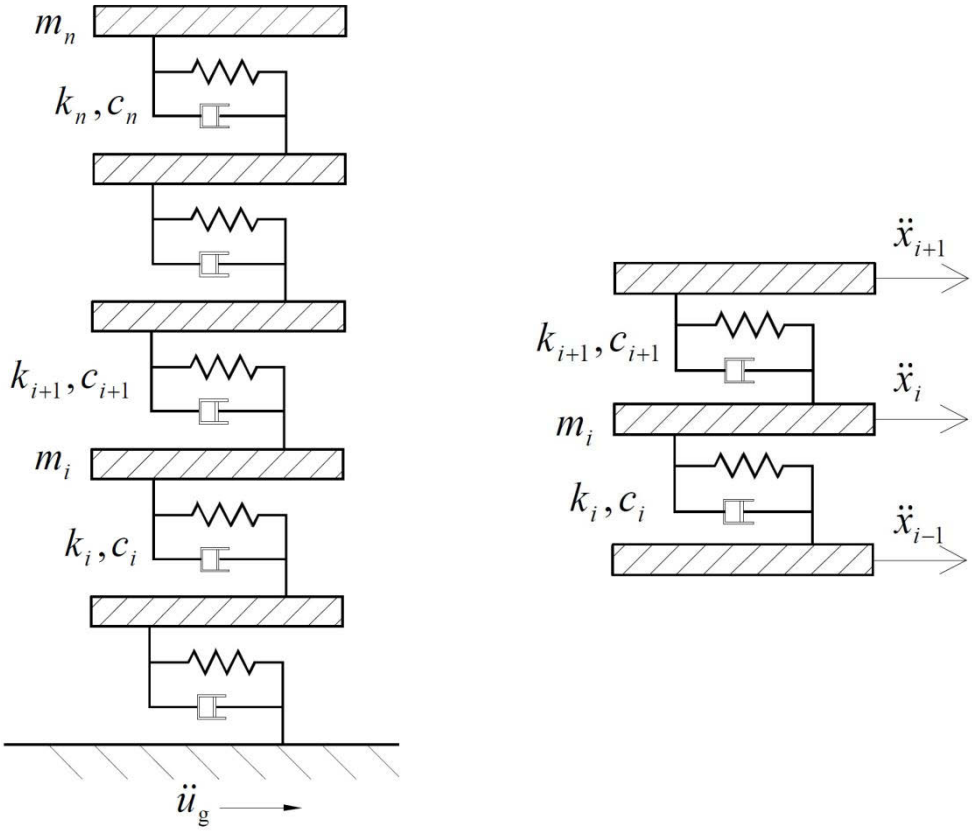

Figure 6.1. A Shear Structure (Left), The two-storey standard substructure (right)

- So far, attention has largely been focused on individual research areas of structural control, sensor technology, and structural health monitoring. These traditional design methodologies treat the structural monitoring and the controller design as two separate procedures. This separate approach is not practical or cost-effective when structures require both a vibration control and a health monitoring system simultaneously. Emerging from recent advances in smart materials, advanced sensing technology, signal processing and advanced control theory, intelligent structures, featuring self-sensing, self-adaptive, self-prognostic and self-repairing abilities, potentially offer ultimate protection to the civil structures as well as their contents and occupants in terms of safety and functionality against undesired dynamic loadings and damage or structural deficiency. In this regard, integration of control and health monitoring is the first and essential step towards development of an intelligent structure. In civil engineering, very limited research on intelligent structures and exploring synergy between SC and SHM are reported. Ray and Tian proposed a method of enhancing modal sensitivity to local damage using feedback

control to aid in damage detection (Ray & Tian 1999). Gattulli and Romeo proposed the use of an integrated procedure for robust control of oscillations and damage detection of linear structural systems (Gattulli & Romeo 2000). Sun and Tong presented a closed-loop control based damage detection scheme aiming at detecting small damage in controlled structures (Sun & Tong 2003). These studies, however, have focused on active control of small-scale structures, which are very different for applications in civil engineering structures in terms of scale and complexity. Xu and Chen have probably performed the most comprehensive work so far in this area (Xu & Chen 2008). They identified the structural parameters by adding a known stiffness using semi-active friction dampers. Then, they considered two types of control strategy for vibration control of the building. A local feedback control strategy with Kalman filter is also designed by which the acceleration response of building is used as feedback signals instead of displacement and velocity measurements. Furthermore, to provide a comparative basis for the local feedback control strategy, the linear quadratic Gaussian (LQG) controller with a modified clipped strategy is also applied to the building with semi-active friction dampers. They applied their methodology to a 5-Storey building and investigated the feasibility of the proposed scenario (Chen & Xu 2008). Results demonstrated that the proposed methodology can successfully identify the mass and stiffness matrices of the building and suppress the vibration. However, their method cannot track the continuing change of stiffness and mass matrices and cannot present an effective strategy to control the vibration in the presence of a growing damage. Also their proposed method cannot be applied to real-time problems. Therefore, further studies are still needed to integrate structural control and health monitoring and develop a framework for the next generation of smart structures.

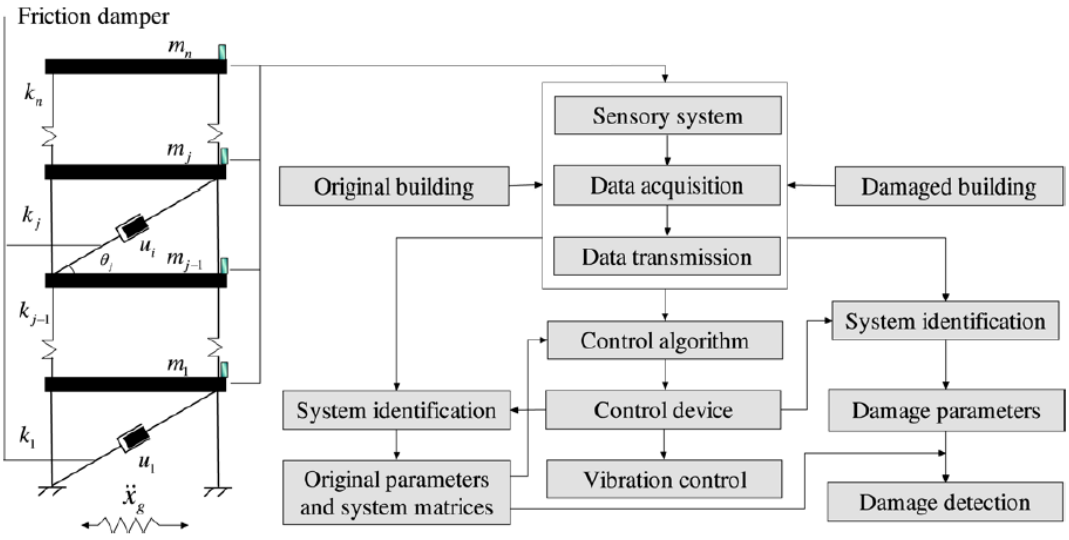

Figure 6.2. Integration of SHM and SC (Chen & Xu 2008)

REFERENCES

Abdullah, M.M., Richardson, A. & Hanif, J. 2001, 'Placement of sensors/actuators on civil structures using genetic algorithms', *Earthquake engineering & structural dynamics*, vol. 30, no. 8, pp. 1167-84.

Amini, F. & Ghaderi, P. 2012, 'Optimal locations for MR dampers in civil structures using improved Ant Colony algorithm', *Optimal Control Applications and Methods*.

Amini, F. & Tavassoli, M.R. 2005, 'Optimal structural active control force, number and placement of controllers', *Engineering structures*, vol. 27, no. 9, pp. 1306-16.

Arbel, A. 1981, 'Controllability measures and actuator placement in oscillatory systems', *International Journal of Control*, vol. 33, no. 3, pp. 565-74.

Askari, M. & Davaie-Markazi, A.H. 2008, 'Multi-objective optimal fuzzy logic controller for nonlinear building-MR damper system', *Systems, Signals and Devices, 2008. IEEE SSD 2008. 5th International Multi-Conference on*, IEEE, pp. 1-6.

Askari, M., Li, J. & Samali, B., 'Semi-Active LQG Control of Seismically Excited Nonlinear Buildings using Optimal Takagi-Sugeno Inverse Model of MR Dampers', *Procedia Engineering*, vol. 14, pp. 2765-72.

Askari, M., Li, J. & Samali, B. 2011, 'Semi-Active LQG Control of Seismically Excited Nonlinear Buildings using Optimal Takagi-Sugeno Inverse Model of MR Dampers', *Procedia Engineering*, vol. 14, pp. 2765-72.

Askari, M. & Markazi, A., 'A new evolving compact optimised Takagi–Sugeno fuzzy model and its application to nonlinear system identification', *International Journal of Systems Science*, vol. 43, no. 4, pp. 776-85.

Barroso, L.R. & Rodriguez, R. 2004, 'Damage detection utilizing the damage index method to a benchmark structure', *Journal of Engineering Mechanics*, vol. 130, no. 2, pp. 142-51.

Bell, B.M. & Cathey, F.W. 1993, 'The iterated Kalman filter update as a Gauss-Newton method', *Automatic Control, IEEE Transactions on*, vol. 38, no. 2, pp. 294-7.

Bernal, D. 2007, 'Damage localization from the null space of changes in the transfer matrix', *AIAA journal*, vol. 45, no. 2, pp. 374-81.

Bernal, D. & Gunes, B. 2003, 'Flexibility based approach for damage characterization: benchmark application', *Journal of Engineering Mechanics*, vol. 130, no. 1, pp. 61-70.

Bezdek, J.C., Ehrlich, R. & Full, W. 1984, 'FCM: The fuzzy ***c***-means clustering algorithm', *Computers & Geosciences*, vol. 10, no. 2, pp. 191-203.

Bitaraf, M. & Hurlebaus, S. 2013, 'Semi-active adaptive control of seismically excited 20-storey nonlinear building', *Engineering structures*, vol. 56, pp. 2107-18.

Brogan, W.L. 1991, 'Modern control theory, 1991', *New Jersy: Prentice Hall*, p. 317.

Brown, A.S., Ankireddi, S. & Yang, H.T. 1999, 'Actuator and sensor placement for multiobjective control of structures', *Journal of Structural Engineering*, vol. 125, no. 7, pp. 757-65.

Caicedo, J., Dyke, S.J. & Johnson, E.A. 2000, 'Health monitoring based on component transfer functions', *Advances in Structural Dynamics*, vol. 2, no. 2, pp. 997-1004.

Caicedo, J.M., Dyke, S.J. & Johnson, E.A. 2003, 'Natural excitation technique and eigensystem realization algorithm for phase I of the IASC-ASCE benchmark problem: Simulated data', *Journal of Engineering Mechanics*, vol. 130, no. 1, pp. 49-60.

Caravani, P., Watson, M. & Thomson, W. 1977, 'Recursive least-squares time domain identification of structural parameters', *Journal of applied mechanics*, vol. 44, p. 135.

Carlson, J.D. & Jolly, M.R. 2000, 'MR fluid, foam and elastomer devices', *Mechatronics*, vol. 10, no. 4, pp. 555-69.

Cha, Y.-J., Agrawal, A.K., Kim, Y. & Raich, A.M. 2012, 'Multi-objective genetic algorithms for cost-effective distributions of actuators and sensors in large structures', *Expert Systems with Applications*.

Chang, C.-C. & Zhou, L. 2002, 'Neural network emulation of inverse dynamics for a magnetorheological damper', *Journal of Structural Engineering*, vol. 128, no. 2, pp. 231-9.

Chang, P.C. & Liu, S.C. 2003, 'Recent research in nondestructive evaluation of civil infrastructures', *Journal of materials in civil engineering*, vol. 15, no. 3, pp. 298-304.

Chase, J.G., Begoc, V. & Barroso, L.R. 2005, 'Efficient structural health monitoring for a benchmark structure using adaptive RLS filters', *Computers & structures*, vol. 83, no. 8, pp. 639-47.

Chase, J.G., Spieth, H.A., Blome, C.F. & Mander, J. 2005, 'LMS-based structural health monitoring of a non-linear rocking structure', *Earthquake engineering & structural dynamics*, vol. 34, no. 8, pp. 909-30.

Chassiakos, A., Masri, S., Smyth, A. & Caughey, T. 1998, 'On-line identification of hysteretic systems', *Journal of applied mechanics*, vol. 65, no. 1, pp. 194-203.

Chatzi, E.N. & Smyth, A.W. 2009, 'The unscented Kalman filter and particle filter methods for nonlinear structural system identification with non-collocated heterogeneous sensing', *Structural Control and Health Monitoring*, vol. 16, no. 1, pp. 99-123.

Chen, B. & Xu, Y. 2008, 'Integrated vibration control and health monitoring of building structures using semi-active friction dampers: Part II—Numerical investigation', *Engineering Structures*, vol. 30, no. 3, pp. 573-87.

Chen, C., Czarnecki, R. & Scholl, R. 1976, *Vibration tests of a 4-storey concrete structure*, Blume (John A.) and Associates, Engineers, San Francisco, CA (USA).

Chen, G. & Chen, C. 2004, 'Semiactive control of the 20-storey benchmark building with piezoelectric friction dampers', *Journal of engineering mechanics*, vol. 130, no. 4, pp. 393-400.

Cheng, F.Y., Jiang, H. & Zhang, X. 2002, 'Optimal placement of dampers and actuators based on stochastic approach', *Earthquake Engineering and Engineering Vibration*, vol. 1, no. 2, pp. 237-49.

Cheung, B.-S., Langevin, A. & Delmaire, H. 1997, 'Coupling genetic algorithm with a grid search method to solve mixed integer nonlinear programming problems', *Computers & Mathematics with Applications*, vol. 34, no. 12, pp. 13-23.

Chiu, S.L. 1994, 'Fuzzy model identification based on cluster estimation', *Journal of intelligent and Fuzzy systems*, vol. 2, no. 3, pp. 267-78.

Chopra, A.K. 1995, *Dynamics of structures: theory and applications to earthquake engineering*, vol. 2, Prentice Hall Englewood Cliffs, NJ.

Das, D., Datta, T. & Madan, A. 2012, 'Semiactive fuzzy control of the seismic response of building frames with MR dampers', *Earthquake engineering & structural dynamics*, vol. 41, no. 1, pp. 99-118.

Deb, K. 2001, 'Multi-objective optimization', *Multi-objective optimization using evolutionary algorithms*, pp. 13-46.

Deb, K., Pratap, A., Agarwal, S. & Meyarivan, T. 2002, 'A fast and elitist multiobjective genetic algorithm: NSGA-II', *Evolutionary Computation, IEEE Transactions on*, vol. 6, no. 2, pp. 182-97.

Deep, K., Singh, K.P., Kansal, M. & Mohan, C. 2009, 'A real coded genetic algorithm for solving integer and mixed integer optimization problems', *Applied Mathematics and Computation*, vol. 212, no. 2, pp. 505-18.

Deep, K. & Thakur, M. 2007a, 'A new crossover operator for real coded genetic algorithms', *Applied Mathematics and Computation*, vol. 188, no. 1, pp. 895-911.

Deep, K. & Thakur, M. 2007b, 'A new mutation operator for real coded genetic algorithms', *Applied mathematics and Computation*, vol. 193, no. 1, pp. 211-30.

Dharap, P. 2006, 'Real-time structural damage detection using interaction matrix formulation and observers', Ph. D. Thesis.

Dhingra, A. & Lee, B. 1995, 'Multiobjective design of actively controlled structures using a hybrid optimization method', *International journal for numerical methods in engineering*, vol. 38, no. 20, pp. 3383-401.

Djajakesukma, S.L. 2003, 'Semi-active control devices for earthquake-resistant structures', University of Technology, Sydney.

Doebling, S.W., Farrar, C.R., Prime, M.B. & Shevitz, D.W. 1996, *Damage identification and health monitoring of structural and mechanical systems from changes in their vibration characteristics: a literature review*, Los Alamos National Lab., NM (United States).

Du, H., Lam, J., Cheung, K., Li, W. & Zhang, N. 2013, 'Direct voltage control of magnetorheological damper for vehicle suspensions', *Smart materials and structures*, vol. 22, no. 10, p. 105016.

Du, H. & Zhang, N. 2008, 'Application of evolving Takagi–Sugeno fuzzy model to nonlinear system identification', *Applied Soft Computing*, vol. 8, no. 1, pp. 676-86.

Duan, Y., Ni, Y. & Ko, J. 2006, 'Cable vibration control using magnetorheological dampers', *Journal of intelligent material systems and structures*, vol. 17, no. 4, pp. 321-5.

Dyke, S., Spencer Jr, B., Sain, M. & Carlson, J. 1996a, 'Modeling and control of magnetorheological dampers for seismic response reduction', *Smart Materials and Structures*, vol. 5, no. 5, p. 565.

Dyke, S., Spencer Jr, B., Sain, M. & Carlson, J. 1996b, 'Seismic response reduction using magnetorheological dampers', *Proceedings of the IFAC world congress*, vol. 50, pp. 145-50.

Dyke, S.J., Caicedo, J.M. & Johnson, E.A. 2000, 'Monitoring of a benchmark structure for damage identification', *Proceedings of the Engineering Mechanics Speciality Conference*.

Fan, W. & Qiao, P. 2011, 'Vibration-based damage identification methods: a review and comparative study', *Structural Health Monitoring*, vol. 10, no. 1, pp. 83-111.

Farrar, C.R., Baker, W., Bell, T., Cone, K., Darling, T., Duffey, T., Eklund, A. & Migliori, A. 1994, *Dynamic characterization and damage detection in the I-40 bridge over the Rio Grande*, Los Alamos National Lab., NM (United States).

Farrar, C.R. & Worden, K. 2007, 'An introduction to structural health monitoring', *Philosophical Transactions of the Royal Society A: Mathematical, Physical and Engineering Sciences*, vol. 365, no. 1851, pp. 303-15.

Fucheng, G., Zhongkang, S. & Kan, H. 2003, 'A modified covariance extended Kalman filtering algorithm in passive location', *Robotics, Intelligent Systems and Signal Processing, 2003. Proceedings. 2003 IEEE International Conference on*, vol. 1, IEEE, pp. 307-11.

Furuya, H. & Haftka, R. 1995, 'Placing actuators on space structures by genetic algorithms and effectiveness indices', *Structural and Multidisciplinary Optimization*, vol. 9, no. 2, pp. 69-75.

Gattulli, V. & Romeo, F. 2000, 'Integrated procedure for identification and control of MDOF structures', *Journal of engineering mechanics*, vol. 126, no. 7, pp. 730-7.

Geoffrey Chase, J., Leo Hwang, K., Barroso, L. & Mander, J. 2005, 'A simple LMS-based approach to the structural health monitoring benchmark problem', *Earthquake engineering & structural dynamics*, vol. 34, no. 6, pp. 575-94.

Ghanem, R. & Ferro, G. 2006, 'Health monitoring for strongly non-linear systems using the Ensemble Kalman filter', *Structural Control and Health Monitoring*, vol. 13, no. 1, pp. 245-59.

Goldberg, D.E. 1989, 'Genetic algorithms in search, optimization, and machine learning'.

Hann, C.E., Singh-Levett, I., Deam, B.L., Mander, J.B. & Chase, J.G. 2009, 'Real-time system identification of a nonlinear four-storey steel frame structure—application to structural health monitoring', *Sensors Journal, IEEE*, vol. 9, no. 11, pp. 1339-46.

Hera, A. & Hou, Z. 2003, 'Application of wavelet approach for ASCE structural health monitoring benchmark studies', *Journal of Engineering Mechanics*, vol. 130, no. 1, pp. 96-104.

Hoshiya, M. & Saito, E. 1984, 'Structural identification by extended Kalman filter', *Journal of Engineering Mechanics*, vol. 110, no. 12, pp. 1757-70.

Hou, Z., Noori, M. & Amand, R.S. 2000, 'Wavelet-based approach for structural damage detection', *Journal of Engineering Mechanics*, vol. 126, no. 7, pp. 677-83.

Hurlebaus, S. & Gaul, L. 2006, 'Smart structure dynamics', *Mechanical Systems and Signal Processing*, vol. 20, no. 2, pp. 255-81.

Inaudi, J.A. 1997, 'Modulated Homogeneous Friction: A Semi-Active Damping Strategy', *Earthquake engineering & structural dynamics*, vol. 26, no. 3, pp. 361-76.

Jang, J.-S.R., Sun, C.-T. & Mizutani, E. 1997, 'Neuro-fuzzy and soft computing-a computational approach to learning and machine intelligence [Book Review]', *Automatic Control, IEEE Transactions on*, vol. 42, no. 10, pp. 1482-4.

Jang, J.-S.R., Sun, C.-T. & Mizutani, E. 2010, *Neuro-fuzzy and soft computing: a computational approach to learning and machine intelligence*, PHI Learning.

Ji, X., Fenves, G.L., Kajiwara, K. & Nakashima, M. 2010, 'Seismic damage detection of a full-scale shaking table test structure', *Journal of structural engineering*, vol. 137, no. 1, pp. 14-21.

Jong, K.A.D. 1975, 'An analysis of the behavior of a class of genetic adaptive systems', University of Michigan.

Juang, J.-N. & Pappa, R.S. 1985, 'An eigensystem realization algorithm for modal parameter identification and model reduction', *Journal of guidance, control, and dynamics*, vol. 8, no. 5, pp. 620-7.

Julier, S.J. & Uhlmann, J.K. 1997, 'New extension of the Kalman filter to nonlinear systems', *AeroSense'97*, International Society for Optics and Photonics, pp. 182-93.

Kaiser, S., Melcher, J., Breitbach, E.J. & Sachau, D. 1999, 'Structural dynamic health monitoring of adaptive CFRP structures', *1999 Symposium on Smart Structures and Materials*, International Society for Optics and Photonics, pp. 51-9.

Karamodin, A., Haji Kazemi, H., Rowhanimanesh, A. & Akbarzadeh Totonchi, M.R. 2009, 'Semi-active control of structures using a neuro-inverse model of MR dampers', *Scientia Iranica*, vol. 16.

Kasabov, N.K. & Song, Q. 2002, 'DENFIS: dynamic evolving neural-fuzzy inference system and its application for time-series prediction', *Fuzzy Systems, IEEE Transactions on*, vol. 10, no. 2, pp. 144-54.

Kim, H.-S., Roschke, P.N., Lin, P.-Y. & Loh, C.-H. 2006, 'Neuro-fuzzy model of hybrid semi-active base isolation system with FPS bearings and an MR damper', *Engineering structures*, vol. 28, no. 7, pp. 947-58.

Kim, H. & Melhem, H. 2004, 'Damage detection of structures by wavelet analysis', *Engineering Structures*, vol. 26, no. 3, pp. 347-62.

Knowles, J. & Corne, D. 1999, 'The pareto archived evolution strategy: A new baseline algorithm for pareto multiobjective optimisation', *Evolutionary Computation, 1999. CEC 99. Proceedings of the 1999 Congress on*, vol. 1, IEEE.

Kwok, N., Ha, Q. & Samali, B. 2007, 'MR Damper Optimal Placement for Semi-Active Control of Buildings Using an Efficient Multi-Objective Binary Genetic Algorithm', *Proceedings of 24th International Symposium on Automation & Robotics in Construction, ISARC*.

Lam, H., Katafygiotis, L. & Mickleborough, N. 2003, 'Application of a statistical model updating approach on phase I of the IASC-ASCE structural health monitoring benchmark study', *Journal of Engineering Mechanics*, vol. 130, no. 1, pp. 34-48.

Leitmann, G. 1994, 'Semiactive control for vibration attenuation', *Journal of Intelligent Material Systems and Structures*, vol. 5, no. 6, pp. 841-6.

Li, L., Song, G. & Ou, J. 2010, 'A genetic algorithm-based two-phase design for optimal placement of semi-active dampers for nonlinear benchmark structure', *Journal of Vibration and Control*, vol. 16, no. 9, pp. 1379-92.

Li, Q., Liu, D., Fang, J. & Tam, C. 2000, 'Multi-level optimal design of buildings with active control under winds using genetic algorithms', *Journal of Wind Engineering and Industrial Aerodynamics*, vol. 86, no. 1, pp. 65-86.

Li, Q., Liu, D., Tang, J., Zhang, N. & Tam, C. 2004, 'Combinatorial optimal design of number and positions of actuators in actively controlled structures using genetic algorithms', *Journal of sound and vibration*, vol. 270, no. 4, pp. 611-24.

Li, S., Suzuki, Y. & Noori, M. 2004, 'Improvement of parameter estimation for non-linear hysteretic systems with slip by a fast Bayesian bootstrap filter', *International Journal of Non-Linear Mechanics*, vol. 39, no. 9, pp. 1435-45.

Lin, C.S. 1990, 'Location of modeling errors using modal test data', *AIAA journal*, vol. 28, no. 9, pp. 1650-4.

Lin, J.-W., Betti, R., Smyth, A.W. & Longman, R.W. 2001, 'On-line identification of nonlinear hysteretic structural systems using a variable trace approach', *Earthquake engineering & structural dynamics*, vol. 30, no. 9, pp. 1279-303.

Liu, D., Yang, Y. & Li, Q. 2003, 'Optimum positioning of actuators in tall buildings using genetic algorithm', *Computers & structures*, vol. 81, no. 32, pp. 2823-7.

Liu, X., Begg, D. & Matravers, D. 1997, 'Optimal topology/actuator placement design of structures using SA', *Journal of Aerospace Engineering*, vol. 10, no. 3, pp. 119-25.

Loh, C.-H., Lin, C.-Y. & Huang, C.-C. 2000, 'Time domain identification of frames under earthquake loadings', *Journal of Engineering Mechanics*, vol. 126, no. 7, pp. 693-703.

Loh, C.H. & Lin, H.M. 1996, 'APPLICATION OF OFF-LINE AND ON-LINE IDENTIFICATION TECHNIQUES TO BUILDING SEISMIC RESPONSE DATA', *Earthquake engineering & structural dynamics*, vol. 25, no. 3, pp. 269-90.

Luo, Y.-C., Guignard, M. & Chen, C.-H. 2001, 'A hybrid approach for integer programming combining genetic algorithms, linear programming and ordinal optimization', *Journal of Intelligent Manufacturing*, vol. 12, no. 5, pp. 509-19.

Lus, H., Betti, R. & Longman, R.W. 1999, 'Identification of linear structural systems using earthquake-induced vibration data', *Earthquake Engineering and Structural Dynamics*, vol. 28, no. 11, pp. 1449-68.

Lus, H., Betti, R., Yu, J. & De Angelis, M. 2003, 'Investigation of a system identification methodology in the context of the ASCE benchmark problem', *Journal of Engineering Mechanics*, vol. 130, no. 1, pp. 71-84.

Lus, H., De Angelis, M., Betti, R. & Longman, R.W. 2003, 'Constructing second-order models of mechanical systems from identified state space realizations. Part I: Theoretical discussions', *Journal of Engineering Mechanics*, vol. 129, no. 5, pp. 477-88.

Maiti, A., Bhunia, A. & Maiti, M. 2006, 'An application of real-coded genetic algorithm (RCGA) for mixed integer non-linear programming in two-storage multi-item

inventory model with discount policy', *Applied Mathematics and computation*, vol. 183, no. 2, pp. 903-15.

Marin, L., Dohler, M., Bernal, D. & Mevel, L. 2013, 'Damage Localization Using a Statistical Test on Residuals from the SDDLV Approach', *Topics in Model Validation and Uncertainty Quantification, Volume 5*, Springer, pp. 143-52.

Masri, S., Smyth, A., Chassiakos, A., Caughey, T. & Hunter, N. 2000, 'Application of neural networks for detection of changes in nonlinear systems', *Journal of Engineering Mechanics*, vol. 126, no. 7, pp. 666-76.

McClamroch, N.H. & Gavin, H. 1995, 'Closed loop structural control using electrorheological dampers', *American Control Conference, 1995. Proceedings of the*, vol. 6, IEEE, pp. 4173-7.

Montalvao, D., Maia, N. & Ribeiro, A. 2006, 'A review of vibration-based structural health monitoring with special emphasis on composite materials', *Shock and Vibration Digest*, vol. 38, no. 4, pp. 295-326.

Ohtori, Y., Christenson, R., Spencer Jr, B. & Dyke, S. 2004, 'Benchmark control problems for seismically excited nonlinear buildings', *Journal of Engineering Mechanics*, vol. 130, no. 4, pp. 366-85.

Onoda, J. & Hanawa, Y. 2012, 'Actuator placement optimization by genetic and improved simulated annealing algorithms', *AIAA journal*, vol. 31, no. 6.

Ponsich, A., Azzaro-Pantel, C., Domenech, S. & Pibouleau, L. 2007, 'Mixed-integer nonlinear programming optimization strategies for batch plant design problems', *Industrial & engineering chemistry research*, vol. 46, no. 3, pp. 854-63.

Rama Mohan Rao, A. & Sivasubramanian, K. 2008, 'Optimal placement of actuators for active vibration control of seismic excited tall buildings using a multiple start guided neighbourhood search (MSGNS) algorithm', *Journal of Sound and Vibration*, vol. 311, no. 1, pp. 133-59.

Ray, L.R. & Tian, L. 1999, 'Damage detection in smart structures through sensitivity-enhancing feedback control', *1999 Symposium on Smart Structures and Materials*, International Society for Optics and Photonics, pp. 314-24.

Sato, T. & Qi, K. 1998, 'Adaptive H∞ filter: its application to structural identification', *Journal of Engineering Mechanics*, vol. 124, no. 11, pp. 1233-40.

Sato, T. & Takei, K. 1997, 'Real-time robust identification algorithm for structural systems with time-varying dynamic characteristics', *Smart Structures and Materials' 97*, International Society for Optics and Photonics, pp. 393-404.

Schurter, K.C. & Roschke, P.N. 2000, 'Fuzzy modeling of a magnetorheological damper using ANFIS', *Fuzzy Systems, 2000. FUZZ IEEE 2000. The Ninth IEEE International Conference on*, vol. 1, IEEE, pp. 122-7.

Shi, Y., Xin, N. & Ningwei, W. 2004, 'Optimal placement of MR damper set in structures', *EARTHQUAKE ENGINEERING AND ENGINEERING VIBRATION-CHINESE EDITION-*, vol. 24, no. 3, pp. 175-8.

Singh, M.P. & Moreschi, L.M. 2002, 'Optimal placement of dampers for passive response control', *Earthquake engineering & structural dynamics*, vol. 31, no. 4, pp. 955-76.

Smyth, A., Masri, S., Chassiakos, A. & Caughey, T. 1999, 'On-line parametric identification of MDOF nonlinear hysteretic systems', *Journal of Engineering Mechanics*, vol. 125, no. 2, pp. 133-42.

Spencer, B., Dyke, S. & Deoskar, H. 1998, 'Benchmark problems in structural control: part I-active mass driver system', *Earthquake Engineering and Structural Dynamics*, vol. 27, no. 11, pp. 1127-40.

Spencer, B., Dyke, S., Sain, M. & Carlson, J. 1997, 'Phenomenological model for magnetorheological dampers', *Journal of engineering mechanics*, vol. 123, no. 3, pp. 230-8.

Stanway, R., Sproston, J. & Stevens, N. 1985, 'Non-linear identification of an electrorheological vibration damper', *IFAC Identification and System Parameter Estimation*, vol. 7, pp. 195-200.

Sun, D. & Tong, L. 2003, 'Closed-loop based detection of debonding of piezoelectric actuator patches in controlled beams', *International Journal of Solids and structures*, vol. 40, no. 10, pp. 2449-71.

Sun, Z. & Chang, C. 2004, 'Statistical wavelet-based method for structural health monitoring', *Journal of structural engineering*, vol. 130, no. 7, pp. 1055-62.

Takagi, T. & Sugeno, M. 1985, 'Fuzzy identification of systems and its applications to modeling and control', *Systems, Man and Cybernetics, IEEE Transactions on*, no. 1, pp. 116-32.

Tan, P., Dyke, S.J., Richardson, A. & Abdullah, M. 2005, 'Integrated device placement and control design in civil structures using genetic algorithms', *Journal of Structural Engineering*, vol. 131, no. 10, pp. 1489-96.

Tang, J.-P., Chiou, D.-J., Chen, C.-W., Chiang, W.-L., Hsu, W.-K., Chen, C.-Y. & Liu, T.-Y. 2011, 'A case study of damage detection in benchmark buildings using a Hilbert-Huang Transform-based method', *Journal of Vibration and Control*, vol. 17, no. 4, pp. 623-36.

Tse, T. & Chang, C. 2004, 'Shear-mode rotary magnetorheological damper for small-scale structural control experiments', *Journal of structural engineering*, vol. 130, no. 6, pp. 904-11.

Ungarala, S. 2012, 'On the iterated forms of Kalman filters using statistical linearization', *Journal of Process Control*, vol. 22, no. 5, pp. 935-43.

Vahidi, A., Stefanopoulou, A. & Peng, H. 2005, 'Recursive least squares with forgetting for online estimation of vehicle mass and road grade: theory and experiments', *Vehicle System Dynamics*, vol. 43, no. 1, pp. 31-55.

Van Der Merwe, R. 2004, 'Sigma-point Kalman filters for probabilistic inference in dynamic state-space models', University of Stellenbosch.

Wang, D. & Liao, W. 2005, 'Modeling and control of magnetorheological fluid dampers using neural networks', *Smart materials and structures*, vol. 14, no. 1, p. 111.

Wang, D. & Liao, W. 2011, 'Magnetorheological fluid dampers: a review of parametric modelling', *Smart Materials and structures*, vol. 20, no. 2, pp. 261-75.

Wen, Y.-K. 1976, 'Method for random vibration of hysteretic systems', *Journal of the Engineering Mechanics Division*, vol. 102, no. 2, pp. 249-63.

Wongprasert, N. & Symans, M. 2004, 'Application of a genetic algorithm for optimal damper distribution within the nonlinear seismic benchmark building', *Journal of engineering mechanics*, vol. 130, no. 4, pp. 401-6.

Wu, M. & Smyth, A.W. 2007, 'Application of the unscented Kalman filter for real-time nonlinear structural system identification', *Structural Control and Health Monitoring*, vol. 14, no. 7, pp. 971-90.

Wu, Y., Hu, D. & Hu, X. 2007, 'Comments on "Performance evaluation of UKF-based nonlinear filtering"', *Automatica*, vol. 43, no. 3, pp. 567-8.

Xiangyi, G. 2004, 'The Study of challenge technology of single observer passive location and tracking using frequency rate and differential direction of arrival', *Changsha: National University of Defense Technology*, pp. 10-28.

Xie, Z. & Feng, J. 2012, 'Real-time nonlinear structural system identification via iterated unscented Kalman filter', *Mechanical Systems and Signal Processing*, vol. 28, pp. 309-22.

Xu, Y. & Chen, B. 2008, 'Integrated vibration control and health monitoring of building structures using semi-active friction dampers: Part I—methodology', *Engineering Structures*, vol. 30, no. 7, pp. 1789-801.

Xu, Y. & Teng, J. 2002, 'Optimum design of active/passive control devices for tall buildings under earthquake excitation', *The Structural Design of Tall Buildings*, vol. 11, no. 2, pp. 109-27.

Yager, R. & Filev, D. 1994, 'Generation of fuzzy rules by mountain clustering', *Journal of Intelligent and Fuzzy Systems*, vol. 2, no. 3, pp. 209-19.

Yang, G. 2001, 'Large-scale magnetorheological fluid damper for vibration mitigation: modeling, testing and control', University of Notre Dame.

Yang, G., Spencer Jr, B., Carlson, J. & Sain, M. 2002, 'Large-scale MR fluid dampers: modeling and dynamic performance considerations', *Engineering structures*, vol. 24, no. 3, pp. 309-23.

Yang, J., Pan, S. & Huang, H. 2007, 'An adaptive extended Kalman filter for structural damage identifications II: unknown inputs', *Structural Control and Health Monitoring*, vol. 14, no. 3, pp. 497-521.

Yang, J.N., Huang, H. & Lin, S. 2006, 'Sequential non-linear least-square estimation for damage identification of structures', *International Journal of Non-Linear Mechanics*, vol. 41, no. 1, pp. 124-40.

Yang, J.N., Lei, Y., Lin, S. & Huang, N. 2003, 'Hilbert-Huang based approach for structural damage detection', *Journal of Engineering Mechanics*, vol. 130, no. 1, pp. 85-95.

Yang, J.N. & Lin, S. 2004, 'On-line identification of non-linear hysteretic structures using an adaptive tracking technique', *International Journal of Non-Linear Mechanics*, vol. 39, no. 9, pp. 1481-91.

Yokota, T., Gen, M. & Li, Y.-X. 1996, 'Genetic algorithm for non-linear mixed integer programming problems and its applications', *Computers & industrial engineering*, vol. 30, no. 4, pp. 905-17.

Yoshida, O. & Dyke, S.J. 2004, 'Seismic control of a nonlinear benchmark building using smart dampers', *Journal of engineering mechanics*, vol. 130, no. 4, pp. 386-92.

Yuen, K.-V., Au, S.K. & Beck, J.L. 2003, 'Two-stage structural health monitoring approach for phase I benchmark studies', *Journal of Engineering Mechanics*, vol. 130, no. 1, pp. 16-33.

Zang, C., Friswell, M. & Imregun, M. 2004, 'Structural damage detection using independent component analysis', *Structural Health Monitoring*, vol. 3, no. 1, pp. 69-83.

Zapico, J., Worden, K. & Molina, F. 2001, 'Vibration-based damage assessment in steel frames using neural networks', *Smart materials and structures*, vol. 10, no. 3, p. 553.

Ze-bing, D., Jin-zhi, H. & Hong-xia, W. 2004, 'Semi-active control of a cable-stayed bridge under multiple-support excitations', *Journal of Zhejiang University SCIENCE*, vol. 5, no. 3, pp. 317-25.

Zhihuan, L., Yinhong, L. & Xianzhong, D. 2010, 'Non-dominated sorting genetic algorithm-II for robust multi-objective optimal reactive power dispatch', *Generation, Transmission & Distribution, IET*, vol. 4, no. 9, pp. 1000-8.

Zong, L.-H., Gong, X.-L., Guo, C.-Y. & Xuan, S.-H. 2012, 'Inverse neuro-fuzzy MR damper model and its application in vibration control of vehicle suspension system', *Vehicle System Dynamics*, vol. 50, no. 7, pp. 1025-41.

APPENDICES

APPENDIX A: STRUCTURAL EVALUATION CRITERIA

Table A-1. Structural evaluation indices (Ohtori et al. 2004)

J_1	Inter-storey Drift Ratio	$\boldsymbol{Max}\left\{\frac{max_{i,t}(\frac{\lvert d_i(t)\rvert}{h_i})}{\delta^{max}}\right\}$
J_2	Level Acceleration	$\boldsymbol{Max}\left\{\frac{max_{i,t}(\ddot{x}_{ai}(t))}{\ddot{x}_{\mathrm{a}}^{\max}}\right\}$
J_3	Base Shear	$\boldsymbol{Max}\left\{\frac{max_t\lvert\sum_{\mathrm{i}} m_i\ddot{x}_{ai}(t)\rvert}{F_b^{max}}\right\}$
J_4	Normed Inter-storey Drift Ratio	$\boldsymbol{Max}\left\{\frac{max_{i,t}(\frac{\lVert d_i(t)\rVert}{h_i})}{\lVert\delta^{max}\rVert}\right\}$
J_5	Normed Level Acceleration	$\boldsymbol{Max}\left\{\frac{max_{i,t}(\lVert\ddot{x}_{ai}(t)\rVert)}{\lVert\ddot{x}_{\mathrm{a}}^{\max}\rVert}\right\}$
J_6	Normed Base Shear	$\boldsymbol{Max}\left\{\frac{max_t\lVert\sum_{\mathrm{i}} m_i\ddot{x}_{ai}(t)\rVert}{\lVert F_b^{max}\rVert}\right\}$
J_7	Ductility	$\boldsymbol{Max}\left\{\frac{max_{i,t}(\frac{\lvert\emptyset_{\mathrm{j}}(\mathrm{t})\rvert}{\emptyset_{\mathrm{yj}}})}{\emptyset^{max}}\right\}$
J_8	Dissipated Energy	$\boldsymbol{Max}\left\{\frac{max_{i,t}\frac{\int \mathrm{dE_j}}{\mathrm{F_{yj}}\emptyset_{\mathrm{yj}}}}{E^{max}}\right\}$

Table A-1. Continue; Structural evaluation indices (Ohtori et al. 2004)

J_9	Plastic Connections	$\boldsymbol{Max}\left\{\frac{N_d^c}{N_d}\right\}$
J_{10}	Normed Ductility	$\boldsymbol{Max}\left\{\frac{max_{i,t}(\frac{\|\emptyset_j(t)\|}{\emptyset_{yj}})}{\|\emptyset^{max}\|}\right\}$
J_{11}	Control Force	$\boldsymbol{Max}\left\{\frac{max_{l,t}\|f_1(t)\|}{W}\right\}$
J_{12}	Control Device Stroke	$\boldsymbol{Max}\left\{\frac{max_{l,t}\|y_1^a(t)\|}{X^{max}}\right\}$
J_{13}	Control Power	$\boldsymbol{Max}\left\{\frac{max_t[\sum_l P_l(t)]}{\dot{X}^{max}W}\right\}$
J_{14}	Normed Control Power	$\boldsymbol{Max}\left\{\frac{\sum_l \frac{1}{t_f}\int_0^t P_l(t)}{\dot{X}^{max}W}\right\}$
J_{15}	Number of control devices	-
J_{16}	Number of required sensors	-
J_{17}	Computational Resource	$\dim(x_k^c)$

where,

t_f : Time of earthquake

$\|.\|$: Norm, computed as follow: $\|.\| = \sqrt{\frac{1}{t_f}\int_0^{t_f}[.]^2 dt}$

d_i (t): Inter-storey drift of the above ground level over the time history of each earthquake

δ^{max} : Maximum inter-storey drift ratio of the uncontrolled structure calculated by equation $\max_{t,i}\left|\frac{d_i(t)}{h_i}\right|$

$\ddot{x}_a^{max}$: Maximum absolute acceleration of uncontrolled structure

$\left\|\delta^{max}\right\| = \max_i \|d_i(t)/h_i\|$

F_b^{max} : Maximum base shear force of the uncontrolled structure

ϕ_j : Curvature at the ends of the *j*-th element (member)

ϕ_{yj} : Yield curvature at the end of the *j*-th member

F_{yj}: Yield moment at the end of the *j*-th member

ϕ^{max}: Maximum curvature of the uncontrolled structure.

E^{max}: Maximum dissipated energy of the uncontrolled structure.

N_d: Number of damaged connections (member ends) without control

N_d^c: Number of damaged connections with control

$f_l(t)$: Force generated by the *l*-th control device at time t

W: Seismic weight of the building based on the above ground mass of the structure

$y_l^a(t)$: Displacement across the *l*-th control device during the earthquake

x^{max}: Maximum uncontrolled displacement of the levels relative to the ground

$p_l(t)$: Measure of the instantaneous power required by the *l*-th control device

$\dot{x}^{max}$: Maximum uncontrolled velocity of the levels relative to the ground

APPENDIX B: EARTHQUAKE SIGNALS

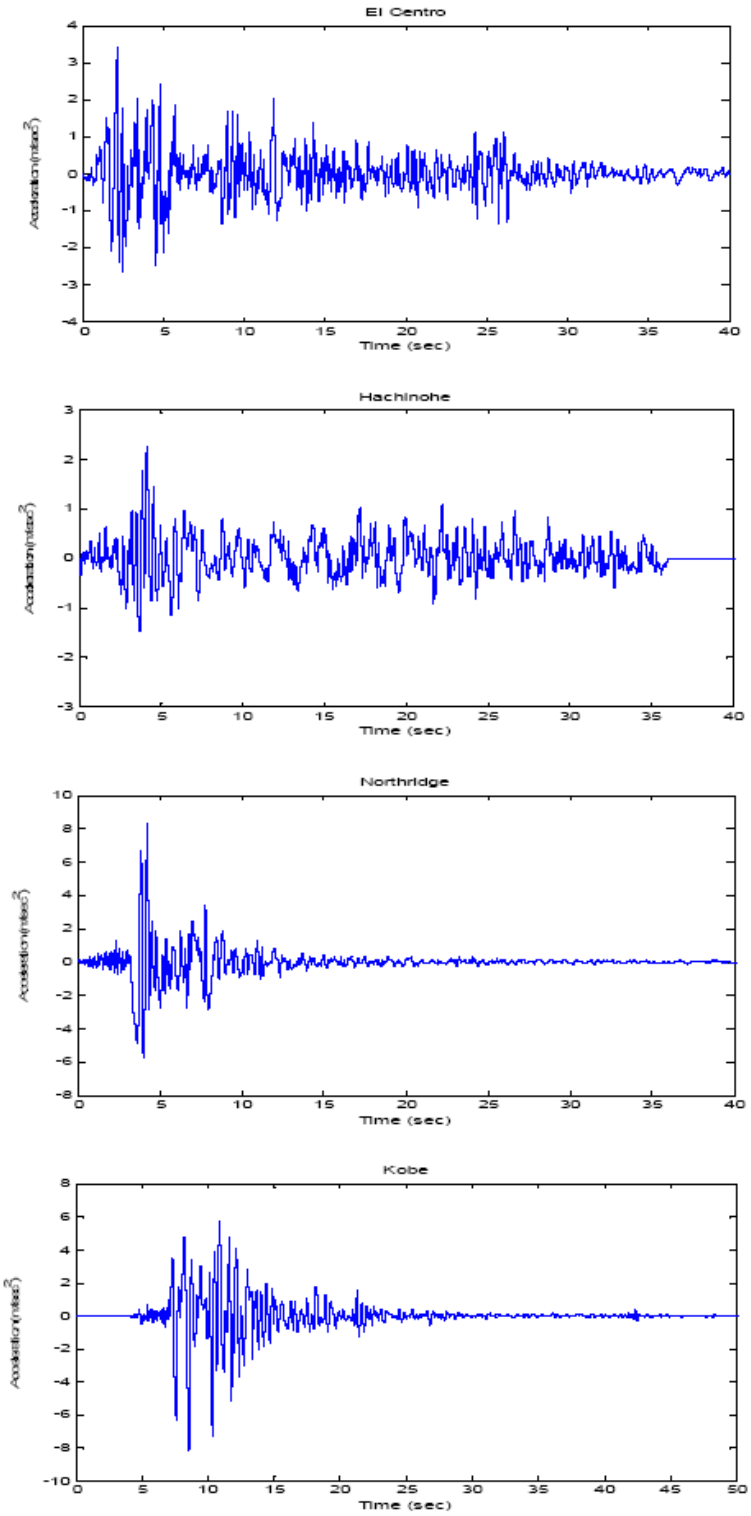

Figure B.1. Earthquake signals used in this thesis

APPENDIX C: STRUCTURAL RESPONSE OF UNCONTROLLED 20-STOREY NONLINEAR BENCHMARK BUILDING

Table C.1. The uncontrolled structural response of 20-storey nonlinear benchmark building used in Chapter 3 and 4

Earthquake	El Centro			Hachinohe			Northridge		Kobe		Max.
(intensity)	0.5	1	1.5	0.5	1	1.5	0.5	1	0.5	1	value
δ^{max}	0.003	0.007	0.010	0.003	0.006	0.009	0.010	0.018	0.010	*0.020*	0.020
$\ddot{x}^{max}(m/s^2)$	2.67	5.34	7.79	1.83	3.66	4.72	6.01	8.51	7.49	*9.97*	9.97
F_b^{max}	3.69	7.38	9.53	3.18	6.36	9.12	10.36	*14.26*	10.08	11.42	14.26
$\lVert\delta^{max}\rVert(m)$	.0007	0.001	0.002	.0006	.0012	.0018	.0019	.0006	.0015	*.0074*	.0074
$\lVert\ddot{x}^{max}\rVert(m/s^2)$	0.39	0.78	*1.13*	0.28	0.55	0.8	0.8	1.01	0.76	1.00	1.13
$\lVert F_b^{max}\rVert$	0.76	1.53	1.27	0.71	1.41	2.08	2.15	*2.39*	1.63	2.03	2.39
$\phi^{max}(rad)$	0.47	0.93	1.5	0.43	0.86	1.4	1.68	*3.36*	1.92	3.20	3.36
E^{max}	-	-	19.5	-	-	6.1	20.6	86.2	18.7	*282.7*	282.7
N_d	-	-	86	-	-	86	96	*192*	78	168	192
$\lVert\phi^{max}\rVert(rad)$	0.099	0.197	0.331	0.094	0.187	0.278	0.363	1.406	0.242	*1.423*	1.423
$x^{max}(m)$	0.152	0.304	0.454	0.174	0.348	0.492	0.489	*0.750*	0.314	0.517	0.750
$\dot{x}^{max}(m/s)$	0.458	0.916	1.301	0.451	0.902	1.268	1.662	*2.039*	1.315	1.846	2.039